



**Politecnico  
di Torino**

**ScuDo**  
Scuola di Dottorato ~ Doctoral School  
WHAT YOU ARE, TAKES YOU FAR

Doctoral Dissertation  
Doctoral Program in Energetics (34<sup>th</sup> Cycle)

# **Energy performance assessment of buildings: a novel approach for model validation**

By

**Giovanna De Luca**

**Supervisor(s):**

Prof. V. Corrado, Supervisor  
Prof. I. Ballarini, Co-Supervisor

**Doctoral Examination Committee:**

Prof. Annamaria Buonomano, Referee, Università degli Studi di Napoli “Federico II”  
Prof. Drury B. Crawley, Referee, Bentley Systems  
Prof. Costanzo Di Perna, Referee, Università Politecnica delle Marche  
Prof. Giampiero Evola, Referee, University degli Studi di Catania  
Prof. Enrico Fabrizio, Referee, Politecnico di Torino

Politecnico di Torino  
2022

## Declaration

I hereby declare that, the contents and organization of this dissertation constitute my own original work and does not compromise in any way the rights of third parties, including those relating to the security of personal data.

Giovanna De Luca  
2022

\* This dissertation is presented in partial fulfilment of the requirements for **Ph.D. degree** in the Graduate School of Politecnico di Torino (ScuDo).





## **Acknowledgment**

My sincere gratitude goes, first and foremost, to my supervisors, professor Corrado and Ballarini, for the passionate attitude towards the Research they conveyed me.

I would also like to acknowledge EdilClima Engineering & Software for supporting my Ph.D. Research, and for hosting me in their offices; a special thank goes to Paola Soma, who encouraged me to see the research also from a professional perspective.

## Abstract

Among the existing calculation methods for the building energy performance assessment, the simplified dynamic models are considered to enable a sufficient level of accuracy while guaranteeing the simplicity of the calculation. To meet these goals, these methods are based on modelling assumptions and simplifications that may lead to inaccuracies in the building energy consumption prediction, both in design phases and in energy audits. The validation of the simplified dynamic models can therefore play a crucial role in fostering their application in the legislative framework, and eventually in addressing their implementation to increase their expected accuracy. However, ensuring a deep, rigorous, and correctly addressed validation is not straightforward. This is mainly due to the shortcomings of the existing validation procedures, which consist in: (i) difficulties in identifying the source of possible errors among uncertainties in the input data or inaccuracies in the calculation method, and (ii) inability in evaluating the effect of specific modelling simplifications, parameters, standard values, etc., on the accuracy of the model. Moreover, the validation is often carried out without any attempt to identify the sources of inaccuracies, or even without any theoretical fundamental on the calculation model under validation.

Within this framework, the Ph.D. research proposes a novel single-process comparative testing validation approach, intended at identifying at which extent, and for which conditions and purposes, specific modelling simplifications can affect the accuracy of the model undergoing validation. The proposed approach, named *aware validation*, is built on a robust and detailed knowledge of the theory behind the calculation model to be validated. This knowledge is achieved through the *comparison map*, a tool developed to catalogue and compare the existing modelling options, assumptions, and simplifications related to the modelling of the built environment. In the *aware validation* approach, an overall input equivalence is achieved, and the effect of given modelling assumptions is assessed by means of

the variation in the accuracy of a reference model due to the implementation of each simplification, one-at-the-time.

The recently introduced EN ISO 52016-1 technical standard presents a (new) simplified dynamic calculation method, whose employment for legislative verifications is currently under discussion in Italy. In the present dissertation, the *aware validation* approach was therefore applied to the validation of the EN ISO 52016-1 dynamic method, as to provide a thorough knowledge of its limitations, problems, and peculiarities.

The research underlined important aspects as regard the building energy model validation, and the simplified dynamic model as well. Firstly, the research demonstrated the advantages of performing the validation separately for the different modelling assumptions, since it allowed different sources of inaccuracies to be distinctly identified in the simplified dynamic method. These consisted in (i) the definition of specific calculation parameters (e.g., definition of convective heat transfer coefficients), and (ii) the simplification of specific heat transfer processes (e.g., shadowing of diffuse radiation, and back reflection of solar radiation). Therefore, the use of single-process validation approaches should be enhanced to guarantee rigorous validations. Moreover, the proposed approach allowed demonstrating that the EN ISO 52016-1 assumptions are suitable for defined conditions (e.g., levels of thermal insulation) and applications (e.g., code compliance checks, etc.); this result may also correctly address the choice of the level of modelling detail for eventual implementations of the method.

Considering these aspects, the outcomes of this Ph.D. research are intended contribute to the enhancement of the standardisation activity by providing a clear overview of the suitability of the EN ISO 52016-1 modelling simplifications and by addressing its implementation.



# Contents

1. Introduction .....	1
2. State of the art .....	6
2.1 Introduction .....	6
2.2 Calculation methods for the building energy performance assessment .....	7
2.2.1 Quality aspects in building energy modelling.....	7
2.2.2 Approaches to building energy modelling .....	8
2.3 Validation techniques of the building energy models .....	13
2.3.1 Empirical validation and analytical verification .....	13
2.3.2 Comparative testing .....	14
2.3.3 Comprehensive validation methodologies .....	16
2.4 Building energy models calibration.....	17
2.5 User's role in building energy modelling .....	18
2.6 Conclusion .....	21
3. Novel validation approach of building energy models .....	22
3.1 Introduction .....	22
3.2 General workflow and objectives .....	23
3.3 Cataloguing of modelling options and assumptions.....	24
3.4 <i>Aware validation</i> approach.....	26
3.5 Discussion and conclusion .....	29
4. Cataloguing of modelling options and assumptions .....	31
4.1 Introduction .....	31
4.2 Common assumptions in building energy simulation .....	32
4.3 Comparison map.....	34
4.3.1 External longwave radiation heat transfer.....	36

4.3.2	External shortwave radiation heat transfer.....	48
4.3.3	External heat convection .....	58
4.3.4	Solar transmission .....	62
4.3.5	Heat conduction and storage .....	68
4.3.6	Internal longwave radiation heat transfer.....	74
4.3.7	Internal shortwave radiation heat transfer.....	79
4.3.8	Internal heat convection .....	83
4.3.9	Heat storage.....	87
4.4	Conclusion .....	88
5.	Validation of the EN ISO 52016-1 simplified dynamic method.....	89
5.1	Introduction .....	89
5.2	The simplified hourly method .....	90
5.2.1	Modelling assumptions .....	96
5.2.2	The Italian National Annex improved modelling options.....	103
5.2.3	Modelling assumptions and options: a summary .....	107
5.2.4	Validation studies on the EN ISO 52016-1 hourly method .....	107
5.3	Validation on building construction archetypes .....	109
5.3.1	Methodology .....	109
5.3.2	Application.....	113
5.3.3	Results .....	115
5.4	Validation on building archetypes.....	122
5.4.1	Methodology .....	122
5.4.2	Application.....	123
5.4.3	Results .....	129
5.5	Validation on a real residential nZEB .....	137
5.5.1	Methodology .....	137
5.5.2	Application.....	139
5.5.3	Results .....	142
5.5.4	Lessons learned from a collective model calibration exercise...	151

5.6 Italian National Annex improved modelling options evaluation.....	154
5.6.1 Methodology .....	154
5.6.2 Application.....	155
5.6.3 Results .....	156
5.7 Suitability of the modelling options .....	161
5.8 Conclusion .....	165
6. Conclusions .....	166
References .....	169
Annex A – Modifications to EnergyPlus’s source code .....	190



# List of Figures

Figure 1: Graphical outline of the research methodology within the Ph.D. thesis (S = Section) .....	4
Figure 2: SERI validation procedure (redrawn from [64]) .....	16
Figure 3: General workflow of the proposed validation approach .....	23
Figure 4: <i>Aware validation</i> approach workflow .....	27
Figure 5: <i>Comparison map</i> .....	35
Figure 6: Illustration of the EN ISO 52016-1 <i>R-C</i> model of an opaque building element.....	99
Figure 7: Illustration of the Italian Annex <i>R-C</i> model of an opaque building element .....	104
Figure 8: Angle dependence of $F_{W,dir}$ for different glazings according to Karlsson and Roos formulation [191] .....	106
Figure 9: Methodology workflow for the evaluation of the EN ISO 52016-1 heat conduction solution algorithm for a thermal zone .....	111
Figure 10: Internal surface temperature <i>RMSD</i> vs. $\kappa_{i,dev}$ for the EN ISO 52016-1 standard conduction model under internal constraint ( <i>IntC</i> ) .....	115
Figure 11: Internal surface temperature <i>RMSD</i> vs. $Y_{ie,dev}$ for the EN ISO 52016-1 standard conduction model under external constraint ( <i>ExtC</i> and <i>SDD</i> ) .....	116
Figure 12: Node temperature comparison ( <i>IntC</i> boundary condition, $t = 0$ h) ....	118
Figure 13: Thermal time constants and temperature decay .....	119
Figure 14: Comparison between hourly internal surface temperatures and heating loads for <i>Class I</i> structure .....	121
Figure 15: 3D visualization of the residential apartment unit (a) and of the office module (b) case studies.....	124

Figure 16: Deviations of the energy needs for heating and cooling for the tested modelling assumptions for the office module.....	130
Figure 17: Deviations of the energy needs for heating and cooling for the tested modelling assumptions for the residential apartment unit.....	131
Figure 18: Existing residential unit in Milan: hourly heating loads and $h_{c,ext}$ values in a winter period for the analysed modelling assumptions.....	132
Figure 19: Operative temperature RMSDs for a winter and a summer month for the tested modelling assumptions for the office module .....	135
Figure 20: Operative temperature RMSDs for a winter and a summer month for the tested modelling assumptions for the residential apartment unit.....	136
Figure 21: Methodology workflow for the evaluation of the EN ISO 52016-1 modelling assumptions to a real building, including the calibration step.....	138
Figure 22: 3D model of the residential building and the surrounding buildings.	140
Figure 23: Plan of the analysed storey (2 <sup>nd</sup> above-ground floor) .....	140
Figure 24: Monitored indoor air temperature for the analysed floor (intermediate) and the adjacent upper and lower floors .....	141
Figure 25: Base model simulations compared to measures .....	143
Figure 26: Sensitivity analysis to internal mass parameters (3 <sup>rd</sup> week).....	144
Figure 27: Sensitivity analysis to building envelope parameters (3 <sup>rd</sup> week) .....	144
Figure 28: Sensitivity analysis to natural ventilation parameters (3 <sup>rd</sup> week).....	145
Figure 29: Sensitivity analysis to internal gains parameters (3 <sup>rd</sup> week) .....	146
Figure 30: Comparison between the base and the calibrated model internal gains profile.....	147
Figure 31: Calibrated models result.....	148
Figure 32: Comparison between the calibrated model and the test model implementing the simplified heat conduction model.....	150
Figure 33: Base models simulations compared to measures for the 3 <sup>rd</sup> week of October 2017.....	152
Figure 34: Performance of the calibrated models in the validation periods .....	153
Figure 35: 3D visualisation of the case study .....	155

Figure 36: Percentage variation of the thermal energy needs due to the implementation of the NA options compared to the EN ISO 52016 1 standard method for Milan (a) and Palermo (b) .....	157
Figure 37: Outdoor air and apparent sky temperature difference in Milan .....	158
Figure 38: Outdoor air and apparent sky temperature difference in Palermo .....	158
Figure 39: Monthly average correction factor of the total solar energy transmittance (FW) for different exposures in Milan.....	159
Figure 40: Monthly average correction factor of the total solar energy transmittance (FW) for different exposures in Palermo .....	159
Figure 41: Modelling assumptions' suitability in predicting thermal energy needs and indoor temperatures (refer to the main text for case studies identifier code)	162

# List of Tables

Table 1: Forward models' classification.....	10
Table 2: Validation techniques (elaboration from [12] and [49]).....	13
Table 3: Decomposition of the built environment into components .....	25
Table 4: General modelling simplifications.....	32
Table 5: External longwave heat transfer .....	46
Table 6: External shortwave heat transfer .....	56
Table 7: External heat convection .....	61
Table 8: Solar transmission.....	67
Table 9: Heat conduction and storage.....	73
Table 10: Internal longwave radiation heat transfer .....	78
Table 11: Internal shortwave radiation heat transfer .....	82
Table 12: Internal heat convection.....	86
Table 13: Distribution of the total areal heat capacity of the structure over the R-C nodes for each mass distribution class.....	100
Table 14: Summary of EN ISO 52016-1's modelling assumptions and options.	107
Table 15: Selected structures description .....	114
Table 16: <i>RMSD</i> of the internal surface temperature [°C].....	115
Table 17: Thermal energy needs for space heating and cooling.....	120
Table 18: <i>RMSD</i> for indoor air temperatures [°C].....	120
Table 19. Main geometrical data of the case studies. ....	124
Table 20: Thermal transmittance values of the reference building in accordance with Interministerial Decree of 26 June 2015 [34] .....	125

Table 21: Parameters varied in the sensitivity analysis .....	142
Table 22: Calibrated models .....	147
Table 23: Accuracy of tested modelling assumptions ( <i>RMSE</i> , in °C).....	149
Table 24: Performance of the revised models (to be compared with Table 22)..	154
Table 25: Computational time vs. thermal energy needs variation for Milan .....	161

# Chapter 1

## Introduction

In the European Union (EU), buildings are currently responsible approximately for 42% of the overall energy consumptions, and for 36% of greenhouse emissions [1]. The energy efficiency improvement in buildings, therefore, plays a key role in achieving the EU's energy, environmental, and carbon neutrality goals. For this reason, stringent targets to be achieved in buildings have been introduced to decrease their energy demand and greenhouse emissions. In particular, Directive 2010/31/EU [2] enforces the Member States to draw up national plans for the transformation of the building stock toward the nearly zero-energy, or even nearly zero-emission [3], building target. Building performance simulation is one of the most powerful tools to address the issue of energy efficiency in buildings by correctly addressing the design of new buildings and the retrofit of existing buildings towards these targets.

The topic of improving energy efficiency in buildings has led to the development of different calculation methods for the energy performance assessment. Several approaches, varying according to the specific purpose or level of accuracy and detail required, can be found. Alongside the rapid evolution of the building performance simulation tools, which advanced from simple “rules of thumbs” to multi-domain tools, also the modellers (users) have changed. In early days, the main users were developers with a deep knowledge of the complex interactions occurring in buildings; currently, the need to verify the buildings' energy efficiency targets led to the broadening of the building energy modelling audience, also including not highly expert users, such as practitioners and

professional figures. To meet this change in the building energy modelling users, and to guarantee reliable and realistic results, simplified dynamic methods were developed as to fulfil the model's requirements of robustness, reproducibility, transparency, accuracy, and simplicity [4]. In 2018, the EN ISO 52016-1 technical standard [5] introduced a simplified dynamic method, whose vital requirement is guaranteeing a balance between these requirements. Although contrasting quality aspects, accuracy and simplicity are reached in the simplified dynamic model thanks to modelling assumptions and simplification chosen as to allow a so-called "balanced accuracy", namely a sufficient level of accuracy with a low amount of input data. Due to these characteristics, the replacement of the currently employed quasi-steady state method with the EN ISO 52016-1 simplified dynamic one for legislative verifications (e.g., compliance with energy performance requirements, energy rating, energy performance certificate generation, etc.) is currently under discussion, for example, in Italy. Unlike the currently used methods, this is furthermore able to account for dynamic effects which cannot be ignored, especially ahead of a significant increase in the energy needs for space cooling due to climate change.

The validation of the calculation energy models plays a crucial role in fostering the application of simplified dynamic methods (not only limited to the EN ISO 52016-1 calculation method) in the legislative framework. As a matter of fact, the modelling assumptions introduced by the simplified methods may lead to inaccurate predictions in the energy consumption of buildings in both design phases and energy audits; assessing the accuracy of the simplified method is thus of foremost importance. Furthermore, the validation process may also address their implementation by identifying for which components (e.g., calculation modules, definition of calculation parameters, etc.) alternative calculation procedures may be required to increase their expected accuracy. This concept underlies the proposal for a new technical standard, the ISO/WD 52016-5 [6], which should complement the EN ISO 52016-1 by allowing, for specific aspects, its opening up to alternative, more detailed, calculation procedures.

Three validation approaches are commonly used, namely empirical validation, analytical verification, and comparative testing. The latter consists in the comparison of the results of a given calculation method to other codes, and it can be applied to the whole model or to single thermophysical processes. Although it is the most used approach since it is inexpensive, quick, and it does not rely on detailed monitoring (empirical) or on the presence of exact analytical solutions (analytical), the comparative testing procedure presents some weaknesses. These were identified in: (i) difficulties in reaching an overall equivalence between input

data, making thus challenging to isolate the inaccuracies due to the uncertainty of input data from those related to the calculation model; (ii) inabilities in the detection of inaccuracies of specific solution algorithms in whole-model applications; and (iii) inabilities in investigating the effect of single processes on the overall building thermal behaviour in single-processes application. Moreover, this approach is often applied without any attempt to understand possible sources of inaccuracies, or even without any theoretical fundamental on the calculation model under validation.

Within this framework, the Ph.D. research proposes a novel single-process comparative testing validation approach, developed to overcome the highlighted limitations. The proposed approach, named *aware validation*, aims at understanding at which extent, for which conditions (e.g., level of thermal insulation, building use, etc.), and application purposes (e.g., code compliance, energy rating, energy audits, etc.), specific modelling options can affect the accuracy of the calculation model to be validated, and thus may require an adjustment. The *aware* approach is based on a deep, robust, and detailed knowledge of the theoretical fundamentals of the calculation model to be validated, and of the modelling differences from a reference model. This is achieved through an extensive documentation phase, resulting in the developed *comparison map* tool, intended at cataloguing the existing modelling options, assumptions, and simplifications related to the modelling of the building fabric. Furthermore, an overall input equivalence is achieved in the proposed approach, and the effects of given modelling assumptions are assessed as the variation in the accuracy of the reference model due to the implementation of each simplification, one-at-the-time.

In the present dissertation, the proposed approach was applied for the validation of the simplified dynamic method introduced by the EN ISO 52016-1 technical standard [5], due to its relevance in the Italian legislation context. Specifically, its main modelling simplifications were analysed and compared with the detailed dynamic method of EnergyPlus, assumed as reference model. Then, their accuracy was assessed on different case studies, including building construction archetypes, building archetypes, and real buildings, as to guarantee a general validity of the outcomes. Through the application of the *aware validation* approach, a thorough knowledge of the suitability and reliability of the EN ISO 52016-1's modelling assumptions, and more in general of its limitations, problems, and peculiarities, is achieved. Thus, the outcomes of the present dissertation are intended to contribute to the enhancement of the standardisation activity, and to address the implementation of the simplified dynamic method to increase its level of accuracy, while guaranteeing the simplicity of the assessment.



Beside the present chapter, intended at introducing the framework and motivations for the research presented, this dissertation is composed by the following chapters, connect as outlined in Figure 1.

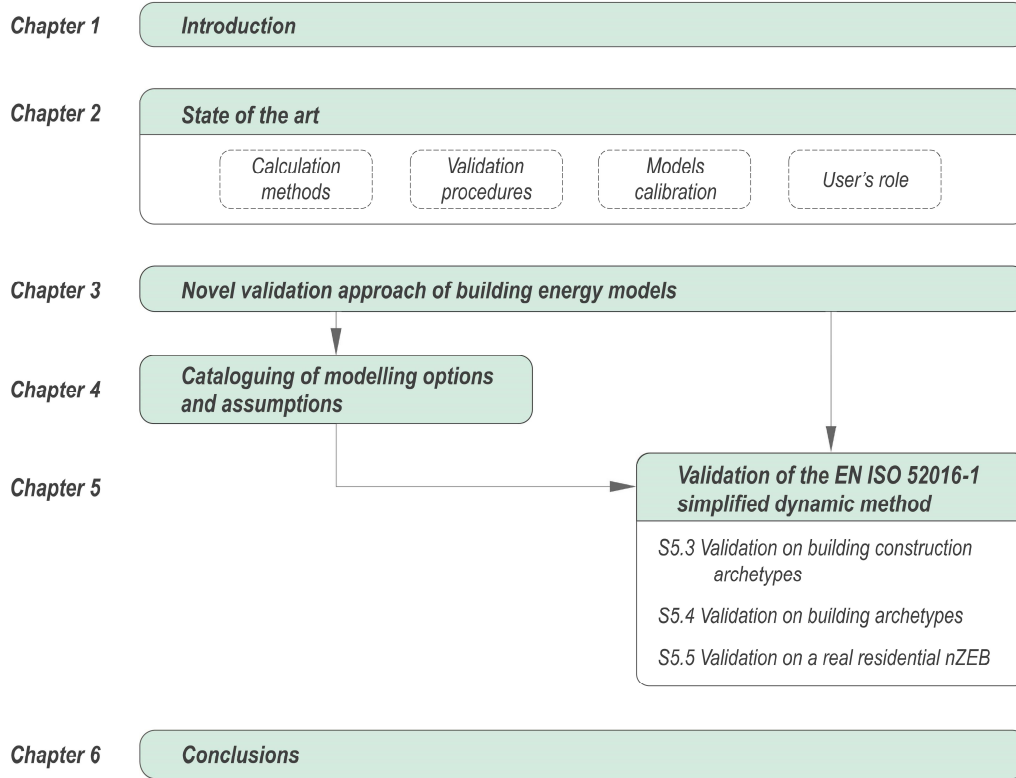


Figure 1: Graphical outline of the research methodology within the Ph.D. thesis (S = Section)

**Chapter 2** provides an analysis of the state of the art, by investigating different aspects related to the building energy modelling. Specifically, it analyses the existing calculation methods for the building energy performance assessment (typologies, quality aspects to be fulfilled, etc.), the existing approach to the validation and the calibration of the building energy models, and the role of the users in the building energy modelling.

**Chapter 3** describes in detail the novel comparative testing validation approach proposed.

**Chapter 4** presents the cataloguing of modelling options, assumptions, and simplifications, implemented in several existing calculation methods. The *comparison map* represents furthermore the starting point for Chapter 5.

**Chapter 5** presents the validation of the EN ISO 52016-1 dynamic method. A detailed description of the model and of its modelling assumptions (derived from

the *comparison map* in Chapter 4) is provided. Four different applications are presented, and the suitability of the tested modelling options for different purposes and conditions is discussed.

**Chapter 6** summarises the main findings of the present research and recommends areas for future works.

# **Chapter 2**

## **State of the art**

### **2.1 Introduction**

Part of the work described in this chapter has been previously published in international peer-reviewed journals [7,8].

The literature review presented in this chapter deals with relevant aspects of building energy simulation. Firstly, an overview of the different calculation methods for the building energy performance assessment is provided in Section 2.2; specifically, advantages and weaknesses of the existing calculation methods are highlighted, along with an analysis of their compliance with prescribed quality aspects. In Section 2.3, the existing validation techniques for building energy models are described, and their relevance in ensuring reliable and realistic building energy performance predictions is examined as well. Similarly, the main open issues related to the building energy model calibration are discussed in Section 2.4. Furthermore, Section 2.5 provides an overview of the influence of the modellers on the accuracy of the building energy performance assessment. Finally, Section 2.6 summarises the main outcomes of the present state of the art analysis.

## **2.2 Calculation methods for the building energy performance assessment**

### **2.2.1 Quality aspects in building energy modelling**

According to the required level of accuracy or detail, as well as for the specific purpose, different calculation models for the building energy performance assessment can be found. Especially for their application in the context of building regulation, these should comply with a number of basic quality aspects (requirements) [9], namely transparency, robustness, reproducibility, accuracy, and simplicity [10].

According to the EN ISO 13790 technical standard [10], the transparency requirement is met when the method is described as a package of equations and parameters complemented by clear rules for their correct application (internal transparency); this requirement also means that the model should allow the user to keep record of each calculation step, and to understand the effects of a specific input data on the calculation results (external transparency). Van Dijk et al. [4] also interpreted the transparency requirement an ideal situation in which each parameter's value has a clarified background, or at least it is within a physically understandable range. The reproducibility requirement is fulfilled when the method is not affected by specific choices of the users, i.e., the same results are achieved by different users. This requires clear and unambiguous specifications of all modelling options. The robustness requirement is achieved when the method can handle different situations with a limited loss of accuracy; this demands that the package of parameters and equations have a physical basis [4]. The accuracy requirement is met when the method produces proper, reasonable, and close to reality results for different solutions.

Finally, the meaning of the simplicity requirement is not straightforward as for the requirements presented before. Although it can be referred to both simple input data and simple methods, a tendency on focusing on the former rather than on the latter was reported [4,10]. However, both aspects should be addressed to achieve the model requirement of simplicity. This means that unambiguous and easily accessible input data are required, as well as a blending of transparency, reproducibility, robustness, and (adequate) accuracy.

Although the above presented model requirements are considered of foremost importance for the application of the calculation procedure within the context of the building regulation [4], other quality aspects are presented in EN ISO 13790, such as legal security, verifiability, distinctiveness, etc. While some quality aspects complement each other, inconsistencies may be found for other aspects. As will be

presented in Section 2.2.2, many existing calculation procedures tends to emphasise one (or more) aspect rather than the others, making them not easily applicable.

### **2.2.2 Approaches to building energy modelling**

According to Beck and Arnold [11], a calculation model describes the behaviour of a system by determining one component among input variables, system structure and parameters, and outputs, when the other two are known. Input variables act on the system, the system structure represents the physical description of the system, and the outputs describe its reaction to the input variables. Applied to the building context, this concept can be adapted to the following statement: *a calculation model describes the behaviour of a building by determining one component among the forcing parameters (e.g., climatic data, geometrical data, thermophysical properties, etc.), the system structure, and the outputs (e.g., energy consumptions, indoor temperatures, etc.), when the other two are known.*

From this description, two different approaches to the building energy modelling can be identified. It is referred to data-driven models (inverse models) when the input and output variables are known; the mathematical description and parameters of the system have to be defined. Instead, it is referred to forward models when the input variables and physical description of the system are known; the outputs of the system (subject to specific input variables) have to be defined. The two modelling approaches will be deepened in the following sections (Section 2.2.2.1 and 2.2.2.2); the existing procedures, application purposes, advantages and disadvantages, and more specifically the compliance with the model's quality aspects, will be presented.

#### **2.2.2.1 Inverse models**

In general, inverse models can be categorised according to two different aspects. Firstly, black- (empirical) and grey-box models are distinguished [12]. In the former approach, the relation between the input and output parameters is identified by means of regression analysis. The latter, instead, consists in a first formulation of a physical model to represent the building (modelling equations), and in a second identification of the modelling equations' relevant parameters by means of statistical analysis. Moreover, the ASHRAE Fundamentals [12] distinguishes the data-driven models into steady-state and dynamic; it also specifies a simple criterion for their identification based on the presence of time-lagged variables, either in the response (outputs) or regressor (input) variables.

The existing black-box approaches are categorised according to the form of regression model used to identify the relation between input and output parameters, which can be either purely statistical or based on general engineering formulation

of energy use in buildings [12]. The most used techniques include linear regression, support vector machine, extreme boosting, random forest, and neural networks [13]. Regardless of the regression technique adopted, black-box models are developed on a large quantity of historical data (either measured or simulated) including building energy consumptions, climatic data, building information, occupant's behaviour, etc.; thus, although no detailed knowledge of on-site physical information is required [14], they are relevant only when the system has already been built and actual performance data are available [12]. For this reason, inverse models are commonly used for energy forecasting [14,15], energy mapping [14,15], energy profiling [14,15], benchmarking prediction [14–16], and retrofit solution evaluation [14,17,18]. However, the identified relation between regressors and response variables is usually not explainable [13]; for this reason, the transparency quality aspect is scarcely met, as well as the simplicity due to the reliance of these models on high amount of not easily accessible historical data.

#### **2.2.2.2 Forward models**

In general, forward energy calculation models can be classified according to three different aspects, namely the considered physical system, the temporal variation of the boundary conditions, and the calculation algorithm employed.

As regards the analysed physical system, the calculation procedures can be applied to the building fabric (which includes the external building envelope components, as well as the internal partitions), the building fabric plus the heat emitters (technical building systems excluding heat generators), and the building fabric plus the technical building systems (including heat generators) [19]. As concerns the temporal variation of the boundary conditions, constant or varying over time quantities (i.e., temperatures, heat flows rates, etc.) can be adopted. In the former case, referred as steady-state regime, the calculation procedures account for quantities integrated over time (e.g., average monthly or seasonal values). In the latter, referred as dynamic regime, the relevant quantities are integrated over short-time intervals (i.e., timesteps); unlike the former approach, this allows to account for thermal phenomena related to the temporal variability of the relevant quantities. Finally, as concerns the calculation algorithm employed, the methods can either solve the convective air heat balance (AHB) equation within the thermal zone (plus the heat balance on the surfaces facing the zone), or calculate the overall thermal load as the sum of the different loads produced by the driving forces (i.e., outdoor environment temperature, ventilation, solar radiation, and internal sources).

According to the aspects presented, three typologies of calculation procedures can be identified (Table 1). In the steady state methods, the overall thermal load of a thermal zone is calculated considering constant boundary conditions for a

sufficiently long period of time. Although these are suitable for the evaluation of the building fabric and the technical building systems, the dynamic phenomena affecting the building thermal inertia are not accounted. Quasi-steady state methods, instead, account for the dynamic effects through simplified aggregated parameters. Finally, in the dynamic methods (also known as hourly methods) the air heat balance is solved considering variable conditions; the dynamic effects of heat accumulated and released by the building structures are accounted in the evaluation of both building fabric and technical building systems.

Table 1: Forward models' classification

Procedure	Physical system	Boundary condition temporal variation	Calculation algorithm	Dynamic effects
<i>Steady state</i>	Building fabric Building fabric plus emitters Building fabric plus technical building systems	Constant	Overall heat balance	Not accounted
<i>Quasi-steady state</i>	Building fabric Building fabric plus emitters	Constant	Overall heat balance	Accounted (simplified)
<i>Dynamic</i>	Building fabric Building fabric plus emitters Building fabric plus technical building systems	Variable	Air heat balance Overall heat balance	Accounted

The EN ISO 52016-1 technical standard [5] (replacing EN ISO 13790 [10]) presents a monthly quasi-steady state and a simplified hourly method for the evaluation of the building thermal energy needs for space heating and cooling (thus, only related to the building fabric). Differently from the simplified dynamic ones, the detailed dynamic methods are not fully prescribed, except for general rules presented in the EN ISO 52017-1 technical standard [20]; they are, in fact, mainly implemented in simulation tools, built and developed for different purposes or to reach different levels of detail.

The quasi-steady state procedure introduced by the EN ISO 52016-1 is based on a monthly balance of heat gains, namely solar and internal gains (i.e., occupancy, appliances, lights, etc.), and heat losses, namely transmission through the building envelope and ventilation, which are assessed considering monthly average boundary and use conditions [21]. Utilisation factors are introduced in this calculation method to account for the dynamic effects on the building thermal energy needs for space heating and cooling; these factors, which are function of heat losses, heat gains, building's time constant, allow to reduce the building energy need for heating or cooling, and can be obtained from hourly thermal energy needs calculation. The simplicity of the assessment, as well as the reproducibility of results [4], made the quasi-steady state methods to be widely applied over the years, especially for annual and monthly evaluations in the regulatory framework. Nevertheless, individual month evaluations may lead to large errors [10].

Furthermore, the ability of the model in predicting the cooling energy needs is often not sufficiently accurate. For example, Bruno et al. [22] demonstrated the consistent overestimation of the thermal energy need for space cooling (ranging from 9% to 60% when compared to the TRNSYS [23] dynamic method). Similar results were also achieved in [24,25] for buildings of the Mediterranean area. While the accuracy requirement is may be difficult to be met in the quasi-steady state methods, they have proved to guarantee the required simplicity, robustness, and reproducibility.

When speaking about detailed dynamic models, it is usually referred to calculation procedures implemented in commercial or open-source tools. In fact, according to Filippi and Fabrizio [26], the detailed dynamic calculation method was developed within the EnergyPlus tool [27]. According to the purpose of application (e.g., evaluation of the building fabric, technical building systems, etc.) and the required level of detail, several simulation tools can be found. The Building Energy Simulation Tools (BESTs) directory [28] provides an extensive classification of the existing tools, while Crawley et al. [29] provides a comparison of the features and capabilities of twenty building energy simulation programs, showing the main modelling differences regarding thermal zone loads, building envelope, ventilation, etc. Most commonly, dynamic methods adopt the air heat balance solution algorithm [19]. Specifically, it accounts for the zone air heat capacity and for several convective driving forces, namely heat convection at internal surface, ventilation, and convective internal (and solar) heat gains. In turn, these heat balance terms depend on the energy balances on the internal and external surfaces of the building envelope components, and on the heat conduction and storage through the structures [19]. Unlike the quasi-steady state procedures, a huge number of equations needs thus to be solved (simultaneously) to calculate the building thermal energy needs, making the dynamic models computationally expensive. Although detailed dynamic methods allow to correctly simulate the most advanced materials, components, and technologies (e.g., chromogenic glazing [30], kinetic façades [31], phase change materials [32], etc.), they require very detailed input data, often not easily accessible, as well as many user's interaction and high level of expertise to correctly carry out the simulations. Certainly, the model requirement of accuracy is fully met in the detailed dynamic methods; however, this brings along a consistent loss of simplicity and reproducibility.

In the middle, the simplified dynamic methods are considered to enable the achievement of the so-called “balanced accuracy” [33,34], namely a sufficient level of accuracy with a low amount of input data. Like the detailed dynamic methods, the EN ISO 52016-1 simplified hourly method adopts the air heat balance solution algorithm. However, some parameters describing the involved heat transfer



phenomena are lumped (e.g., convective and radiative surface heat transfer), or certain heat transfer phenomena are even neglected (e.g., nonlinearity of radiant heat transfer). The modelling assumptions and simplifications on which the EN ISO 52016-1 hourly method is based allow to guarantee the simplicity of the model; the simplicity requirement related to the input data is met as well due to the use of the same input data as in the quasi-steady state method (i.e., low amount and easily accessible data). As for the quasi-steady state method, also the simplified dynamic one is fully prescribed in the technical standard, thus the transparency requirement is achieved. Since its recent introduction, the existing research studies are not sufficient yet to establish the accuracy of the simplified hourly method. Although the process of validation has been successfully completed [33], more effort could be required to assess its suitability for different purposes and specific conditions.

Although the different types of forward model differ in several aspects and meet different quality aspects, they enable the explicit description (more or less accurate, according to the model chosen) of the heat transfer phenomena that occur within the building [16]; unlike the inverse models, the relationship between the dependent and independent variable is easily explainable, and no historical data are required to build the model [13]. On the other hand, robust knowledge and expertise is needed to correctly perform the simulations, as well as a significant amount of effort to input the required building information and parameters [13]. Despite these disadvantages, the majority of the studies concerning the building energy performance assessment are conducted through forward models [19]. In fact, they have been employed for several applications, including energy needs assessment [35], overheating assessment [36], economic analysis and energy efficiency measures evaluations (retrofit design) [37–39], energy audits [40,41], and legislative verifications [42].

Except for legislative verifications, the employment of a calculation model rather than another is not regulated, nor practical advice were found in literature. In the regulatory framework, the European Commission [43] requires the Member States to apply calculation methods that are consistent with European standards and relevant legislation. In most of the Member States, quasi-steady state methods are currently applied to check the compliance with minimum energy requirements in building, for energy rating, or for energy performance certificate generation. Nevertheless, the need to correctly evaluate the summer thermal behaviour of buildings, ahead of a significant increase in the energy needs for space cooling due to climate change, is foresting the employment of simplified dynamic models. As a matter of fact, the replacement of the currently employed quasi steady-state method with the simplified dynamic one for legislative verifications is currently under

discussion, for example, in Italy. Specifically, the Italian National Agency for New Technologies, Energy and Sustainable Economic Development (ENEA) promoted a research activity aimed at analysing the applicability of the EN ISO 52016-1 simplified dynamic method in the legislative context for different types of buildings [44,45], and in updating of the National methodology for the assessment of cost-optimal energy performance requirements [46].

## 2.3 Validation techniques of the building energy models

The calculation model's ability to produce proper, reasonable, and reliable results [47] is assessed through its validation<sup>1</sup>. Three approaches are commonly used for the building energy model validation (Table 2), namely empirical validation, analytical verification, and comparative testing [48].

Table 2: Validation techniques (elaboration from [12] and [49])

Technique	Advantages	Disadvantages
<i>Empirical</i>	<ul style="list-style-type: none"> <li>» Approximate truth standard within experimental accuracy</li> <li>» Any level of complexity</li> </ul>	<ul style="list-style-type: none"> <li>» Experimental uncertainties</li> <li>» High-quality, detailed measurement are expensive and time consuming</li> <li>» Only a limited number of test cases are practical</li> <li>» Diagnostic can be difficult</li> <li>» Requires empirical determination of inputs</li> <li>» Only a limited number of sensitivity test cases are practical</li> </ul>
<i>Analytical</i>	<ul style="list-style-type: none"> <li>» No input uncertainty</li> <li>» Exact mathematical or secondary mathematical truth standard for given model</li> <li>» Inexpensive</li> </ul>	<ul style="list-style-type: none"> <li>» No test of model validity or suitability</li> <li>» Limited to highly constrained cases for which analytical or quasi-analytical solutions can be developed</li> </ul>
<i>Comparative</i>	<ul style="list-style-type: none"> <li>» No input uncertainty</li> <li>» Any level of complexity</li> <li>» Many diagnostic comparisons possible</li> <li>» Inexpensive and quick</li> </ul>	<ul style="list-style-type: none"> <li>» No absolute truth standard (only statistically based acceptance ranges are possible)</li> <li>» Dependency on the accuracy of the reference model</li> <li>» Overall input equivalence is impossible</li> </ul>

### 2.3.1 Empirical validation and analytical verification

Empirical validation consists in the comparison between the calculated results from a simulation tool, subroutine, or algorithm, and the monitored data from a real building, test cell, or laboratory experiment; for this reason, it is agreed that the empirical validation allows to establish an absolute truth standard (within the experimental accuracy) [49] for assessing the ability of a calculation model in analysing specific physical behaviours. However, this approach has to deal with experimental uncertainties, including those related to measurement instruments,

<sup>1</sup> The meaning of the word validation has been widely discussed. In the present dissertation, the term validation refers to the process of assessing the accuracy of a calculation model for specific conditions and purposes; it is thus used to address the question "It is good enough for [whatever purpose]?" [51].

unknown exact design details (e.g., material properties), and overall experimental design. Thus, the description of the experimental apparatus requires a thorough effort to minimise the possible uncertainties [49].

Analytical verification consists in the comparison between the calculated results from a simulation tool, subroutine, or algorithm, and the results from a known analytical solution, or a generally accepted numerical method, for isolated heat transfer under very simple, highly constrained boundary conditions [49]. This approach is inexpensive, it compares the simulation tool results to a so-called “mathematical truth”, and it is not subject to any input uncertainty; however, it can be applied only to constrained cases of thermophysical phenomena with known exact solution.

### **2.3.2 Comparative testing**

Comparative testing consists in the comparison of the calculated results from a simulation tool, subroutine, or algorithm, and the calculated data from the same or another simulation tool, assumed as reference model. Although it relies on the accuracy of the reference model – which represents what is commonly accepted as current state of the art in the building energy simulation, not necessarily an absolute truth [50] – the comparative testing approach can be a very powerful approach to identify errors and to assess the accuracy of the tested model [51]. In fact, it has been widely applied, and it proved its valuable capabilities in code debugging activities [52,53], in assessing the accuracy of building energy performance calculation models [54,55], and in the validation of several simulation programs.

The comparative testing approach can be applied to the whole calculation model (whole model comparative testing approach), or to single portions (single process comparative testing approach). In the former approach, the entire calculation model architecture (e.g., the interaction between the thermophysical phenomena) is tested; the latter, instead, is focused in analysing specific solution algorithms, modelling assumptions, etc. Both the comparative testing applications can handle any level of complexity, are inexpensive and not time consuming (thus, many comparisons are possible), and do not rely on the accuracy of the measurements (thus, they are not subject to input uncertainties). However, their main weakness concerns the achievement of a sufficient input equivalence to ensure that each model is using comparable data [56]. Several research studies have introduced different approaches for minimizing the errors due to differences in the input data [57], where a set of consistency options were suggested to ensure comparable results between the test and the reference model. However, input equivalence is not always a straightforward issue (especially where the modelling

approach varies significantly between programs [58]), and it may be difficult to reach a global equivalence in the input; it may be thus challenging to isolate the inaccuracies due to the uncertainty of input data from those related to the calculation models. The whole model and the single process approaches differ in two aspects; the former enables the analysis of the overall thermal behaviour of the building, while the latter allows to detect inaccuracies in the algorithms or in the assumptions related to single portions of the tested calculation method [59].

Different validation approaches employing the comparative testing have been developed in the last decades. The most applied approach is the International Energy Agency (IEA) Building Energy Simulation Test (BESTEST) [50], then adopted in the ASHRAE Standard 140 [60]. This approach was developed to systematically test whole building energy simulation tools, and to diagnose possible sources of predictive discrepancies. It consists in forty comparative test cases (ranging from simple to realistic tests), built as to incrementally test different models, including thermal mass, solar gains through the transparent envelope components, window's shading, sunspaces, etc. In the BESTEST approach, the results of the tested calculation model (relative to the consisted test cases) are compared to an acceptance range, namely the results of several detailed public domain models, considered to be the representative of what is commonly accepted as the current state of the art in whole-building energy simulation. The attempt of evaluating specific models is, however, influenced by the overall calculation model architecture, thus it is challenging to isolate their specific effects. The BESTEST test cases have been updated to account for improved equivalent surface heat transfer input parameters [58], and to adapt them to the current modelling state-of-the-art [61].

The (withdrawn) EN ISO 13791 technical standard [62] introduced a validation procedure based on four different test cases. In the first three, single portions of a calculation model are tested, namely heat conduction through opaque components, internal long-wave radiation heat transfer, and shadowing of the windows due to external obstacles (short-wave radiation heat transfer); in the latter, instead, all the thermophysical phenomena are considered (whole model validation procedure).

SimQuality [63] is a recently introduced test suite for the validation of building energy performance simulation tools (based on the BESTEST and EN ISO 13791 test suites), and a platform for the publication and the documentation of the validation status of the tools. Currently, it consists in twelve different tests, including single-process (e.g., solar gains calculation, solar distribution, internal gains, outer shadings, etc.) and whole-building tests (e.g., real building geometries and complex case for the evaluation of the summer overheating protection).

Through the specified tests, the SimQuality test suite aims to limit the errors occurring in each calculation model component (single-process tests), and in any components' combination as well (whole-building tests).

### 2.3.3 Comprehensive validation methodologies

The empirical validation, analytical verification, and comparative testing are generally coupled into comprehensive methodologies for the building energy model validation. The Solar Energy Research Institute (SERI) [64] proposed a validation procedure based on three phases (Figure 2). Firstly, the tested code is run against analytical test cases to check the accuracy of the major heat transfer algorithms, and eventually repaired. Then, it is compared to monitored data, and eventually repaired. In the last phase, the code is compared with several codes with different thermal solution approaches for various representative test cases. If the tool completes all the three phases, it is considered validated within the range of cases defined by the comparative studies; otherwise, the source of disagreement is identified, and the validation procedure starts again from the first phase (analytical verification).

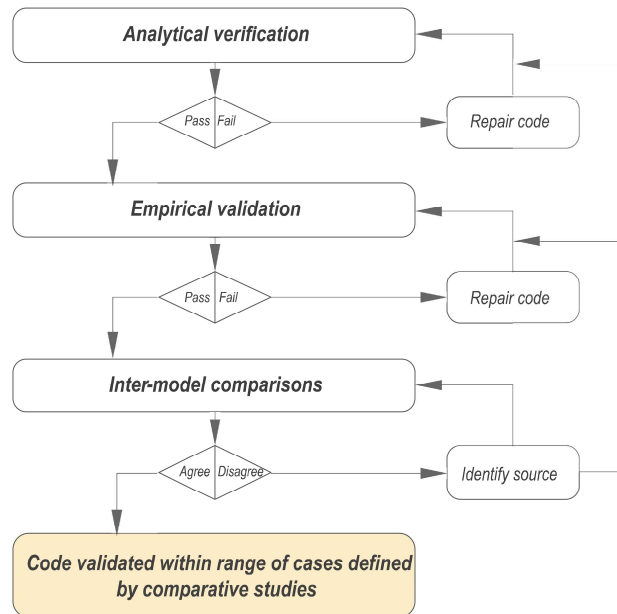


Figure 2: SERI validation procedure (redrawn from [64])

Alongside the SERI approach, the three testing techniques are also included in the European Union PASSYS Project methodology [59]. The PASSYS approach includes several steps, among which the application of analytical and inter-model comparisons, the use of sensitivity analysis to investigate the model overall uncertainty, and the application of empirical validation experiments. Moreover, it

highlights two fundamental aspects related to the model validation. Firstly, it suggests that the model validation should be applied not only to the whole calculation model, but also to its single components (the proposed procedure may vary if applied to the whole model or to single components). The main advantage of such validation method is the possibility to clearly detect inaccuracies in the algorithms or in the assumptions related to single portions of the tested calculation method [59]. Secondly, it includes a critical literature review in which the theory behind the different heat transfer processes is evaluated, and possible alternatives are investigated. The importance of this last aspect is also highlighted in the “Management of Information” System (MIS), a prototype tool developed by the IEA Annex 21 Subtask A [51] to assist the program development and validation. The developers and users are asked to document each choice made in terms of solving algorithm, or assumed simplification, or level of detail. Through the MIS, it is therefore possible to easily catch the causes of the discrepancies, for example while conducting several simulations or in validation activities.

## **2.4 Building energy models calibration**

Initially, building energy modelling was mainly focused on building design phases; currently, instead, it is becoming relevant in post-construction phases [65], including building retrofit design. A widely applied technique to evaluate building retrofit solutions is the calibrated simulation approach [66], which is of foremost importance to reduce the energy consumption of the existing building stock.

Calibration is the process of fine-tuning the modelling parameters (i.e., input data, standard parameters, etc.) to reduce the discrepancies between the building energy simulation predictions and the actual monitored building energy behaviour. Although the calibration has been widely applied for different purposes (including to provide insight to an owner of the actual building’s thermal behaviour, to evaluate the impact of different load control measures, to support investment-grade recommendations, etc. [66]), this is not a standard process, and no consensus on a shared methodology has been achieved yet. Different approaches are currently applied, mainly categorised into manual and automatic approaches [67–69]. In manual calibration, the user modifies the model parameters affected by uncertainties iteratively to reach a required matching between the simulated and monitored data. Due to the considerable variety of parameters that may be affected by modelling uncertainties, and the amplitude of the corresponding range of variation, a methodical manual calibration is difficult to be performed. For this reason, the process mainly depends on the user’s experience and expertise [66]. The modeller also drives the automatic calibration process; in fact, the user has to firstly identify

the uncertain parameters (defined through a sensitivity analysis to reduce the number of parameters to be calibrated [66]) and their range of variation. Then, the calibration is performed by an automated process based on mathematical, statistical, or optimisation methods [70]. Other calibration approaches can be based on graphical comparative displays, and on special tests and analytical procedures [66]. The heuristic manual calibration can be combined with graphical comparative approaches, which allows to easily highlight the discrepancies between measured and simulated performance on monthly or diurnal plots, so that the modeller is guided in deciding which parameters to be tuned in the calibration iterative process. Common plots include carpet plots, time series plots, etc.; their use is widely described in the ASHRAE Guidelines 14 [71]. Among the special tests and analytical procedures based calibration procedures, Reddy [66] included intrusive blink-tests, STEM Tests, and signature analysis methods.

The issues related to the building energy model calibration go beyond the absence of a shared methodology. In fact, the calibration lacks unique solutions as well. Especially if manual processes are applied, many calibrated models are usually identified. Such result may be more robust than searching a single optimal solution [72]; however, not all the identified calibrated models may be representative of the actual building behaviour outside of the calibration period. Thus, an additional verification process, in which the calibrated model predictions are tested on different periods, is usually recommended, often leading to a refinement of the calibrated model [73].

Moreover, there is also a lack of standardised calibration criteria, meaning that the current calibration guidelines (e.g., ASHRAE Guidelines 14) only specify acceptable error ranges for long-term building simulations, not accounting for input uncertainties, sub-metering calibration, or zone-level discrepancies [67].

Finally, both validation and verification of the calibrated models demand for high quantity and quality of monitored data, often expensive and time consuming to be obtained. The kind of information available to the modeller can largely vary, so that different levels of calibration can be identified [68]; as well, the available data resolution may orientate and impact on the calibration approach and the subsequent results. Thus, important efforts should be devoted to address to what extent detailed metering is necessary to produce high-fidelity calibrated models.

## **2.5 User's role in building energy modelling**

*“[...] BPS suffers from a credibility gap and [...] its full potential will only be realized once we adequately prepare users to effectively apply tools with full knowledge of their applicability,*

*modelling limitations, and default methods and data, and provide them the skill set to scrutinize their results.” [74]*

The accuracy in the prediction of the building's energy performance is of foremost importance to address the energy efficiency improvements in buildings. In literature, it is recognised that it depends on three main factors [66,75,76], namely the input data, the calculation method, and the user.

Errors and uncertainties in the building's performance prediction may arise from inaccurate input data used to represent the building. These may be affected by errors, caused by different sources (e.g., lack of information, mistakes in data processing, etc.), or by uncertainties [77]. The issue related to the input data uncertainty has been widely investigated in the last years; in the work of Tian et al [78], an extensive state of the art regarding input data uncertainties is presented, including weather, building envelope, technical building systems, and occupant behaviour data as source of uncertainty in the building energy performance analysis. The dependency of the simulation output's accuracy to the calculation method employed concerns several issues, including the applicability of the method to the building and/or climate analysed [76], its modelling detail and resolution [75], and the use of different levels of modelling assumption and simplification, or numerical solutions for the description of the physical processes [75,76]. Finally, both the aspects covered above are affected by the users, and specifically by their domain knowledge [75]. This, in fact, may intensify the errors and uncertainties affecting building simulation. Firstly, the users may commit errors in deriving the input data due to lack of experience and expertise, or even negligence [66]; moreover, they may choose to use standard input data [74] which may not be appropriate for the building analysed. On the other hand, the choice to adopt specific modelling simplifications it is up to the user [66,76], as well as the use of different numerical approaches to describe the thermal mechanisms [75], or even to avoid some of them. Last but not least, the evaluation of the simulation outputs is entirely a responsibility of the users, who will base the decision making on their professional expertise and knowledge [79].

In the last years, different studies assessed the relevance of the user on the building performance simulation accuracy and analysed the errors' occurrence. The work of the IEA Annex 21 Subtask B [80,81] illustrated a variation of four to one in the prediction of the building energy performance for twenty users using the same simulation tool. In a validation exercise submitted to twelve users, Guyon [82] proved that the users' choices can affect the prediction of the energy consumptions for a residential building by a  $\pm 40\%$ . The users were provided with identical specifications for the case study, including a detailed geometrical description of the



building, the data related to the windows and to the heat transfer coefficients. Similarly, the users' modelling choices, while still reasonable, had a significant effect on simulation results in the research of Berkeley et al. [83]; a wide variety of users were included, from master degree graduated to professional figures with experience in the building simulation field. Errors related to lack of attention, selection of the calculation model, input data elaboration, and user's awareness were identified. The input data-related errors included the incorrect data processing or extrapolation [81,83], and use of default (standard) data [83,84]. Instead, the user's awareness-related errors included the adoption of not suitable modelling simplifications [81], the incorrect evaluation of heat transfer mechanisms [82], and the lack of awareness of the most influencing parameters on the simulation results [83]. This latter behaviour was also proved by the work of Imam et al. [85]. The Authors asked a huge number of building modellers to sort common modelling input variables by their importance and influence when estimating building annual energy needs; the sorted lists were then compared to a reference rank (obtained by means of a sensitivity analysis against monitored data). The results showed a little correlation between the variables considered important by the modellers and the ones objectively important. Thus, their work showed a lack of consensus between the users on which inputs matter most, and therefore where they should invest their time when applying building performance simulation [74].

Alongside the evolution of the building performance simulation tools, also the users have changed. In early days, the main users were developers with a deep knowledge of the physical phenomena that occur in buildings, and how to correctly model them [74]. Then, the simulation tools advanced with two different purposes. On the one hand, they became more accessible also to not expert users [74], increasing thus the chance of an improper or outside the range of applicability tools' use [79]. On the other hand, they increased in complexity to correctly simulate the most advanced technologies, requiring more expertise to get reliable outcomes and increasing the uncertainty sources [86]. A huge effort in developing building performance simulation training paradigms have been put in the last years [74,84,87–90]. Since data entry errors can and will occur (and may be hopeless trying to avoid them), the proposed paradigms underlined the importance of preliminary understanding of the fundamentals of building performance simulation; these are thus intended to act on the user awareness-related errors. In fact, increasing the awareness in the use of the building energy simulation may help to ensure accurate energy performance prediction. A deep knowledge may allow the users to realise which models, assumptions, or simplification are applicable in

which situations and to understand the effect of modelling choices and default modelling input data [74].

## 2.6 Conclusion

From the analysis of the state of the art, some critical issues related to different aspects of building energy modelling have emerged.

The fulfilment of the calculation methods for the building energy performance assessment with the quality aspects prescribed is hardly achieved. Among the existing forward methods, the simplified dynamic ones stand out for their simplicity and accuracy (the so-called “balanced accuracy”), enhancing their suitability for the employment in the legislative framework to verify the building energy performance requirements. As a matter of fact, the application of the simplified dynamic method introduced by the EN ISO 52016-1 in the Italian regulatory context is currently under discussion. However, this may be fostered only by a rigorous validation of the proposed calculation method. The current validation processes though lack in certain aspects. Firstly, they show limitations in isolating the source of errors related to the calculation method from the ones due to input data uncertainties, and the detection of inaccuracies in specific solution algorithms, modelling assumptions, and parameters is challenging. Moreover, a validation procedure that makes no attempt in understanding the source of errors (i.e., similar to how building energy simulation is used as well) is often favoured by many practitioners and simulation tool developers, which prevents definite conclusions about the accuracy of the model under validation [48]. The building energy simulation users furthermore may consistently influence the accuracy in the prediction of building energy performance, often due to lack of sufficient knowledge in the building physics or building simulation domains, or awareness of the effect of modelling choices and default modelling input data.

The research activity was aimed at overcoming the highlighted research gaps, in order to address a correct, rigorous, and aware validation of the building energy models. In particular, the Ph.D. thesis proposed a novel validation procedure aimed at enhancing the user awareness (Chapter 4) and intended at identifying at which extent specific modelling simplifications can affect the accuracy of the EN ISO 52016-1 calculation method (Chapter 5).

## **Chapter 3**

# **Novel validation approach of building energy models**

### **3.1 Introduction**

Part of the work described in this chapter has been previously published in international peer-reviewed journals [7] or presented at international conferences [91].

The validation of the calculation methodologies plays a crucial role in fostering both the application of simplified dynamic methods in legislative framework and their implementation to increase their level of accuracy. However, from the investigation of the state of the art presented in Chapter 2, it emerged how the existing comparative testing validation approaches present some weaknesses. Three main limitations were identified: (i) difficulty in reaching an overall equivalence between input data, in both whole model- and single process-applications; (ii) inability in the detection of inaccuracies of specific solution algorithms for whole-model applications; and (iii) inability in investigating the effect of single processes on the overall building thermal behaviour. Moreover, inter-model comparisons are often applied without any attempt in understanding the sources of discrepancies, or without any theoretical fundamental on the calculation model under validation [51].

Starting from these premises, a novel comparative testing validation approach was developed to overcome the highlighted limitations. Section 3.2 introduces the

objectives and the workflow of the proposed validation approach. The main phases are instead detailed in Sections 3.3 and 3.4.

### 3.2 General workflow and objectives

To correctly address the implementation of a given building energy performance calculation model, there is the need to understand which components of the method (e.g., calculation modules, definition of calculation parameters, etc.) lead to inaccuracies in the results, and thus may require an adjustment. Moreover, a clear and detailed picture of the possible implementation alternatives may be potentially very valuable in an implementation activity.

Starting from these premises, the workflow of this dissertation was organised into two main phases to address the needs presented above, as presented in Figure 3.

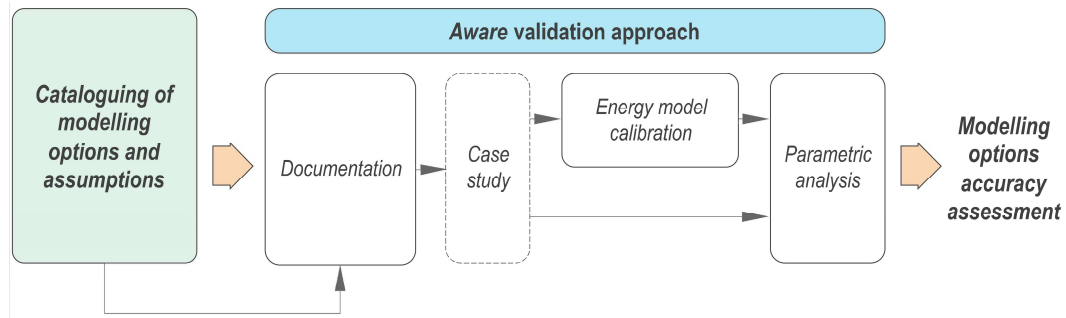


Figure 3: General workflow of the proposed validation approach

In a preliminary phase, a detailed documentation of the state of the art related to the modelling of the main heat transfer processes in buildings was provided. This review was specifically intended to document and classify the existing modelling options, assumptions, and simplifications applied in dynamic calculation models, and it was extended to both simplified and detailed methods. The specific methodology developed in the present thesis for reviewing the existing modelling simplifications is deeply presented in Section 3.3.

In the second phase, instead, the accuracy of the modelling assumptions and simplification of a given calculation model, documented in the previous phase, was assessed. To this purpose, a single-process validation approach, fitting into the comparative testing technique, was proposed. Differently from other comparative testing approaches (Section 2.3.2), the proposed approach, named *aware validation*, is built on a robust and detailed knowledge of the modelling assumptions implemented in the calculation model to be validated, achieved through the first documentation phase. The *aware* approach is a case-study based approach mainly

consisting in a parametric analysis in which the documented modelling assumptions are tested one-at-the-time. The parametric analysis may be preceded by a calibration phase if the considered case study is a real building. The phases composing the proposed *aware validation* approach are described in Section 3.4.

As mentioned, the documentation phase concerned a wide range of dynamic calculation methods; in the framework of the present dissertation, the *aware validation* approach was instead applied in the validation of the recent simplified dynamic method introduced by the EN ISO 52016-1 technical standard [5].

### 3.3 Cataloguing of modelling options and assumptions

The review of the existing assumptions and simplifications was focused on the modelling of the building fabric, and it was structured as an analysis of the interaction between the components composing the built environment. To this purpose, the review was carried out following three different steps.

#### *Step 1 – Decomposition of the built environment*

To identify the components to be studied, the built environment was firstly decomposed into four systems (i.e., indoor environment, opaque building envelope, transparent building envelope, and outdoor environment); then, the components (and subcomponents) characterising each system were identified. The defined built environment components are reported in Table 3.

The indoor environment was decomposed into indoor air, internal sources (e.g., occupants, appliances, lights, etc.), thermal mass (i.e., internal thermal capacity of the zone), furniture, and HVAC terminal units. It is worth highlighting that furniture is also included in the thermal mass component, since it adds participating thermal mass to the zone. However, it was necessary to distinguish thermal mass and furniture since the latter may also participate in the radiation and convection heat exchange. Even though the technical building system modelling was not the object of the present dissertation, the HVAC terminal units were included in the built environment components as the system heating/cooling loads affects the zone air heat balance, as well as the indoor surface heat balance. As for the opaque building envelope, the external components, indoor partitions, and components adjacent to the ground were considered separately since they are subject to different driving forces. For each of the opaque building envelope components, the investigation was focused on the inside and/or outside surfaces (considered as subcomponents) and on their constructions (consisting of both solid and only-resistance layers). The transparent envelope was decomposed into holes, glasses (subdivided as the opaque building envelope components), frames and dividers, and shading devices. Finally,

the outdoor environment was decomposed into outdoor air, sky vault, sun, surface of the ground, objects considered at outdoor air temperature, and other objects (at different temperatures).

Table 3: Decomposition of the built environment into components

System	Component	Subcomponents	
<i>Indoor environment</i>	Air		
	Furniture		
	HVAC terminal units		
	Internal heat sources		
	Internal thermal mass		
<i>Opaque envelope</i>	External component	Inside surface	
		Construction	Solid layer Air layer
		Outdoor surface	
	Internal partitions	Surfaces	
		Construction	Solid layer Air layer
	Adjacent to ground	Inside surface	
		Construction	Solid layer Air layer
	Thermal bridges		
<i>Transparent envelope</i>	Holes		
	Glass	Inside surface	
		Construction	Solid layer Air layer
		Outdoor surface	
	Frame/Divider	Inside surface	
		Construction	Solid layer Air layer
		Outdoor surface	
	Shading device	Shading layer Air gap	
	Thermal bridges		
<i>Outdoor environment</i>	Air		
	Sky vault		
	Sun		
	Ground		
	Objects at air temperature		
	Objects at different temperature		

### *Step 2 – Identification of interaction between components*

The second step consisted in identifying the interaction between the built environment components, and the heat transfer processes involved. This analysis was performed through the creation of a “component vs. component” array, in which each row and column represent one of the components identified in the first phase. The array elements (i.e., the intersection of a row and a column) were then filled if the respective components interact with each other. Finally, for each interaction between the components, the heat transfer phenomena involved were identified. In particular, the analysis included longwave radiation heat transfer, shortwave radiation heat transfer, heat convection, heat conduction, and heat storage phenomena.

The “component vs. component” array, called *comparison map*, represents the tool employed in the next step to document the existing modelling options and assumptions.

#### *Step 3 – Review of modelling options*

In the third phase, three levels of modelling assumptions were investigated for each identified interaction between couples of components, and for each heat transfer process involved.

Firstly, the existing strategies for the modelling of the analysed heat transfer phenomenon were explored, and the modelling assumptions linked to the use of a specific modelling strategy were highlighted. For example, the longwave radiation heat transfer can be modelled by means of the Stefan-Boltzmann law or its linearisation; if the latter is considered, the non-linearity of the phenomenon is assumed. The second level of assumptions studied concerned to the determination of the driving forces, and to their temporal discretisation as well. Lastly, the same investigation was applied to the definition and temporal discretisation of calculation parameters.

The review was carried out by analysing research papers, technical standards (e.g., CEN, ISO, ASHRAE), books, and the documentation of different dynamic simulation tools (e.g., EnergyPlus [92], TRNSYS [23], ESP-r [93], etc.).

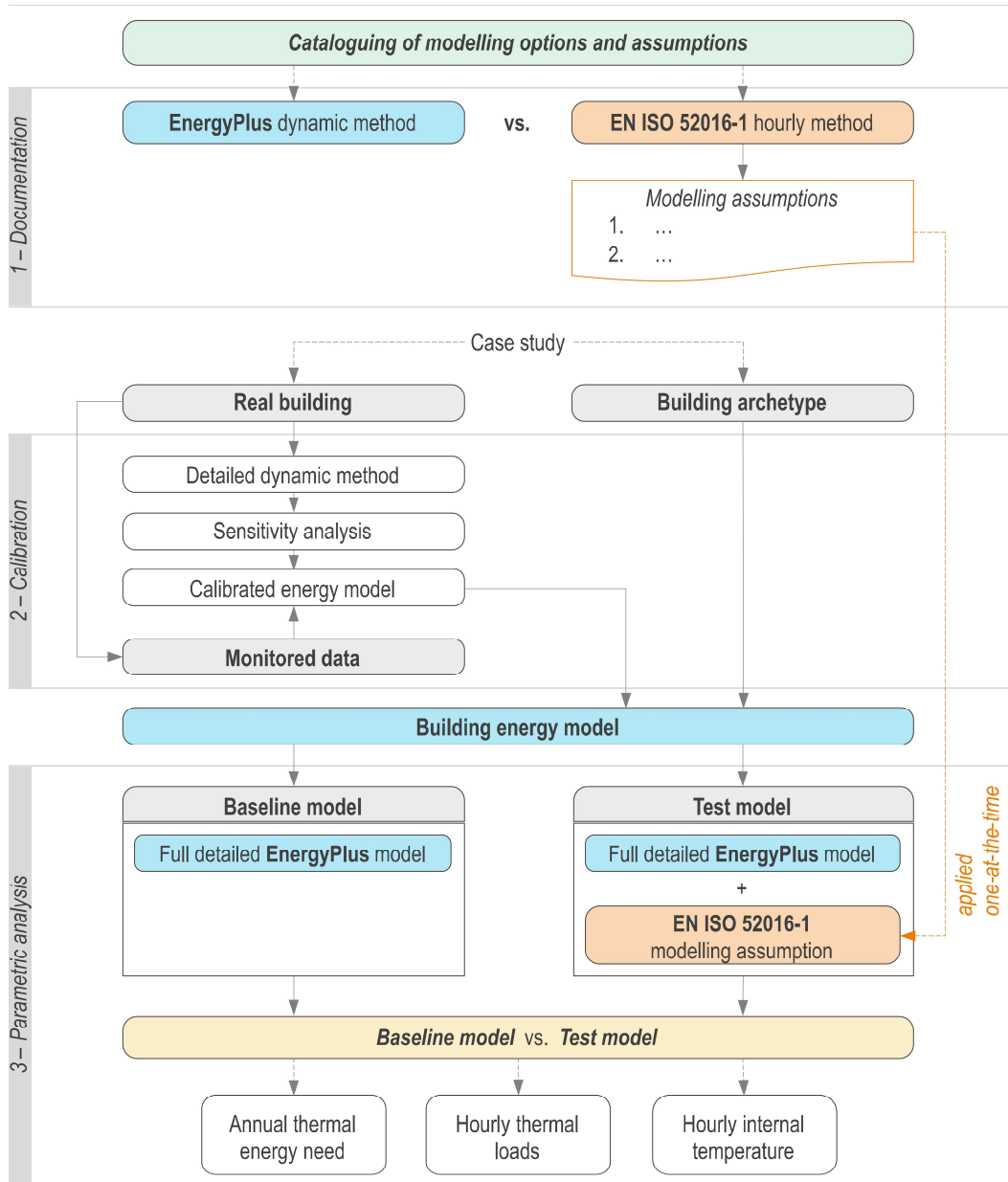
### **3.4 Aware validation approach**

As introduced, the proposed *aware validation* approach is aimed at assessing the accuracy of the modelling options implemented in the simplified EN ISO 52016-1 hourly method. It consists in four different steps (Figure 4); a first theoretical phase, and three applicative steps.

As a comparative testing approach, the proposed one is based on the comparison of the test model to a reference model, which should be a fully validated model [51], or at least more detailed than the tested one [50]. In the present thesis, the full detailed dynamic method of EnergyPlus [92], validated in several research such as [5,6], was assumed as the reference model.

#### *Step 1 – Modelling assumption comparison and documentation*

In the first step, the modelling assumptions of the EN ISO 52016-1 hourly method are compared to the ones of the reference model of EnergyPlus. This theoretical step is of crucial importance; in fact, through the robust knowledge of the differences in the solving algorithms, or modelling assumptions, it is possible to catch the causes of the discrepancies between the two models.

Figure 4: *Aware validation approach workflow*

To facilitate the research goals, the applicative steps of the *aware validation* approach are applied to different case studies. Since the investigated modelling assumptions may influence the accuracy of a simulation depending on the building being analysed [48], different building categories, levels of thermal insulation of the building envelope and weather conditions are considered to guarantee a general validity of the outcomes. Specifically, the case studies considered in the present dissertation include both real buildings and building archetypes. If real buildings are considered, the key phase of the proposed approach (parametric analysis) is



preceded by a calibration phase, in which the building energy model is calibrated against monitored data.

#### *Step 2 – Building energy model calibration*

The second phase of the *aware validation* approach consists in a manual calibration of the parameters describing the building fabric of the considered real building case studies. It is aimed at minimizing the discrepancies between the results of the simulations and the monitored data. Since the proposed approach is focused on the modelling of the building fabric, the considered monitored data mainly regards the indoor air temperatures, or the building envelope components surface temperatures and heat flow densities.

The applied calibration methodology firstly consists in the creation of the case study energy model by means of the detailed dynamic method of EnergyPlus, starting from the available data. To the case study energy model is then applied a sensitivity analysis to the main building envelope and user behaviour parameters, which are varied one-at-the-time, to identify the most influencing parameters on the results of the simulations. The considered parameters may vary depending on the considered case study, according to its specific characteristics. Following the sensitivity analysis, the most influential parameters are combined and adjusted to reach the calibration target. The accuracy of the calibration is verified by means of different statistical indices, according to the considered monitored data.

#### *Step 3 – Parametric analysis*

In the last phase, an energy model is firstly created by means of the detailed dynamic model of EnergyPlus for the considered case study (calibrated energy model if a real building is considered); this model is referred as “baseline model”. The EN ISO 52016-1 modelling assumptions are then implemented one-at-the-time in the baseline model, thus creating the “test model”. In this way, an overall input equivalence between the baseline and the test model is achieved since the only difference between them is related to the tested modelling option. On the practical side, the implementation of the modelling assumptions to be tested may vary according to the simplifications their self and to the capabilities of the assumed reference model. In the present dissertation, the implementation of the tested modelling assumptions in EnergyPlus was carried out in three different ways, characterised by different levels of expertise required:

1. By overwriting specific parameters within the EnergyPlus file (.idf file), when allowed by the tool. Generally, the considered parameters were overwritten by means of the Python’s pyEp [94] external interface of EnergyPlus, which

- allows to exploit the computational capabilities of Python to allocate either constant or calculated (by means of customised equations) variable's values,
2. By developing specific workaround and modelling strategies (generally, by means of pyEp), as to correctly model the considered simplifications, and
  3. By modifying the EnergyPlus's source code, for those modelling assumptions for which appropriate modelling strategies and workarounds could not be developed.

The implementation of the specific modelling assumptions, the modelling strategies applied, as well as the required modifications to the source code, are thoroughly described in Chapter 5 for the specific applications considered; the specifications related to the modified source code are instead presented in Annex A.

The effect of the modelling assumptions is assessed as the variation in the accuracy of dynamic model due to the implementation of each simplification. This variation is evaluated for two different situations. Firstly, the variation in the annual sensible energy needs for heating and cooling is assessed for each test model, in comparison with the baseline model. Secondly, the errors in the prediction of the indoor operative temperatures, as well as surface temperatures and heat fluxes, are evaluated in a free-floating situation. The numerical assessment of the accuracy of the model is performed by means of different statistical indexes, according to the evaluated quantity.

The procedure presented is applied separately for each tested modelling option.

### 3.5 Discussion and conclusion

The present chapter presented a novel validation approach for the building energy performance calculation methods. The novelty and advantages of the proposed approach lies in two main issues that are here presented.

Firstly, the fundamental of the *aware validation* approach is a robust and detailed knowledge of the differences between the model to be validated and the reference model, achieved through the *comparison map*. Moreover, the documentation phase was also aimed at (i) increasing the knowledge in the use of the dynamic simulation, by making the users aware of the modelling assumptions implemented in the used calculation models and their effect, or by guiding them in the choice of this or another modelling options, and at (ii) providing the developers of a well-documented set of implementation options for choosing the ones that allow to guarantee the expected model requirements.

Moreover, the proposed validation approach differs from the existing comparative testing methods in an attempt of overcoming their underlined limitations and of exploiting the potentiality of the single-process validation

approach. In particular, the uncertainties due to input inconsistencies were minimised, thus enabling to emphasize only the inaccuracies related to the modelling assumptions; moreover, the *aware validation* approach gives the change to analyse the effect of single modules of the calculation method (e.g., solution algorithms, modelling assumptions, etc.) on the overall building thermal behaviour.

Finally, pursuing the conceptual issues mentioned by Bloomfield in [51], the proposed approach tries to answer to the question: “Is it good enough for [*whatever purpose*]?” . In fact, it also allows to determine the expected accuracy and limitation of the tested model for different purposes and applications [95], such as energy performance evaluations or the energy requirements compliance check, or the energy audits or the thermal comfort evaluations.

On the other hand, the main limitations of the *aware validation* approach concern two aspects. Firstly, it requires a high level of expertise for its correct application; in fact, it is intended and appropriate for qualified figures (academic and professional) with an advanced knowledge of building physics, who are interested in either validating (or implementing) an existing calculation method or developing a new (simplified) calculation procedure. Even if applied for the presented purposes, the proposed approach moreover requires a multidisciplinary knowledge. In fact, the implementation of the modelling assumptions to be tested may not be straightforward, and the development of specific modelling strategies and workarounds may be necessary for their correct application. Thus, a thorough knowledge of the simulation tool assumed as reference model is required, as well as a (basic) computer programming knowledge, for eventual modifications of the simulation tool’s source code. Besides the complexity of the proposed approach, the specific application of the proposed approach may vary according to either the tested simplifications or the reference model, making it not easily reproducible.

## Chapter 4

# Cataloguing of modelling options and assumptions

### 4.1 Introduction

The proposed validation approach, presented in Chapter 3, consists in a first cataloguing phase in which the existing modelling options, assumptions, and simplification applied in dynamic calculation models are documented and classify. In order to increase the user awareness in the use of dynamic simulation, such a cataloguing is of crucial importance; in fact, it allows to provide the user with the modelling assumptions and simplification implemented in a given calculation model, or to guide them in the choice of a modelling strategy rather than another.

The results of the cataloguing of the existing modelling options and assumptions are presented in this Chapter. As introduced in Section 3.3, the built environment was firstly decomposed into its characteristic components, and the components interaction was then analysed by means of the *comparison map* tool. Since the built environment is a very elaborate system, general assumptions are commonly adopted in most calculation methods. Starting from these premises, the presented documentation includes the modelling options and assumptions that are consistent with the commonly adopted simplifications.

In Section 4.2, the common assumptions in building energy modelling are presented, while in Section 4.3 the *comparison map* is presented, and the documented modelling assumptions are analysed.

## 4.2 Common assumptions in building energy simulation

Building energy performance simulation is considered as an attempt to replicate the reality [96]. However, the building is a very elaborate system that needs to be simplified to reduce the complexity of the simulated processes and the computational effort; thus, certain modelling assumptions have been considered as reasonable and appropriate by building physics researchers and practitioners [97]. During the last decades, these simplifications have been tested to prove their suitability for a wide range of conditions, and finally were also included in technical standards, such as the EN ISO 52017-1 [20] which provides the guidelines for calculation procedures under transient conditions.

Therefore, the built environment is commonly modelled by assuming the simplifications summarised in Table 4; however, the use of other approaches going beyond these assumptions, or even more simplified models, for specific purposes or for modelling complex building systems is not excluded.

Table 4: General modelling simplifications

System	Modelling assumption
<i>Zone air</i>	<ul style="list-style-type: none"> <li>» Uniform through the building zone</li> <li>» Transparent to longwave radiation</li> </ul>
<i>Envelope component surfaces</i>	<ul style="list-style-type: none"> <li>» Isothermal</li> <li>» Uniform radiative properties</li> <li>» Diffuse emission and reflection</li> <li>» Act like grey bodies (Kirchhoff's law)</li> </ul>
<i>Transparent component surfaces</i>	<ul style="list-style-type: none"> <li>» No heat storage</li> </ul>
<i>Envelope components</i>	<ul style="list-style-type: none"> <li>» Perpendicular and one-dimensional heat flow</li> </ul>
<i>Sky hemisphere</i>	<ul style="list-style-type: none"> <li>» Isotropic behaviour (for longwave radiation exchange)</li> </ul>
<i>Foreground</i>	<ul style="list-style-type: none"> <li>» Homogeneous</li> <li>» Isotropic reflection process</li> </ul>

The fundamental assumption for heat balance calculation methods is the modelling of zone air as well mixed (or well-stirred), meaning that the zone air temperature is considered uniform through the building zone, and it is modelled as a single control volume (one capacitive node) [98]. Although this assumption proved to be reasonable and valid over a wide range of conditions [97,98], in the last years several researches focused on developing room air models with increasing levels of detail and accuracy, proposing both nodal [99–101] or zonal models [98], or Computational Fluid Dynamics (CFD) models. Moreover, zone air is also assumed to be completely transparent to longwave radiation, and thus it does not participate in the longwave exchange between internal surfaces [92,97,102].

Besides the modelling simplifications applied to the zone air, other assumptions are commonly applied to the building envelope components' surfaces. Firstly, the internal and external surfaces are considered uniform considering both temperatures (i.e., isothermal), heat fluxes, and radiative properties. More detailed approaches

suggest to subdivide the surfaces into patches (or meshes), for which temperatures and irradiances are simulated; those approaches are mainly adopted in studies concerning solar distribution on internal surfaces [103,104], and in daylight applications [105]. Other approaches consisting in the calculation of temperature gradients over the surfaces, instead, were developed, for example, for the evaluation of glass thermal stress [106].

Moreover, building envelope component surfaces are generally considered as grey bodies absorbing and emitting radiation independently from both wavelength and direction, and hence their radiative properties (transmittance, absorptance, and reflectance). Furthermore, the thermal emissivity of the surfaces is assumed to be equal to the absorption coefficient (Kirchhoff's law). Finally, the surfaces are assumed to diffusely reflect thermal and solar radiation.

Regarding the transparent envelope components, they are thin enough [107] that the heat storage in the various planes of a glazed element can be neglected [5,20,92].

Perpendicular and one-dimensional heat flows due to heat conduction is generally assumed in a wide range of applications; however, the modelling of two- or tri-dimensional heat conduction effects is considered for heat conduction to the ground [108], for thermal bridges evaluations [109], or to consider space varying boundary conditions at building component surfaces [110].

Although not reported in [20], other modelling assumptions concerning the outdoor environment were documented. An isotropic behaviour of the sky vault is generally adopted regarding the longwave radiation exchange. In fact, an uniform intensity of the atmospheric radiation is assumed over the sky vault (isotropic behaviour), and, consequently, the apparent sky temperature [111] usually applied in longwave heat fluxes calculations. However, in a few research a varying intensity of atmospheric radiation due to variation in the relative depth of water vapour over the sky vault is considered [112], or formula for atmospheric radiation at various angles above the horizon are suggested [113]. On the other hand, both isotropic and anisotropic models are widely adopted for the definition of diffuse solar radiation emission from the sky vault.

Furthermore, an isotropic ground reflection process is commonly assumed, meaning that a constant radiance originates from every point of the ground [114], including both longwave and shortwave irradiances (purely diffuse ground reflectance [115]). However, anisotropic approaches have been proposed in different studies, such as [116] and [117]. These mainly concerned an appropriate modelling of the ground albedo (ground reflection coefficient), considering its daily variation for departure of the isotropy simplification, or changes in ground

properties [115]. In this sense, a “semi-anisotropic” behaviour is considered in EnergyPlus [107] in which the ground albedo varies on a monthly basis (user defined parameter). Moreover, a homogeneous foreground is generally assumed, meaning that no variation in materials, colours, and temperatures, is considered.

Starting from these premises, the review in Section 4.3 analyses the modelling options and assumptions that are consistent with the commonly adopted simplifications.

### 4.3 Comparison map

As introduced in Section 3.3, the *comparison map* is a “component vs. component” array representing the interactions between the built environment’s components. The *comparison map* is presented in Figure 5.

The grey-filled elements of the array represent the interaction between a couple of components; moreover, in each filled element, identification initials representing the physical processes involved in the interaction between the two components is reported as well. The identified phenomena include longwave radiation (LW), shortwave radiation (SW), heat convection (CV), heat conduction and storage (CD), heat storage (HS), heat production (HP), mass production (MP), and mass transfer (MT). Within this dissertation, the components interaction highlighted in Figure 5 (dark grey filled elements) were analysed, and the simplifications relative to the modelling of the component interactions (i.e., modelling options, driving forces, and calculation parameters) were deepened. For the sake of clarity, the analysed components interactions were grouped by physical phenomenon, and the related modelling assumptions were summarised in different tables. In particular, they were grouped into the following groups:

1. External longwave radiation heat transfer (Section 4.3.1, Table 5),
2. External shortwave radiation heat transfer (Section 4.3.2, Table 6),
3. External heat convection (Section 4.3.3, Table 7),
4. Solar transmission (Section 4.3.4, Table 8),
5. Heat conduction and storage (Section 4.3.5, Table 9),
6. Internal longwave radiation heat transfer (Section 4.3.6, Table 10),
7. Internal shortwave radiation heat transfer (Section 4.3.7, Table 11),
8. Internal heat convection (Section 4.3.8, Table 12),
9. Heat storage (Section 4.3.9).

			Indoor environment					Opaque envelope							Transparent envelope										Outdoor environment											
			Air	Furnitures	HVAC terminal units	Internal sources	Thermal mass	External components			Internal partitions		Adjacent to ground		Therma bridges	Holes	Glass			Frame/Divider			Shading device		Therma bridges	Air	Sky vault	Sun	Ground	Objects at air temperature	Objects at different temperature					
								Inside surface	Construction	Outdoor surface	Inside surface	Construction	Inside surface	Construction			Inside surface	Construction	Inside surface	Construction	Outdoor surface	Inside surface	Construction	Outdoor surface								Inside surface	Construction	Outdoor surface	Shading layer	Air gap
Indoor environment	Air			CV	CV HP MP	CV HP MP	HS	CV				CV			CV			MT MP	CV				CV	MT	MT		CV			MT	SW	SW	SW			
	Furniture		CV			SW LW	SW LW		LW				LW		LW				LW				LW							SW	SW	SW				
	HVAC terminal units		CV HP MP	SW LW					SW LW			SW LW			SW LW				SW LW				SW LW				SW LW									
	Internal heat sources		CV HP MP	SW LW			SW LW	SW LW			SW LW			SW LW					SW LW				SW LW			SW										
	Internal thermal mass		HS				SW LW																													
Opaque envelope	External component	Inside surface		CV	LW	SW LW	SW LW		LW	CD			LW			LW			LW				LW													
		Construction	Solid layer							CD	CD	CV LW	CD					CD										CD								
			Air layer									CV LW																								
			Outdoor surface									CD		LW										LW			LW	LW			CV	LW	SW	SW	SW	LW
	Internal partitions	Surfaces		CV	LW	SW LW	SW LW		LW				LW	CD		LW			LW				LW			LW										
		Construction	Solid layer											CD	CD	CV LW			CD										CD							
			Air layer												CV LW																					
	Adjacent to ground	Inside surface		CV	LW	SW LW	SW LW		LW				LW			CD							LW			LW										
		Construction	Solid layer													CD	CD	CV LW	CD										CD							
			Air layer													CV LW																				
			Thermal bridges									CD				CD			CD					CD												
Transparent envelope	Holes		MT																										MT							
	Glass	Inside surface		CV	LW	SW LW	SW LW		LW				LW			LW			LW	CD			LW			LW	CV LW									
		Construction	Solid layer																	CD	CD	CV LW	CD						CD							
			Air layer																		CV															
			Outdoor surface											LW								CV									CV	LW	SW	LW	SW	LW
	Frame/Divider	Inside surface		CV	LW	SW LW	SW LW		LW				LW			LW			LW				LW	CD			LW	CV LW								
		Construction	Solid layer		MT															CD	CD	CV LW	CD						CD	MT						
			Air layer		MT																				CV						MT					
	Shading device	Outdoor surface											LW											LW			LW	CV LW			CV	LW	SW	LW	SW	LW
		Shading layer		CV	LW	SW LW	SW		LW		LW	LW			LW				LW			LW	LW			LW				CV	LW	SW	SW	SW	LW	SW
Air gap																	CV LW				CV LW	CV LW			CV LW											
Thermal bridges									CD				CD			CD							CD													
Outdoor environment	Air		MT								CV					MT				CV		MT	MT	CV	CV							CV		CV		
	Sky vault		SW	SW							LW	SW								LW	SW			LW	SW	LW	SW				LW	SW	LW	SW	SW	
	Sun		SW	SW							SW									SW	LW			SW	LW	SW	LW				SW	SW	SW			
	Ground		SW	SW							SW	LW									SW	LW			SW	LW	SW	LW		CV	LW	SW	SW		LW	
	Objects at air temperature										SW	LW									SW	LW			SW	LW	SW	LW			LW	SW	SW			
	Objects at different temperature										SW	LW									SW	LW			SW	LW	SW	LW		CV	LW	SW	SW	SW		

Figure 5: Comparison map



The tables (from Table 5 to Table 12) in which the modelling assumptions are summarised are organised as follows. Firstly, they are divided for each component interactions; then, for each interaction, in the first column, the existing modelling options documented to describe the involved phenomenon are reported from the most accurate to the simplest one (and named with a specific identification name). In the second and third columns, the assumptions and simplifications related to the definition of the involved driving forces and calculation parameters are respectively reported. For both driving forces and calculation parameters, their temporal discretisation (in column named *T.D.*) is indicated as well; in particular, it is specified whether if they vary (indicated as *v*) or are kept constant (indicated as *c*) during the simulation period. Furthermore, since the determination of the driving forces and calculation parameters may depend on the modelling option adopted to describe the analysed phenomenon, an indication of the related model is given (in column named *Model*) referring to the identification name given to the modelling options.

### **4.3.1 External longwave radiation heat transfer**

Longwave radiation heat exchange between the outdoor surfaces and the environment is treated as a surface-to-surface phenomenon [112], determined as the difference between the radiation emitted by the considered surface and that emitted by the objects composing the outdoor environment. These are characterised by various temperatures, which are generally unpredictable [118], thus it is reasonable to split the external longwave heat transfer into the heat exchanged with the following components:

1. the sky vault (Section 4.3.1.1),
2. the foreground (Section 4.3.1.2),
3. other objects assumed at the external air temperature (Section 4.3.1.3), and
4. other objects at specific temperatures (Section 4.3.1.4).

The interaction between an external surface and each of the components listed above is analysed in the following sections, and the related modelling assumptions are highlighted and summarised in Table 5.

#### **4.3.1.1 Outdoor surfaces vs. sky vault**

##### *Modelling of the phenomenon*

The documented approaches for the modelling of the longwave radiation heat exchange between an external building envelope surface and the sky vault can belong to two categories with different level of accuracy. The most accurate approach employs the Stefan-Boltzmann's law, while its linearisation is used in

simplified calculation models. The two documented approaches are here presented (named as in Table 5).

- a) **Stefan-Boltzmann's (SB) law**: in this approach, the net heat exchange between the surface and the sky vault ( $q_{\text{LW,ext,sky}}$ , in  $\text{W}\cdot\text{m}^{-2}$ ) is calculated as presented in Equation (1),

$$q_{\text{LW,ext,sky}} = F_{\text{sky}} \cdot \varepsilon \cdot \sigma \cdot (T_{\text{surf,ext}}^4 - T_{\text{sky}}^4) \quad (1)$$

where  $F_{\text{sky}}$  is the view factor to the sky vault,  $\varepsilon$  is the thermal emissivity of the surface (equal to the thermal absorption for the Kirchhoff law),  $\sigma$  is the Stefan-Boltzmann constant ( $5,67 \cdot 10^{-8} \text{ W}\cdot\text{m}^{-2}\cdot\text{K}^{-4}$ ), and  $T_{\text{surf,ext}}$  and  $T_{\text{sky}}$  are the external surface temperature and the so called apparent (or equivalent) sky vault temperature (in K). The latter, which will be deepened later in the text, was introduced to provide a practical approach to calculate this heat exchange [119,120],

- b) **Linearised SB's law**: according to [121], the outside longwave radiation component has been simplified by many researchers, considering either simplified modelling strategies or a simplified determination of driving forces and calculation parameters. In fact, the Stefan-Boltzmann law is generally reduced to its simple linear expression [112] in a wide range of applications. Following this approach, the longwave radiation exchange ( $q_{\text{LW,ext,sky}}$ , in  $\text{W}\cdot\text{m}^{-2}$ ) between the outdoor surfaces and the sky vault is calculated by introducing the radiant heat transfer coefficient, as in Equation (2),

$$q_{\text{LW,ext,sky}} = F_{\text{sky}} \cdot h_{\text{r,ext,sky}} \cdot (\theta_{\text{surf,ext}} - \theta_{\text{sky}}) \quad (2)$$

where  $F_{\text{sky}}$  is the view factor to the sky vault,  $h_{\text{r,ext,sky}}$  is the radiant heat transfer coefficient (in  $\text{W}\cdot\text{m}^{-2}\cdot\text{K}^{-1}$ ), and  $\theta_{\text{surf,ext}}$  and  $\theta_{\text{sky}}$  are the surface and the apparent sky temperatures ( $^{\circ}\text{C}$  or K), respectively. This approach does not consider the nonlinearity of the phenomenon, but it prevents from the need of iterative predictor-corrector approaches for calculating the longwave heat transfer due to the fourth power temperature relationship [122], which requires an high computational effort, especially if a large number of surfaces are considered [122]. However, the impact of a linearised longwave heat transfer approach on the building thermal behaviour and energy needs has not been determined yet. Different versions of the linearised longwave heat transfer approach were documented.

- b.1) *Component separately modelled*: following this approach, the heat flux exchanged between the surface and the sky vault is calculated separately

from the other components of the outdoor environment, and the net heat flux is calculated as in Equation (2),

- b.2) *Extra-thermal radiation to sky approach*: in this approach, the outdoor environment is assumed to be at the outdoor air temperature, and the extra-thermal radiation to sky is introduced to consider the different temperature of the sky vault. Hence, the extra-thermal radiation to sky ( $q_{LW,ext,air-sky}$ , in  $W \cdot m^{-2}$ ) models the heat flux exchanged between the outdoor environment (at air temperature) and the sky vault (at its specific temperature), and it can be calculated according to Equation (3),

$$q_{LW,ext,air-sky} = F_{sky} \cdot h_{r,ext} \cdot (\theta_{air,ext} - \theta_{sky}) \quad (3)$$

where  $h_{r,ext}$  is the radiant heat transfer coefficient (in  $W \cdot m^{-2}K^{-1}$ ) between the surface and the outdoor environment at air temperature. Reasonably, the  $h_r$  may be also referred specifically to the interaction between the outdoor air and the sky vault; however, any reference was documented to support this assumption.

The extra-thermal radiation to sky approach is applied in the simplified dynamic method of EN ISO 52016-1 [5], and in both the detailed and simplified hourly method of EN ISO 13790 [10],

- b.3) *Precalculated extra-thermal radiation to sky*: in this approach, a precalculated value for the extra-thermal radiation is assumed. This approach is implemented in the DOE-2 calculation method [123]; since presence of clouds effects the thermal radiation coming from sky, and thus its effective temperature [119], the calculation method assumes two different values for clear ( $63,1 W \cdot m^{-2}$ ) and overcast sky conditions (is assumed that no sky radiation exchange occurs). Under partly cloudy skies, the extra-thermal radiation to sky is calculated as a linear interpolation between the two extreme conditions, according to the level of cloud sky cover. Differently from the approaches previously presented in which the heat exchange is driven by the temperature difference between the sky and the surface (or external air), the constraint in this approach is a parameter accounting for the cloud cover of sky,
- b.4) *Aggregated with heat convection*: in simplified models, the combination of heat convection and longwave radiation heat transfer has been generally adopted [118], including all components of the outdoor environment. In this approach, an overall external heat transfer coefficient is employed ( $h_{ext}$ ), such as in the BLAST simple model [124].

The driving forces, boundary conditions, and calculation parameters employed in modelling options presented are analysed in the following paragraphs.

#### *Driving forces*

The main driving force involved in the longwave radiation heat exchange between an external surface and the sky vault is the sky temperature. As introduced, the sky temperature is generally introduced for practical issues [120]; it can be derived by means of different approaches, including empirical methods, radiation charts, and computer program models [119,125]. The radiation chart approach consists in calculating monthly sky temperature in charts formats [112,125], while detailed atmospheric constituents are used in the latter approach to estimate the sky vault temperature. Empirical models, instead, are based on measured data, and are generally preferred and more used [120].

Generally, the empirical models for the calculation of the sky vault temperature are classified into two categories, namely sky emissivity and direct models. The use of correlations belonging to the first group entails to assume that the atmosphere acts like a grey body characterised by a specific thermal emissivity. According to this assumption, the sky temperature is derived from the emissivity of the sky ( $\varepsilon_{\text{sky}}$ ) by means of Equation (4),

$$T_{\text{sky}} = \varepsilon_{\text{sky}}^{0,25} \cdot T_{\text{air}} \quad (4)$$

where  $T_{\text{sky}}$  and  $T_{\text{air}}$  are the absolute sky vault and outdoor air temperature (in K), respectively. In the second group, instead, are included the correlations that assumes the black body assumptions for the atmosphere; therefore, the sky vault can be described by means of an effective temperature, that is directly derived by means of different correlations. Since the sky temperature is affected by the sky cloud cover, both sky emissivity and direct models provide different correlations for clear, overcast, and cloudy skies.

Around sixty different empirical correlations have been catalogued in the last twenty years in different researches. In 1998, Adelard et al. [126] reviewed ten different correlations including both sky emissivity models and direct models, and the Authors tested two direct models in comparison with a neural network approach to evaluate the difference in the estimation of the sky vault temperature for clear sky conditions during the day and the night. Algarni and Nutter [125,127] provided an extensive survey of sky temperature models, highlighting their applicability to calculate the sky longwave radiative exchange in buildings under various climate conditions. The three different sky emissivity correlations implemented in the calculation models of EnergyPlus, TRNSYS, and ESP-r were extensively deepened

by Zhang et al. [120], and their differences were highlighted compared to measured data for different locations and time periods. In 2019, Karn et al. [119] presented around thirty different sky emissivity models, highlighting both diurnal and nocturnal variation in sky temperature, as well as seasonal disparities. Finally, Evangelisti et al. [111] classified and described around forty correlations, including both sky emissivity, direct, and computer (or detailed) models. The simplified direct correlations suggested in the European standardisation (e.g., ISO 13790 [10], and EN ISO 52016-1 [5]) was firstly surveyed in [111], and were used as a comparison to assess the influence of different selected correlations on building annual energy needs for various significant locations all over the world.

Beside the effect of a chosen sky temperature correlation on the building energy performance, which was evaluated for some algorithms in the previously presented works, the choice of a correlation may also influence the complexity of the calculation by increasing the computational time or requiring complex, or difficulty available, input data. Generally, the existing sky temperature correlations depends on traditional weather data, such as the outdoor environment temperature, and relative or absolute humidity, or on easily derivable data, such as the dew-point temperature, and water vapour partial pressure, accordingly to the considered correlation. However, most of the correlations to estimate both sky emissivity and temperature under cloudy sky conditions depends on a parameter accounting for the sky cloud cover, which can be defined in several ways according to the correlation, and it is generally difficult to obtain for both real (whose measurement can hardly be achieved objectively and, in particular, cannot be carried out by an automatic weather station [128]) or standard conditions (in weather data files). For example, this parameter is not available in the typical meteorological years used in Italy for standard evaluations [129], thus making unfeasible the application of cloudy sky temperature correlations.

Generally, most applications imply a variable sky temperature on a timestep basis, which can be either hourly or sub-hourly, accordingly to the time discretisation of the considered calculation model.

#### *Calculation parameters*

The calculation parameters on which the determination of the longwave radiation heat exchange between the outdoor surfaces and the sky vaults depend are the radiant heat transfer coefficient ( $h_r$ ), and the view factor to sky ( $F_{\text{sky}}$ ).

The introduction of the concept of radiant surface heat transfer coefficient is generally linked to the linearisation of the longwave heat transfer phenomenon (approach *b*). For consistency with linear terms of the surface heat balance, the radiant heat transfer coefficient may also be used even if the phenomenon is

described by means of the Stefan-Boltzmann law (approach *a*). In this case, the radiative coefficient is determined iteratively during the timestep by solving the fourth-power law; thus, this approach does not imply a linearisation of the phenomenon. This approach is used in the EnergyPlus dynamic model [107]; the radiative coefficient is variable on a timestep basis and it is calculated independently for each surface of the considered building.

If not used in this way (i.e., iteratively defined solving the forth power Stefan-Boltzmann law), the radiant heat transfer coefficient's introduction represents an over-simplification of the heat exchange process [112]. The radiative coefficient is generally calculated by means of an approximation of the Stefan-Boltzmann law [130–132], described through Equation (5),

$$h_r = 4 \cdot \varepsilon \cdot \sigma \cdot T_m^3 \quad (5)$$

where  $\varepsilon$  is the surface thermal emissivity,  $\sigma$  is the Stefan-Boltzmann constant ( $5,67 \cdot 10^{-8} \text{ W} \cdot \text{m}^{-2} \cdot \text{K}^{-4}$ ), and  $T_m$  is the mean thermodynamic temperature of the surface and of its radiative surrounding, for whose definition no specific indications can be found in literature, as stated by Cole in [112]. For this reason, the Author may assume that the  $T_m$  can be calculated considering the outdoor surface temperature and the considered outdoor environment component temperature (i.e., in this case, the sky vault); although this assumption may be considered feasible, any research was found in literature to support this assumption. On the other hand, a commonly adopted assumption considers the outdoor environment to radiate as a black body at air temperature [112], thus the  $T_m$  can be defined as the mean temperature of the surface and the outdoor air. Although this assumption is not representative of the real outdoor conditions [112], it is assumed in many different applications.

Following this approach, the linear radiant heat transfer coefficient can be assumed variable or constant over the simulation period. In the first case, the radiative coefficient is calculated by considering the temperatures at the previous timestep. Beside considering variable conditions in the determination of the  $h_r$ , this approach also allows to solve the issue related to its iterative definition [122]. Also in this case, the determination of the radiative coefficient is related to a single surface, since it is dependent on its specific temperature at the previous timestep.

Another common simplification consists in considering a constant value of the radiant heat transfer coefficient over the simulation period; this is the case, for example, of the dynamic method of TRNSYS, in which the radiant coefficients are determined considering initial simulation temperatures, but can also be updated during the simulation [133]. Reference conditions are instead used by the EN ISO

13789 technical standard [134]; in particular, the  $h_r$  is determined by means of Equation (5) assuming a reference surface emissivity equal to 0,9, and a mean thermodynamic temperature of the surface and of its radiative surrounding ( $T_m$ ) equal to 0 °C.

Finally, the radiant heat transfer can be treated together with heat convection; in this case, the radiative coefficient is determined as coupled with the convective heat transfer coefficient.

As regards the sky view factor, it is generally described as the fraction of the view from a base surface obstructed by a given other surface [122]; it is a purely geometry dependent parameter that can be calculated numerically or analytically [122,135]. Detailed calculation procedures for the determination of the view factor to sky are extensively analysed in urban building energy modelling (UBEM) applications. For example, Miao et al. [136] listed the existing methods used to calculate sky view factors in urban street canyons; however, the reviewed approaches generally calculate the view factor of a point on the ground, thus their application is not reasonable in external radiant heat transfer of building envelope components, at least for vertical surfaces (i.e., walls). In traditional building simulation application, the view factors are generally determined by means of geometrical models dependent on surface tilt angle. They can be derived from tabular values, which are generally defined using fixed surface tilt angles; for example, a sky view factor equal to 0,5 is assumed for vertical surfaces in EN ISO 52016-1 [5], while for horizontal surfaces it is assumed equal to 1. Tabular view factors are also used in ESP-r [93]. On the other hand, sky view factors can be calculated for specific tilt angles, thus for specific surfaces. The presence of obstructions for longwave radiation heat transfer is generally considered in the definition of view factors through an additional correction factor. For example, EnergyPlus calculates the view factor to sky for shaded surfaces considering a shading factor dependent on the sunlit area fraction of the surface (see Section 4.3.2.1); in TRNSYS, instead, to the reference value of 0,5 for vertical surfaces is subtracted the specific view factor to the considered obstructions (e.g., wingwall or overhang). External obstructions are instead not considered in the determination of the view factors to sky in standardised calculation methods, such as in the EN ISO 52016-1 [137].

#### **4.3.1.2 Outdoor surfaces vs. ground**

##### *Modelling of the phenomenon*

The existing strategies for modelling the longwave radiation heat transfer between an external surface and the ground are similar to the ones presented in

Section 4.3.1.1, as regards the heat exchange with the sky vault, with the exception of the extra-thermal radiation to sky approaches. In particular, two different approaches were documented, and presented below (named as in Table 5).

- a) **Stefan-Boltzmann's (SB) law**: in this approach, the net heat exchange between the surface and the sky vault is calculated by means of the fourth-power Stefan-Boltzmann law, as presented in Equation (1). The parameters used in Equation (1) are, in this case, referred to the ground; thus, they are the view factor to the ground ( $F_{\text{gnd}}$ ), and the foreground surface absolute temperature ( $T_{\text{gnd}}$ , in K),
- b) **Linearised SB law**: following this approach, the longwave radiation exchange between the outdoor surfaces and the foreground is calculated by introducing the radiant heat transfer coefficient, as presented in Equation (2). Also in this case, the radiant heat transfer coefficient is referred to the ground ( $h_{\text{r,ext,gnd}}$ , in  $\text{W}\cdot\text{m}^{-2}\cdot\text{K}^{-1}$ ), as well as the foreground temperature ( $\theta_{\text{gnd}}$ , in  $^{\circ}\text{C}$ ), respectively. Two different versions of the linearised longwave heat transfer approach were documented.
  - b.1) *Component separately modelled*: in this approach, the foreground is modelled separately from the others outdoor environment components (i.e., at its specific temperature),
  - b.2) *Aggregated with heat convection*: in simplified models the combination of heat convection and longwave radiation heat transfer has been generally adopted, as described in Section 4.3.1.1.

#### *Driving forces*

Different levels of detail in determining the ground surface temperature were found in literature. Firstly, the temperature can be derived from inner layers energy balance which can involve the use of detailed models for solving heat conduction through the ground. An improved approach to define the ground surface temperature was proposed by Evins et al. in [122], in which daily temperature variation is calculated considering convection, shortwave and longwave radiation and evaporation at the soil surface [92,122]. Moreover, as stated by the Authors, more detailed ground temperature models could be included in the longwave calculation.

Most applications, however, assumes the ground surface temperature at outdoor air temperature [5,92]. In this way, the ground is aggregated with the outdoor air; such an assumption can be applied in both nonlinear (approach *a*) and linear (approach *b*) modelling approaches. For example, EnergyPlus (which implements the approach *a*) generally assumes that the foreground is at air temperature [107]; such an assumption is assumed in the EN ISO 52016-1 hourly method [5] as well, which implements instead the linearised longwave heat transfer formulation



(approach *b*). Another common assumption is to consider the foreground at a sol-air temperature, thus considering the effect of solar radiation absorption and heat convection and longwave radiation [93,138]. Finally, the surface ground temperature may also be defined by the user, with a user-defined time discretisation.

If the foreground temperature is derived from ground energy balance or is considered equal to the air or the sol-air temperature, it is assumed to vary over the simulation period on a timestep basis. In TRNSYS [23], instead, the foreground temperature is assumed constant over the simulation period and it is calculated as an average value of the annual outdoor air temperature.

#### *Calculation parameters*

As for the heat exchange to the sky vault (Section 4.3.1.1), the considered calculation parameters are the radiant heat transfer coefficient, and the view factor to ground. If the approaches for the determination of the radiative coefficient are consistent with the one presented in Section 4.3.1.1, some differences can be instead found for the definition of the ground view factor. In fact, it can be calculated depending on the surface tilt angle by means of geometric methods, and it can be either calculated for specific or predefined angles (tabular view factors). However, differently from the determination of the sky view factors, there is no documentation in literature about the consideration the eventual shading from the longwave radiation emitted by the ground. A reference to this issue appears in the EnergyPlus Engineering Reference [107], in which it can be found that the software does not automatically calculates the shadowing from the ground, but user defined view factors accounting for the specific conditions can be used in the simulation. Finally, the view factor may also be included in the view factor to objects at air temperature (Section 4.3.1.3), if the ground is modelled together with outdoor air.

#### **4.3.1.3 Outdoor surfaces vs. objects at air temperature**

Generally, the longwave heat transfer process with other objects at the air temperature is referred as *longwave radiation to air*, even though the medium (i.e., outdoor air) it is assumed as not participating in the longwave heat transfer process [107]. For consistency with the literature on this phenomenon, it will be referred as *longwave radiation to air* in this dissertation as well.

As for the processes presented in Sections 4.3.1.1 and 4.3.1.2, the heat exchanged between an outdoor surface and the outdoor air can be modelled by means of the fourth power Stefan-Boltzmann law (approach *a* in Table 5) or by means of its linearisation (approach *b* in Table 5), and it depends on the outdoor air temperature (i.e., the driving force), the radiant heat transfer coefficient to air, and the view factor to air (i.e., the calculation parameters).

As regards the outdoor air temperature, a site air temperature can be assumed, or it can be corrected to accounts for variation in the air temperature due to the actual height from the ground of the considered surface [107].

The radiant heat transfer coefficient can be derived by applying the different approaches described in Section 4.3.1.1. As for the view factor to air, it can be derived from the view factor to sky (Section 4.3.1.1) [107], or tabular values can be used.

#### **4.3.1.4 Outdoor surfaces vs. objects at different temperature**

As for the processes presented previously, the heat exchanged between an outdoor surface and other surfaces at a specific temperature can be modelled by means of the fourth power Stefan-Boltzmann law (approach *a* in Table 5) or by means of its linearisation (approach *b* in Table 5), and it depends on the other objects surface temperature (i.e., the driving force), the radiant heat transfer coefficient, and the view factor (i.e., the calculation parameters).

As regards the other objects temperature, it can be derived from simplified energy balance on the other object surface [107], or it can be defined by the user, as suggested by Evins et al. in [122].

The radiant heat transfer coefficient can be derived by applying the different approaches described in Section 4.3.1.1; as for the view factor to other objects, it is generally calculated by means of geometric methods.

Table 5: External longwave heat transfer

Phenomenon modelling	Driving forces		Calculation parameters	
	Determination	T.D.	Determination	T.D.
<b>Outdoor surfaces vs. sky vault</b>				
<b>a. Stefan-Boltzmann (SB) law</b>	<b>Sky vault temperature</b>		<b>Radiative heat transfer coefficient</b>	
<b>b. Linearised SB law</b>	» Atmospheric sky emissivity models	$\nu$	» SB law (iterative determination) <sup>6</sup>	$\nu$
b.1. Component separated modelled	- Cloudy skies <sup>1</sup>	$a, b, 1, b, 2$	» Approximated SB law	$a, b$
b.2. Extra-thermal radiation to sky approach	- Clear skies <sup>2</sup>		- From previous timestep	$\nu$
b.3. Precalculated extra-thermal radiation to sky	» Direct models	$\nu$	- At initial temperature	$c$
b.4. Aggregated with heat convection	- Cloudy skies <sup>3</sup>	$a, b, 1, b, 2$	- At reference conditions	$c$
	- Clear skies <sup>4</sup>	$b, 4$	» Coupled with heat convection	$\nu, c$
	» Equal to air temperature			
	<b>Cloud cover index</b> <sup>5</sup>	$\nu$	<b>View factor to sky</b>	$b, 4$
			» Photographic method <sup>7</sup>	$c$
			» Geometric method	$c$
			- With obstruction	$a, b$
			- Without obstruction	$a, b$
			» Tabular	$c$
<b>Outdoor surfaces vs. ground</b>				
<b>a. Stefan-Boltzmann (SB) law</b>	<b>Ground surface temperature</b>		<b>Radiative heat transfer coefficient</b>	
<b>b. Linearised SB law</b>	» Derived from inner layers energy balance	$\nu$	» SB law (iterative determination) <sup>5</sup>	$\nu$
b.1. Component separated modelled	» Equal to sol-air temperature	$\nu$	» Approximated SB law	$a, b$
b.2. Aggregated with heat convection	» Equal to air temperature	$\nu$	- From previous timestep	$\nu$
	» User defined	$\nu, c$	- At initial temperature	$c$
			- At reference conditions	$c$
			» Coupled with heat convection	$\nu, c$
			<b>View factor to ground</b>	$b, 2$
			» Geometric method	$c$
			- With obstruction	$a, b$
			- Without obstruction	$a, b$
			» Tabular	$c$

**Notes**<sup>1</sup> Depending on clear sky emissivity ( $\epsilon_{clear}$ ), vapour partial pressure ( $P_v$ ), and/or sky cloudiness parameters (various), according to the considered correlation<sup>2</sup> Depending on dew point temperature ( $T_{dp}$ ), vapour partial pressure ( $P_v$ ), and/or outdoor ambient temperature ( $T_{amb}$ ), according to the considered correlation<sup>3</sup> Depending on outdoor ambient temperature ( $T_{amb}$ ), vapour partial pressure ( $P_v$ ), and/or sky cloudiness parameters (various), according to the considered correlation<sup>4</sup> Depending on outdoor ambient temperature ( $T_{amb}$ )<sup>5</sup> It is a weather data (input data)<sup>6</sup> Introduced for consistency with the other heat balance terms<sup>7</sup> Fish-eye photographs taken looking upwards towards the zenith [136], usually implemented in UBEMs

Table 5: External longwave heat transfer (continues)

Phenomenon modelling		Driving forces		Calculation parameters	
		Determination	T.D.	Determination	T.D.
Outdoor surfaces vs. objects at air temperature ("to air")					
<i>Air temperature</i>					
a. <i>Stefan-Boltzmann (SB) law</i>	» Local air temperature (at certain height) <sup>s</sup>	$\nu$	$a, b$	<b>Radiative heat transfer coefficient</b>	$\nu$
b. <i>Linearised SB law</i>	» Site air temperature	$\nu$	$a, b$	» SB law (iterative determination)	$a$
				» Approximated SB law	
				- From previous timestep	$\nu$
				- At initial temperature	$c$
				- At reference conditions	$c$
				» Coupled with heat convection	$\nu, c$
					$a, b$
<b>View factor to objects at air temperature</b>					
				» Derived from view factor to sky	$c$
				» Tabular	$a, b$
					$a, b$
Outdoor surfaces vs. objects at different temperature					
<b>Other objects surface temperature</b>					
a. <i>Stefan-Boltzmann (SB) law</i>	» Derived from energy balance (surface <i>U</i> -value)	$\nu$	$a, b$	<b>Radiative heat transfer coefficient</b>	$\nu$
b. <i>Linearised SB law</i>	» User defined			» SB law (iterative determination)	$a$
				» Approximated SB law	
				- From previous timestep	$\nu$
				- At initial temperature	$c$
				- At reference conditions	$c$
				» Coupled with heat convection	$\nu, c$
					$a, b$
<b>View factor to sky</b>					
	» Geometric method				$c$
					$a, b$

**Notes**

<sup>s</sup> Accounts for variation in the air temperature due to the actual height from the ground of the considered surface

### 4.3.2 External shortwave radiation heat transfer

The heat balance on an outdoor opaque surface includes, among all the considered terms, the absorbed solar radiation. The amount of absorbed solar radiation depends on the solar absorptance of the surface (assumed time-invariant and uniform over the surface) and on the incident solar radiation, which can be either beam, diffuse, or reflected.

In Section 4.3.2.1, the interaction between the outdoor opaque surfaces and the sun, responsible of beam solar radiation, is deepened (Table 6); the modelling of sky diffuse radiation is instead investigated in Section 4.3.2.2. The diffuse reflected solar radiation is studied in Section 4.3.2.3 and 4.3.2.4, respectively solar radiation reflected from the ground surface and from other outdoor objects (e.g., surrounding buildings, overhangs, etc.).

#### 4.3.2.1 Outdoor opaque surfaces vs. sun

##### *Modelling of the phenomenon*

The absorption of beam solar can be modelled following two different approaches, applied also in the modelling of absorbed diffuse (Section 4.3.2.2) and reflected solar irradiance (Sections 4.3.2.3 and 4.3.2.4), described below and named as in Table 6.

- a) **Absorbed solar irradiance as separate HB term:** firstly, the absorbed solar (shortwave) irradiance can be modelled as a separate surface heat balance term. Thus, the solar heat flux ( $q_{\text{sol,b}}$ , in  $\text{W}\cdot\text{m}^{-2}$ ) is calculated as reported in Equation (6),

$$q_{\text{sol,b}} = \alpha \cdot F_{\text{sh,b}} \cdot I_{\text{b}} \quad (6)$$

where  $\alpha$  is the surface solar absorption,  $F_{\text{sh,b}}$  is the shading reduction factor for beam solar irradiance, and  $I_{\text{b}}$  is the incident beam irradiance on the surface (in  $\text{W}\cdot\text{m}^{-2}$ ),

- b) **Sol-air temperature approach (global solar irradiance):** alternatively, the effect of the absorbed solar irradiance can be modelled by means of the sol-air temperature, generally defined as the outside air temperature which, in the absence of solar radiation, would give the same temperature trend inside the component, as well as the heat transfer rate, as in reality (i.e., in presence of solar radiation) [139]. The sol-air temperature accounts for a combined effect of the actual outdoor temperature distribution and the incident solar radiation; for this reason, this modelling approach assumes a coupling of the absorption

of the global solar irradiation (beam, diffuse, and reflected) with the thermal processes of heat convection and longwave radiation.

#### *Driving forces*

The sole driving force involved in the interaction between an opaque outdoor surface and the sun is the incident beam solar irradiance on the considered surface, which is commonly derived from the horizontal beam solar irradiance through transposition models. These are purely geometrical models [114] that accounts for the cosine effect for the incidence angle of sun rays on a considered surface. Following these transposition models, the incident beam solar irradiance ( $I_b$ , in  $\text{W}\cdot\text{m}^{-2}$ ) on a given surface is calculated as in Equation (7),

$$I_b = R_b \cdot I_{b,h} = \frac{\cos\beta_i}{\cos\beta_z} \cdot I_{b,h} \quad (7)$$

where  $I_{b,h}$  is the horizontal beam solar irradiance (in  $\text{W}\cdot\text{m}^{-2}$ ), and  $R_b$  is the beam transposition factor, defined as the ratio between the incidence angle ( $\beta_i$ ) cosine and the solar azimuth angle ( $\beta_z$ ) cosine. The horizontal beam solar irradiance ( $I_{b,h}$ ) can be calculated through atmosphere transmittance or decomposition models [140], which are here briefly described. In the former models, the wavelength averaged  $I_{b,h}$  is derived from the extraterrestrial irradiance by means of atmosphere transmittance, accounting for different extinction process. In decomposition models, instead, the determination of the horizontal beam solar irradiance depends on a correction factor that represents the fraction between beam and global horizontal solar irradiance. Different empirical correlation can be found in literature for the determination of this correction factor, including univariate [141,142], bivariate [143], and multivariate models [144], all dependent on the clearness index of the atmosphere (i.e., the ratio of the measured global solar radiation at the ground surface to the extra-terrestrial solar radiation [145]). For more specific details as concern the determination of horizontal beam solar irradiance the reader should refer to the research of Lam and Li [146], Gueymard [147], Bird [148], and Perez et al. [144].

The incident beam solar irradiance, together with the diffuse and reflected irradiance, is required also for the determination of the sol-air temperature. This, defined in [139], can be calculated considering the longwave radiation loss [139], or just the effect of solar absorption and heat convection [149].

#### *Calculation parameters*

The shading reduction factor for beam solar irradiance is the only calculation parameter required for determining the amount of absorbed irradiance, beside the

solar absorption coefficient. It is commonly referred as sunlit fraction, and it is defined as the fraction of a given surface which is irradiated by the sun. The sunlit fraction can be estimated through ray tracing, pixel counting, and geometric methods. The former approach works by shooting parallel rays from a planar grid, and by computing the ratio of respawned rays from the considered surface [150]. An image processing technique [151] is instead employed in pixel counting methods to assess the sunlit fraction. Finally, geometric methods (such as polygon clipping [152] and shadow projection method [153]) consist in the determination of the instantaneous shadow shapes cast on the considered surface [154]. While ray tracing and pixel counting methods can account for complex boundary conditions (e.g., surrounding buildings, vegetation, etc.), geometric approaches are generally limited to simple objects and geometries [153,155], such as overhangs or side fins, and neglect the shadowing from far obstacles, which is instead considered in the geometric method developed by Cascone et al. [155].

#### 4.3.2.2 Outdoor opaque surfaces vs. sky vault

##### *Modelling of the phenomenon*

As introduced in Section 4.3.2.1, the options for modelling the absorption of diffuse solar radiation are consistent with the ones described for beam solar radiation, i.e., modelled as a separate surface heat balance term, or by means of the sol-air temperature.

- a) ***Absorbed solar irradiance as separate HB term***: the application of this former approach depends on the assumed sky model. In fact, due to the high variability over the hemisphere [156], diffuse irradiance distribution requires the use of simplifying assumptions to be correctly modelled; according to the assumed simplification, the sky vault behaviour can be classified as isotropic or anisotropic. Accordingly, the determination of the incidence diffuse solar radiation follows different approaches which are described below (named as in Table 6).
  - a.1) ***Anisotropic radiance distribution***: studies on clear skies have recognised a strong anisotropy in the diffuse solar irradiance distribution over the sky vault [156]. Thus, many research have presented models that consider the anisotropic nature of the hemisphere, and describe the diffuse solar irradiance as composed of three different terms. The reference model is the one proposed by Perez et al. [157], which splits the diffuse irradiance into a sky dome component, a circumsolar brightening component (i.e., concentrated in an area close to the sun,

resulting from solar radiation scattering), and an horizon brightening components (i.e., concentrated in a band near the horizon).

Although the anisotropic sky models do not incorporate all the structures of the radiance distribution [156], they represent an improvement over the simplest uniform radiance distribution. Assuming an anisotropic sky vault behaviour, and its decomposition into the components proposed in [157], the absorbed diffuse solar radiation ( $q_{\text{sol,d}}$ , in  $\text{W}\cdot\text{m}^{-2}$ ) on the outdoor surface of the opaque building envelope is calculated as in Equation (8),

$$q_{\text{sol,d}} = \alpha \cdot \left( F_{\text{sh,d,dome}} \cdot I_{\text{d,dome}} + F_{\text{sh,d,cir}} \cdot I_{\text{d,cir}} + F_{\text{sh,d,hor}} \cdot I_{\text{d,hor}} \right) \quad (8)$$

where  $I_{\text{d,dome}}$ ,  $I_{\text{d,cir}}$ , and  $I_{\text{d,hor}}$  are the diffuse irradiances (in  $\text{W}\cdot\text{m}^{-2}$ ) coming from the sky dome, the circumsolar brightening, and the horizon brightening, respectively, and  $F_{\text{sh,d,dome}}$ ,  $F_{\text{sh,d,cir}}$ , and  $F_{\text{sh,d,hor}}$  are the respective shading reduction factors.

- a.2) *Isotropic radiance distribution*: in isotropic sky models, the distribution of the diffuse radiation is assumed to be uniform over the sky vault (or sky dome) [114,140,158]; thus, the absorbed diffuse solar irradiance ( $q_{\text{sol,d}}$ , in  $\text{W}\cdot\text{m}^{-2}$ ) on the outdoor surface is calculated as in Equation (9),

$$q_{\text{sol,d}} = \alpha \cdot F_{\text{sh,d,dome}} \cdot I_{\text{d,dome}} \quad (9)$$

where  $I_{\text{d,dome}}$  is the diffuse solar irradiance from the sky dome (in  $\text{W}\cdot\text{m}^{-2}$ ), and  $F_{\text{sh,d,dome}}$  is the shading reduction factor. Since the radiative properties of the surfaces are assumed to be not dependent on angle of incidence, the solar absorption coefficient  $\alpha$  for diffuse radiation is equal to the beam radiation absorption. Equation (9) can be seen as a simplification of Equation (8), i.e., anisotropic sky vault behaviour. In fact, assuming an uniform distribution of diffuse irradiance over the sky vault (isotropic behaviour), the circumsolar brightening and the horizon brightening components are assumed equal to zero [114].

- b) *Sol-air temperature approach (global solar irradiance)*: alternatively, together with the beam solar radiation, the effect of the absorbed diffuse solar irradiance can be modelled by means of the sol-air temperature, as described in Section 4.3.2.1.



*Driving forces*

The driving forces involved in the interaction between an opaque outdoor surface and the sky vault are the three components of the diffuse solar irradiance, i.e., sky dome, circumsolar brightening, and horizon brightening.

The diffuse solar irradiance coming from the sky dome, which represents the only driving force in isotropic sky models, is commonly considered to be uniformly distributed over the sky dome. According to this assumption, the incident diffuse solar radiation on a tilted surface ( $I_{d,dome}$ , in  $W \cdot m^{-2}$ ) is generally derived from the horizontal diffuse solar irradiance through transposition models, as reported in Equation (10),

$$I_{d,dome} = R_{d,dome} \cdot I_{d,h} \quad (10)$$

where  $I_{d,h}$  is the horizontal diffuse solar irradiance (in  $W \cdot m^{-2}$ ), and  $R_{d,dome}$  is the diffuse transposition factor, which depends only on the angle of incidence on the plane and the solar elevation under clear sky conditions; complex equations depending on clearness index are instead employed for partial cloudy sky conditions.

The determination of the diffuse solar irradiance from the circumsolar brightening sky vault component is generally performed by means of a circumsolar transposition factor ( $R_{d,cir}$ ), as for the sky dome diffuse irradiance. The circumsolar transposition factor definition generally depends on the solar position and the surface tilt angle, as well as on the clearness index for cloudy sky conditions. In some simplified methods, the incidence diffuse solar irradiance from the circumsolar brightening is calculated as a fixed percentage of the beam irradiance on the considered surface (for example, equal to 5% in the Bugler's model [159]). Finally, the circumsolar brightening component is not considered in isotropic sky models.

In most of the investigated correlations, including both isotropic and anisotropic sky models, the diffuse irradiance coming from the horizon brightening component is computed with the isotropic sky dome irradiance. Where separately considered, e.g., the Reindl et al. [160] model – implemented in TRNSYS, or the Perez et al. [157] model – implemented in EnergyPlus, it is determined by means of the horizon brightening transposition factor ( $R_{d,hor}$ ). In these models, the transposition factor depends on the solar position, the surface tilt angle, and the clearness index.

Dozens of researches have been published in the last decades reviewing and surveying the existing approaches for the determination the diffuse solar irradiance incident on a tilt surface. For more specific details, the reader should refer to the

research of, but not limited to, Hay [161], Loutzenhiser et al. [162], David et al. [163], Demain et al. [114], Yang [158], and Simón-Martín et al. [140].

In less common approaches, the sky vault is assumed to be discretised into infinitesimal portions [155] (or patches), each characterised by a specific radiance value. This is the case, for example, of matrix-based radiance models, in which the incident irradiance at a receiving surface is determined by summing the irradiance contributions from all the sky segments [164]. Although these approaches allow to describe the diffuse radiation distribution more realistically, they are computationally time-consuming, and are commonly adopted in daylight simulations, but a few research applied this approach for thermal purposes [164].

#### *Calculation parameters*

The calculation parameter required in the definition of the absorbed diffuse solar irradiance on an external surface is the shading reduction factor. A unique reduction factor is considered in isotropic sky models, and it is referred to the shading reduction factor for the diffuse irradiance coming from the sky dome. On the other hand, if an anisotropic sky model is assumed, the shading reduction factor for each component needs to be determined.

The shading reduction factor for sky dome is generally calculated as the integral of the sunlit fraction (for beam solar irradiance) over the sky dome, considering its discretisation into segments, as proposed by Brunger and Hooper [165] and implemented in many software, such as EnergyPlus [107]. The same approach is also applied for the determination of the shading reduction factor for horizon brightening. Eventually, the shading reduction factor for diffuse solar irradiance coming from the sky dome can be assumed equal to the sky view factor [166]. Finally, no shadowing for diffuse solar irradiance is considered in one of the two methods (Method 1) proposed by the simplified hourly method of the EN ISO 52016-1 [5], thus no shading factor is applied to any of the sky vault components. Such an approach assumes that the obstacles produce, by reflection, the same amount of solar radiation that they obstruct [10].

As for the shadowing reduction factor for the circumsolar brightening, it is generally assumed equal to the sunlit fraction in different applications, such as in EnergyPlus [92] and in the Method 2 proposed by the EN ISO 52016-1 [5] technical standard. The sunlit fraction is defined as described in Section 4.3.2.1.

Finally, the detailed dynamic model of TRNSYS [23] assumes an isotropic sky model when calculating the shadowing for diffuse solar irradiance; thus, the shading reduction factors for circumsolar and horizon brightening are assumed equal to the one for the sky dome.

### 4.3.2.3 Outdoor opaque surfaces vs. ground

#### *Modelling of the phenomenon*

The solar irradiance diffusely reflected on the ground is absorbed by the outdoor surface of the building envelope components. This process can be modelled as a separate surface heat balance term (approach *a* in Table 6), or through the sol-air temperature (approach *b* in Table 6). As regard the former approach, the absorbed solar irradiance ( $q_{\text{sol,r,gnd}}$ , in  $\text{W}\cdot\text{m}^{-2}$ ) is calculated as in Equation (11),

$$q_{\text{sol,r,gnd}} = \alpha \cdot F_{\text{sh,r,gnd}} \cdot I_{\text{r,gnd}} \quad (11)$$

where  $I_{\text{r,gnd}}$  is the reflected solar irradiance incident on the surface (in  $\text{W}\cdot\text{m}^{-2}$ ), and  $F_{\text{sh,r,gnd}}$  is relative shading reduction factor.

#### *Driving forces*

Even though the foreground is hit by both beam and diffuse solar radiation, no distinction between the two solar radiation components in the ground reflection process is made, due to the commonly adopted modelling assumption of purely diffuse ground reflectance. Thus, the amount of reflected solar irradiance that reaches the outdoor surface ( $I_{\text{r,gnd}}$ , in  $\text{W}\cdot\text{m}^{-2}$ ) depends on the reflection coefficient of the ground surface (ground albedo), on the global horizontal solar irradiance, and on the transposition factor for ground reflected solar irradiance. It is calculated as in Equation (12),

$$I_{\text{r,gnd}} = \rho_{\text{gnd}} \cdot R_{\text{r,gnd}} \cdot I_{\text{gl,h}} = \rho_{\text{gnd}} \cdot \frac{(1 - \cos\beta_i)}{2} \cdot I_{\text{gl,h}} \quad (12)$$

where  $\rho_{\text{gnd}}$  is the ground albedo,  $I_{\text{gl,h}}$  is the global (beam plus diffuse, in  $\text{W}\cdot\text{m}^{-2}$ ) horizontal solar irradiance, and its transposition factor  $R_{\text{r,gnd}}$ . Assuming the simplifications described in Section 4.2 (i.e., uniformity of the foreground, absence of shadowing on the foreground, and purely diffuse ground reflectance), the transposition factor can be derived by means of a simple formula depending of the surface tilt angle [114,140,158,167] (shown in Equation (12), where  $\beta_i$  is the surface tilt angle); in some proposed models, the  $R_{\text{r,gnd}}$  slightly differs from the one reported in Equation (12), such as in [168] or [169], and it may also be integrated with the clearness index to accounts for partly cloudy sky conditions [170].

As introduced in Section 4.2, some Authors have proposed improved models to overcome the general modelling assumptions adopted in the ground reflectance process. Firstly, Gueymard et al. [115] observed the dependence of the ground albedo on solar elevation and on the beam-to-diffuse solar radiation ratio; thus, the Authors introduced an albedo for diffuse radiation, independent of solar elevation

and valid for any sky conditions, and one for beam radiation, which can be defined for both nearly isotropic or specular reflectance conditions. Moreover, anisotropic models for the determination of the ground albedo have been proposed by Arnfield [116] and Temps and Coulson [117], considering its hourly variation depending on solar elevation, sky conditions, and ground properties.

#### *Calculation parameters*

The shading reduction factor for reflected solar radiation is generally assumed equal to the view factor to ground (Section 4.3.1.2), that takes into account how the ground is viewed from the surface [171], or it is an user defined parameter [92].

#### **4.3.2.4 Outdoor opaque surfaces vs. other objects**

Generally, the reflection of solar radiation on external surfaces is computed in dynamic simulation tools, such as EnergyPlus [92]. In particular, it considers the reflection from both shadowing surfaces (e.g., overhang, side fin, other buildings, etc.) and exterior building surfaces (i.e., in buildings characterised by complex geometries, one section of the building may reflect solar radiation onto another section). The solar radiation that hits the shadowing surfaces can be both specularly and diffusely reflected; on the other hand, the reflection process on exterior building surface is instead driven by the pure diffusely reflectance assumption (Section 4.2), commonly adopted in building energy performance calculation models.

Table 6: External shortwave heat transfer

Phenomenon modelling	Driving forces		Calculation parameters	
	Determination	T.D.	Determination	Model
<b>Outdoor opaque surface vs. sun (beam solar radiation)</b>				
<b>a) Absorbed solar irradiance as separate HB term</b>  <b>b) Sol-air temperature approach (global solar irradiance)</b>	<b>Incident beam solar radiation<sup>1</sup></b> » Transposition model	$\nu$	<b>Shading reduction factor (sunlit fraction)</b> » Ray tracing method » Pixel counting method » Geometric methods - Polygon clipping method - Shadow projection method	$\nu$ $\nu$ $\nu$ $a, b$ $a, b$ $a, b$
	<b>Sol-air temperature</b> » Analytical calculation » Tabular	$\nu$ $\nu, c$ $b$		
<b>Outdoor opaque surface vs. sky vault (diffuse solar radiation)</b>				
<b>a) Absorbed solar irradiance as separate HB term</b> a.1) Anisotropic radiance distribution a.2) Isotropic radiance distribution  <b>b) Sol-air temperature approach (global solar irradiance)</b>	<b>Diffuse incident solar radiation from sky dome</b> » Anisotropic models - Matrix-based radiance models <sup>2</sup> » Isotropic models (transposition model) <sup>3</sup>	$\nu$ $\nu$	<b>Shading reduction factor for sky dome</b> » Integral of sunlit fraction over a sky dome spatial discretization » None (not shadowing of diffuse radiation)	$\nu$ $c$ $a, b$ $a, b$
	<b>Diffuse incident solar radiation from circumsolar brightening</b> » Matrix-based radiance models <sup>2</sup> » Decomposition model » Percentage of beam irradiance on surface » Absent	$\nu$ $\nu$ $\nu$ $c$	<b>Shading reduction factor for circumsolar brightening</b> » Equal to sunlit fraction - Including far obstacles - Not including far obstacles » Equal to shading reduction factor for sky dome » None	$\nu$ $a, 1, b$ $a, 1, b$ $a, 1, b$ $a, 1, b$ $a, 2$
	<b>Diffuse incident solar radiation from horizon brightening</b> » Matrix-based radiance models » Decomposition model » Included in diffuse radiation from sky dome » Absent	$\nu$ $\nu$ $\nu$ $c$	<b>Shading reduction factor for horizon brightening</b> » Integral of sunlit fraction over a horizon line spatial discretization » Equal to shading reduction factor for sky dome » None	$\nu$ $a, 1, b$ $a, 1, b$ $a, 1, b$ $a, 1, b$ $a, 2$
	<b>Sol-air temperature</b> » Analytical calculation » Tabular	$\nu$ $\nu$		$b$ $b$

**Notes**<sup>1</sup> Transposition of horizontal beam solar irradiance<sup>2</sup> Discretisation of the sky into segments of radiance values; the irradiance at the receiving surface is the sum of the irradiance contributions from all sky segments [164]<sup>3</sup> Transposition of horizontal diffuse solar irradiance

Table 6: External shortwave heat transfer (continues)

Phenomenon modelling	Driving forces		Calculation parameters	
	Determination	T.D.	Determination	T.D.
<b>Outdoor opaque surface vs. ground (reflected solar radiation)</b>				
<b>a) Absorbed solar irradiance as separate HB term</b>	<b>Reflected incident solar radiation from ground</b>		<b>Shading reduction factor for ground</b>	
	» Anisotropic models <sup>4</sup>	$\nu$	» Equal to view factor to ground	$\nu$
	» Isotropic models (dependent on surface tilt angle)	$\nu$	» User defined	$c$
<b>b) Sol-air temperature approach (global solar irradiance)</b>	<b>Sol-air temperature</b>			
	» Analytical calculation	$\nu$		$a, b$
	» Tabular	$c$		$a, b$

**Notes**

<sup>4</sup> Anisotropic behaviour of ground is modelled by means of a variable reflectance coefficient (albedo), which depends on solar elevation, sky conditions, and ground properties

### 4.3.3 External heat convection

Differently from the previously presented heat transfer processes, the external heat convection is involved only in the interaction between the outdoor surfaces of the building envelope components (both opaque and transparent) and the outdoor air. The detected modelling assumptions related to the modelling of the heat transfer phenomenon, and to the determination of both driving forces and calculation parameters are deepened below and are summarised in Table 7.

#### *Modelling of the phenomenon*

The heat flux transferred between the outdoor surface and the environment due to heat convection ( $q_{\text{conv,ext}}$ , in  $\text{W}\cdot\text{m}^{-2}$ ) is generally determined by means of the classical Newton's law (approach *a* in Table 7), as presented in Equation (13),

$$q_{\text{conv,ext}} = h_{\text{c,ext}} \cdot (\theta_{\text{surf,ext}} - \theta_{\text{air}}) \quad (13)$$

where  $h_{\text{c,ext}}$  is the convective heat transfer coefficient (in  $\text{W}\cdot\text{m}^{-2}\cdot\text{K}^{-1}$ ), and  $\theta_{\text{surf,ext}}$  and  $\theta_{\text{air}}$  are the outdoor surface and the ambient temperatures (in  $^{\circ}\text{C}$ ), respectively. As well known, the external heat convection can be driven by natural or forced constraints [172]; in natural, or buoyancy-driven, heat convection, the driving force is the temperature difference between air and surface, while wind (speed and direction) is the main constraint in forced, or wind-driven, convection. Moreover, the convective heat transfer coefficient is dependent on these driving forces as well.

#### *Driving forces*

Differently from internal convection, the forced component is predominant in the external heat convection, and thus it is the wind, its main driving force. Although it is the main parameter employed in the determination of the convective heat transfer coefficients [173,174], there still no consensus regarding the definition of the wind speed [175,176], even though a consistent literature has discussed over this issue [172,175,176].

Generally, the wind speed employed in the correlation for convective heat transfer coefficients was identified to belong to three categories (referred to in Table 7):

1. Local wind speed, which accounts for increases of wind speed with building height, as well as for wind-blocking effects due to neighbouring buildings [173]. In particular, it can be determined at a certain height, which can be at roof top, at 10 meters above the ground level, at the surface centroid, and/or at a certain distance from the surface,
2. Site wind speed, which is generally determined far away from any object or physical boundary to avoid any disturbance by any object [175],

3. Reference wind speed, generally adopted to define reference convective heat transfer coefficients in technical standards, e.g., EN ISO 6946 [132].

Generally, local and site wind speed is assumed to vary during the simulation period, according to the weather conditions, and thus the convective coefficients; a constant value is adopted, instead, for the reference wind speed. For example, the EN ISO 6946 technical standard assumes a constant reference wind speed equal to  $4 \text{ m}\cdot\text{s}^{-1}$  to calculate the external convective heat transfer coefficient. A more detailed analysis on the determination of the wind speed can be found in the research of Defraeye et al. [176], Mirsadeghi et al. [175], and Evangelisti et al. [172].

The outdoor ambient temperature is the thermal constraint, instead, in buoyancy-driven heat convection, which can be either local air temperature or site air temperature, as described in Section 4.3.1.3. Moreover, the outdoor wet-bulb temperature may be assumed under rainy conditions [107].

#### *Calculation parameters*

Convective heat transfer coefficients can be calculated by means of analytical methods, numerical methods, or experimental methods [172,173,175]; the latter is the currently the main source [175], while analytical methods can be applied for specific conditions (i.e., flow regime, and simple geometries). Experimental methods were developed to account for both mixed heat convection and for forced convection. In mixed convection, the heat transfer coefficient is determined as the sum between the convective coefficients for natural and forced convection [177]. The former is generally dependent on the temperature difference between the surface and the air; instead, the latter is derived by means of a variety of correlations, widely surveyed in literature [172–176,178,179], depending on different parameters, including:

1. Wind speed, which is the main (or only) dependent parameter [173],
2. Wind direction, or surface orientation in relation to the wind direction (windward or leeward surfaces [175]),
3. Surface texture and roughness,
4. Surface geometry, explicitly expressed in terms of surface area, height, or perimeter, or implicitly described through the Nusselt number [178],
5. Building shielding (accounting for sheltering effects), including terrain type, sheltering by nearby buildings, neighbouring building geometry, etc. [175].

Although most of the identified correlations focus on the wind speed, comprehensive methods employ many of the presented dependent parameters; for more details on the specific correlations, the reader may refer to the research of, but not limited to, Evangelisti et al. [172], Montazeri and Blocken [173],



Awol et al. [174,179], Misardeghi et al. [175], Defraeye et al. [176], and Palyvos [178]. In particular, Misardeghi et al. [175] have also highlighted the modelling assumptions adopted to implement the reviewed correlations in seven different building energy simulation tools.

The convective heat transfer coefficients can be considered as variable over the simulation period, or constant values can be used. Moreover, their definition can be achieved by implying reference conditions (e.g., wind speed, temperature difference) or the specific conditions. In the former case, such as for the EN ISO 6946 formulation [132], a reference wind speed value is assumed to calculate the external convective heat transfer coefficient, which is thus assumed to be constant over the simulation period. Under rainy conditions, the convective heat transfer coefficients are generally assumed fixed [175]; for example, in EnergyPlus the exterior surfaces are assumed to be wet, and a convective coefficient of  $1\,000\text{ W}\cdot\text{m}^{-2}\cdot\text{K}^{-1}$  is used [107].

Table 7: External heat convection

Phenomenon modelling	Driving forces		Calculation parameters	
	Determination	T.D.	Determination	T.D.
Outdoor surface vs. air <i>a. Newton law</i>	<b>Wind speed</b> » Local wind speed <sup>1</sup> - At certain height and distance from surface - At certain height » Site wind speed » Reference wind speed	$v$	<b>Convective heat transfer coefficient</b> » Mixed convection experimental correlations <sup>3</sup> » Forced convection experimental correlations <sup>4</sup> - Dependent on wind speed - Dependent on wind direction - Dependent on surface roughness - Dependent on surface geometry - Dependent on building shielding » Combined with longwave radiation	$v$ $v, c$
	<b>Wind direction</b> » Prevalent wind direction » Reference wind direction	$v, c$ $c$		
	<b>Air temperature</b> » Local air temperature (at certain height) <sup>2</sup> » Site air temperature	$v$ $v$		$a$ $a$

**Notes**<sup>1</sup> Accounts for increase of wind speed with height and wind-blocking effect due to neighbouring buildings [173]<sup>2</sup> Accounts for variation in the air temperature due to the actual height from the ground of the considered surface<sup>3</sup> Determined as the sum of the convective heat transfer coefficients for natural (buoyancy-driven) and forced (wind-driven) convection<sup>4</sup> The dependent variables can be coupled in the reviewed correlations

#### 4.3.4 Solar transmission

In the present section, the solar transmission through the transparent building envelope components is analysed. This process accounts for the solar heat flux entering the zone. In this sense, the solar transmission heat transfer process is involved in the interaction between the transparent surfaces and the sun, the sky vault, the ground surface, and the external objects characterised by both specular and isotropic reflectance. In particular, the interaction between the sun and specular reflectivity objects are analysed together in Section 4.3.4.1, since both are responsible of beam solar irradiance incidence on an external surface; in Section 4.3.4.2, instead, solar transmission due to diffuse solar radiation is analysed, including the sky vault and isotropic reflectivity objects.

The interaction between an external surface and each of the components listed above is analysed in the following sections, and the related modelling assumptions are highlighted and summarised in Table 8.

##### 4.3.4.1 Transparent surfaces vs. sun and other objects (beam reflection)

###### *Modelling of the phenomenon*

It is well known that incident solar flux on a window is partly transmitted as shortwave radiation, partly reflected, and partly absorbed by the glass layers; the latter then interacts with the indoor and outdoor environment by heat convection and longwave thermal radiation. This phenomenon is commonly referred to as "secondary heat transfer" [180,181] toward inside and outside, respectively. The existing modelling approaches for solar transmission differ in how the transmitted solar radiation and the secondary heat transfer are considered; complete models account for the two components separately, while they are aggregated in more simplified models. The two approaches found in literature are here presented (named as in Table 8).

- a) ***Separated shortwave transmitted and secondary heat transfer toward the inside***: this approach separately accounts for the directly transmitted solar radiation and the secondary heat transfer. The former enters the zone as shortwave radiation, and it is distributed over and absorbed by the internal surfaces in a prescribed manner (described in Section 4.3.7.1); this represents a surface heat balance term which affects the surface longwave thermal radiation, heat convection, and conduction heat transfer. Similarly, the absorbed solar radiation (secondary heat transfer toward inside) contributes to the internal longwave heat transfer (between the transparent surface and the other internal surfaces), and to the heat convection with the ambient air.

The amount of transmitted solar radiation depends on the glass optical properties (i.e., solar transmittance, absorptance, and reflectance), whose determination is analysed later in the text,

- b) ***Aggregated shortwave transmitted and secondary heat transfer toward inside (g-value)***: this approach, instead, aggregates the directly transmitted solar radiation and the secondary heat transfer by means of the global solar energy transmittance (*g*-value or *SHGC*), which is determined to consider both the effects [180,181]. Through this approach, the so-called solar heat gains are determined, and either loaded on the zone air node or distributed over the surfaces, according to the calculation model considered. Two variants of the presented approach have been documented.
  - b.1) *Considered as shortwave and longwave radiation*: in the first variant, the effect of both short- and longwave radiation is accounted. In fact, the solar heat gains are determined by the directly shortwave transmitted solar radiation, and by the re-emission of the absorbed solar radiation as longwave,
  - b.2) *Considered as shortwave radiation*: in the second variant, instead, the solar heat gains are determined just by the transmission of solar radiation as shortwave radiation. In this case, the secondary heat transfer toward inside is neglected. This is the case, for example, of the EN ISO 52016-1 hourly method [5], which the total transmitted solar radiation is assumed to be completely shortwave radiation,

As introduced, the solar heat gains depend on the global solar energy transmittance, whose determination is analysed later in the text.

#### *Driving forces*

The thermal constraint involved in the here presented physical process is the beam solar irradiance incident on the building transparent components, determined as described in Sections 4.3.2.1 (outdoor surfaces vs. sun) and 4.3.2.4 (outdoor surfaces vs. other objects).

#### *Calculation parameters*

In the first modelling approach (*a*), the glass optical properties determine the amount of solar radiation transmitted into the thermal zone. Generally, these properties are characteristic of the glazing system to be modelled, and thus they are considered an input data. The adopted modelling assumptions regarding the glass optical properties concern their variation during the simulation period, depending on wavelength and angle of incidence.

In most application, the glass optical properties are spectral averaged values, determined by averaging the spectral data over the solar wavelength band [182] independently from the atmospheric conditions [180]. The spectral average optical properties are then assumed to be dependent or not on the angle of incidence of solar irradiance. In the first case, the glass properties are varied at each timestep simulation accordingly to the considered model for angular dependency; different approaches to extract the angular dependency of glass properties include [183] Fresnel ‘exact’ calculations, semi-physical models, empirical models, and template models. A detailed description of these approaches can be found in the work of [184]. Most commonly, dynamic simulation tools use the Fresnel equation to derive the angular dependency of glass optical properties [107,185]. On the other hand, technical standards suggest the use of constant optical properties for simplification [180,181] (i.e., spectral averaged properties calculated at normal incidence), as well as simplified models such as the multizone building model developed by Khoury et al [186].

In the second modelling approach (*b*), the global solar energy transmittance (*g*-value) determines the solar heat gains. The *g*-value, defined as the portion of radiant solar energy incident on a window that reaches the conditioned space of a building in [182], can be determined as the area-weighted value of three components: centre of the glass, edge of the glass, and frame (accounting for the solar gain that occurs through the frame [182]). This approach it is not widespread; in fact, it is documented only in the research of Wright [182] which was then implemented in the ASHRAE cooling load procedure [97,187,188]. The *g*-value at the centre of the glass is reasonably assumed in other applications. As for the specific glass optical properties, a spectral averaged *g*-value can be considered for not strongly spectrally selective glazing systems [187], and it can be assumed to be dependent or not on the angle of incidence of solar irradiance. Differently from the approaches presented previously, only empirical and template models can be used to extract the angular dependency of the total solar energy transmittance [183,189]. In particular, Montecchi and Polato [190] and Karlsson and Ross [191] developed two similar models based on the *g*-value at normal incidence, the angle of incidence, and different parameters assuming different values for different glazing types. Moreover, Singh and Garg [192] have developed an angular dependency model depending only on the angle of incidence and the *g*-value at normal incidence. In simplified methods, the total solar energy transmittance is considered solar angle-independent, and the *g*-value at normal incidence, or a time-averaged value lower than the *g*-value is assumed [5,10].

Finally, the  $g$ -value is assumed to be equal to the solar transmission coefficient if the transmitted solar radiation is considered to be all shortwave radiation, thus the absorption and re-emission processes are neglected [5].

#### 4.3.4.2 Transparent surfaces vs. sky vault, ground, and other objects (diffuse reflection)

##### *Modelling of the phenomenon*

As for beam solar radiation presented in Section 4.3.4.1, the existing modelling approaches for diffuse solar transmission includes both models accounting separately for the directly transmitted solar radiation and the secondary heat transfer toward inside, or aggregating them. Beside these approaches, presented below (named as in Table 8), another simplified approach aggregates the transmission of diffuse solar radiation with beam irradiance, differently from the previous approaches.

- a) ***Separated shortwave transmitted and secondary heat transfer toward the inside***: this approach is consistent with approach *a*, defined for beam solar transmission, in Section 4.3.4.1. In this case, the glass optical properties are referred to diffuse solar radiation. This approach is applied in detailed dynamic tools, as in EnergyPlus [107], TRNSYS [23], and it is suggested in the EN ISO 52017-1 technical standard [20],
- b) ***Aggregated shortwave transmitted and secondary heat transfer toward inside (g-value)***: this approach is consistent with approach *b*, defined for beam solar transmission, in Section 4.3.4.1. Two variants have been documented as well, but they consistently differ from the ones presented for beam solar transmission.
  - b.1) *Separated from beam solar irradiance*: in the first variant, beam and diffuse solar irradiance are separately considered. In fact, solar heat gains due to diffuse solar transmission are calculated by means of a specific total solar energy transmittance of diffuse radiation, which is different from beam  $g$ -value, and its determination is described below. This is the case of the ASHRAE cooling load procedure [187,188],
  - b.2) *Aggregated with beam solar irradiance*: in the second variant, instead, the solar heat gains are determined for the global (beam plus diffuse) solar transmission. This is the case, for example, of the EN ISO 52016-1 hourly method [5].

*Driving forces*

The thermal constraint involved in the here presented physical process is the diffuse solar irradiance incident on the building transparent components, determined as described in Sections 4.3.2.2 (outdoor surfaces vs. sky vault), 4.3.2.3 (outdoor surfaces vs. ground), and 4.3.2.4 (outdoor surfaces vs. other objects).

*Calculation parameters*

As introduced, the glass optical properties are referred to the diffuse radiation in the first modelling approach (*a*). The definition of diffuse glass optical properties based on the anisotropic behaviour of the sky vault is considered in a few calculation models; in particular, this approach implies the definition of three different values for each glass optical property referred to the diffuse radiation coming from the sky dome, the circumsolar brightening, and the horizon brightening, respectively. Even though this approach is reasonably the most complete approach in determining the transmission of diffuse solar radiation, its application is documented only for tabular daylighting devices in EnergyPlus [107], and no other references were found for this approach. On the other hand, the most common approach for determining the diffuse glass optical properties assumes an isotropic sky model, meaning that a single value is considered for the calculation of the diffuse transmitted solar radiation. Following this approach, the diffuse transmittance, reflectance, and absorptance, is derived from the beam glass optical properties. In particular, the glass properties can be calculated by integrating the beam properties over all directions (i.e., hemispherical averaged values) [187], or beam properties at specific solar angles are considered. The latter is the case of the TRNSYS detailed dynamic model, in which the diffuse optical properties are calculated considering a reference solar angle of 60° [23].

Similar considerations can be referred to the second approach (*b.1*), even though referred to the total solar energy transmittance *g*-value. In particular, the *g*-value can be a hemispherical value *g*-value can be assumed [187], as well as a *g*-value at a specific solar angle.

Finally, the beam total solar energy transmittance (Section 4.3.4.1) is also applied also diffuse solar radiation in the third approach (*b.2*), neglecting the different glass behaviour for diffuse and beam solar irradiance.

Phenomenon modelling	Driving forces		Calculation parameters	
	Determination	<i>t.d.</i>	Determination	<i>t.d.</i>
<b>Transparent surfaces vs. sun and other objects (beam reflection)</b>				
<i>a) Separated shortwave transmitted and secondary heat transfer toward inside</i>	<b><i>Incident beam solar irradiance</i></b> Sections 4.3.2.1 and 4.3.2.4, Table 6		<b><i>Glass optical properties</i></b> » Solar angle-dependent (spectral average) <sup>1</sup> » At normal incidence (spectral average)	<i>v</i> <i>c</i>
<i>b) Aggregated shortwave transmitted and secondary heat transfer toward inside (g-value)</i>			<b><i>g-value</i></b> » Three components g-value (centre of glass, edge of glass, and frame/divider) » One component g-value (centre of glass) - Solar angle-dependent (spectral average) <sup>2</sup> - Time-weighted g-value at normal incidence (spectral average) - At normal incidence (spectral average)	<i>v, c</i>  <i>b, l</i>  <i>c</i>
<i>b.1) Considered as shortwave and longwave radiation</i>				<i>b, l</i>
<i>b.2) Considered as shortwave radiation</i>				<i>b, l</i>
<b>Transparent surfaces vs. sky vault, ground, and other objects (diffuse reflection)</b>				
<i>a) Separated shortwave transmitted and secondary heat transfer toward inside</i>	<b><i>Incident diffuse solar irradiance</i></b> Sections 4.3.2.2, 4.3.2.3 and 4.3.2.4, Table 6		<b><i>Glass optical properties</i></b> » Anisotropic model <sup>3</sup> » Beam optical properties (isotropic model) - Hemispherical averaged - At certain solar angle	<i>v, c</i>  <i>c</i> <i>c</i>
<i>b) Aggregated shortwave transmitted and secondary heat transfer toward inside (g-value)</i>			<b><i>g-value</i></b> » Beam g-value - Hemispherical averaged - At certain solar angle » Equal to beam g-value	<i>a</i>  <i>a</i> <i>a</i>
<i>b.1) Separated from beam solar irradiance</i>				<i>b, l</i>
<i>b.2) Aggregated with beam solar irradiance</i>				<i>b, l</i> <i>b, 2</i>

Angle-dependency correction factors can be derived using the 'exact' (Fresnel calculation) approach, semi-physical models, empirical models, or template models<sup>1</sup>.

## 2 Angle-dependency correction factors can be derived using empirical or template models

<sup>3</sup> Reported in literature only for tubular daylighting devices [92]



### 4.3.5 Heat conduction and storage

#### *Modelling of the phenomenon*

Probably, there are more ways to formulate the building envelope components conduction process than any other process [97]. Among the existing models for modelling heat conduction, the ones applied more frequently in building energy performance calculation include numerical models (i.e., finite difference and lumped capacitance methods), time series methods (i.e., conduction transfer function, and response factor methods), and analytical methods [12,193–196]. These are summarised in Table 9, together with the modelling assumption related to the definition of the driving forces and calculation parameters.

- a) ***Finite difference methods***: this approach is based on the spatial and temporal discretisation of the building envelope components [196] into a variable number of discrete – or lumped – elements [195], in accordance with the thermal-electrical analogy [195,197]. Practically, this approach involves the discretisation of the reference domain (i.e., structure layer, or a finite volume) into several resistive-capacitive (R-C) nodes, to which the algebraic difference equations are applied to determine the solution of the conductive problem. The finite difference approach has been widely applied in different calculation methods, such as in EnergyPlus [92], ESP-r [93], or in the conduction model proposed by Mazzarella et al. [198] and implemented in the Italian National Annex to the EN ISO 52016-1 hourly calculation method [137]. In fact, it is attractive since it mimics the physical heat flow process as in the reality [196], and it is the only documented approach able to consider materials with variable thermophysical properties; however, since its accuracy relies on the density of the temporal- and spatial-discretisation of the building envelope components, it might be costly and time-consuming [195,199], thus other approaches are usually preferred over this,
- b) ***Lumped parameters methods***: this approach can be considered as simplifications of the finite difference methods. In fact, also in this approach the structures are discretised into resistive-capacitive nodes; however, in this case, predefined numbers of nodes are used, according to the considered variant. These can be categorised into schemes assuming capacitive (approach *b.1*) or non-capacitive surface nodes (approach *b.2*),

***Conduction transfer function methods***: in this approach, considered an extension of the thermal response factor method [195], the wall distribution of resistance and capacity is continuous, but the time is discretised [196]. This transfer function equation relates the heat flux at one surface of the element to

the heat flux and temperature histories at both surfaces of the structure [107,194]. This approach is appealing since the knowledge of the heat flux and temperature distribution inside the structure is not required [199], contrary to what happens in the finite difference and lumped parameters methods, and the solution of the conduction heat transfer depends only on the definition of the transfer function coefficients, which is analysed in the following paragraphs. This approach is widely implemented in different calculation methods, such as in EnergyPlus and in TRNSYS,

- c) **Response factor method:** differently from the transfer function approach, in this approach the heat flux at one surface depends only on the temperatures of the surfaces, and not on the previous heat fluxes [194]. As in the previous approach, the solution of the conduction heat transfer depends on the definition of the response factor coefficients.

#### *Driving forces*

The driving forces for the conduction heat transfer are the indoor and outdoor surface temperatures, which depends on all the heat transfer phenomena analysed in the *comparison map*. Alternatively, in simplified methods, such as the “air-to-air” conduction transfer function method [194] the driving forces involved are the indoor and outdoor air temperature.

#### *Calculation parameters*

As regards the finite difference and the lumped parameters approach (approach *a* and *b* in Table 9, respectively), the conduction solution depends on the discretisation density into R-C nodes and their position, and on the distribution of the resistance and capacitance over the R-C nodes.

As regards the density of the spatial discretisation of the structure, in conduction finite difference methods (approach *a*) the number of nodes is generally defined for each construction layer. The density of the nodes grid for each layer can be defined depending on the layer’s Fourier number and a space discretisation constant, such as in the conduction finite difference method implemented in EnergyPlus [107], or through a reference Fourier number, for instance in the conduction model employed in the EN ISO 52016-1 Italian National Annex [137,198]. A predefined number of nodes for each layer is instead required in the simplified conduction finite difference approach proposed by Luo et al. [200], in which layer is discretised into three discrete volumes with four resistive-capacitive nodes.

In lumped parameters methods (approach *b*), the number of nodes is predefined, regardless of the real characteristics (e.g., layer sequence, thermophysical

properties of each material, etc.) of the considered structure. In lumped parameters methods considering capacitive surfaces (approach *b.1*), the structures are assumed to be described by two surface nodes and by different internal nodes, according to the considered model. In particular, in fourth-power order models, the structure is described by means of four capacitive nodes (two placed on the inner and outer surfaces) and three resistances (3R4C), such as in the model proposed by Fraisse et al. [201]; in EN ISO 52016-1 hourly method [5], instead, each opaque component is assumed to be discretised into five capacitive nodes (two placed on the structure surfaces) and four resistances (4R5C), while the transparent components are characterised by two surface nodes and one internal node. On the other hand, in lumped parameters methods considering non-capacitive surfaces (approach *b.2*), the structures are described by means of one capacitive node and two resistances in first-order models (2R1C), such as the one proposed by Laret in [202], or by means of two capacitive nodes and three resistances in second-order models (3R2C), such as the one proposed by Gouda et al. [203].

As concerns, instead, the position of the nodes inside the structure, in lumped parameters methods this is not defined, with the exception for the surface nodes in 3R4C and 4R5C models. In the conduction finite difference approaches, instead, the node placement is a critical and widely discussed modelling step. Generally, two nodes are always placed on the inner and outer surfaces of the structure. As regards the inner nodes, instead, it is a common practise to consider the nodes to reside in the middle of a volume element [204], and to separate them by an equal distance. This is what is generally assumed in models considering capacitive nodes on the surfaces, such as in EnergyPlus [107]; on the other hand, in case of non-capacitive surface nodes, all interior nodes are separated by the same distance, while the distance between the last interior node and the surface node is half of the node spacing [204], as assumed in the finite volume method proposed by Mazzearella et al. [198]. Another discussed issue is related to the position of node on the internal boundary between two materials in multilayer structures. Waters and Wright [205] proved that the placement of interface nodes may allow to avoid gross error at any part of the system, and this procedure was employed in the EnergyPlus finite difference model. Mazzearella et al. [198] analysed the chance of positioning interlayer nodes as well, but this strategy proved to not increase significantly the model accuracy, but to increase the computational effort.

The distribution of heat capacity and thermal resistance over the structure nodes is another widely discussed issue. In the conduction finite difference methods (approach *a*), to each node is associated a thermal resistance and heat capacity referred to the relative thickness portion of the layer. Moreover, these can be either

calculated at the beginning of the simulation and kept constant, or can vary at each timestep for considering materials with variable thermophysical properties (e.g., phase change material, etc.). The distribution of resistances and capacitances in lumped parameters models, instead, has been widely discussed, and different approaches have been proposed to assure an acceptable accuracy of these methods [199]. The approximation of the R-C network can be performed through numerical approaches, analytical procedures, or it can be predefined. In the former approach, optimisation algorithms are used to find the parameters that allow to match the actual heat transfer through building envelope the best [206,207]. Among the documented analytical methods, more complex approaches are based on the hypothesis that the position of the capacitance within the element varies in every timestep in response to changes in the excitation value, such as in the model proposed by Rodríguez Jara et al. [199] in which the resistances and capacitances distribution varies during the simulation period, or they relies on the analysis of the relative influence of the different layers within a construction, basing the resistance-capacitance distribution on the so called ‘dominant layer’ [197]. Finally, in simplified approaches, predefined distribution of the thermal resistance and heat capacity is considered; for example, fixed ratios of the overall thermal resistance of the structure are associated to each node of the 4R5C model of the EN ISO 52016-1 technical standard [5], while the heat capacity is distributed considering a qualitative mass position of the structure.

Coming to the transfer function method (approach *c*), this is based on the definition of the transfer function coefficients (TFCs), which reflect the transient response of a given structure [194], and they depends only of the thermophysical properties of the materials composing the structure. The TFCs are constant coefficients that need to be calculated once at the beginning of the simulation [107], thus they are not able to account for phase change materials. As for the distribution of the resistances and capacitances in the lumped parameters methods (approach *b*), also in this case the accuracy of the response factor method relies on the determination of the TFCs [208]. Thus, several approaches have been developed for the TFCs derivation, including analytical and experimental methods. A summary of the existing methods for deriving the transfer function coefficient is reported in the research of Haghighat and Liang [195]. Moreover, the coefficients can be calculated for arbitrary structure configurations [194], or tabular values can be assumed [209,210]. For example, the ASHRAE Fundamental [211] provided a set of conduction transfer function coefficients for representative structures. Finally, the derivation of the TFCs from response factors was also documented [195,210].

Similar considerations can be also drawn for the determination of the response factor coefficients (RFCs), which can be calculated for specific structure configurations, or can be derived from the transfer function coefficients [194].

Table 9: Heat conduction and storage

Phenomenon modelling	Driving forces		Calculation parameters	
	Determination	T.D.	Model	Model
a) <i>Finite difference method</i>			<b>Number of nodes</b> » Calculated for each construction layer » Predefined for each construction layer » Predefined for construction <sup>1</sup>	c c c
b) <i>Lumped capacitance method</i> b.1) <i>Capacitance on elements surfaces</i> b.2) <i>No capacitance on elements surfaces</i>			<b>Spatial distribution of nodes</b> » On surfaces (int. and ext.), on interlayer surfaces, inside each layer » On surfaces (int. and ext.), inside each layer » On surfaces (int. and ext.), not specified for inside each layer » Not specified	c c c c
c) <i>Transfer function method</i>			<b>Heat capacity associated to each node</b> » Proportional to node spacing in each layer » Ratio of overall construction heat capacity - Depending on construction characteristics - Precalculated (qualitative mass position) - Precalculated	v, c c
d) <i>Response factor method</i>			<b>Thermal resistance associated to each node</b> » Proportional to node spacing in each layer » Ratio of overall construction thermal capacity - Depending on construction characteristics - Precalculated	v, c c
			<b>Transfer function parameter</b> » Calculated for the specific construction » Derived from response factor coefficients » Tabular	c c c
			<b>Transfer function parameter</b> » Calculated for the specific construction » Derived from transfer function coefficients » Tabular	c c c

### 4.3.6 Internal longwave radiation heat transfer

Indoor surfaces are subject to longwave radiation exchange with other indoor surfaces facing the thermal zone, with furniture, and with internal sources, such as appliances and occupants (Table 10). The modelling assumptions adopted in modelling the longwave radiation heat exchange between surfaces are presented in Section 4.3.6.1; in Section 4.3.6.2, instead, the modelling of furniture is analysed, while the longwave radiation from internal sources is deepened in Section 4.3.6.3.

#### 4.3.6.1 Indoor surface vs. indoor surfaces

##### *Modelling of the phenomenon*

A wide range of calculation methods characterised by different levels of details and complexity have been developed to calculate the longwave radiation heat exchange between surfaces facing a thermal zone. Due to the simplification adopted, the documented modelling strategies have been categorised into four different groups, presented below.

- a) **Uniform radiosity**: the uniform radiosity method calculates the difference between the surface radiosity and irradiation, which represent the net radiation exchange at a given indoor surface [133]. It consists in a network of equations (as the number of surfaces facing the thermal zone) aimed at calculating, at each simulation timestep, the incident radiation (i.e., irradiation) and the reflected and remitted radiation (i.e., radiosity) for each surface, based on the longwave radiation Stefan-Boltzmann law. It represents an accurate model to predict longwave heat transfer between surfaces, however it requires a high computational effort at each timestep iteration, since it allows to consider variable surface properties [133]. This approach depends on surfaces emissivity and view factors between surfaces; their determination is deepened below,
- b) **Stefan-Boltzmann (SB) law**: in this approach, the net heat exchange between two surfaces depends on their absolute temperatures, the view factor, and the surface emissivities, and it is calculated as presented in Equation (14),

$$q_{LW,surf,i} = F_{surf,i-surf,j} \cdot \varepsilon_i \cdot \sigma \cdot (T_{surf,i}^4 - T_{surf,j}^4) \quad (14)$$

where  $F_{surf,i-surf,j}$  is the view factor between surface  $i$  and  $j$  (the “other” surface”),  $\varepsilon_i$  is the thermal emissivity of the surface,  $\sigma$  is the Stefan-Boltzmann constant ( $5,67 \cdot 10^{-8} \text{ W} \cdot \text{m}^{-2} \cdot \text{K}^{-4}$ ), and  $T_{surf,i}$  and  $T_{surf,j}$  are the indoor temperatures of surface  $i$  and  $j$  respectively. In particular, the fourth-power nonlinear longwave heat transfer can be formulated considering the radiant enclosure (i.e.,

participating surfaces in the longwave heat exchange) into two ways, as presented below.

- b.1) *Enclosure explicit modelled*: in this approach, the participating surfaces are geometrically modelled, and each surface is characterised by its thermal properties,
- b.2) *Enclosure implicit modelled*: in this approach, commonly called “mean radiant temperature” method [212], the considered surface is assumed to interact with a fictitious surface representing the whole radiant enclosure [133]. Beside the advantages of this method in reducing the computational effort (just two equations have to be solved simultaneously), it also allows to include furnishings in the radiant enclosure, avoiding the need of specific information to their modelling (i.e., position, view factors). However, this inclusion assumes the thermal equilibrium of furniture with indoor air,
- c) ***Linearised SB law***: in this approach the linearisation of the longwave heat transfer phenomenon is assumed, and it is based on the introduction of the radiant heat transfer coefficient ( $h_r$ ). Three variants of the Stefan-Boltzmann linearised approach were documented, and they are described below.
  - c.1) *Enclosure explicit modelled*: in this approach, the participating surfaces are explicitly modelled, as described in (b.1),
  - c.2) *Enclosure implicit modelled*: in this approach, the participating surfaces are implicitly modelled by means of a fictitious radiant surface, as described in (b.1). This approach is a simplification of the Walton’s mean radiant temperature method [212], and it is applied in the CISBE model and in the IES-VE calculation method (ApacheSim) [185],
  - c.3) *Aggregated with heat convection*: in this approach, the heat convection and longwave radiation heat transfer are combined by means of an overall surface heat transfer coefficient. This approach is based on the modelling assumption that the zone air completely absorbs the longwave radiation from the surfaces within the zone [97]; thus, the radiant enclosure is assumed to be at air temperature.

#### *Driving forces*

In longwave radiation heat transfer, the main driving force is the difference between the considered surface and the radiant enclosure temperatures. While the former is the outcome of the surface heat balance, the enclosure temperature can be estimated in different ways, according to the modelling strategy considered. In particular, the specific temperature of the surfaces facing the thermal zone are required if the uniform radiosity ( $a$ ), the nonlinear Stefan-Boltzmann approach with



explicit modelling of the enclosure (*b.1*), and the linear one (*c.1*) are assumed; they are usually derived from the specific surface heat balances.

The radiant enclosure can be moreover described by means of the mean radiant temperature (approaches *b.2* and *c.2*), which is defined as an area- and emissivity-weighted average value of the surfaces facing the thermal zone [102,133]. The mean radiant temperature can be also calculated as an radiant heat transfer coefficients-weighted average value [213].

#### *Calculation parameters*

The introduction of the radiant heat transfer coefficient ( $h_r$ ) is generally linked to the linearisation of the longwave heat transfer phenomenon. For consistency with the other linear terms of the surface heat balance (e.g., heat convection), the radiant heat transfer coefficient may also be employed in the nonlinear longwave heat transfer description (approach *b*). In this case, the radiative coefficient is determined iteratively during the timestep by solving the fourth-power Stefan-Boltzmann law. If not used in this way but in the linearised Stefan-Boltzmann law approach (*c*), the radiant heat transfer coefficient is generally calculated by means of an approximation of the Stefan-Boltzmann law [130–132], described as in Section 4.3.1.1 in Equation (5). Following this approach, the linear radiant heat transfer coefficient depends on the surface emissivity and on the mean temperature between the considered surface and the participating surface(s). The  $h_r$  can be assumed variable or constant over the simulation period. In the first case, the radiative coefficient is calculated by considering the temperatures at the previous timestep. In the second case, the radiative coefficient is calculated considering static conditions; in this case, the  $h_r$  is calculated ones at the beginning of the simulation, or it can be updated periodically during the simulation [97]. Initial temperatures and specific surface emissivities are used for example in TRNSYS [23], while reference conditions are used in the EN ISO 13798 technical standard [134]; in particular, a reference surface emissivity equal to 0,9 is assumed in the indoor  $h_r$  determination, as well as a 20 °C mean temperature of the surface and the radiant enclosure. Finally, the radiant heat transfer coefficient can be coupled with the convective heat transfer coefficient, and it can be considered either variable or constant during the simulation period.

The other dependent parameter is the view factor to other surfaces. Many approaches for the view factor determination were documented; in particular, it be calculated by means of exact calculations, or through approximated definitions [133]. Among the exact definition approaches, ray-tracing methods, integral expressions, and the so called “grey interchange factor” methods [214] were documented. In ray-tracing methods, the view factor to other surfaces is computed

by recording the interactions of a large number of rays shot from random points on the considered surface at random angles into the 3D environment [215]. If ray-tracing methods provide a purely geometric value, the “grey interchange factor” method allows to determine an exchange coefficient that includes all exchange paths between a pair of surfaces, i.e., all reflections, absorptions, and re-emission [214]. It is thus reasonable to state that the “grey interchange factor” accounts for both the geometric view factor and the emissivity of the surfaces. This approach is implemented in EnergyPlus [107]. Finally, the view factors can be determined by means of the classical integral expression formulation.

On the other hand, the view factor determination can be simplified using an area-weighted calculation [39]. Otherwise, tabular view factors can be employed for simplified geometries.

#### **4.3.6.2 Indoor surface vs. furniture**

Furnishings increase the surface area participating in the internal longwave radiation and convection heat exchange, as well as the thermal heat capacity of the thermal zone. While other approaches only account for the increase of thermal heat capacity (Section 4.3.9), equivalent planar element approaches [216] allow also to model the furniture involvement in the longwave radiation heat transfer. In particular, the modelled planar element representing the furnishings can be modelled as a geometrical element, or as a virtual element.

The former approach, developed by Raftery et al. [217], consists in the geometric representation and location of the furniture inside the thermal zone [216]. This allows to account for the effect of direct and diffuse solar radiation on furnishing, as well as for the shading on other surfaces in the zone [217]. In the latter approach, instead, the furniture are not geometrically represented in the thermal zone, meaning that they are not taken into account for the internal solar distribution [216].

#### **4.3.6.3 Indoor surface vs. internal sources**

The classical, and only documented, procedure for modelling the longwave radiation from internal sources is to define a radiative/convective split for the zone equipment heat gain. The radiative heat gains are distributed over the surfaces facing the thermal zone by considering an area- and emissivity-based distribution [107], or a uniform distribution (i.e., area-weighted) [5].

Table 10: Internal longwave radiation heat transfer

Phenomenon modelling	Driving forces		Calculation parameters	
	Determination	T.D.	Determination	Model
<b>Indoor surfaces vs. indoor surfaces</b>				
<b>a) Uniform radiosity</b>				
<b>b) Stefan-Boltzmann (SB) law</b>				
b.1) Enclosure explicit modelled	» Other surface temperatures derived from energy balance	$\nu$	<b>Radiative heat transfer coefficient</b>	$\nu$
b.2) Enclosure implicit modelled	» Mean radiant temperature	$\nu$	» SB law (iterative determination)	$b$
	» Air temperature	$\nu$	» Approximated SB law	$c$
			- From previous timestep	$c$
			- At initial temperature	$c$
			- At reference conditions	$c$
			» Coupled with heat convection	$\nu, c$
<b>c) Linearised SB law</b>				
c.1) Enclosure explicit modelled			<b>View factor to other surfaces</b>	
c.2) Enclosure implicit modelled			» Exact definition	$c$
c.3) Aggregated with heat convection			- Ray-tracing method	$a, b, c$
			- "Grey interchange factor"	
			- Integral expression	
			» Approximated definition	$c$
			- Area-weighted calculation (approx. integral expression)	$a, b, c$
			» Tabular	$c$
				$a, b, c$
<b>Indoor surfaces vs. furnitures</b>				
<b>a) Equivalent planar element<sup>1</sup></b>				
a.1) Geometrical element <sup>2</sup>	<b>Furniture temperature</b>	$\nu$		$a$
a.2) Virtual element <sup>3</sup>	» Derived from energy balance	$\nu$		$a$
	» Mean radiant temperature	$\nu$		$a$
<b>Indoor surfaces vs. internal sources</b>				
<b>a) Radiative fraction of heat gain on surface node</b>				
	<b>Heat gain</b>	$\nu, c$	<b>Distribution of radiative fraction on internal surfaces</b>	
	» Calculated	$\nu, c$	» Area- and emissivity-based distribution	$c$
	» Tabular	$\nu, c$	» Uniform distribution (area-weighted)	$c$
	<b>Radiative fraction</b>			$a$
	» Tabular	$\nu, c$		$a$

**Notes**<sup>1</sup> Once modelled, they interact with the indoor surfaces as classical surfaces<sup>2</sup> This approach also accounts for the computation of the beam solar irradiance reaching internal surfaces, diffuse solar irradiance and radiant mean temperature [217]<sup>3</sup> This approach does not account for the internal solar distribution, while the equivalent furniture element interacts with the enclosure by radiation heat transfer and with the air node by convection [216]

### 4.3.7 Internal shortwave radiation heat transfer

In practise, after its transmission through the transparent building envelope components, solar radiation is partly absorbed by interior surfaces, transmitted through adjacent zones and back out through transparent envelope components, and a part is transmitted to internal air [103,218,219]. Among these processes, the latter represent a solar convective heat gain immediately delivered to the indoor air [216], which is not involved in the radiant heat transfer with internal surfaces; this process is thus analysed in Section 4.3.8.3. As for the other processes, some of them may be neglected in building energy modelling, according to the calculation method adopted.

Early models have considered the transmitted beam solar irradiance leaves the inner glass surface as diffuse solar radiation into the indoor space [220]; however, this assumption is generally not applied in current building energy models, and the exterior windows are considered the source for beam and diffuse solar radiation [221]. The two components are generally considered separately; the modelling options and assumptions concerning the transmitted beam solar radiation are analysed in Section 4.3.7.1, while in Section 4.3.7.2 the diffuse solar radiation is deepened.

#### 4.3.7.1 Indoor surfaces vs. sun and other objects (beam reflection)

##### *Modelling of the phenomenon*

Although the processes of absorption and re-transmission of solar radiation are phenomena of a different nature, their modelling is closely related. Generally, the absorbed solar irradiance is modelled as a separate term of the indoor surface heat balance (approach a in Table 11); then, it is re-emitted as longwave radiation and released to the air by convection [133]. Two variants in the application of this approach were documented and are presented below (referred as in Table 11).

- a.1) *Solar irradiance back reflected*: in this approach, the interior surfaces are assumed to act as grey bodies, thus part of the incident solar irradiance is reflected from the surface outside toward windows, or to adjacent thermal zones through interior windows. This component is usually referred as “back reflection”, and it is determined by means of the optical glass properties (Sections 4.3.4.1 and 4.3.4.2),
- a.2) *Solar irradiance all absorbed*: in this approach, a black body cavity approach is considered; thus, incident solar radiation is completely absorbed by the internal surfaces, and no back reflection is considered. This is the case of technical standards such as EN 13790 [10] and EN ISO 52016-1 [5].

*Driving forces*

The thermal constraint involved in the here presented physical process is the beam solar irradiance transmitted through the building transparent components, determined as described in Section 4.3.4.1.

*Calculation parameters*

Beside the consideration or not of the back reflection process, the main issue related to the absorption of solar irradiance on internal surface is its distribution. The fraction of beam solar radiation incident on the interior surfaces (considered here as a calculation parameter) can be defined through different approaches. The more accurate approach consists in the definition of beam sun patches that are formed as the beam solar irradiance is transmitted through external windows [222]. This approach considers the fact that the transmitted solar beam is directional and strikes defined locations on internal surfaces [220]; ray-tracing [138,223], pixel counting [104], or geometrical methods [23,107,224] are generally employed for the sun patches definition. Although they allows to describe the distribution of beam solar irradiance in a realistic way, these approaches require a high computational time to trace beam solar rays, as well as detailed geometrical information with regard to internal surfaces [222]. In compliance with the commonly adopted assumption of isothermal surfaces, the beam solar radiation that hits an internal surface (sun patch) is then uniformly distributed over the surface.

Simplified beam solar irradiance distribution on internal surfaces were documented; in particular, it can be uniformly distributed (i.e., area-weighted distribution [222]), or distributed assigning precalculated fractions [225]. The most simplified approach is one of the procedures implemented in EnergyPlus [107], in which the beam solar irradiance is assumed to fall all on floor.

According to the generally adopted grey body assumption, purely diffuse reflection process is considered for surfaces. In this sense, beam solar irradiance is generally traced from the point where it leaves the interior surface of the transparent envelope components to its first encounter surface inside the enclosure [221], and then it is reflected and converted as diffuse solar radiation. This is then distributed over the interior surfaces, as described in Section 4.3.7.2.

**4.3.7.2 Indoor surfaces vs. sky vault, ground and other objects (diffuse reflection)**

The process of absorption of diffuse solar irradiance on internal surface is equal to the absorption of beam irradiance. They differ in the approaches for distribution of the diffuse solar radiation. Due to the angular independent nature of diffuse radiation, simplified approaches can be used to define the distribution of diffuse

solar irradiance on internal surfaces. In particular, it can be distributed based on a view factor-based distribution [220], and area- and solar absorptance-weighted distribution [107,224], a uniform distribution [5], and fraction on surfaces.

Table 11: Internal shortwave radiation heat transfer

Phenomenon modelling	Driving forces		Calculation parameters	
	Determination	T.D.	Determination	T.D.
<b>Indoor surfaces vs. sun (beam solar irradiance)</b>				
<b>a) Absorbed solar irradiance as separate HB term</b>				
a.1) Solar irradiance back reflected	<i>Transmitted beam solar irradiance</i> Section 4.3.4.1, Table 8		<i>Distribution of beam solar irradiance on internal surfaces</i>	
a.2) Solar irradiance all absorbed			» Sun patches definition - Ray tracing method - Pixel counting method - Geometrical methods » Uniform distribution (area-weighted) » Fixed fraction on surface » All on floor	$\nu$     $c$ $c$ $c$
<b>Indoor surfaces vs. sky vault (diffuse solar irradiance) / vs. ground (diffusely reflected solar irradiance)</b>				
<b>a) Absorbed solar irradiance as separate HB term</b>				
a.1) Solar irradiance back reflected	<i>Transmitted diffuse solar irradiance</i> Section 4.3.4.2, Table 8		<i>Distribution of diffuse solar irradiance on internal surfaces</i>	
a.2) Solar irradiance all absorbed			» View factor-based distribution » Area- and absorptance-weighted distribution » Uniform distribution (area-weighted) » Fixed fraction on surface	$c$ $c$ $c$ $c$

### 4.3.8 Internal heat convection

Internal heat convection is involved in the interaction between different components. Firstly, indoor surfaces exchange with indoor air by convection (Section 4.3.8.1); moreover, a fraction of internal heat gains is generally considered as convective, and it is loaded on the indoor air node (Section 4.3.8.2), as well as a fraction of solar heat gains in a few calculation methods (Section 4.3.8.3). The modelling assumptions relative to the internal heat convection are presented in Table 12.

#### 4.3.8.1 Indoor surfaces vs. indoor air

##### *Modelling of the phenomenon*

The heat flux transferred between the indoor surface and the environment due to heat convection is generally determined by means of the classical Newton's law, as presented in Equation (15),

$$q_{\text{conv,int}} = h_{\text{c,int}} \cdot (\theta_{\text{surf,int}} - \theta_{\text{air}}) \quad (15)$$

where  $h_{\text{c,int}}$  is the convective heat transfer coefficient (in  $\text{W} \cdot \text{m}^{-2} \text{K}^{-1}$ ), and  $\theta_{\text{surf}}$  and  $\theta_{\text{air}}$  are the indoor surface and the ambient temperatures (in  $^{\circ}\text{C}$ ), respectively. The only involved calculation parameter is the convective heat transfer coefficient, which can be calculated by means of different approaches, as presented below.

##### *Driving forces*

The use of a reference temperature different from the mean zone air temperature as driving force for the internal heat convection, such as local, supply, or return air temperature, has been widely discussed, such as in the research of Spitler et al. [226] and Fisher and Pedersen [227]. However, this does not comply with the well-mixed zone air temperature assumption [228], thus the mean zone air temperature is generally assumed.

##### *Calculation parameters*

As well known, the internal heat convection can be driven by natural or forced constraints; contrary to the external heat convection, buoyancy-driven heat convection is dominant in indoor applications [229], even if mechanical forces cannot be neglected. Thus, the convective heat transfer coefficients can be determined for mixed convection, natural convection, or forced convection, by means of specific correlations.



The convective coefficients for mixed convection are generally calculated by blending two different coefficients for natural and forced convection, respectively, as specified in Equation (16) [230],

$$h_{c,int} = \left( h_{c,int,nat}^n + h_{c,int,for}^n \right)^{\frac{1}{n}} \quad (16)$$

where  $h_{c,int}$  is the internal convective heat transfer coefficient (in  $\text{W} \cdot \text{m}^{-2} \cdot \text{K}^{-1}$ ) for natural (nat) and forced (for) convection, respectively. These coefficients can be calculated by means of specific correlations developed for both natural and forced convection, which are described below.

As regard natural convection, the existing correlations for the derivation of the heat transfer coefficient generally depending different parameters that have been widely discussed by Peeters et al. in [231], including temperature difference between the surface and the air, the geometric characteristic of the surface, the heat flow direction, and the position of the surface compared to the location of the heat emitters; the latter parameter accounts for the fact that the overall airflow pattern affects the flow on a specific surface [228]. Based on these dependent parameters, convective heat transfer coefficients can be derived by means of flat-plates (i.e., assuming that the convective heat transfer at the surfaces of an enclosure is the same as that along isolated flat plates [228]) or experimental correlations, and are usually variable on a timestep basis.

Both flat-plate and experimental correlations can be applied to derive convective heat transfer coefficients for forced convection. They generally depend on the different parameters and conditions [231], such as the heat flow direction, the ventilation rates, the geometric characteristic of the surface, and the type and location of HVAC emitters.

For more details on the specific correlations, the reader may refer to the research of, but not limited to, Peeters et al. [228], Camci et al. [229], and Khalifa for isolated vertical and horizontal surfaces [232], and surfaces in two- and three-dimensional enclosures [233].

In simplified approaches, constant values for the convective heat transfer coefficients are generally assumed. This is the case, for example, of the EN ISO 52016-1 hourly method [5], which implements constant convective heat transfer coefficients depending on the heat flow direction, as specified by the EN ISO 6946 technical standard [132]. Moreover, Camci et al. [229] reviewed a large number of constant convective heat transfer coefficients for specific and limited boundary conditions and applications.

#### **4.3.8.2 Indoor air vs. internal sources**

The classical, and only documented, procedure for modelling the convection heat transfer from internal sources is to define a radiative/convective split for the zone equipment heat gain; then, the convective fraction of heat gains is loaded on the zone air node.

#### **4.3.8.3 Indoor air vs. sun, sky vault, ground, and other objects (solar radiation)**

In some simplified calculation methods, a fraction of the radiation entering through a glazing which is immediately delivered as a convective heat flow to the indoor air [234]. This fraction is defined by means of a solar to air factor, depending on the presence of carpets or furniture [216]. Tabular values for the solar to air factor are generally assumed; for example, a 0,1 value is specified in EN ISO 52016-1 [5].

Table 12: Internal heat convection

Phenomenon modelling		Driving forces		Calculation parameters			
		Determination	T.D.	Model			
Indoor surfaces vs. air							
a) <i>Newton law</i>		<i>Air temperature</i> » Mean air temperature	<i>v</i>	<i>a</i>	<i>Convective heat transfer coefficient</i> » Mixed convection » Natural convection <sup>1,2</sup> <ul style="list-style-type: none"><li>- Dependent on temperature difference</li><li>- Dependent on heat flow direction</li><li>- Dependent on surface geometry</li><li>- Dependent on the surface position <sup>3</sup></li></ul> » Forced convection <sup>1,4</sup> <ul style="list-style-type: none"><li>- Dependent on heat flow direction</li><li>- Dependent on ventilation rates</li><li>- Dependent on surface geometry</li><li>- Dependent on heat emitters <sup>5</sup></li></ul> » Combined with longwave radiation » Reference value <sup>6</sup>	<i>v</i> <i>v, c</i>  <i>v, c</i>  <i>v, c</i> <i>c</i>	<i>a</i>      <i>a</i>     <i>a</i> <i>a</i>
Internal sources vs. air							
a) <i>Convective fraction of heat gain on air node</i>		<i>Heat gain</i> » Calculated (e.g., heat gain from occupants) » User defined » Tabular  <i>Convective fraction</i> » Tabular	<i>v, c</i> <i>v, c</i> <i>v, c</i>	<i>a</i> <i>a</i> <i>a</i>			
Sun, sky vault, ground, and other objects vs. air							
a) <i>Convective fraction of solar radiation on air node</i>		<i>Solar to air factor</i> » Tabular	<i>c</i>	<i>a</i>			

**Notes**

<sup>1</sup> Either experimental or similarity-based correlations (the latter derived from flat plate or enclosure theory, neglecting the potential impact of airflow at adjacent surfaces)

<sup>2</sup> Dependent variables can be coupled according to the considered correlations

<sup>3</sup> Position of the surface respect to the location of the heat emitters

<sup>4</sup> Dependent variables can be coupled according to the considered correlations

<sup>5</sup> Type and position of heat emitters

<sup>6</sup> Dependent on heat flux direction, or defined for specific conditions and boundary conditions

### 4.3.9 Heat storage

Beside heat storage in the building envelope components, objects inside the thermal zone add participating thermal mass that increases the thermal heat capacity of the zone. In particular, the internal thermal mass is composed of all the furnishing elements, the finishing parts that are not directly integrated in the building envelope (e.g., carpets, drapery, etc.), and other objects (e.g., books, small appliances, etc.).

A realistic modelling of indoor thermal mass would require the knowledge of the placement, the geometries, and the surface temperature of all objects, resulting in complex systems [107,216]; it is thus commonly adopted to simplify these systems.

Generally, the existing approaches for the modelling the heat storage in indoor thermal mass assume that this does not participate in any of the heat transfer processes inside the thermal zone, i.e., heat convection, longwave radiation heat transfer, and distribution of solar (shortwave) radiation. The existing approaches, which can be classified as lumped capacitance methods, describe the indoor thermal mass as an additional capacitance that is added either to the inner node of building envelope surfaces [235] or to the air node. In the former approach, the heat capacity of the furniture and other objects affects the heat conduction process in the building envelope components, and thus the inner surface temperatures. In the latter, the indoor thermal mass is assumed to be perfectly isothermal and in equilibrium with the indoor air node [216]; thus, the heat capacity of the furniture and other objects is added to the air volume heat capacity. This approach is implemented in the simplified EN ISO 52016-1 hourly method [5], while it is one of the modelling options considered in the detailed dynamic methods of EnergyPlus [92] and TRNSYS [23].

The furniture and other objects heat capacity can be calculated from internal mass characteristics (i.e., material and thickness hypothesis) or a reference value can be assumed. In particular, in the EN ISO 52016-1 technical standard a reference value of  $10 \text{ kJ} \cdot \text{m}^{-2} \cdot \text{K}^{-1}$  is adopted. It includes both air and furniture heat capacity, and it is calculated assuming an (average) net height of the thermal zone of 2,4 m (approx.  $3 \text{ kJ} \cdot \text{m}^{-2} \cdot \text{K}^{-1}$ ), and a default value for the furniture (approx.  $7 \text{ kJ} \cdot \text{m}^{-2} \cdot \text{K}^{-1}$ ), the determination of which is not specified.

More complete approaches accounting for these physical processes are presented in Sections 4.3.6.2.

## 4.4 Conclusion

In the present chapter, the existing modelling assumptions relative to the building fabric and its interaction with the indoor and outdoor environment were documented and analysed. This cataloguing of modelling option was intended to make the users aware of the existing simplifications found in literature or implemented in a given calculation model, or to guide them in the choice of this or another modelling options. Moreover, it also allows to provide the developers of a well-documented set of implementation options for choosing the ones that allow to guarantee the expected model requirements.

Although this cataloguing of modelling assumption was extended to different calculation models (implemented in simulation tools and in standardised documents, or developed in standalone research), a special focus was given to the EN ISO 52016-1 [5]. In fact, starting from this documentation, the modelling assumptions of the EN ISO 52016-1 hourly method are compared to the ones of the reference model of EnergyPlus [92] in Chapter 5, in order to address its validation.

# **Chapter 5**

## **Validation of the EN ISO 52016-1 simplified dynamic method**

### **5.1 Introduction**

Part of the work described in this chapter has been previously published in international peer-reviewed journals [7,8,236] or presented at international conferences [91,237,238].

The simplified dynamic method introduced by the EN ISO 52016-1 technical standard [5] challenges the need for too detailed input data from the user [34], typical of the detailed dynamic methods, relying on assumptions and simplifications selected as to guarantee a balance between the accuracy and the simplicity of the assessment. However, these may lead to inaccurate predictions in the energy consumption of buildings in both design phases and energy audits. The validation of the method may play a crucial role in fostering its application in legislative framework and, eventually, its implementation to increase the expected accuracy. The present chapter presents the accuracy assessment of the simplifications related to the modelling of the building fabric introduced by the simplified dynamic method.

In Section 5.2, an overview of the EN ISO 52016-1 hourly method is provided; specifically, its main modelling simplifications, as well as the improved modelling options proposed by the Italian National Annex to the technical standard, were thoroughly analysed and compared with the reference model of EnergyPlus.

Section 5.3 presents the evaluation of the simplified heat conduction model proposed by the standard method; this was conducted on five building construction archetypes, firstly through a stand-alone construction analysis then extended to a simple, basic enclosed office. In Section 5.4, the validation of the simplifications concerning the modelling of external and internal driving forces is presented. To guarantee a general validity of the outcomes, different building uses, levels of thermal insulation, and climatic zones (for a total of eight case studies) were considered. Section 5.5 addresses the open issues concerning to the building energy model calibration (underlined in Section 2.4) by presenting a collective calibration exercise performed on an existing nearly zero-energy residential building. The building was furthermore considered in the evaluation of the certain EN ISO 52016-1 modelling assumptions (i.e., related to those parameters identified as most influencing on the thermal behaviour of the analysed building). In Section 5.6, the effects of improved modelling options, introduced by the Italian National Annex, on the thermal energy needs of a residential building is provided. Finally, Section 5.7 discusses the suitability of the tested modelling assumptions for different purposes, and conditions, and Section 5.8 summarises the main outcomes of the analysis presented in the chapter.

## **5.2 The simplified hourly method**

The international standards developed under European Commission Mandate M/480 [239] are aimed to harmonise the methodology for assessing the energy performance of buildings by developing detailed calculation models that meet requirements for accuracy, simplicity, robustness, and transparency. Among them, the EN ISO 52016-1 technical standard [5] specifies two different calculation methods; a quasi-steady state monthly method, and a simplified hourly method. The latter is aimed at calculating indoor temperatures and hourly energy loads and needs for heating and cooling, accounting also for the dynamic effects that hourly variations of the climatic condition and building operation have on the aforementioned parameters. The EN ISO 52016-1 simplified dynamic method is based on the EN ISO 52017-1 technical standard [20], which specifies general assumptions, boundary conditions and equations.

In the following paragraphs, an overview of the simplified dynamic method is provided, with a specific regard to the required input data and to the calculation workflow (i.e., energy balance at zone level and at building construction level, and calculation of indoor operative and mean radiant temperatures).

*Input data*

As a simplified dynamic method, the EN ISO 52016-1 hourly method is based on different modelling assumptions and simplifications (which are thoroughly described in Section 5.2.1) chosen so as to reach a so-called “balanced accuracy” [34], namely a sufficient accuracy with a minimum of required input data. Indeed, the input data required are generally equivalent to the input data for the quasi-steady state monthly method, also provided by the technical standard. These regard external climatic conditions (e.g., dry bulb temperature, wind speed, solar irradiance for different orientations, etc.), geometrical data (e.g., floor area, volume, etc.), building’s operational data (e.g., set-point temperature, internal gains, air and furniture heat capacity, etc.), and thermophysical properties of the building components. Differently from the detailed dynamic methods, the thermal transmittance (or resistance) and the areal heat capacity are the only parameters required by the EN ISO 52016-1 model to describe the building components; in fact, neither component’s layers information nor their thermophysical properties are needed. This aspect is attractive especially for its application to existing buildings, generally characterised by a low availability of input data.

*Calculation workflow – General procedure*

Based on the input data presented above, the EN ISO 52016-1 can be applied to calculate, on an hourly basis, the sensible thermal load for space heating and cooling, the latent load for the (de-)humidification, the internal temperature (operative, air and/or mean radiant temperature), the sensible energy need for space heating and cooling, the latent energy need for (de-)humidification, the sensitive and latent design heat load for space heating and cooling and the conditions of the supply air to guarantee any humidification and/or dehumidification. The calculations are performed separately for the different thermal zones, which can be either coupled or not.

For each thermal zone and for each calculation timestep, the internal operative temperature and the heating or cooling loads are calculated applying a step-wise procedure [240], developed on the following steps:

1. Check if heating or cooling is needed (i.e., there is no need for heating/cooling if the indoor operative temperature – calculated in absence of any system – is within the range of the heating and cooling set-point temperatures),
2. Calculate the heating/cooling load if cooling or heating is needed (i.e., the heating or cooling load required to reach the heating or cooling set-point),
3. Check if the available cooling or heating power is sufficient,
4. Calculate the internal temperature, if the available heating or cooling power is insufficient,



5. Calculation of the actual energy load for heating and cooling as output of the calculation.

The EN ISO 52016-1 dynamic method adopts an air heat balance (AHB) algorithm, which is solved on an hourly timestep [33] to estimate the heating and cooling loads to reach the indoor set-point temperature. It is a revised version of the three-node method (5RC1) presented in EN ISO 13790 [10], and it is based on a thermal-electric analogy in which the thermal zone can be represented by a resistive-capacitive node for the internal air and a few nodes for each building component [241]. Differently from the EN ISO 13790 method, each building element is considered separately (not aggregated to a few lumped parameters [33]), and are described by a variable number of resistive-capacitive nodes.

*Calculation workflow – Energy balance on zone level*

The indoor air temperature is calculated, at each timestep, by solving an AHB equation on the air node, which considers the zone heat capacity (i.e., air, furniture), the heat exchanged by convection with the surfaces facing the zone, the ventilation heat transfer, and the convective heat gains. The AHB equation is presented in Equation (17),

$$\left[ \frac{C_{\text{int},ztc}}{\Delta t} + \sum_{eli=1}^{eln} (A_{eli} \cdot h_{ci,eli}) + \sum_{ven=1}^{ven} H_{ve,vei,t} + H_{tr,tb,ztc} \right] \cdot \theta_{\text{int},a,ztc,t} =$$

$$\frac{C_{\text{int},ztc}}{\Delta t} \cdot \theta_{\text{int},a,ztc,t-1} + \sum_{eli=1}^{eln} (A_{eli} \cdot h_{ci,eli} \cdot \theta_{pln,eli,t}) + \sum_{ven=1}^{ven} (H_{ve,vei,t} \cdot \theta_{\text{sup},vei,t}) +$$

$$+ H_{tr,tb,ztc} \cdot \theta_{\text{ext},a,ztc,t} + f_{\text{int},c} \cdot \Phi_{\text{int},ztc,t} + f_{\text{sol},c} \cdot \Phi_{\text{sol},ztc,t} + f_{\text{H/C},c} \cdot \Phi_{\text{H/C},ztc,t} \quad (17)$$

where, for each thermal zone  $ztc$  at timestep  $t$ :

$C_{\text{int},ztc}$  is the internal thermal capacity of the zone (in  $\text{J} \cdot \text{K}^{-1}$ ), which should include both air and furniture thermal capacity,

$\Delta t$  is the length of the timestep  $t$  (in s),

$\theta_{\text{int},a,ztc,t}$  is the internal air temperature (in  $^{\circ}\text{C}$ ),

$\theta_{\text{int},a,ztc,t-1}$  is the internal air temperature at the previous timestep (in  $^{\circ}\text{C}$ ),

$A_{eli}$  is the area of the building element  $eli$  (in  $\text{m}^2$ ),

$h_{ci,eli}$  is the internal convective heat transfer coefficient at building element  $eli$  (in  $\text{W} \cdot \text{m}^{-2} \cdot \text{K}^{-1}$ ),

$\theta_{pln,eli,t}$  is the internal surface temperature of the building element  $eli$  (in  $^{\circ}\text{C}$ ),

$H_{ve,k,t}$  is the heat exchange coefficient by ventilation for the ventilation flow  $k$  (in  $\text{W} \cdot \text{K}^{-1}$ ),

$\theta_{\text{sup},k,t}$  is the supply temperature of the ventilation flow  $k$ ,

$\theta_{\text{e},a,t}$  is the external air temperature (in  $^{\circ}\text{C}$ ),

$H_{tr,tb,ztc}$  is the overall heat transfer coefficient for thermal bridges (in  $W \cdot K^{-1}$ ) – directly thermally coupled to the internal and outdoor temperatures – obtained by means of the length and the linear thermal transmittance (obtained from the EN ISO 13789 technical standard [134]) for the considered thermal bridges,

$f_{int,c,ztc}$ ,  $f_{sol,c,ztc}$ , and  $f_{H/C,c,ztc}$  are the convective fraction of internal gains, solar radiation, and heating/cooling system respectively, and

$\Phi_{int,ztc,t}$ ,  $\Phi_{sol,ztc,t}$ , and  $\Phi_{H/C,ztc,t}$  are the total internal heat gains, the directly transmitted solar heat gain into the zone, and the heating/cooling load at timestep  $t$  (in W).

#### *Calculation workflow – Energy balance on building element level*

Simultaneously, a heat balance at each building construction adjacent to the zone is solved. Specifically, each of the nodes representing a building component is involved in a heat balance by means of different equations depending on the position of the node (i.e., indoor surface, outdoor surface, internal). At the indoor surface node, the heat balance accounts for the convective heat transfer with the indoor air, the longwave radiation exchanged with the other components indoor surface nodes, and the radiative fraction of the internal heat gains; similarly, the heat balance at the outdoor surface node accounts for the convective heat transfer with the outdoor air, the longwave radiation exchanged with the outdoor environment (e.g., sky vault, ground, etc.), and the absorption of solar (shortwave) radiation. Finally, the heat balance at the internal nodes (i.e., nodes within building structure) consider the conductive heat exchanges with adjacent nodes. The heat balance equation at the internal, external, and inside nodes are presented respectively in Equation (18), Equation (19), and Equation (20),

$$\begin{aligned}
 & -\left(h_{pli-1,eli} \cdot \theta_{pli-1,eli,t}\right) + \left[\frac{\kappa_{pli,eli}}{\Delta t} + h_{ci,eli} + h_{ri,eli} \cdot \sum_{eli=1}^{eln} \left(\frac{A_{eli}}{A_{tot}}\right) + h_{pli-1,eli}\right] \cdot \theta_{pli,eli,t} + \\
 & -h_{ci,eli} \cdot \theta_{int,a,ztc,t} - \sum_{eli=1}^{eln} \left(\frac{A_{eli}}{A_{tot}} \cdot h_{ri,eli} \cdot \theta_{pli,eli,t}\right) = \frac{\kappa_{pli,eli}}{\Delta t} \cdot \theta_{pli,eli,t-1} + \\
 & + \frac{1}{A_{tot}} \cdot \left[\left(1 - f_{int,c}\right) \cdot \Phi_{int,ztc,t} + \left(1 - f_{sol,c}\right) \cdot \Phi_{sol,ztc,t} + \left(1 - f_{H/C,c}\right) \cdot \Phi_{H/C,ztc,t}\right]
 \end{aligned} \tag{18}$$

$$\begin{aligned}
& \left[ \frac{\kappa_{pli,eli}}{\Delta t} + h_{ce,eli} + h_{re,eli} + h_{pli,eli} \right] \cdot \theta_{pli,eli,t} - h_{pli,eli} \cdot \theta_{pli+1,eli,t} = \\
& = \frac{\kappa_{pli,eli}}{\Delta t} \cdot \theta_{pli,eli,t-1} + (h_{ce,eli} + h_{re,eli}) \cdot \theta_{e,t} + \\
& + \alpha_{sol,pli,eli} \cdot (I_{sol,dif,eli,t} + I_{sol,dir,eli,t} \cdot F_{sh,obst,eli,t}) - \Phi_{sky,eli,t}
\end{aligned} \tag{19}$$

$$\begin{aligned}
& - (h_{pli-1,eli} \cdot \theta_{pli-1,eli,t}) + \left[ \frac{\kappa_{pli,eli}}{\Delta t} + h_{pli,eli} + h_{pli-1,eli} \right] \cdot \theta_{pli,eli,t} + \\
& - h_{pli,eli} \cdot \theta_{pli+1,eli,t} = \frac{\kappa_{pli,eli}}{\Delta t} \cdot \theta_{pli,eli,t-1}
\end{aligned} \tag{20}$$

where:

$pli$  is the number of node (from  $pli = 1$  for external surface nodes to  $pln$  – total number of nodes – for internal surface nodes),

$A_{elk}$  is the area of the building element  $k$  (in  $m^2$ ),

$A_{tot}$  is the sum of the areas of  $A_{elk}$  of all building elements (in  $m^2$ ),

$\theta_{pli,eli,t}$  is the temperature at node  $pli$  (in  $^{\circ}C$ ),

$\theta_{pli-1,eli,t}$  is the temperature at node  $pli-1$  (in  $^{\circ}C$ ),

$\theta_{pli+1,eli,t}$  is the temperature at node  $pli+1$  (in  $^{\circ}C$ ),

$h_{pli,eli}$  is the conductance between node  $pli+1$  and  $pli$  (in  $W \cdot m^{-2} \cdot K^{-1}$ ), derived from the component overall thermal resistance as specified in Section 5.2.1.5 (or in Section 5.2.2.1 for the Italian National Annex approach),

$h_{pli-1,eli}$  is the conductance between node  $pli$  and  $pli-1$  (in  $W \cdot m^{-2} \cdot K^{-1}$ ), derived from the component overall thermal resistance as specified in Section 5.2.1.5 (or in Section 5.2.2.1 for the Italian National Annex approach),

$\kappa_{pli,eli}$  is the areal heat capacity of node  $pli$  (in  $J \cdot m^{-2} \cdot K^{-1}$ ), derived from the component overall heat capacity as specified in Section 5.2.1.5 (or in Section 5.2.2.1 for the Italian National Annex approach),

$h_{ci,eli}$  and  $h_{ri,eli}$  are respectively the internal convective and radiative surface heat transfer coefficients (in  $W \cdot m^{-2} \cdot K^{-1}$ ),

$\theta_{pli,eli,t-1}$  is the temperature at node  $pli$  at previous timestep  $t-1$  (in  $^{\circ}C$ ),

$f_{int;c;ztc}$ ,  $f_{sol;c;ztc}$ , and  $f_{H/C;c;ztc}$  are the convective fraction of internal gains, solar radiation, and heating/cooling system respectively,

$\Phi_{int;ztc,t}$ ,  $\Phi_{sol;ztc,t}$ , and  $\Phi_{H/C;ztc,t}$  are the total internal heat gains, the directly transmitted solar heat gain into the zone, and the heating/cooling load at timestep  $t$  (in  $W$ ),

$\theta_{int;a;ztc,t}$  is the internal air temperature (in  $^{\circ}C$ ),

$\theta_{e;a,t}$  is the external air temperature (in °C),  
 $h_{ce;eli}$  and  $h_{re;eli}$  are respectively the external convective and radiative surface heat transfer coefficients (in  $\text{W} \cdot \text{m}^{-2} \cdot \text{K}^{-1}$ ),  
 $a_{sol;eli}$  is the solar absorption coefficient at the external surface,  
 $I_{sol;dir;tot;eli;t}$  and  $I_{sol;dif;tot;eli;t}$  are respectively the beam and diffuse solar irradiance on the element  $eli$  (in  $\text{W} \cdot \text{m}^{-2}$ ),  
 $F_{sh;obst;eli;t}$  is the shading reduction factor for external obstacles for the element, and  
 $\Phi_{sky;eli;t}$  is the total extra thermal radiation to sky (in  $\text{W} \cdot \text{m}^{-2}$ ).

*Calculation workflow – Calculation of mean radiant and operative temperature*

As previously said, the outcome of the energy balance at the zone level is the indoor air temperature; the internal surface temperatures, instead, are the outcomes of the energy balance solved at each building surface. The mean radiant and the operative temperatures are derived from these outcomes. Specifically, the mean radiant temperature is calculated as the area-weighted average value of the internal surface temperatures of all building elements (facing the thermal zone). The operative temperature, instead, is calculated as an arithmetic average of the indoor air and the mean radiant temperatures.

To ensure the compliance with the requirements of robustness, unambiguity, and transparency, all the technical standards developed under mandate M/480 [239] follow specific rules [33]; they also provide a discrete flexibility that allows specific choices based on the national or regional context [242] through the “National Annex” approach [243]. In fact, all EPB (Energy Performance of Buildings) standards contain a legislative annex (Annex A) – providing a template to be used to specify the national or regional choices [20] – and an informative annex (Annex B), which provides default choices for all options, boundary conditions and input data presented in Annex A. However, these choices are based on the expert awareness, and not on studies involving national preferences and limitations [243]. Each Member State can thus replace the default choices for the assessment of the energy performance in the context of their building regulations, and is obligated to describe the deviations of the national choices from the default ones [244] by means of National Annexes (NA) or National Data Sheets. Therefore, National Annexes may contain information on those data and options, such as modelling options, parameters, and boundary conditions, where alternatives are given in the EPB standards (examples of the type of choices are presented in [245]), and may refer to national standards in place of other EPB standards [243]. This is the case of the Italian National Annex to the EN ISO 52016-1 standard [137], currently at the final drafting stage, which introduces improved options on different aspects of the

building energy performance assessment. In particular, an improved modelling procedure that takes into account the characteristics and mass distribution of the component layer was introduced for the resistive-capacitive nodes determination. Moreover, hourly variations of the sky temperature and of the total solar energy transmittance of the glazed components were introduced. The coupling of the thermally conditioned zones was also specified.

### 5.2.1 Modelling assumptions

As mentioned, the EN ISO 52016-1 hourly method is aimed at reaching a balance between the accuracy of the calculation results and the simplicity of the assessment. To this purpose, it is based on easily available input data, and on different modelling assumptions and simplifications. As prescribed by the EN ISO 52017-1 technical standard, the simplified dynamic method is built upon basic, generally adopted modelling simplifications (introduced in Section 4.2), including (but not limited to) the uniformity of the air temperature through the thermal zone, isothermal zone surfaces, and one-dimensional thermal conduction through the building components. Beside these assumptions, the EN ISO 52016-1 introduces some specific simplifications which are analysed in the present section. In particular, the modelling assumptions are documented and compared with the full detailed dynamic calculation model of EnergyPlus (from Section 5.2.1.1 to Section 5.2.1.8); this theoretical comparison is of crucial importance to address the evaluation of their accuracy, which is carried out in the present Chapter.

#### 5.2.1.1 External longwave radiation heat transfer

The external longwave radiation heat transferred between the surface, the sky, and the ground ( $q_{\text{lwr,ext}}$ , expressed in  $\text{W}\cdot\text{m}^{-2}$ ) is calculated by applying the Stefan-Boltzmann law in EnergyPlus, as presented in Equation (21),

$$\begin{aligned} q_{\text{lwr,ext}} = & F_{\text{gnd}} \cdot \varepsilon \cdot \sigma \cdot (T_{\text{gnd}}^4 - T_{\text{surf,ext}}^4) + F_{\text{sky}} \cdot \varepsilon \cdot \sigma \cdot (T_{\text{sky}}^4 - T_{\text{surf,ext}}^4) + \\ & + F_{\text{air}} \cdot \varepsilon \cdot \sigma \cdot (T_{\text{air,ext}}^4 - T_{\text{surf,ext}}^4) \end{aligned} \quad (21)$$

where  $\varepsilon$  is the surface thermal emissivity,  $\sigma$  is the Stefan-Boltzmann constant ( $5,67 \cdot 10^{-8} \text{ W}\cdot\text{m}^{-2}\cdot\text{K}^{-4}$ ), while  $T_{\text{gnd}}$ ,  $T_{\text{sky}}$ ,  $T_{\text{air,ext}}$  and  $T_{\text{surf,ext}}$  are respectively the ground, the sky, the outdoor air, and the surface temperatures (in K), and  $F_{\text{gnd}}$ ,  $F_{\text{sky}}$  and  $F_{\text{air}}$  are the view factors between the surface and the ground, the sky, and the air, respectively. The linearised formulation is instead applied in the simplified hourly method of the EN ISO 52016-1 technical standard; the  $q_{\text{lwr,ext}}$  (in  $\text{W}\cdot\text{m}^{-2}$ ) is calculated as

$$q_{\text{lwr,ext}} = h_{\text{r,ext}} \cdot (T_{\text{surf,ext}} - T_{\text{air,ext}}) - h_{\text{r,ext}} \cdot F_{\text{sky}} \cdot \Delta T_{\text{sky}} \quad (22)$$

where  $h_{\text{r,ext}}$  is the external radiant heat transfer coefficient (in  $\text{W} \cdot \text{m}^{-2} \cdot \text{K}^{-1}$ ),  $T_{\text{surf,ext}}$  and  $T_{\text{air,ext}}$  are the surface and the outdoor air temperatures (in K), respectively, and  $\Delta T_{\text{sky}}$  is the difference between the outdoor air temperature and the apparent sky temperature (in K). According to this formulation, the outdoor environment is assumed to be at the air temperature. To consider the difference between the sky and the air temperatures, the second term in Equation (22) represents the extra thermal radiation to the sky, namely the correction for the longwave radiation exchanged from the surface to the sky.

The radiant heat transfer coefficient used in Equation (22) is assumed time-independent and is calculated by means of the EN ISO 6946 formulation [132], as

$$h_{\text{r}} = 4 \cdot \varepsilon \cdot \sigma \cdot T_{\text{m}}^3 \quad (23)$$

where  $T_{\text{m}}$  is the average temperature of the surface and of its surroundings (in K). Reference conditions, derived from [134], are assumed in the determination of the external radiant heat transfer coefficient; namely, a surface emissivity equal to 0,9 and a  $T_{\text{m}}$  temperature of 0 °C. Moreover, the determination of the view factor between the surface and the sky, which is used in Equations (21) and (22), takes into account the presence of external obstacles (such shadings or other buildings) in EnergyPlus, while this aspect is not considered in the simplified method.

Finally, the apparent sky temperature is determined by applying a direct model (see Section 4.3.1.1) in the simplified hourly method; in fact, a constant difference between the apparent sky and the air temperature, equal to 11 °C for intermediate climatic zones, is assumed [5]. In EnergyPlus, instead, the sky temperature is determined by applying an atmospheric emissivity model; in particular, the Clark-Allen correlation [246] is applied. Site values and local values (at the height above ground of the surface centroid) of the outdoor air temperature are assumed by the simplified and by the detailed method, respectively.

### 5.2.1.2 External shortwave radiation heat transfer

The solar gains on any exterior surface are a combination of the absorption of direct and diffuse solar radiation both in the EN ISO 52016-1 hourly method and in EnergyPlus. In case of shaded surfaces, both the methods consider the reduction of the direct radiation reaching the surface by means of the sunlit fraction, while the shadowing of the diffuse solar radiation component is considered only by EnergyPlus through a correction factor. This factor takes into account the angle between the surface and the sky, and the radiance distribution of the sky.

### 5.2.1.3 External heat convection

The external convective heat transfer phenomenon is described by means of the classical formulation for the convective heat transfer by both the EN ISO 52016-1 simplified method and the detailed method of EnergyPlus. The areal heat flux transferred between the outdoor surface and the environment ( $q_{\text{conv,ext}}$ , expressed in  $\text{W}\cdot\text{m}^{-2}$ ) is calculated as in Equation (24),

$$q_{\text{conv,ext}} = h_{\text{c,ext}} \cdot (T_{\text{air,ext}} - T_{\text{surf,ext}}) \quad (24)$$

where  $h_{\text{c,ext}}$  is the external convective heat transfer coefficient (in  $\text{W}\cdot\text{m}^{-2}\cdot\text{K}^{-1}$ ), and  $T_{\text{air,ext}}$  and  $T_{\text{surf}}$  are the temperatures (in K) of the outdoor air and of the surface, respectively.

In EN ISO 52016-1, the convective heat transfer coefficient (used in Equation (24)) is defined by applying the wind-speed correlation (forced convection) presented in EN ISO 6946 [132], as

$$h_{\text{c,ext}} = 4 + 4 \cdot v \quad (25)$$

where  $v$  is the wind speed (in  $\text{m}\cdot\text{s}^{-1}$ ). On the other hand, EnergyPlus offers a wide selection of calculation models for the  $h_{\text{c,ext}}$  determination; for the sake of the studies presented in this Chapter, the Thermal Analysis Research Program (TARP) algorithm [247] was assumed as reference. According to the TARP formulation, the external convection is split into its natural and forced components, and  $h_{\text{c,ext}}$  is calculated as the sum of the respective heat transfer coefficients. The forced component is calculated by means of the Sparrow et al. [177] formulation, which takes into account the surface geometrical characteristics, roughness and wind exposure, and the wind speed. The natural component is instead calculated by means of three different formulations for vertical, upward, and downward facing surfaces [247]. In the EN ISO 52016-1 hourly method, a time-independent (constant over the calculation period) convective heat transfer coefficient is assumed, while a timestep variable coefficient is adopted in EnergyPlus, if not explicitly required by the user.

Finally, outdoor air temperatures and wind speed relative to the site (used in Equations (24) and (25)) are considered in the simplified method, while local values calculated at the height above ground of the surface centroid are assumed in EnergyPlus.

### 5.2.1.4 Solar transmission

As far as the definition of the solar radiation entering the zone through the transparent envelope is concerned, the simplified and the detailed methods differ

under two main aspects. Firstly, the total transmitted solar radiation is assumed to be completely shortwave radiation in EN ISO 52016-1, while EnergyPlus accounts for the effect of the secondary heat transfer toward the inside (see Section 4.3.4).

Secondarily, the solar properties of windows are considered solar angle-dependent in EnergyPlus, and are determined by means of the Fresnel's equation, while a weighted time average value of the total solar energy transmittance ( $g$ -value or  $SHGC$ ) is assumed over the simulation period in EN ISO 52016-1. This is calculated by means of the exposure correction factor ( $F_W$ ), as in Equation (26),

$$g_{gl} = g_{gl,n} \cdot F_W \quad (26)$$

where  $g_{gl,n}$  is the total solar energy transmittance at normal incidence. The solar properties of the windows are considered time independent in EN ISO 52016 1, and the  $F_W$  factor is assumed constant and equal to 0,9.

### 5.2.1.5 Heat conduction and storage

In compliance with the thermal-electrical analogy, the EN ISO 52016-1 heat conduction model considers each building envelope component to be discretised into up to five resistance-capacitance nodes (R-C). As far as the opaque components are concerned, five R-C nodes are considered regardless of the specific characteristics and thermal properties of the component, as shown in Figure 6.

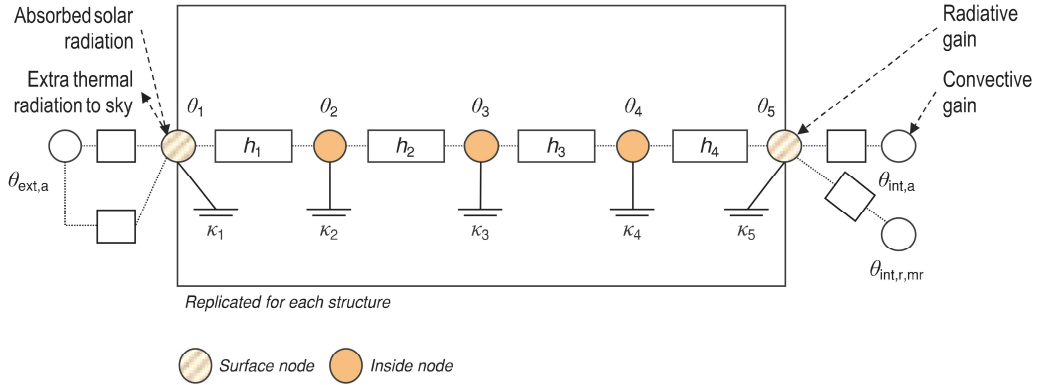


Figure 6: Illustration of the EN ISO 52016-1 R-C model of an opaque building element

Two nodes are placed on the external and on the internal surface, respectively, while the others are placed inside the construction element. The R-C nodes are interconnected by four conductances ( $h_{pli}$ , with  $pli$  from 1 to 5), defined in Equation (27) as fixed ratios of the total thermal resistance of the component ( $R_c$ ). In the same way, to each R-C node is associated a thermal capacity ( $\kappa_{pli}$ ), defined as a portion of the total areal heat capacity of the structure ( $\kappa_m$ ). Each component is assumed to belong to one of the five mass distribution classes, defined in function of the mass



position inside the component, and specified by the technical standard [5] as follows:

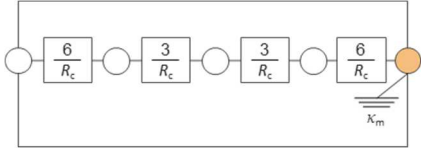
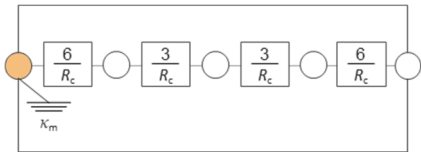
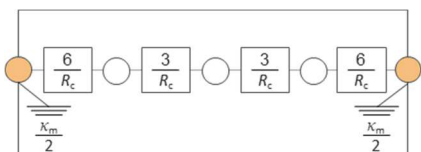
1. Class I, where the mass is concentrated at internal side,
2. Class E, where the mass is concentrated at external side,
3. Class IE, where the mass is divided over internal and external side,
4. Class D, where the mass is equally distributed (e.g., uninsulated constructions), and
5. Class M, where the mass is concentrated inside.

Depending on the assumed mass distribution class, the total areal heat capacity of the structure is distributed over the five R-C nodes, as shown in Table 13. In addition to the mass distribution classes, EN ISO 52016-1 also introduces pre-calculated areal heat capacity values to be used whenever the actual value is unknown.

$$\begin{aligned} h_1 = h_4 &= \frac{6}{R_c} \\ h_2 = h_3 &= \frac{3}{R_c} \end{aligned} \quad (27)$$

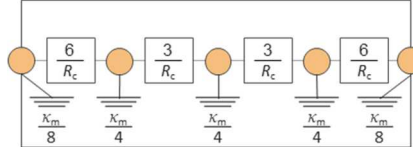
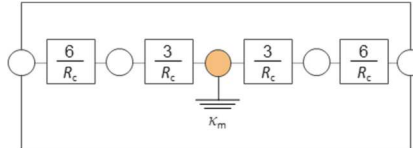
For the sake of the studies presented in this chapter, the Crank-Nicolson finite difference solution algorithm was adopted in the reference model of EnergyPlus.

Table 13: Distribution of the total areal heat capacity of the structure over the R-C nodes for each mass distribution class

Mass distribution class	Heat capacity distribution
Class I	$\kappa_1 = \kappa_2 = \kappa_3 = \kappa_4 = 0, \quad \kappa_5 = \kappa_m$ 
Class E	$\kappa_2 = \kappa_3 = \kappa_4 = \kappa_5 = 0, \quad \kappa_1 = \kappa_m$ 
Class IE	$\kappa_2 = \kappa_3 = \kappa_4 = 0, \quad \kappa_1 = \kappa_5 = \frac{\kappa_m}{2}$ 

Orange filled nodes are capacitive nodes; white filled nodes are non-capacitive nodes

Table 13: Distribution of the total areal heat capacity of the structure over the R-C nodes for each mass distribution class (continue)

Mass distribution class	Heat capacity distribution
Class D	$\kappa_2 = \kappa_3 = \kappa_4 = \frac{\kappa_m}{4}, \quad \kappa_1 = \kappa_5 = \frac{\kappa_m}{8}$ 
Class M	$\kappa_1 = \kappa_2 = \kappa_4 = \kappa_5 = 0, \quad \kappa_3 = \kappa_m$ 

Orange filled nodes are capacitive nodes; white filled nodes are non-capacitive nodes

### 5.2.1.6 Internal longwave radiation heat transfer

In both EN ISO 52016-1 and EnergyPlus, the longwave radiation heat transfer includes the radiation exchange between the surfaces facing the thermal zone, and the radiation from internal sources.

The longwave radiation heat transferred between the zone surfaces is determined by means of the Stefan-Boltzmann law in EnergyPlus, while its linearised formulation is considered in EN ISO 52016-1. In particular, it is calculated as

$$q_{lwr,surf,eli} = h_{r,int,eli} \cdot \sum_{elk=1}^{eln} \frac{A_{elk}}{A_{tot}} \cdot \theta_{surf,eli} - \sum_{elk=1}^{eln} h_{r,int,eli} \cdot \frac{A_{elk}}{A_{tot}} \cdot \theta_{surf,elk} \quad (28)$$

where *eli* refers to the considered surface, and *elk* refers to the other surfaces facing the thermal zone, *A* is surface area (in m<sup>2</sup>), *h<sub>r,int</sub>* is the radiant heat transfer coefficient (in W·m<sup>-2</sup>·K<sup>-1</sup>), *θ<sub>surf</sub>* is the indoor surface temperature (in K). As for the external radiant heat transfer coefficient, also the internal coefficient is assumed time-independent, and it is calculated by means of the EN ISO 6946 formulation [132] in Equation (23). Also in this case, reference conditions are assumed and derived from [134]; namely, a surface emissivity equal to 0,9 and a *T<sub>m</sub>* temperature of 20 °C.

As far as the radiation from internal sources is concerned, both the models define a radiative and convective split for the heat introduced into the thermal zone from the equipment. However, the models differ as regards the distribution of the radiative part over the surfaces. In particular, in EN ISO 52016-1, the radiative fraction of internal gains is uniformly distributed over the surfaces (*q<sub>lwr,int</sub>*, expressed in W·m<sup>-2</sup>). It is calculated according to Equation (29),

$$q_{\text{lwr,int}} = \frac{1}{A_{\text{tot}}} \cdot (1 - f_{\text{int,c}}) \cdot \Phi_{\text{int}} \quad (29)$$

where  $A_{\text{tot}}$  is the sum of the surface areas facing the thermal zone (in  $\text{m}^2$ ) – including thermal mass surfaces,  $f_{\text{int,c}}$  is the convective fraction of internal gains, and  $\Phi_{\text{int}}$  is the total internal heat gains (in W). In EnergyPlus, instead, the radiant fraction of internal gains is distributed proportionally to the surface area and the surface emissivity ( $\Phi_{\text{lwr,int}}$ , expressed in W), according to Equation (30),

$$\Phi_{\text{lwr,int}} = \frac{A_{\text{eli}} \cdot \varepsilon_{\text{eli}}}{\sum_{\text{elk}=1}^{\text{eln}} A_{\text{elk}} \cdot \varepsilon_{\text{elk}}} \cdot (1 - f_{\text{int,c}}) \cdot \Phi_{\text{int}} \quad (30)$$

where *eli* refers to the considered surface, and *elk* refers to the other surfaces facing the thermal zone, and  $A$  and  $\varepsilon$  are the surface area (in  $\text{m}^2$ ) and the emissivity, respectively. The other parameters are described in Equation (29).

Although both the models are not completely realistic, alternative methods are not easily applicable, since they would require knowledge of the placement and the surface temperature of all equipment [107].

#### 5.2.1.7 Internal shortwave radiation heat transfer

As far as the solar radiation transmitted into a thermal zone is concerned, the EN ISO 52016-1 method and EnergyPlus differ under three aspects. Firstly, the solar heat gains are considered to be all radiative heat gains in EnergyPlus; on the other hand, a fraction of solar heat entering the zone through the glazing is considered to be immediately transferred to the internal air [20] in EN ISO 52016-1. Secondly, the radiative fraction of solar heat gains is distributed uniformly over the zone surfaces in the simplified method ( $q_{\text{swr,sol}}$ , in  $\text{W} \cdot \text{m}^{-2}$ ), according to Equation (31),

$$q_{\text{swr,sol}} = \frac{1}{A_{\text{tot}}} \cdot (1 - f_{\text{sol,c}}) \cdot \Phi_{\text{sol}} \quad (31)$$

where  $A_{\text{tot}}$  is the sum of the surface areas facing the thermal zone (in  $\text{m}^2$ ) – including thermal mass surfaces,  $f_{\text{sol,c}}$  is the convective fraction of solar gains, and  $\Phi_{\text{sol}}$  is the total solar heat gains (beam plus diffuse solar radiation, in W). In EnergyPlus, instead, different approaches for the distribution of solar radiation are offered. For the sake of the studies presented in this chapter, the “full exterior with reflections” distribution model [107] of EnergyPlus was assumed as a reference. According to this approach, beam solar radiation entering the zone is assumed to fall on the floor, where it is absorbed according to the floor solar absorptance coefficient. The reflected solar radiation by the floor is added to the transmitted diffuse radiation

(and eventual shortwave radiation from the lighting system), which is then distributed over the internal surfaces proportionally to the surface area and the surface solar absorptance ( $\Phi_{\text{swr,sol}}$ , expressed in W), as in Equation (32),

$$\Phi_{\text{swr,int}} = \frac{A_{eli} \cdot \alpha_{eli}}{\sum_{elk=1}^{eln} A_{elk} \cdot (1 - \rho_{eli})} \cdot \Phi_{\text{sol,diff}} \quad (32)$$

where  $eli$  refers to the considered surface, and  $elk$  refers to the other surfaces facing the thermal zone,  $A$ ,  $\alpha$  and  $\rho$  are, respectively, the surface area (in  $\text{m}^2$ ), the absorption and the reflection coefficients, and  $\Phi_{\text{sol,diff}}$  is the diffuse solar radiation (transmitted solar radiation plus reflected beam solar radiation, in W). Finally, the solar reflectance is calculated according to Equation (33) for transparent surfaces,

$$\rho = 1 - \alpha - \tau \quad (33)$$

where  $\tau$  is the direct solar transmission coefficient of the transparent surface. This represents the “lost” fraction of the solar radiation entering the zone that is reflected back to the external environment. In the EN ISO 52016-1 hourly method, instead, the solar radiation back reflection is not considered.

### 5.2.1.8 Internal heat convection

Similarly to the external convective heat transfer, the areal heat flux transferred between the surface and the indoor environment ( $q_{\text{conv,int}}$ , expressed in  $\text{W} \cdot \text{m}^{-2}$ ) is calculated both in the EN ISO 52016-1 simplified method and in the detailed method of EnergyPlus as in Equation (34),

$$q_{\text{conv,int}} = h_{\text{c,int}} \cdot (T_{\text{air,int}} - T_{\text{surf,int}}) \quad (34)$$

where  $h_{\text{c,int}}$  is the internal convective heat transfer coefficient (in  $\text{W} \cdot \text{m}^{-2} \cdot \text{K}^{-1}$ ), and  $T_{\text{air,int}}$  and  $T_{\text{surf,int}}$  are the indoor air and the surface temperatures (in K), respectively.

In Equation (34), constant values of the convective heat transfer coefficient over the simulation period are applied in the EN ISO 52016-1 hourly method, and are derived from the EN ISO 13789 [134] technical standard, in accordance with the direction of the heat flux. The definition of  $h_{\text{c,int}}$  on a timestep basis is instead performed by means of the TARP algorithm [247] in EnergyPlus, assumed as a reference for the sake of the studies presented in this chapter.

## 5.2.2 The Italian National Annex improved modelling options

As introduced in Section 5.2, the EN ISO 52016 1 hourly method [5] provides for different assumptions and simplifications regarding different aspects of the building energy performance assessment. To increase the accuracy of the standard hourly

method, the Italian National Annex [137] instead introduces improved options regarding the modelling of the conduction heat transfer (Section 5.2.2.1), the extra thermal radiation to the sky (Section 5.2.2.3), the shortwave radiation heat transfer (Section 5.2.2.2), and the coupling of thermally conditioned zones (Section 5.2.2.4). The improved modelling options are described in the following sections, and the differences between the standard and the improved Italian NA methods are highlighted as well.

### 5.2.2.1 Heat conduction model

The conduction model of the Italian National Annex to EN ISO 52016-1 [137] is an improved version of the one presented in the standard (Section 5.2.1.5); in particular, it provides a more detailed approach for the opaque components discretisation into R-C nodes that is more in line with the physical characteristics of the layers composing the structure, as shown in Figure 7.

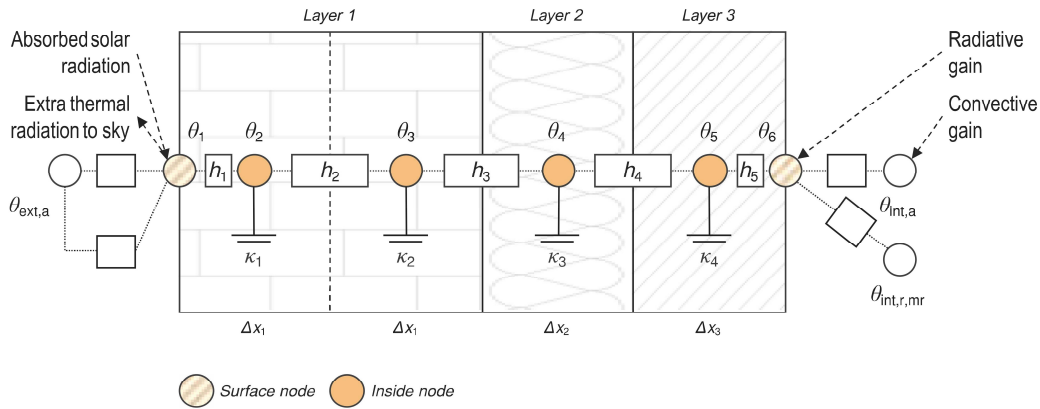


Figure 7: Illustration of the Italian Annex R-C model of an opaque building element

As for the EN ISO 52016-1 method, two nodes are placed on the internal and on the external surface, respectively. However, in the improved method, no heat capacity is associated to the surface R-C nodes. The main difference between the standard and the improved method is the definition of the number and position of the R-C nodes inside the structure. Each layer is in fact discretised into at least one node; the number of nodes ( $N_{cnj}$ ) in the  $j$ -layer is defined based on a correlation between the Fourier number for the  $j$ -layer ( $Fo_j$ ) and a reference Fourier number ( $Fo_{ref}$ ) assumed equal to 0,5, as defined in Equation (35). To each node is associated a ratio of the layer thickness ( $\Delta x_j$  in Figure 7), of the layer heat capacity ( $\kappa_{pli,j}$  with  $pli$  from 1 to  $N_{cnj}$ ), and of the layer thermal resistance ( $R_{pli,j}$ ), as defined in Equations (36), (37) and (38), respectively. The node is placed in the middle of its associated  $\Delta x_j$ . The internode conductances ( $h_{pli,j}$  with  $pli$  from 1 to  $N_{cnj}$ ) are determined

considering half of the thermal resistances associated to each node, as defined in Equation (39).

$$Ncn_j = \max \left[ 1; \text{int} \left( \left( \frac{Fo_{\text{ref}}}{Fo_j} \right)^{\frac{1}{2}} + 0,999999 \right) \right] \quad (35)$$

$$\Delta x_j = \frac{d_j}{Ncn_j} \quad (36)$$

$$\kappa_{\text{pli},j} = \rho_j \cdot c_j \cdot \Delta x_j \quad (37)$$

$$R_{\text{pli},j} = \frac{\Delta x_j}{\lambda_j} \quad (38)$$

$$h_{\text{pli},j} = \frac{1}{\frac{R_{\text{pli}-1,j}}{2} + \frac{R_{\text{pli},j}}{2}} \quad (39)$$

### 5.2.2.2 Solar gains through windows

The solar properties of windows are considered time independent in EN ISO 52016-1, and the  $F_W$  factor is assumed constant over the calculation period. On the other hand, a solar angle-dependent  $F_W$  is considered in the Italian National Annex, and it is calculated according to Equation (40),

$$F_W = \frac{F_{W,\text{diff}} \cdot I_{\text{sol,diff},t} + F_{W,\text{dir}} \cdot I_{\text{sol,dir},t} \cdot F_{\text{sh,obst},t}}{I_{\text{sol,diff},t} + I_{\text{sol,dir},t} \cdot F_{\text{sh,obst},t}} \quad (40)$$

where,  $F_{W,\text{diff}}$  and  $F_{W,\text{dir}}$  are the correction factors, respectively, for the diffuse and for the beam incident solar irradiance on a window,  $I_{\text{sol,diff},t}$  and  $I_{\text{sol,dir},t}$  are, respectively, the diffuse and the beam incident solar irradiance at timestep  $t$ , and  $F_{\text{sh,obst},t}$  is the reduction factor for the beam incident solar irradiance due to external obstacles at timestep  $t$ . The  $F_{W,\text{diff}}$  correction factor is assumed equal to 0,8 [137] over the calculation period, while the  $F_{W,\text{dir}}$  correction factor is calculated on a time-step basis according to the empirical model introduced by Karlsson and Roos [191]. According to this formulation, the  $F_{W,\text{dir}}$  depends on the angle of incidence of beam incidence solar irradiance, and on the type of glazing considered (number of panes).

The solar-angle dependence of the correction factor is presented in Figure 8 for a single glazing (1 pane), a double- (2 panes) and a triple-glazed unit (3 panes).

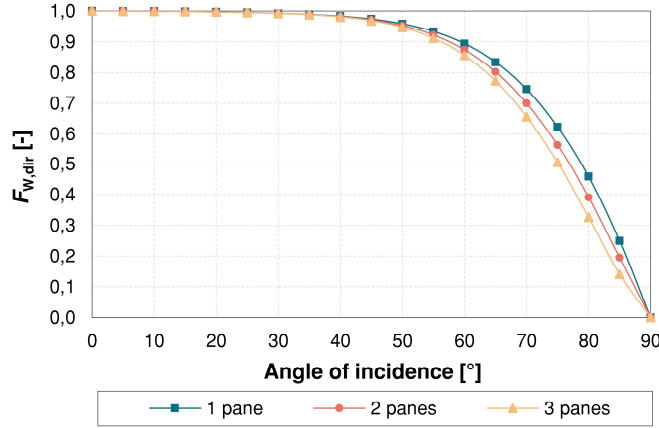


Figure 8: Angle dependence of  $F_{w,dir}$  for different glazings according to Karlsson and Roos formulation [191]

### 5.2.2.3 Extra thermal radiation to the sky

The longwave radiation heat transfer between a surface and the sky is considered in both the European standard and the improved Italian NA models by means of the extra thermal radiation to the sky. The two models differ in the determination of the apparent sky temperature. Differently from the European standard, the Italian NA proposes a correlation based on the partial pressure of water vapour [248]. The apparent sky temperature is calculated as in Equation (41), where  $p_{v,e}$  is the partial pressure of water vapour (in Pa).

$$\theta_{sky} = 18 - 51,6 \cdot e^{-\frac{p_{v,e}}{1000}} \quad (41)$$

### 5.2.2.4 Coupling of thermally conditioned zones

The standard hourly method of EN ISO 52016 1 performs a multi-zone calculation without thermal coupling between zones, i.e., it does not account for any heat transfer between thermally conditioned zones, neither by thermal transmission nor by ventilation or infiltration. The heat transfer between conditioned zones is instead considered in the Italian NA. In particular, the heat flow through internal partitions between adjacent thermal zones is calculated by considering an equivalent thermal resistance and an outdoor surface temperature (seen from the thermal zone being calculated) for each partition. As for the air flow exchange, if the air flow is considered to pass from a thermal zone “A” to a thermal zone “B” (mono-directional air flow), the calculation is done first for zone “A”, then its air

temperature is used to solve the thermal balance of zone “B”. If instead the air flow is considered to be bi-directional, zone “A” and “B” are assumed to be a single thermal zone.

### 5.2.3 Modelling assumptions and options: a summary

The specific modelling assumptions introduced by the EN ISO 52016-1 technical standard were thoroughly described in Section 5.2.1; in Section 5.2.2, instead, the improved modelling options introduced by the Italian National Annex were presented. For a simpler and clearer access to all these modelling assumptions and options, these are herein summarised and compared in Table 14.

Table 14: Summary of EN ISO 52016-1’s modelling assumptions and options

Heat transfer phenomenon	EN ISO 52016-1	Italian National Annex to EN ISO 52016-1
<i>External longwave radiation</i>	<ul style="list-style-type: none"> <li>» Linearised Stefan-Boltzmann law</li> <li>» Outdoor environment at external air temperature (excluding the sky)</li> <li>» Direct model for the determination of the apparent sky temperature (constant difference with the external air temperature)</li> <li>» Time-independent radiant heat transfer coefficient (standard value from EN ISO 6946)</li> </ul>	<ul style="list-style-type: none"> <li>» Linearised Stefan-Boltzmann law</li> <li>» Outdoor environment at external air temperature (excluding the sky)</li> <li>» Direct model for the determination of the apparent sky temperature (correlation based on the partial pressure of water vapour)</li> <li>» Time-independent radiant heat transfer coefficient (standard value from EN ISO 6946)</li> </ul>
<i>External shortwave radiation</i>	» Not shadowing of diffuse solar radiation	
<i>External convection</i>	» Time-independent convective heat transfer coefficient (forced convection, standard value from EN ISO 6946)	
<i>Solar transmission</i>	<ul style="list-style-type: none"> <li>» Transmitted solar irradiance as shortwave radiation</li> <li>» Time- and solar angle-independent glazing optical properties</li> </ul>	<ul style="list-style-type: none"> <li>» Transmitted solar irradiance as shortwave radiation</li> <li>» Time- and solar angle-dependent glazing optical properties</li> </ul>
<i>Heat conduction and storage</i>	<ul style="list-style-type: none"> <li>» Lumped parameter approach</li> <li>» Predefined number of R-C nodes</li> <li>» Capacitive surfaces</li> <li>» Position of nodes inside the structure (excluding surface nodes) is not defined</li> <li>» Fixed distribution of thermal resistance over the nodes</li> <li>» Distribution of heat capacity over the R-C nodes depending on qualitative mass distribution classes</li> </ul>	<ul style="list-style-type: none"> <li>» Finite volume approach</li> <li>» Calculated number of R-C nodes per layer</li> <li>» Not capacitive surfaces</li> <li>» R-C nodes are placed in the middle of the associated finite volume (portion of layer thickness)</li> <li>» Distribution of thermal resistance and heat capacity over the R-C proportionally to the associate finite volume (portion of layer thickness)</li> </ul>
<i>Internal longwave radiation</i>	<ul style="list-style-type: none"> <li>» Linearised Stefan-Boltzmann law</li> <li>» Time-independent radiant heat transfer coefficient (standard value from EN ISO 6946)</li> <li>» Approximated defined view factors between surfaces (area-weighted)</li> <li>» Uniform distribution of radiant heat gains over internal surfaces</li> </ul>	
<i>Internal shortwave radiation</i>	<ul style="list-style-type: none"> <li>» Uniform distribution of solar radiation over internal surfaces</li> <li>» Fraction of solar radiation directly transmitted to internal air (convective heat gain)</li> <li>» Back reflection of solar radiation outside through windows is neglected</li> </ul>	
<i>Internal convection</i>	» Time-independent convective heat transfer coefficient (standard value from EN ISO 6946)	

### 5.2.4 Validation studies on the EN ISO 52016-1 hourly method

Since the release of the technical standard in 2017, the effect of the model simplifications on the accuracy of the calculation method has been the central topic



of a growing, but not yet sufficient, body of literature, in which the EN ISO 52016-1 method has been compared to detailed numerical simulation models.

Among the simplifications introduced, the research of Ballarini et al. [57,241] showed that, for a single family house in northern Italy, the main cause of the differences in the results between the standard hourly method and the detailed dynamic calculation of EnergyPlus was found in the use of constant values for the surface convective and radiant heat transfer coefficients. Zakula et al. [249], analysing the simplification introduced by the EN ISO 52016-1 hourly method on the modelling of the transparent envelope components, underlined the significance of using fixed windows solar properties; this assumption, in fact, led to relevant differences in the results between the standard method and the detailed hourly method applied in TRNSYS (Transient System Simulation Tool) for ten Croatian reference buildings. These results were then confirmed by the same Authors, by extending the analysis and applying it to more than 147 thousand case studies [250]. Similar results were found by Magni et al. in [251]. The authors applied both constant and variable windows thermal properties (total solar energy transmittance and thermal resistance) in the EN ISO 52016-1 calculation and compared the outcomes obtained implementing the TRNSYS model. The results emphasised the considerable deviation resulting from the application of constant windows thermal properties. In fact, the use of these latter led to consistent differences in the heating demand for an office building, while the discrepancies between the two models are significantly reduced if variable properties are considered (from 40% to 5%). Summa et al. [252] have studied the variation in the indoor ambient temperature, as well as in the indoor surface temperatures, related to the variation in the mass distribution in the external walls for a room in a highly insulated residential building. Specifically, they have tested four different structures characterised by the same level of thermal insulation, but with different mass positions (i.e., four out of the five mass distribution classes specified by the EN ISO 52016-1 technical standard). The Authors observed that the extent of the errors in the prediction of both indoor temperature and surface temperatures vary according to the assumed mass distribution when compared to the results of the detailed dynamic method of TRNSYS; the highest discrepancies were found for the construction characterised by the massive layer placed on the outer side.

To date, the introduction of the improved modelling option of the Italian NA was evaluated in a few research, therefore it is essential to widen current knowledge of the modelling techniques implemented in the Italian NA. In the study of Mazzarella et al. [198], the improved conduction model introduced by the Italian NA was compared to the exact analytical solution, and it showed better results with

respect to the standard model in terms of internal and external heat flux amplitude and phase difference. A sensitivity analysis to the Italian NA improved algorithms was performed by Bianco Mauthe Degerfeld et al. [253] for a residential existing building in Rome (Italy), while a parametric analysis to evaluate the influence of the NA improved method was performed for an existing office building [254]. Considerable variations in the thermal energy need for space heating were observed for both NA improved models applied separately and for their combined application in the considered case studies. Finally, Palladino et al. [255] compared the currently adopted calculation method in Italy (quasi steady-state model) with the simplified hourly method as transposed in the Italian national standard, in terms of thermal energy needs of three reference nearly-zero energy building (nZEB) case studies.

### **5.3 Validation on building construction archetypes**

The work presented in this section concerns the evaluation of the hypothesis of the simplified heat conduction model introduced by the EN ISO 52016-1 technical standard, and the improved solution provided by its Italian National Annex.

#### **5.3.1 Methodology**

The hypotheses of the EN ISO 52016-1 heat conduction model were evaluated in a multi-step analysis. Firstly, the analysis was applied to stand-alone structures, subject to different simplified boundary conditions, including both cyclical and realistic variation of indoor and outdoor air temperature; the effect of the simplified heat conduction models (i.e., European and Italian National Annex) on the prediction of the internal surface temperature was assessed for different building components, covering a wide range of structure heat capacity and mass position. The analysis was then extended to evaluate the influence of the heat conduction models on the overall thermal zone heat balance (i.e., indoor air temperature, thermal energy needs) for those components characterised by significant errors in the prediction of the internal surface temperatures, resulting from the preliminary analysis. In the second step, realistic boundary conditions (i.e., real climate data, thermal constraints, etc.) were considered.

A detailed description of the proposed evaluation phases is provided in the following paragraphs.

##### **5.3.1.1 Stand-alone component analysis**

The first evaluation phase was performed by applying a code-to-code comparison methodology. Five structures, each representing one of the five mass distribution classes provided by the EN ISO 52016-1 hourly method [5], and described in

Section 5.2.1.5, were selected. Each structure was simulated with the standard (i.e., EN ISO 52016-1) and the improved (i.e., Italian National Annex) algorithms, and with the Crank-Nicolson (finite difference) solution algorithm taken as the baseline. A 24 hours simulation was performed for each structure in a steady periodic regime; in particular, the structures were assumed to be only exposed to the convective heat transfer. Thus, the effect of the longwave radiant heat transfer was annulled and neither solar gains nor internal heat gains were considered. Three different boundary conditions were considered:

1. *IntC*, with cyclical variation of the indoor air temperature (unitary amplitude, 24 h period of variation) and constant outdoor air temperature,
2. *ExtC*, with cyclical variation of the outdoor air temperature (unitary amplitude, 24 h period of variation) and constant indoor air temperature, and
3. *SDD*, that represents the summer design day external boundary conditions of a south-facing wall exposed to solar radiation and constant indoor air temperature. The wall was assumed to be placed in Rome (Italy), and the effect of solar radiation was considered by means of the sol-air temperature.

Both the standard and the improved algorithms were implemented by means of a custom-built Python script developed by the Author, while the Crank-Nicolson algorithm was simulated through the EnergyPlus calculation engine. Since EnergyPlus does not allow the simulation of a stand-alone building component (i.e., not included in a thermal zone), a specific simulation environment, devised for the purposed of the calibration of the thermo-physical properties of a single wall in [256] and modified for the purpose of the present work, was adopted for a single component simulation in EnergyPlus. The proposed simulation procedure requires the creation of a fictitious thermal zone (a simple shoebox), in which the same construction, namely the one to be tested, is attributed to each wall, to the roof and the slab; these structures are assumed to be exposed neither to solar radiation nor to wind. The thermal emissivity of the internal and external surfaces of each component is set to zero to annul the longwave radiation heat transfer and to ensure that these are exposed only to the convective heat transfer; a specific (constant or variable) convective heat transfer coefficient is attributed to each surface, consistent with the simulation carried out with the EN ISO 52016-1 algorithm. Finally, the considered boundary conditions (*IntC*, *ExtC*, and *SDD*) are applied as climatic conditions on the external side, and as indoor air temperature setpoint on the internal side (guaranteed by means of an ideal heating and/or cooling system).

The accuracy of the simplifying modelling assumptions of the standard and the improved algorithms was evaluated by means of the Root Mean-Square Deviation

(*RMSD*) of the internal surface temperature compared to the results of the finite difference solution algorithm simulations, as described in Equation (42),

$$RMSD = \left( \frac{1}{n} \cdot \sum_{t=1}^n \left( \theta_{\text{model},t} - \theta_{\text{CondF},t} \right)^2 \right)^{0,5} \quad (42)$$

where,  $\theta_{\text{CondF}}$  and  $\theta_{\text{model}}$  are the internal surface temperatures at timestep  $t$ , resulting from the simulations with the finite difference and the standard/improved solution algorithms, respectively, and  $n$  is the number of time-steps evaluated (in this case, 24 steps).

### 5.3.1.2 Thermal zone analysis

In the second phase, the analysis was extended to a building unit (i.e., thermal zone) by applying the methodology workflow proposed in the present dissertation (Section 3.4). In particular, its specific application is presented in Figure 9.

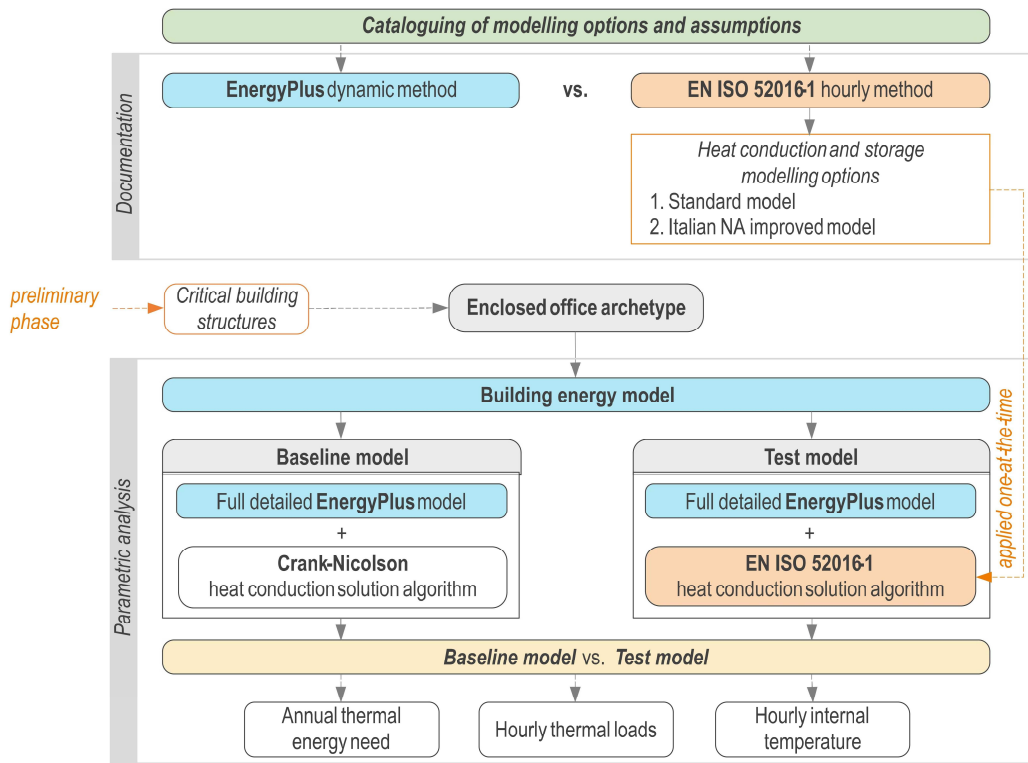


Figure 9: Methodology workflow for the evaluation of the EN ISO 52016-1 heat conduction solution algorithm for a thermal zone

Starting from the results of the preliminary phase, the structures for which the higher errors in the prediction of the internal surface temperatures occur were selected and applied, one-at-the-time, to the considered case study – an enclosed

office archetype, representative of the Italian building stock. Therefore, the analysed case studies are as many as the selected structures. Differently from the preliminary analysis, the structures were assumed to be exposed to all thermal constraints (i.e., longwave radiation, solar radiation, internal gains, etc.); moreover, a realistic building use and real climatic conditions were considered in the simulations. The “baseline model” was firstly created in EnergyPlus for the case studies, assuming the Crank-Nicolson heat conduction solution algorithm as baseline. In the “test models”, the standard (i.e., EN ISO 52016-1) and the improved models (i.e., Italian NA to EN ISO 52016-1) were implemented one-at-the-time to the baseline model. The effect of the simplified heat conduction models was assessed as the variation in the accuracy of test model due to the implementation of each simplification, compared to the baseline model. This variation was evaluated in terms of both annual thermal energy needs for space heating and cooling, and hourly indoor air temperatures.

To simulate the simplified opaque component discretisation, the EnergyPlus source code was modified according to EN ISO 52016-1 specifications. In particular, the code was implemented to consider the number of resistive-capacitive nodes specified by the technical standard, as well as the heat capacity associated to each node and the internode conductances (these calculated parameters are described in Section 5.2.1.5). The modified source code, as well as some specifications regarding the modifications, is provided in Annex A of the present dissertation.

The accuracy of the simplified conduction model in the prediction of the indoor air temperature was evaluated by means of the *RMSD*, calculated as in Equation (42); the hourly Mean Bias Error (*MBE*) index was instead used for the annual energy needs evaluation, and was calculated as specified in [71]:

$$MBE_{H/C} = \frac{\sum_{t=1}^n (\Phi_{H/C, \text{test}, t} - \Phi_{H/C, \text{baseline}, t})}{\sum_{t=1}^n |\Phi_{H/C, \text{baseline}, t}|} \cdot 100 \quad (43)$$

where  $\Phi_{H/C}$  is the heating (H) or cooling (C) load (in W) at timestep  $t$ , for the test model and for the baseline, respectively, and  $n$  is the number of timesteps considered for the calculation (8760 for annual evaluations). The *MBE* is expressed as a percentage error, and measures how closely the predicted hourly heating or cooling loads corresponds to the baseline data. The variations in the energy needs are considered acceptable with *MBE* values in the range of  $\pm 10\%$  (when using hourly data) [71].

### 5.3.1.3 Mass distribution deviation

The evaluation of the different approaches for the structure mass distribution was carried out by means of two specific parameters, introduced for this specific purpose, namely the “internal areal heat capacity deviation” ( $\kappa_{i,\text{dev}}$ ) and the “periodic thermal transmittance deviation” ( $Y_{ie,\text{dev}}$ ). Both the parameters allow the numerical assessment of the mass distribution differentiation between a model and the actual component, and are calculated for each of the considered structures. An “artificial” structure, that represents the mass distribution for the considered heat conduction model, is introduced for the calculation of both the parameters. The “internal areal heat capacity deviation” is considered for the validation of the heat conduction models when the structures are exposed to an internal constraint, and it is defined in Equation (44) as the difference between the internal areal heat capacity for the “artificial” structure ( $\kappa_{i,\text{model}}$ ,  $\text{J}\cdot\text{m}^{-2}\cdot\text{K}^{-1}$ ) and for the actual structure ( $\kappa_i$ ,  $\text{J}\cdot\text{m}^{-2}\cdot\text{K}^{-1}$ ), calculated according to the EN ISO 13786 technical standard [257].

$$\kappa_{i,\text{dev}} = \kappa_{i,\text{model}} - \kappa_i \quad (44)$$

The “periodic thermal transmittance deviation” is instead employed when an external constraint is considered. It is defined in Equation (45) as the module of the difference between the periodic thermal transmittance for the “artificial” structure ( $Y_{ie,\text{model}}$ ,  $\text{W}\cdot\text{m}^{-2}\cdot\text{K}^{-1}$ ) and for the actual structure ( $Y_{ie}$ ,  $\text{W}\cdot\text{m}^{-2}\cdot\text{K}^{-1}$ ), both calculated according to the EN ISO 13786 technical standard [257].

$$Y_{ie,\text{dev}} = \left| \vec{Y}_{ie,\text{model}} - \vec{Y}_{ie} \right| \quad (45)$$

## 5.3.2 Application

### 5.3.2.1 Representative construction of the Italian building stock

The selection of the structures to be analysed in the preliminary analysis was based on the mass distribution classes specified by EN ISO 52016-1 [5]; in fact, each selected structure is representative of one of the five mass distribution classes. Each of the five structures selected corresponds to a typical construction of the Italian existing building stock, and was derived from the UNI/TR 11552 technical report [258]. In Table 15, the selected structures, which are named as the corresponding mass distribution class, are described and the layers’ thermal properties are reported. In absence of structures consistent with the mass distribution class in [258] (e.g., Class M structure), an *ad hoc* structure was hypothesised.

Table 15: Selected structures description

Material	$d$ [m]	$\lambda$ [W·m <sup>-1</sup> ·K <sup>-1</sup> ]	$\rho$ [kg·m <sup>-3</sup> ]	$c$ [J·kg <sup>-1</sup> ·K <sup>-1</sup> ]	$R$ [m <sup>2</sup> ·K·W <sup>-1</sup> ]	$R_c$ [m <sup>2</sup> ·K·W <sup>-1</sup> ]	$\kappa_m$ [kJ·m <sup>-2</sup> ·K <sup>-1</sup> ]
<b>Class I</b>							
(ext) Plaster	0,02	0,90	1800	1000	-	3,55	472
Fiberglass insulation	0,12	0,04	30	670	-		
Concrete panel	0,30	0,58	1400	1000	-		
(int) Plaster	0,01	0,70	1400	1000	-		
<b>Class E</b>							
(ext) Plaster	0,02	0,90	1800	1000	-	3,55	472
Concrete panel	0,30	0,58	1400	1000	-		
Fiberglass insulation	0,12	0,04	30	670	-		
(int) Plaster	0,01	0,70	1400	1000	-		
<b>Class IE</b>							
(ext) Plaster	0,02	0,90	1800	1000	-	3,54	380
Bricks	0,25	0,40	1000	1000	-		
Wool rock insulation	0,12	0,05	30	570	-		
Hollow bricks	0,08	0,40 <sup>a</sup>	800	1000	-		
(int) Plaster	0,02	0,70	1400	1000	-		
<b>Class D</b>							
(ext) Plaster	0,02	0,90	1800	1000	-	0,74	224
Bricks	0,25	0,39	800	1000	-		
Air gap	0,12	-	-	-	0,18		
Hollow bricks	0,08	0,40 <sup>a</sup>	800	1000	-		
(int) Plaster	0,02	0,70	1400	1000	-		
<b>Class M</b>							
(ext) Plasterboard	0,019	0,20	700	837	-	5,88	110
Wool rock insulation	0,12	0,04	70	1030	-		
XLAM panel	0,10	0,12	470	1600	-		
Wool rock insulation	0,05	0,04	70	1030	-		
(int) Plasterboard	0,019	0,20	700	837	-		

**Notes**<sup>a</sup> Equivalent thermal conductivity**5.3.2.2 Enclosed office representative of the Italian building stock**

In the second analysis phase, an enclosed office – representative of the Italian existing building stock – was assumed as case study. It is a single office of a multi-storey office building, and it was assumed to be adjacent to identical conditioned offices. The only exposed building envelope component is characterised by a window of 4,8 m<sup>2</sup> area. The external wall was assumed to be characterised by the structures selected from the preliminary analysis, thus it varies from case study to case study. The internal vertical partitions are instead characterised by a single concrete panel ( $R_{\text{wall,int}} = 0,20 \text{ m}^2 \cdot \text{K} \cdot \text{W}^{-1}$ ,  $\kappa_{\text{wall,int}} = 168 \text{ kJ} \cdot \text{m}^{-2} \cdot \text{K}^{-1}$ ), while masonry and bricks slabs were assumed as internal horizontal partitions ( $R_{\text{slab,int}} = 0,38 \text{ m}^2 \cdot \text{K} \cdot \text{W}^{-1}$ ,  $\kappa_{\text{slab,int}} = 294 \text{ kJ} \cdot \text{m}^{-2} \cdot \text{K}^{-1}$ ). The external window is a double-glazing unit with wooden frame ( $U_{\text{win}} = 2,8 \text{ W} \cdot \text{m}^{-2} \cdot \text{K}^{-1}$ ,  $g_{\text{gl}} = 0,75$ ). In the present study, thermal bridges were neglected.

A standard user behaviour, regarding the occupancy profile, internal heat sources, ventilation air flow rate, and HVAC operation, was assumed and was derived from the draft of the Italian Annex of the EN 16798-1 technical standard

[259]. The ideal load air system of EnergyPlus was considered to evaluate the energy needs for heating and cooling, considering a dead band internal temperature set point of 20 °C and 26 °C, respectively. The HVAC system was instead switched off all year long in the indoor operative temperature evaluation (free-floating condition). The evaluations were carried out using the International Weather for Energy Calculations (IWEC) data file [260] for the Italian city of Milan.

### 5.3.3 Results

#### 5.3.3.1 Stand-alone components analysis

The accuracy of the simplified heat conduction models was assessed with respect to the finite difference solution algorithm. In particular, the analysis of the results was mainly focused on the internal surface temperature, whereas it is involved in the thermal balance of the indoor environment. In Table 16, the *RMSDs* of the internal surface temperature of the analysed structures are reported for the standard and the improved algorithms, and for the three boundary conditions, respectively. The *RMSDs* related to the *SDD* boundary condition were normalised to the amplitude of the sol-air temperature variation, to make them comparable to the *ExtC* results.

Table 16: *RMSD* of the internal surface temperature [°C]

Boundary condition	Heat conduction model	Class I	Class E	Class IE	Class D	Class M
<i>IntC</i>	<i>Improved (UNI)</i>	0,028	0,012	0,036	0,026	0,013
	<i>Standard (CEN)</i>	0,298	0,097	0,231	0,032	0,084
<i>ExtC</i>	<i>Improved (UNI)</i>	0,010	0,005	0,001	0,003	0,006
	<i>Standard (CEN)</i>	0,012	0,014	0,011	0,006	0,006
<i>SDD</i>	<i>Improved (UNI)</i>	0,001	0,001	0,001	0,001	0,001
	<i>Standard (CEN)</i>	0,007	0,014	0,011	0,003	0,002

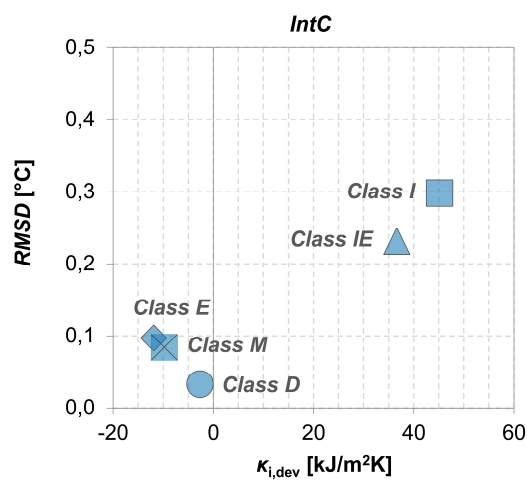


Figure 10: Internal surface temperature *RMSD* vs.  $\kappa_{i,dev}$  for the EN ISO 52016-1 standard conduction model under internal constraint (*IntC*)



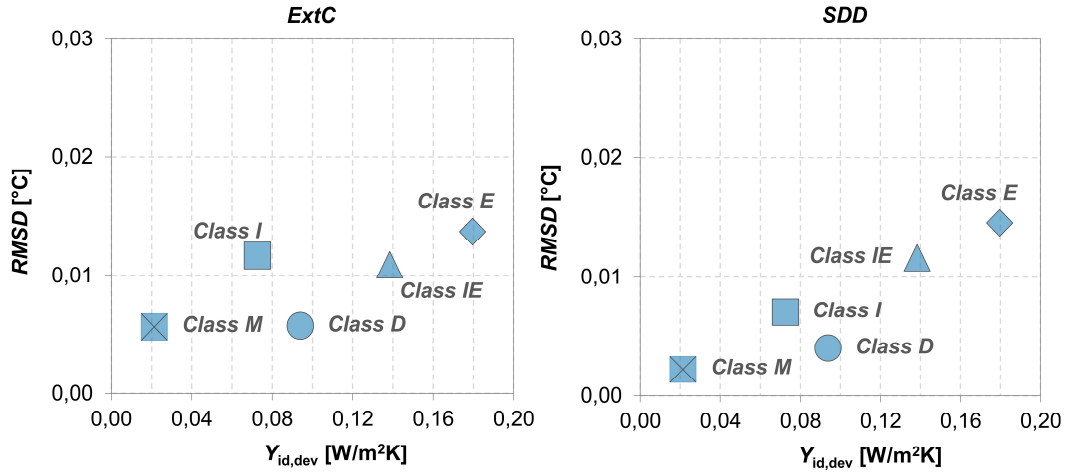


Figure 11: Internal surface temperature  $RMSD$  vs.  $Y_{ie,dev}$  for the EN ISO 52016-1 standard conduction model under external constraint ( $ExtC$  and  $SDD$ )

Generally, the improved solution algorithm introduced by the Italian National Annex ensures very close results to those of the Crank-Nicolson model. As shown in Table 16, negligible values of  $RMSD$  are reported for all the structures considered, regardless of the thermal constraint stressing the structure. On the other hand, less accurate results can be highlighted for the standard conduction model. To deepen the reasons for these results, it is necessary to separately analyse the structures response when internal ( $IntC$ ) and external constraints ( $ExtC$  and  $SDD$ ) are considered. To this purpose, in Figure 10 and Figure 11 the  $RMSDs$  for the standard conduction model are correlated to  $\kappa_{i,dev}$  and  $Y_{ie,dev}$ , respectively for the boundary condition  $IntC$ , and the boundary conditions  $ExtC$  and  $SDD$ . From the charts, a linear correlation between the  $RMSDs$  and the parameters introduced by the Authors can be observed for the considered structures, both under internal and external constraints. In fact, the deviations in the prediction of the internal surface temperatures increase with the increment of the mass distribution deviation. Nevertheless, the accuracy in the prediction of the internal surface temperature is not sensitive to the implementation of the standard conduction model when an external constraint is considered. In fact, negligible deviations (comparable to the improved method results) are reported for both the  $ExtC$  and the  $SDD$  boundary conditions. On the other hand, higher discrepancies are reported when the structures are stressed by an internal constraint. In particular, the highest deviations are relative to the structures characterised by the main massive component placed near the inner side of the structure. Thus, the hypothesis of distribution of the total areal heat capacity on the internal surface  $R-C$  node (Class I) and half of it (Class IE) leads to an overestimation of the heat capacity effectively stressed by the thermal constraint ( $\kappa_{i,dev}$  equal to  $45,2$  and  $36,6 \text{ kJ} \cdot \text{m}^{-2} \text{K}^{-1}$  for Class I and IE, respectively).

This overestimation results in considerable discrepancies in the internal surface temperature prediction, with errors in the range of 0,3 °C (i.e., 0,3 °C and 0,23 °C for the Class I and Class IE structures, respectively).

For a better understanding of this last result, the temperature trend inside the structures was analysed. The graphs in Figure 12 represent the *R-C* nodes position inside the structure and the relative temperature at the first calculation time-step ( $t = 0$  h), for the three heat conduction models (black, pink, and blue lines for the finite difference, the improved and the standard solution algorithms, respectively).

As far as the Italian approach is concerned, the node temperature analysis confirms the results previously presented. In fact, the temperature trend inside the structure of the improved method is highly consistent with the finite difference algorithm through the whole wall thickness, especially for the Class I, IE, and D structures. Negligible deviations can be instead found for the Class E and M structures, specifically in the massive layers (e.g., the concrete and the XLAM panels, respectively in Class E and M). Moving to the standard model analysis, a very good agreement between the standard and the finite difference algorithm can be found for the Class E and Class D structures. The temperature trend through the wall thickness is in fact highly consistent with the other heat conduction models, resulting in negligible deviations in the prediction of the internal surface temperature (i.e., 0,1 and 0,03 °C *RMSDs* values for Class E and Class D, respectively). With regards to the structures characterised by the massive layers on the inner side (Class I and Class IE), it is possible to observe that the errors in the temperatures mainly occur nearby the nodes on which the structure heat capacity is distributed (i.e., the internal surface node). This may be due to the fact that the distribution of the whole heat capacity (or half of it) of the structure on the inner surface node leads the inner layers to be less responsive to the temperature variations, with respect to the finite difference and the improved algorithm results, thus resulting in differences in the internal surface temperatures.

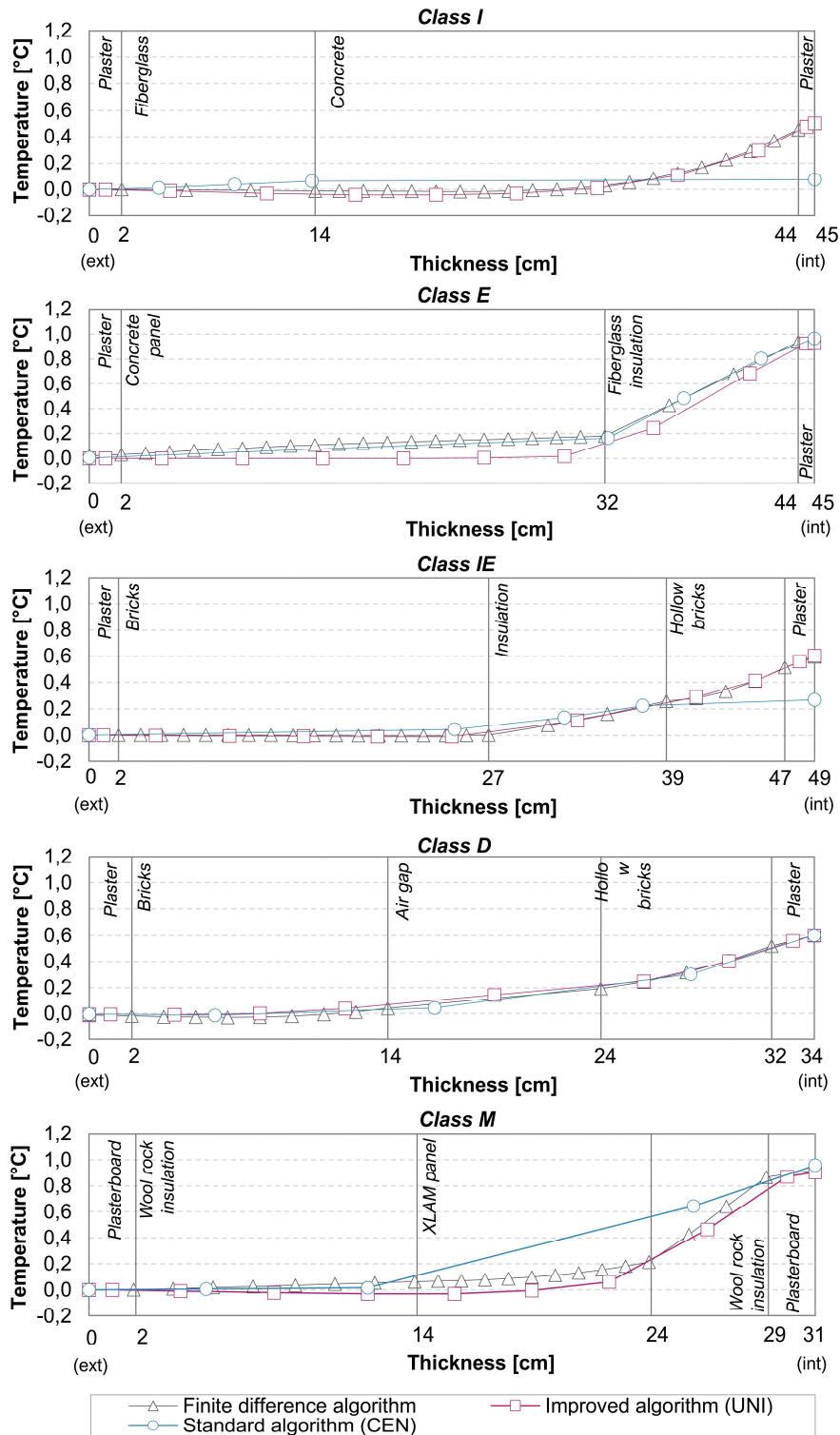


Figure 12: Node temperature comparison (*IntC* boundary condition,  $t = 0$  h)

### 5.3.3.2 Thermal zone analysis

The preliminary analysis showed that the standard conduction model may lead to not negligible errors in the prediction of the internal surface temperature of the structures characterised by the massive layers placed on the inner side (Class I and Class IE), when compared to the finite difference heat conduction model. Although the reported errors are in the order of 0,3 °C, it is conceivable that higher errors may occur if these structures are exposed to additional driving forces. For this reason, the analysis was extended to an enclosed office (single thermal zone) for the Class I and IE components to evaluate the components' response considering additional driving forces.

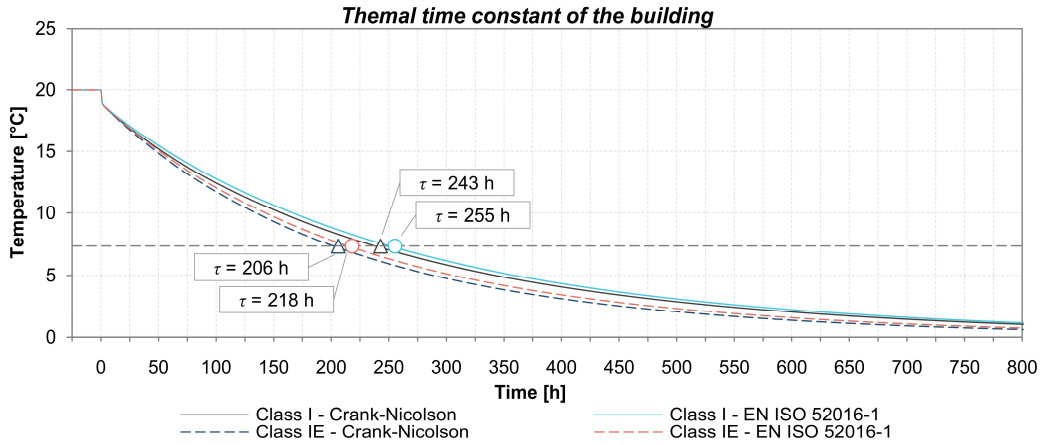


Figure 13: Thermal time constants and temperature decay

Firstly, an analysis on the building thermal time constant was performed for the analysed enclosed office implementing the Class I and IE components. The thermal time constant,  $\tau$  (expressed in h), represents the thermal decay of the internal temperatures when the outdoor temperature is kept constant. It is defined as in Equation (46):

$$\theta_{i,t} = \theta_e + (\theta_{i,\text{init}} - \theta_e) \cdot e^{-\frac{t}{\tau}} \quad (46)$$

where  $\theta_{i,t}$  is the indoor temperature at timestep  $t$ ,  $\theta_e$  is the constant outdoor air temperature, and  $\theta_{i,\text{init}}$  is the initial indoor temperature. Thus,  $\tau$  is the time required for the difference between the indoor and outdoor air temperature to decrease up to a  $e^{-1}$  factor [241]. To calculate the  $\tau$  for the baseline (EnergyPlus) and the test model (EN ISO 52016-1), a simulation was performed assuming an indoor air temperature equal to 20°C (stabilised), a constant outdoor air temperature equal to 0°C, no internal and solar gains, and no ventilation heat exchange (as suggested in [241]). The thermal time constants and the temperature decays are presented in Figure 13.

The temperature trends presented in Figure 13 are characterised by a first drop, common to all structures, and by a further slow decrease, which is instead specific for each structure (and considered conduction model); the former represents the internal air temperature decrease, while the latter is influenced by the heat capacity of the building components. Generally, the distribution of the whole heat capacity (or half of it) of the structure on the inner surface node results in higher thermal time constant values in the test model when compared to the baseline (characterised by the actual mass distribution of the structure), thus resulting in a delayed temperature decrease. Nevertheless, the  $\tau_s$  of the test and the baseline model differ for a few hours (from 243 to 255 h for Class I, and from 206 to 218 h for Class IE).

These findings allow to better understand the results presented below in terms of thermal energy needs for space heating and cooling (Table 17), and of indoor temperatures (Table 18).

Table 17: Thermal energy needs for space heating and cooling

Model	Class I		Class IE	
	$EP_{H,nd}$ [kWh·m <sup>-2</sup> ]	$EP_{C,nd}$ [kWh·m <sup>-2</sup> ]	$EP_{H,nd}$ [kWh·m <sup>-2</sup> ]	$EP_{C,nd}$ [kWh·m <sup>-2</sup> ]
<i>EnergyPlus (Crank-Nicolson)</i>	18,8	50,0	18,9	50,1
<i>Standard (CEN)</i>	18,9	50,0	19,0	50,1
<i>Improved (UNI)</i>	18,8	50,0	18,9	50,1

Table 18: *RMSD* for indoor air temperatures [°C]

Model	Class I		Class IE	
	January [°C]	July [°C]	January [°C]	July [°C]
<i>Standard (CEN)</i>	0,08	0,11	0,09	0,07
<i>Improved (UNI)</i>	0,00	0,00	0,00	0,00

The results of the analysis confirm what found in the preliminary phase. On the one hand, the improved solution algorithm introduced by the Italian National Annex ensures very close results to those of the Crank-Nicolson model, in terms of both thermal energy needs for space heating and cooling and indoor temperatures. As shown in Table 17, no variation in the accuracy of the model occurs in predicting the thermal energy needs for both the analysed structures (*MBE*'s values equal to 0%). Equally, the improved conduction model (Italian NA) allows to predict the indoor air temperatures with negligible errors in free-floating condition.

In the preliminary analysis, the standard heat conduction model led to not negligible errors (although low) in the prediction of the internal surface temperatures for the Class I and IE structures when stressed by an internal thermal constraint. In the present analysis, instead, the EN ISO 52016-1 simplified model ensures a high accuracy in the results. In particular, the standard model tends to slightly overestimate the thermal energy need for space heating for both the analysed structures. Nevertheless, the overestimation is almost negligible; in fact,

the *MBE* committed in the prediction of the  $EP_{H,nd}$  is equal to 0,6% (from 18,8 to 18,9 kWh·m<sup>-2</sup>) and 0,3% (from 18,9 to 19,0 kWh·m<sup>-2</sup>) for Class I and IE, respectively. On the other hand, no variation in the accuracy of the model in the prediction of both thermal energy needs for space cooling and indoor temperature occurs, as shown respectively in Table 17 and Table 18.

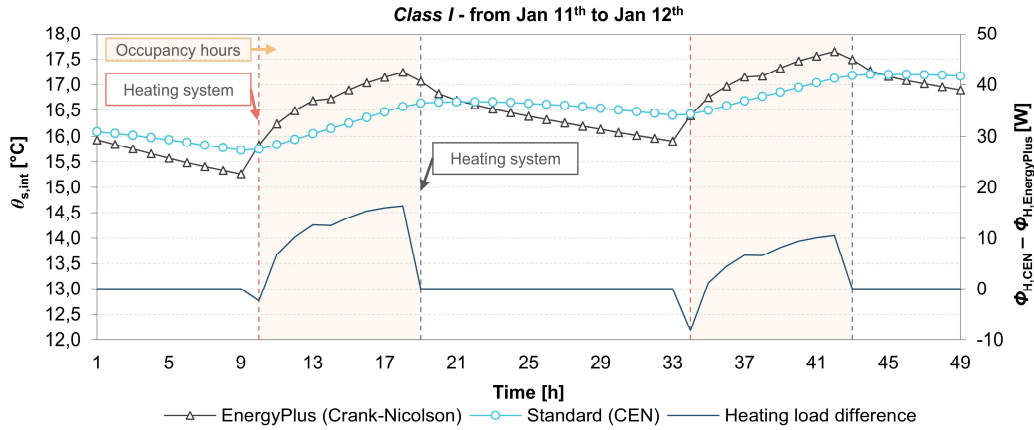


Figure 14: Comparison between hourly internal surface temperatures and heating loads for *Class I* structure

Even though the reported discrepancies are negligible, it is worth to analyse the thermal response of the structures to the main thermal constraints. In Figure 14, the internal surface temperature trend (for the external wall) is reported for the Class I structure case study; the heating load hourly difference between the test (EN ISO 52016-1) and the baseline model (EnergyPlus) is presented as well (a negative value indicates that the test model underestimates the hourly heating load with respect to the baseline model). As shown in the result analysis of the preliminary phase, the standard heat conduction model leads to an overestimation of the Class I structure internal areal heat capacity, compared to the actual structure ( $\kappa_{i,dev}$  equal to 45,2 kJ·m<sup>-2</sup>K<sup>-1</sup>). This overestimation causes a flattening in the thermal response of the structure to the internal constraints. In fact, in the unoccupied hours (i.e., free-floating condition, no internal gains) the external internal surface temperature decays less than the baseline model (e.g., temperature difference at time 9 h equal to ~1°C). On the other hand, the modelling of the whole thermal mass on the structure inner node (internal surface node) makes the inner layers to be less responsive to the heat gains (internal and solar gains) in the occupied hours, whose effect is thus reduced (and delayed) compared to the baseline model, resulting in lower internal surface temperatures. These temperature trends lead to a lower thermal power required to reach the internal set-point temperature when the heating system is switched on (–3 W and –8 W at time 10 and 34 h, respectively) compared to the baseline model; in the occupied hours, instead, a higher heating power is

required to maintain the set-point temperature, leading thus to the reported slight overestimation of the annual thermal energy need for space heating.

## 5.4 Validation on building archetypes

The present work investigates the effect of the main modelling assumptions related to the heat balance on the outdoor and the indoor envelope surfaces, introduced by the EN ISO 52016-1 technical standard [5]. To guarantee a general validity of the outcomes, two building archetypes, representative of the Italian existing building stock, two levels of thermal insulation (i.e., uninsulated/scarcely insulated, and highly insulated), and two Italian climatic zones were considered, for a total of eight case studies. Moreover, to explore different applications of the standard method, the analysis was performed both to evaluate the accuracy of the model in predicting the indoor operative temperatures (in free-floating conditions), and to assess the annual thermal energy needs for space heating and cooling.

### 5.4.1 Methodology

The methodology workflow proposed in Section 3.4 (except for the calibration phase) was applied to assess the accuracy of the EN ISO 52016-1 assumptions relative to the modelling of external and internal driving forces. Specifically, the tested modelling assumptions are those presented in Sections 5.2.1.1–5.2.1.4 and 5.2.1.6–5.2.1.8.

Firstly, the baseline model was created by means of the EnergyPlus simulation engine; then, each tested modelling assumptions were applied one-at-the-time in the test models. The effect of the modelling assumptions on the accuracy of the model was evaluated for two different situations. Firstly, the variation in the annual sensible energy needs for heating and cooling was assessed; secondly, the errors in the prediction of the indoor operative temperatures are evaluated in a free-floating situation. These two different analyses allow to determine the expected accuracy of the model for different purposes, such as the energy performance evaluation or the energy requirements compliance check, or the energy audits or the thermal comfort evaluations.

Two statistical indexes were calculated to numerically assess the accuracy of the models. In particular, the hourly mean bias error (*MBE*) was used for the annual energy needs evaluation, and was calculated as specified in [71]:

$$MBE_{H/C} = \frac{\sum_{t=1}^n (\Phi_{H/C, \text{test}, t} - \Phi_{H/C, \text{baseline}, t})}{\sum_{t=1}^n |\Phi_{H/C, \text{baseline}, t}|} \cdot 100 \quad (47)$$

where  $\Phi_{H/C}$  is the heating (H) or cooling (C) load (in W) at timestep  $t$ , for the test model and for the baseline, respectively, and  $n$  is the number of timesteps considered for the calculation (8760 for annual evaluations). The *MBE* is expressed as a percentage error, and measures how closely the predicted hourly heating or cooling loads corresponds to the baseline data. The variations in the energy needs are considered acceptable with *MBE* values in the range of  $\pm 10\%$  (when using hourly data) [71]. The root-mean-square deviation (*RMSD*) was instead used to measure the variability in the prediction of the indoor operative temperatures (in K), and was calculated as

$$RMSD = \left( \frac{1}{n} \cdot \sum_{t=1}^n (\theta_{\text{op}, \text{test}, t} - \theta_{\text{op}, \text{baseline}, t})^2 \right)^{0,5} \quad (48)$$

where  $\theta_{\text{op}}$  is the indoor operative temperature at timestep  $t$ , for the test model and for the baseline, respectively, and  $n$  is the number of timesteps considered for the calculation (8760 for annual evaluations). In this case, acceptable deviations in the prediction of the indoor operative temperatures are considered for *RMSD* values lower than 0,5 °C [62].

The procedure presented is applied separately for each tested modelling option. All simulations were performed through the Python applicative pyEp [94], which implements the Ptolemy EnergyPlus's external interface.

## 5.4.2 Application

### 5.4.2.1 Case studies

The cases considered in the present study are two buildings, an office module and a residential apartment unit, each one characterised by two levels of thermal insulation of the building envelope and sited into two different Italian climatic zones, for a total of four variants for two case studies.

A thermally uninsulated or scarcely insulated existing building (referred as ExtB from so on) was assumed as first; a well-insulated building envelope (referred as DM from so on), in compliance with the Italian minimum energy performance requirements for new buildings as specified by the Interministerial Decree of 26 June 2015 [261], was considered as well. The case studies were assumed to be placed in Milan (Northern Italy) and Palermo (Southern Italy).



The residential case study is an apartment unit of a multi-storey residential building (Figure 15a), representative of the Italian residential existing building stock, built in the period 1946-76 [262]. The main geometrical characteristics of the case study are presented in Table 19. It was assumed to be adjacent to identical residential units; thus, only the South-, West- and North-oriented façades are exposed to the outdoor environment. The internal partitions were assumed as adiabatic components, and were explicitly modelled for the sake of internal mass. The South-oriented façade is characterised by two windows of 2,8 m<sup>2</sup> area each, shaded by an overhang of 1 m depth; the North-oriented façade is instead characterised by two windows of 1,5 m<sup>2</sup> and 2,0 m<sup>2</sup> areas, respectively. As concerns the existing building variant (ExtB), the external walls are made of uninsulated hollow brick masonry with air gap ( $U_{\text{wall,res,ExtB}} = 1,1 \text{ W}\cdot\text{m}^{-2}\cdot\text{K}^{-1}$ ), while the transparent components are characterised by a single glazing with wooden frame ( $U_{\text{win,res,ExtB}} = 4,9 \text{ W}\cdot\text{m}^{-2}\cdot\text{K}^{-1}$ ,  $g_{\text{res,ExtB}} = 0,85$ ).

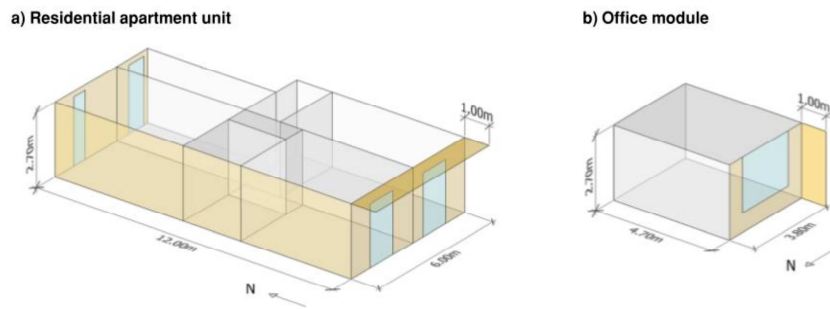


Figure 15: 3D visualization of the residential apartment unit (a) and of the office module (b) case studies

Table 19. Main geometrical data of the case studies.

Parameters	Residential apartment-Unit	Office module
Conditioned net floor area, $A_n$	66,3 m <sup>2</sup>	17,8 m <sup>2</sup>
Conditioned net volume, $V_n$	179,0 m <sup>3</sup>	48,1 m <sup>3</sup>
Transparent area (vs. external), $A_{\text{env,w}}$	9,1 m <sup>2</sup>	4,8 m <sup>2</sup>
Opaque area (vs. external), $A_{\text{env,op}}$	52,7 m <sup>2</sup>	5,5 m <sup>2</sup>
Compactness ratio, $S/V$	0,35 m <sup>-1</sup>	0,21 m <sup>-1</sup>
Windows-to-wall ratio, $WWR$	0,34 (South wall)	0,47 (West wall)
	0,00 (West wall)	
	0,27 (North wall)	

The office module is a single office (Figure 15b, Table 19) of a multi-storey office building, representative of the Italian existing office building stock, built in the 90s [263]. As for the residential unit, the office module was assumed to be adjacent to identical conditioned offices. The only exposed building envelope component (West-oriented façade) is characterised by a window of 4,8 m<sup>2</sup> area, shaded by a side fin of 1 m depth. As concerns the existing building variant (ExtB),

the external wall is made of a prefabricated concrete wall ( $U_{\text{wall,off,ExtB}} = 0,8 \text{ W}\cdot\text{m}^{-2}\cdot\text{K}^{-1}$ ) with interposed low thickness thermal insulation material, while the window is a double-glazing unit with wooden frame ( $U_{\text{win,off,ExtB}} = 2,8 \text{ W}\cdot\text{m}^{-2}\cdot\text{K}^{-1}$ ,  $g_{\text{off,ExtB}} = 0,75$ ).

For both the case studies, the thermo-physical features of the opaque envelope components were derived from the UNI/TR 11552 technical report [258] that provides typical Italian building components. As concerns the well-insulated building variants (DM), the opaque and transparent building envelope components were modified in order to achieve the thermal transmittance values of the reference building, as specified by the Italian legislation [261] for the considered climatic zones (Table 20). In both case studies, thermal bridges were neglected.

Table 20: Thermal transmittance values of the reference building in accordance with Interministerial Decree of 26 June 2015 [34]

Envelope Component	Milan (Climatic Zone E) <sup>1</sup>	Palermo (Climatic Zone B) <sup>2</sup>
External wall ( $U_{\text{wall,DM}}$ )	$0,26 \text{ W}\cdot\text{m}^{-2}\cdot\text{K}^{-1}$	$0,43 \text{ W}\cdot\text{m}^{-2}\cdot\text{K}^{-1}$
Windows ( $U_{\text{win,DM}}$ )	$1,4 \text{ W}\cdot\text{m}^{-2}\cdot\text{K}^{-1}$ ( $g = 0,50$ )	$3,0 \text{ W}\cdot\text{m}^{-2}\cdot\text{K}^{-1}$ ( $g = 0,75$ )

<sup>1</sup> 2274 °C·d HDD, 81 °C·d CDD.

<sup>2</sup> 1121 °C·d HDD, 166 °C·d CDD. Heating Degree Days (HDD) and Cooling Degree Days (CDD) calculated according to the UNI 10349-3 technical standard [264] using 20 °C and 26 °C, respectively, as base temperatures.

A standard user behaviour, regarding the occupancy profile, internal heat sources, ventilation air flow rate, and HVAC operation, was assumed for both the case studies, and was derived from the draft of the Italian Annex of the EN 16798-1 technical standard [259]. The ideal load air system of EnergyPlus was considered to evaluate the energy needs for heating and cooling, considering a dead band internal temperature set point of 20 °C and 26 °C, respectively. The HVAC system was instead switched off all year long in the indoor operative temperature evaluation (free-floating condition).

The evaluations were carried out using the International Weather for Energy Calculations (IWECC) data file [260] for the cities of Milan and Palermo.

#### 5.4.2.2 Modelling options

From the documentation analysis presented in Section 5.2.1, fourteen different modelling options were selected to be tested. In this paragraph, a detailed description of the parameters used in the tested modelling assumptions is provided. For some of these, the implementation in EnergyPlus was not straightforward. The strategies used for the correct modelling of these assumptions are therefore outlined.

##### *External convection heat transfer*

With regards to the external convection heat transfer (External CV) assumptions, the TARP algorithm [247] was adopted in the baseline model for the

definition of the external convection heat transfer coefficient; four evaluation steps were considered instead in the test models, representing increasing levels of simplifications in its determination.

1. *HC-V<sub>w-av</sub>*: the effect of a lack of detailed input data regarding the wind speed was assessed. In particular, the convective heat transfer coefficient was considered time-dependent and was calculated by means of the TARP algorithm [247]. Differently from the baseline model, the forced component is calculated by implementing annual average wind speed values; specifically, wind speeds of 0,9 and 3,8 m·s<sup>-1</sup> were used for Milan and Palermo, respectively,
2. *HC-V*: the effect of the formulation specified in Equation (25) for the  $h_{c,ext}$  determination was evaluated. The convective heat transfer coefficient was considered variable on a timestep basis, and the site hourly wind speed was used,
3. *HC-C<sub>w-av</sub>*: the annual average wind speed was implemented in Equation (25) to calculate an average heat transfer coefficient, assumed constant over the simulation period,
4. *HC-C<sub>st</sub>*: the effect of the  $h_{c,ext}$  standard values was evaluated, assuming a constant convective heat transfer coefficient equal to 20 W·m<sup>-2</sup>·K<sup>-1</sup> over the simulation period, calculated by means of the reference wind speed value of 4 m·s<sup>-1</sup> (Equation (25)).

#### *External longwave radiation heat transfer*

As far as the external longwave radiation heat transfer (External LW) is concerned, the heat transferred between the surface and the external environment is assessed by means of Equation (21) in the baseline model. In particular, the Clark and Allen correlation [265] is used for the apparent sky temperature determination. Three evaluation steps were considered.

1. *SKY*: the influence of the direct sky temperature model for the apparent sky temperature calculation was assessed; specifically, the sky temperature was assumed 11 °C below the outdoor air temperature,
2. *HR*: in EnergyPlus, the external net longwave radiation heat flux is calculated by applying the Stefan-Boltzmann law. Thus, the definition of the radiant heat transfer coefficients as input values was not possible. To assess the influence of the linearisation of the longwave heat transfer (Equation (22)), a simple modelling strategy was applied. Firstly, the outdoor surface emittances were set equal to 0 to annul the external longwave heat transfer automatically calculated by EnergyPlus. Then, an additional heat balance term, calculated as specified in Equation (22), was added to the external surface of the envelope

components. The standard radiant heat transfer coefficient ( $h_{r,ext}$ ) equal to  $4,14 \text{ W}\cdot\text{m}^{-2}\cdot\text{K}^{-1}$  was used, and was calculated by assuming a surface emissivity equal to 0,9 and a reference mean temperature of  $0 \text{ }^{\circ}\text{C}$  [132]. The EnergyPlus's calculated view factor between the surface and the sky ( $F_{sky}$ ) was assumed, as well as the Clark and Allen [265] calculated sky temperature,

3. *HR-EU*: the parameters described for the HR test model were used in this step, while the apparent sky temperature was calculated as direct difference from outdoor air ( $11 \text{ }^{\circ}\text{C}$ ).

Due to software limitations, the HR and HR-EU modelling assumptions were implemented only on the opaque building envelope components.

#### *Solar transmission*

Concerning the solar radiation entering the zone through windows (External SW), two steps were considered.

1. *GV-EU*: the effect of considering the solar radiation entering the thermal zone as all shortwave radiation was assessed. The glazing solar properties were considered time- and solar angle-independent, by assuming a constant exposure factor ( $F_w$  in Equation (26)) equal to 0,9 over the simulation period [5],
2. *GV-ITA*: as in GV-EU, the solar radiation entering the thermal zone was considered as all shortwave radiation, while the glazing solar properties were considered solar angle- and time-dependent, by assuming a variable exposure factor ( $F_w$  in Equation (26)) calculated by means of the Italian National Annex approach [137] (Equation (40)).

Differently from other tested modelling assumptions, the EnergyPlus code was modified to correctly model the GV-EU and GV-ITA evaluation steps. In particular, it was adapted as to consider the solar transmission coefficient of windows (for beam-to-beam, beam-to-diffuse, and diffuse-to-diffuse solar irradiance) equal to the  $g$ -value at normal incidence (while 0 was assumed for the absorption factor), and corrected by means of the  $F_w$  exposure factor calculated within in the EnergyPlus code.

#### *Internal convection heat transfer*

About the internal convection heat transfer (Internal CV), the variation in the accuracy of the model resulting from the use of the standard values of the heat transfer coefficient was assessed, compared to the baseline implementing the TARP algorithm [265] for the definition of the internal convective heat transfer coefficients. Specifically,

1. *HC-Cst*: A constant value of the convective heat transfer coefficient was considered over the simulation period, whose determination depends on the direction of the heat flow. As specified by the EN ISO 6946 technical standard [132], the  $h_{c,int}$  values were assumed equal to 5,0, 2,5 and 0,7  $W \cdot m^{-2} \cdot K^{-1}$ , for horizontal, upward and downward heat fluxes, respectively.

#### *Internal longwave radiation heat transfer*

Although the linearisation of the internal longwave heat transfer (Internal LW) represents a simplification in the modelling on the considered physical phenomenon, this assumption was not tested in the present work. In fact, the temperature difference between the surfaces facing the thermal zone can be considered minimal, thus this approach may influence the energy behaviour of a building in a negligible way. Instead, the effect of the uniform distribution of the radiant fraction of internal gains was assessed, as follows.

1. *IG*: Firstly, only the convective fraction of internal gains (occupancy, appliances, and lighting) was set as input data in the EnergyPlus model (test model). Then, their radiative fraction was directly applied to the internal surfaces as additional heat balance term, calculated for each timestep as in Equation (29). For the sake of this test, different thermal emissivities were assumed for surfaces facing the zone (i.e., floor and ceiling, walls, and windows).

#### *Internal shortwave radiation heat transfer*

Finally, three assumptions were tested as regards the solar radiation and solar heat gains (Internal SW) in the thermal zone, as follows.

1. *BR*: The assumption of EN ISO 52016-1 to not consider a fraction of solar radiation that is reflected back outside the zone from windows was evaluated. To this purpose, the “lost” solar radiation (Equation (33)) was added as an additional heat balance term to each surface, proportionally to the respective surface areas and solar absorption factors (Equation (32)),
2. *UD*: The effect of the uniform distribution of solar radiation on the internal surfaces, specified by the EN ISO 52016-1 hourly method, was evaluated. A simple modelling procedure was applied; the internal surface solar absorption was set equal to 0 to annul the absorbed solar radiation automatically calculated by EnergyPlus. Then, the global (beam plus diffuse) solar radiation entering the zone at each timestep was distributed uniformly on the internal surfaces (Equation (31)). Solar heat gains were considered all radiant heat gains. For the sake of this test, different solar absorption factors were assumed for surfaces facing the zone (i.e., floor and ceiling, and walls),

3. *UD-CSG*: The influence of the fraction of solar radiation directly transferred to the in-ternal air as convective heat gain was evaluated. The modelling approach of UD was applied. Differently from the UD test model, the solar radiation distributed over the internal surfaces was decreased by a 10%, considered as a convective heat gain.

### 5.4.3 Results

The effects of the tested modelling options on the thermal behaviour of the case studies are presented in this section; in Section 5.4.3.1, the deviations of the annual energy needs for heating and cooling are presented for each case study variant, while the errors in the prediction of the indoor operative temperatures are presented in Section 5.4.3.2.

#### 5.4.3.1 Energy needs evaluation

Figure 16 and Figure 17 show the deviations in the energy needs for heating and cooling for the tested modelling assumptions for the office module and the residential apartment unit, respectively. The labels represent the variation of both heating and cooling energy needs ( $\Delta EP_{H/C,nd}$ ), while the red and bold highlighted values represent the tested assumptions for which the mean bias error (*MBE*) exceeds the acceptable value ( $\pm 10\%$  [71]). Significant discrepancies between the baseline and the test models are highlighted when the EN ISO 52016-1 assumptions related to the definition of the external convective heat transfer coefficients are concerned. Generally, an increase of the annual energy needs for heating, and a decrease in the one for cooling occur for all the case study variants. Firstly, the effect related to the lack of specific input data regarding the local wind speed was assessed. The use of an average wind speed value for the determination of the  $h_{cs}$  following the TARP algorithm (*HC-Vw-av*, variable heat transfer coefficient) leads to negligible variations in the cooling energy needs for all the considered building variants. In fact, the energy needs for cooling decreases with variations within  $-0,3 \text{ kWh}\cdot\text{m}^{-2}$ , with respective Mean Bias Errors (*MBEs*) lower than  $-1\%$ . Slightly increases occur instead in the energy needs for heating, especially for the residential apartment unit at the existing building (ExtB) insulation level in Milan (i.e.,  $\Delta EP_{H,nd}$  equal to  $+1,3 \text{ kWh}\cdot\text{m}^{-2}$ , and *MBE* equal to  $+2\%$ ). Negligible variations instead are reported for the cooling dominated climatic zone (Palermo), as well as for the well-insulated case studies (DM) in Milan.

The use of a constant value of the heat transfer coefficient, calculated considering either an average (*HC-Cw-av*) or a reference wind speed (*HC-Cst*), leads to the highest variations of the energy need for heating among all the tested modelling assumptions. This is particularly true for the apartment unit at the ExtB

insulation level in both climatic zones. In Palermo for the *HC-Cst* assumption,  $EP_{H,nd}$  variations of  $+4,2 \text{ kWh}\cdot\text{m}^{-2}$  (compared to  $5,2 \text{ kWh}\cdot\text{m}^{-2}$  of the baseline), and  $EP_{C,nd}$  variations of  $-4,3 \text{ kWh}\cdot\text{m}^{-2}$  (compared to  $22,2 \text{ kWh}\cdot\text{m}^{-2}$  of the baseline) are reported, with *MBEs* both exceeding the acceptable values ( $+83\%$  and  $-19\%$  for the heating and the cooling needs, respectively). Comparable situations occur in Milan for both the *HC-Cw-av* and *HC-Cst* tests (for heating,  $+11\%$  and  $+24\%$ , respectively; for cooling,  $-19\%$  and  $-42\%$ , respectively).

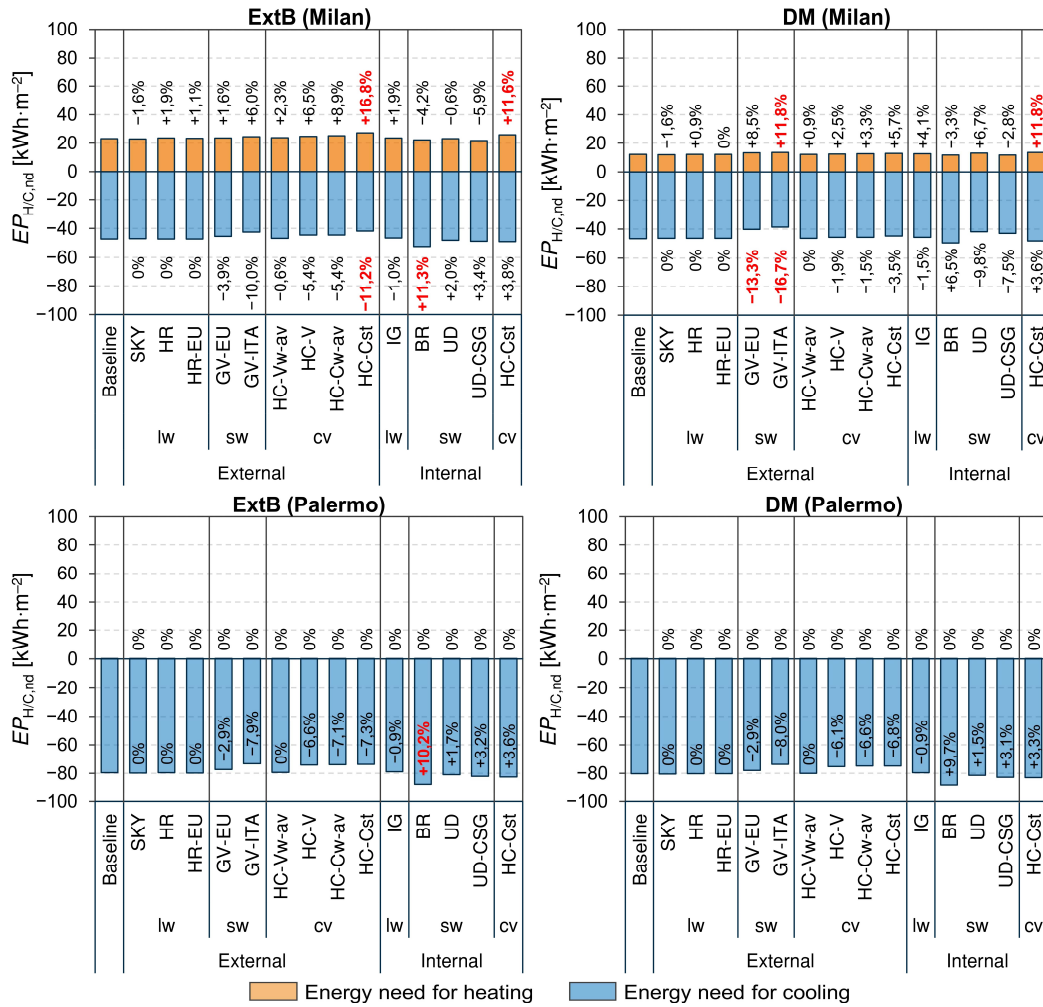


Figure 16: Deviations of the energy needs for heating and cooling for the tested modelling assumptions for the office module

Consistent discrepancies occur also for the ExtB office module in Milan when the *HC-Cst* assumption is implemented; in this case, the variations in the energy needs for heating and cooling are characterised by *MBEs* equal to  $+17\%$  and  $-11\%$ , respectively. Nevertheless, the implementation of the reference  $h_c$  values specified by the EN ISO 13798 technical standard [134] leads to acceptable variations of the

energy needs for all case studies characterised by the DM insulation level (e.g., for the DM apartment unit in Milan, +5% and −9% for the heating and the cooling energy needs, respectively), as well as for the existing office module in Palermo.

Finally, a decrease in the model accuracy occurs when variable external heat transfer coefficients, calculated by means of the EN ISO 6946 formulation (Equation (25)), are considered. In fact, this formulation applied on a timestep basis leads to increases in the heating needs comparable to the *HC-Cw-av* assumption for the all the considered cases (e.g., +9% for the ExtB residential building in Milan), as well as decreases in the cooling needs (e.g., −19% for the ExtB residential building in Milan).

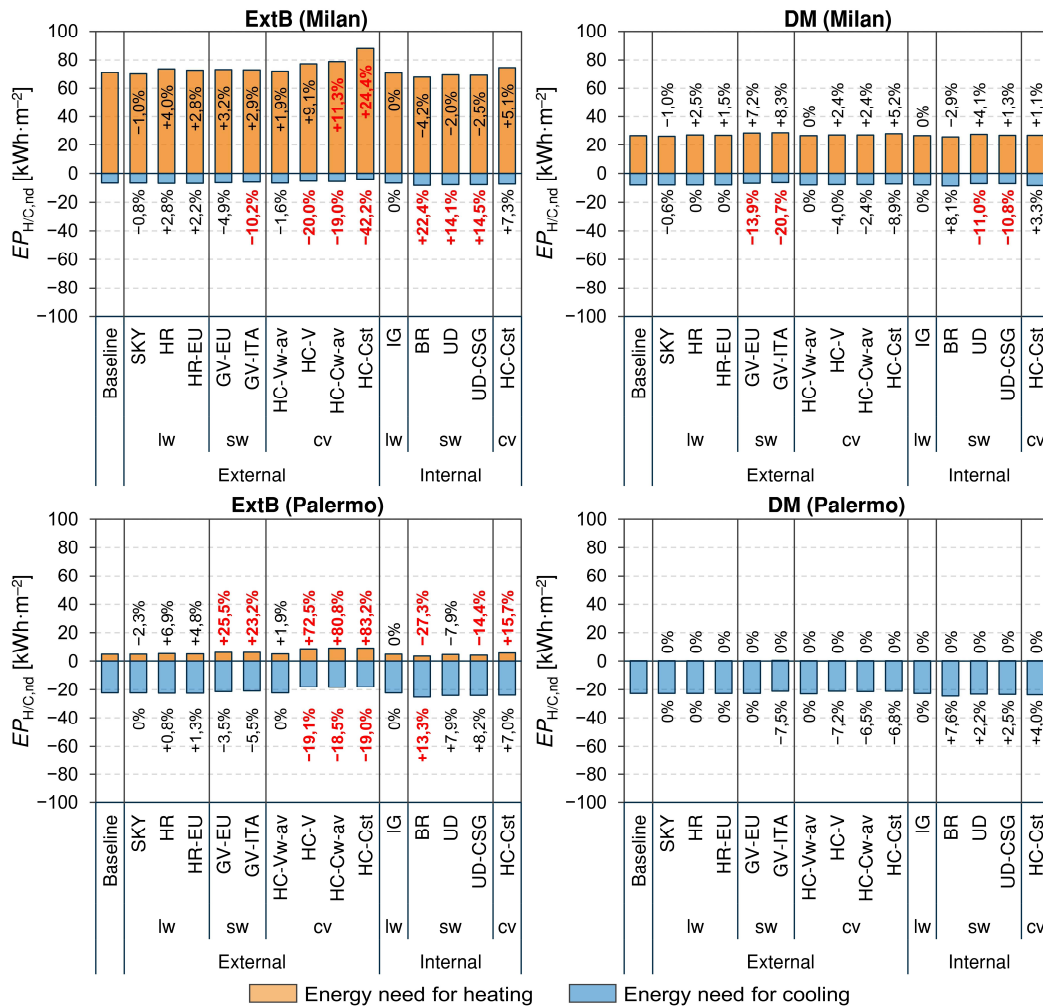


Figure 17: Deviations of the energy needs for heating and cooling for the tested modelling assumptions for the residential apartment unit

These similarities in the results can be explained by analysing the convective coefficient profiles shown in Figure 18, in which the different  $h_{c,ext}$  hourly profiles



(left-hand side graph in Figure 18) for the residential apartment unit (ExtB) in Milan are presented for a typical winter week (from 13 to 20 January). The hourly thermal loads are presented as well (right-hand side graph in Figure 18). The  $h_{c,ext}$  values calculated by means of the formulation in Equation (25) on an hourly basis (*HC-V*) are consistently higher than the ones calculated by means of the TARP algorithm, using either a variable (baseline model) or an average constant wind speed (*HC-Vw-av*). Higher convection heat transfer rates occur for the *HC-V* assumption, leading to the reported discrepancies between the outcomes both on the annual energy needs and on the hourly thermal loads. The *HC-Cw-av* assumption leads to similar results to *HC-V*, since the constant  $h_{c,ext}$  used in *HC-Cw-av* can be considered an average mean value of the hourly *HC-V* values. However, since *HC-V* is sensitive to the hourly fluctuation of the wind speed, slight discrepancies can be highlighted between *HC-Cw-av* and *HC-V*. In particular, the *HC-V* test model tends to overestimate the  $h_c$  values with respect to the baseline when high values of wind speed are reported, and thus to overestimate heating loads, while the *HC-Cw-av* constant value is similar to the baseline one.

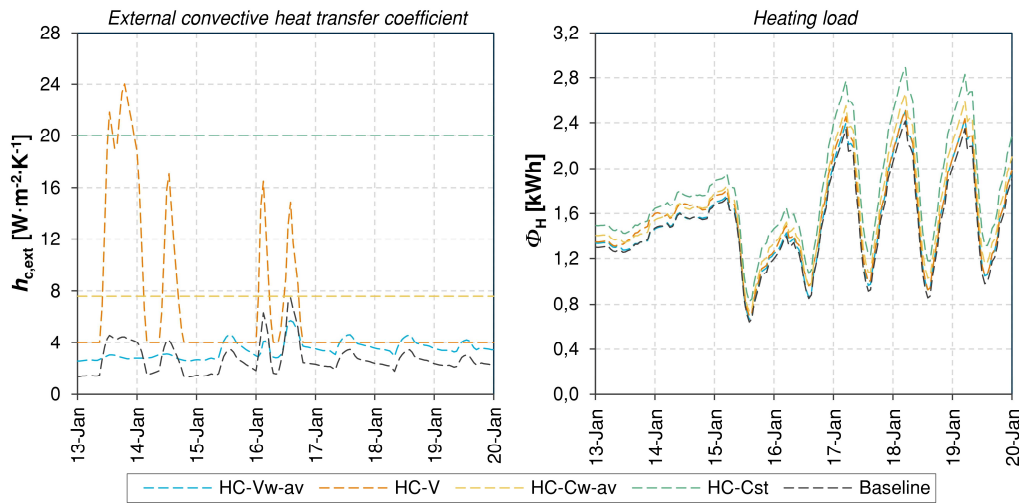


Figure 18: Existing residential unit in Milan: hourly heating loads and  $h_{c,ext}$  values in a winter period for the analysed modelling assumptions

As far as the modelling assumptions related to the longwave heat transfer phenomenon are concerned, a general increase in the energy need for heating and a decrease in the one for cooling can be observed. The linearisation of the longwave heat transfer phenomenon (*HR* and *HR-EU*) results to influence the energy need of the case studies more than the simplified definition of the sky temperature (*SKY*). For example, the energy need for heating increases of +2,8 and +0,7 kWh·m<sup>-2</sup> for the residential unit in Milan, for the existing building and the DM insulation levels, respectively, when the standard constant  $h_{r,ext}$  and the EnergyPlus sky temperature

are considered (*HR*). The introduction of the EN ISO 52016-1 assumption related to the sky temperature definition (*HR-EU*) shows comparable results with the *HR* modelling option. This is due to the fact that the actual average difference between the apparent sky and the outdoor air temperatures is similar to the reference value of 11 °C (i.e., equal to 11,5 °C for Milan, and 11,2 °C for Palermo) used in the simulations. Likewise, good agreements between the baseline and the test models can be found when the sky temperature is assumed to be 11°C below the external air temperature (*SKY*). In fact, the variation in the energy need for heating is around  $\pm 0,5 \text{ kWh}\cdot\text{m}^{-2}$  for all the case studies, with mean errors within  $\pm 2\%$ . For all the considered case study variants, the modelling assumptions related to the external longwave radiation guarantee a variation in the accuracy of the calculation model never exceeding the *MBE* assumed limits ( $\pm 10\%$ ).

When the solar radiation entering the thermal zone is considered as all shortwave radiation, and the glazing parameters are considered to be solar angle- and time-independent (*GV-EU*), the energy need for heating slightly increases compared to the baseline model, while the energy need for cooling decreases. The same trend occurs also for the *GV-ITA* test model.

The implementation of a time-independent internal convective heat transfer coefficient (*HC-Cst*), calculated for reference conditions [132], leads to a general increase of the energy needs for both heating and cooling. Differently from the external convective heat transfer, the simplification introduced by the EN ISO 52016-1 on the definition and time discretisation of the internal convective heat transfer coefficients guarantees an acceptable level of accuracy for almost all the considered cases. In fact, the average errors in the prediction of the energy needs for cooling vary between +3% and +7% for all the considered case studies. As for the energy needs for heating, good agreements between the baseline and the test models are reported for the office module in Palermo (i.e.,  $\Delta EP_{H,nd}$  equal to 0  $\text{kWh}\cdot\text{m}^{-2}$  for both the ExtB and the DM insulation levels), and for the ExtB residential apartment in Milan (i.e.,  $\Delta EP_{H,nd}$  equal to +3,6  $\text{kWh}\cdot\text{m}^{-2}$ , corresponding to *MBE* of +5%).

The simplification related to the uniform distribution of the radiant fraction of internal gains on the internal surfaces does not affect the accuracy of the model. The extent of the variation in the energy needs for both heating and cooling is negligible for the residential apartment; in fact, they range within a  $\pm 0,1 \text{ kWh}\cdot\text{m}^{-2}$  variation, with relative mean bias errors tending towards 0%. For the office module, in which the internal heat gains are consistently higher than in the residential building (overall 28  $\text{W}\cdot\text{m}^{-2}$  compared to 7,6  $\text{W}\cdot\text{m}^{-2}$ ), the variations in the energy needs are slightly higher (e.g., +0,5 and -0,7  $\text{kWh}\cdot\text{m}^{-2}$  for heating and cooling,

respectively, for the well-insulated office module in Milan); the *MBE* values never exceed the acceptable values.

As introduced, the EN ISO 52016-1 hourly method does not consider back reflection of solar radiation to the external environment (*BR*). As expected, a decrease in the energy needs for space heating occurs due to the higher solar gains; an increase in the energy needs for cooling is reported, as well. This trend is particularly clear for the case studies characterised by the existing building insulation level; in fact, the high values of windows solar transmittance (typical for low-performance transparent building components) entail a high amount of back reflected solar radiation (baseline model), and thus higher solar gains in the test models. For example, the energy need for cooling of the ExtB office building in Palermo increases of  $+8,1 \text{ kWh}\cdot\text{m}^{-2}$  compared to the baseline model, while a decrease of  $-3,0 \text{ kWh}\cdot\text{m}^{-2}$  is reported for the ExtB residential apartment in Milan. Similar variations also occur for the case studies in Palermo, when the DM level of thermal insulation is considered (e.g., for the office module,  $-3\%$  and  $+7\%$  of the energy needs for heating and cooling, respectively). For four out of eight cases considered, the variations in the energy needs exceed the accepted ranges.

Generally, considering a uniform distribution of solar radiation on the zone surfaces (*UD*) leads to a slight increase of the annual energy needs for heating, and a decrease in the one for cooling, in the heating dominated climatic zone (Milan), while an opposite trend is reported in Palermo (cooling dominated). The EN ISO 52016-1 solar distribution approach causes a consistent underestimation of the surface solar heat gain for the floor, while a higher solar radiation amount is distributed over the surfaces facing the outdoor environment, compared to the baseline model. Finally, the same trend, but with opposite signs, is reported when a fraction of solar radiation is considered to be immediately transferred to the internal air (*UD-CSG*). In fact, this approach leads to a decrease in the energy need for heating, and an increase in the energy need for cooling, with respect to the *UD* test model. If compared to the baseline model, the *UD* and *UD-CSG* variants show an opposite deviation on the energy needs for heating and cooling that, if applied together, they might produce compensations in the results. The variations of the heating energy needs are almost negligible for all the considered case studies, while a general increase in the energy needs for cooling occurs. The effect of this assumption is particularly consistent in the office module, which is characterised by a noteworthy transparent surface with respect to the conditioned volume. The solar radiation immediately transferred to the air consists in an annual average additional heat gain equal to  $2,5 \text{ W}\cdot\text{m}^{-2}$  for the office module, compared to  $0,9 \text{ W}\cdot\text{m}^{-2}$  for the apartment unit.

### 5.4.3.2 Indoor temperatures evaluation

The errors in the prediction of the indoor operative temperatures are presented in Figure 19 and Figure 20 for a winter month (yellow squared dots), and for a summer month (blue diamond dots), respectively for the office module and the residential apartment unit. In particular, a free-floating simulation was performed for each tested assumption and for each case study variant, and the effect of the simplifications was assessed for two months (from 15 January to 15 February – referred as Winter month, and from 15 July to 15 August – referred as Summer month). The dashed red line in each chart represents the assumed root-mean-squared deviation acceptable limit (0,5 °C).

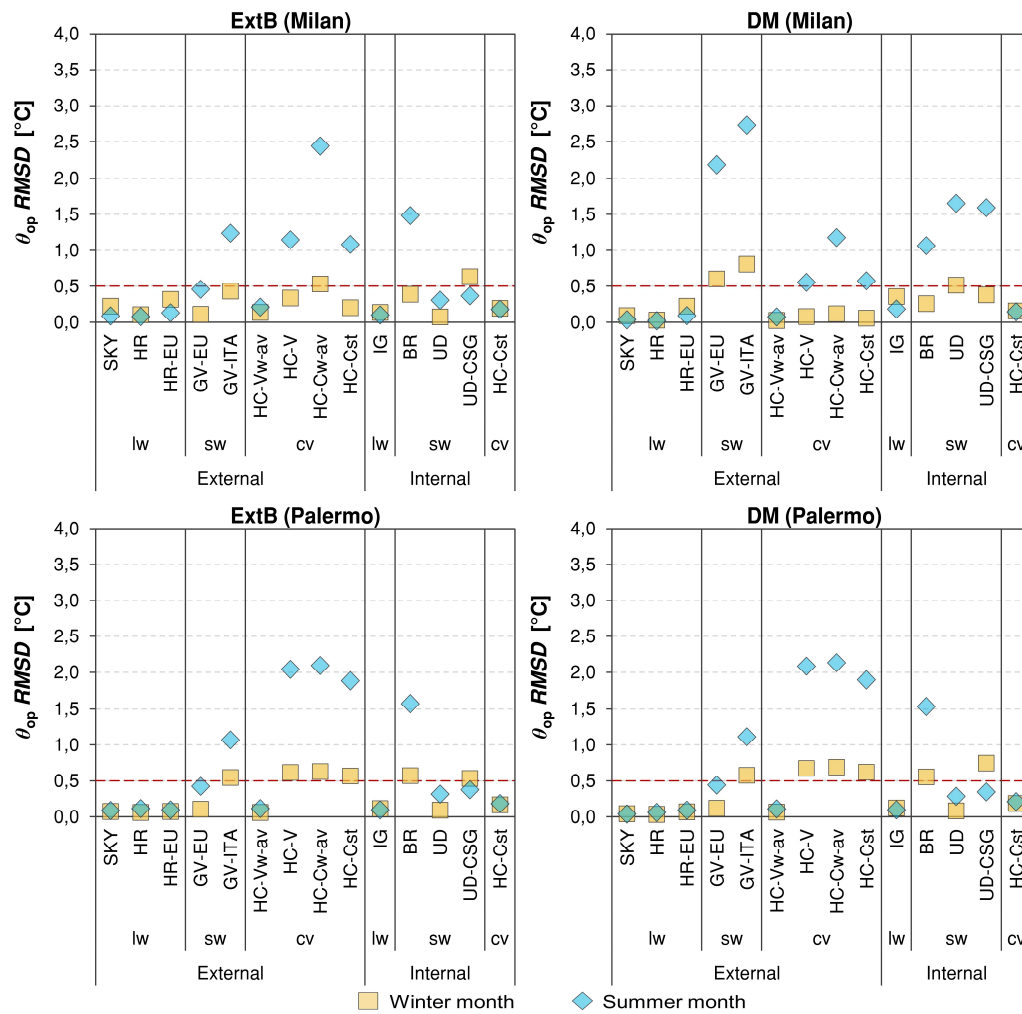


Figure 19: Operative temperature RMSDs for a winter and a summer month for the tested modelling assumptions for the office module

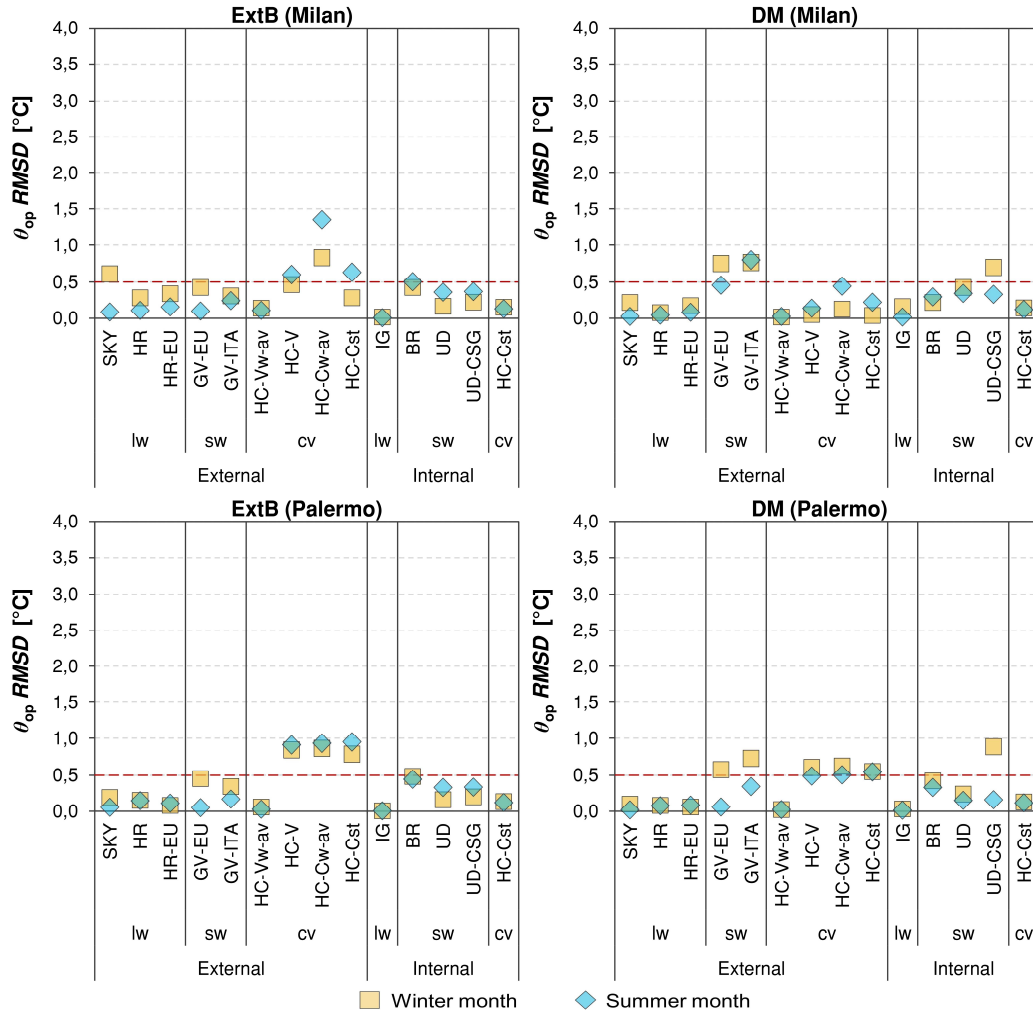


Figure 20: Operative temperature RMSDs for a winter and a summer month for the tested modelling assumptions for the residential apartment unit

The evaluations on the operative temperatures partially confirm the findings of the previous analysis on the annual energy needs for heating and cooling. As far as the existing building insulation level is concerned, the accuracy of the model in predicting the indoor operative temperatures results to be not sensitive to the modelling assumptions related to the longwave radiation heat transfer (on both the internal and external surfaces), and to the inside heat convection. The simplified algorithms used in the determination of the external convective heat transfer coefficients (HC-V, HC-Cw-av, and HC-Cst) are the simplifications that lead to consistent discrepancies in the operative temperature estimation in all the ExtB cases. Discrepancies in the prediction of the indoor operative temperatures also occur when the back reflection of the solar radiation entering the thermal zone is neglected (BR test case), as well as when a weighted  $g$ -value is considered in the

simulations (GV-EU and GV-ITA), especially in the office module case study due to its large windowed surface (compared to the conditioned volume).

The results related to the well-insulated buildings are consistently different between the office module and the residential unit. The residential apartment results to be less sensitive to the modelling assumptions related to the external heat convection than the office building, for which RMSDs between 0,55 and 1,2 °C are reported for Milan and around 2,0 °C for Palermo in summer, if either an hourly variable (HC-V) or constant heat transfer co-efficient (HC-Cw-av and HC-Cst) is applied. Differently from the ExtB building, in the well-insulated building the GV assumptions (GV-EU and GV-ITA) result to influence more the winter-performance than the summer one; however, the acceptable variance of the indoor operative temperatures is not guaranteed for both summer and winter, for all the considered cases.

## **5.5 Validation on a real residential nZEB**

The present work is intended at finalising the research developed in this dissertation, gathering the activities presented in the previous sections. It investigates, on the one hand, the effect of the EN ISO 52016-1 simplifications related the modelling of the building fabric on the thermal behaviour of a real residential nearly-zero building; on the other hand, it addresses the open issues concerning the building energy model calibration. As for the latter analysis, this was performed through a collective calibration exercise involving research groups from four Italian universities, namely Politecnico di Milano, Politecnico di Torino, Università di Trento, and Università degli Studi di Roma Tor Vergata (the main outcomes are presented in Section 5.5.4).

### **5.5.1 Methodology**

The present analysis evaluates the effect of the EN ISO 52016-1 modelling assumptions on a real building; differently from the analyses presented in the previous sections, the application on a real building requires a preliminary step of building energy model calibration. The evaluation of the simplification was performed by applying the methodology workflow proposed in the present dissertation (Section 3.4); its specific application is presented in Figure 21.

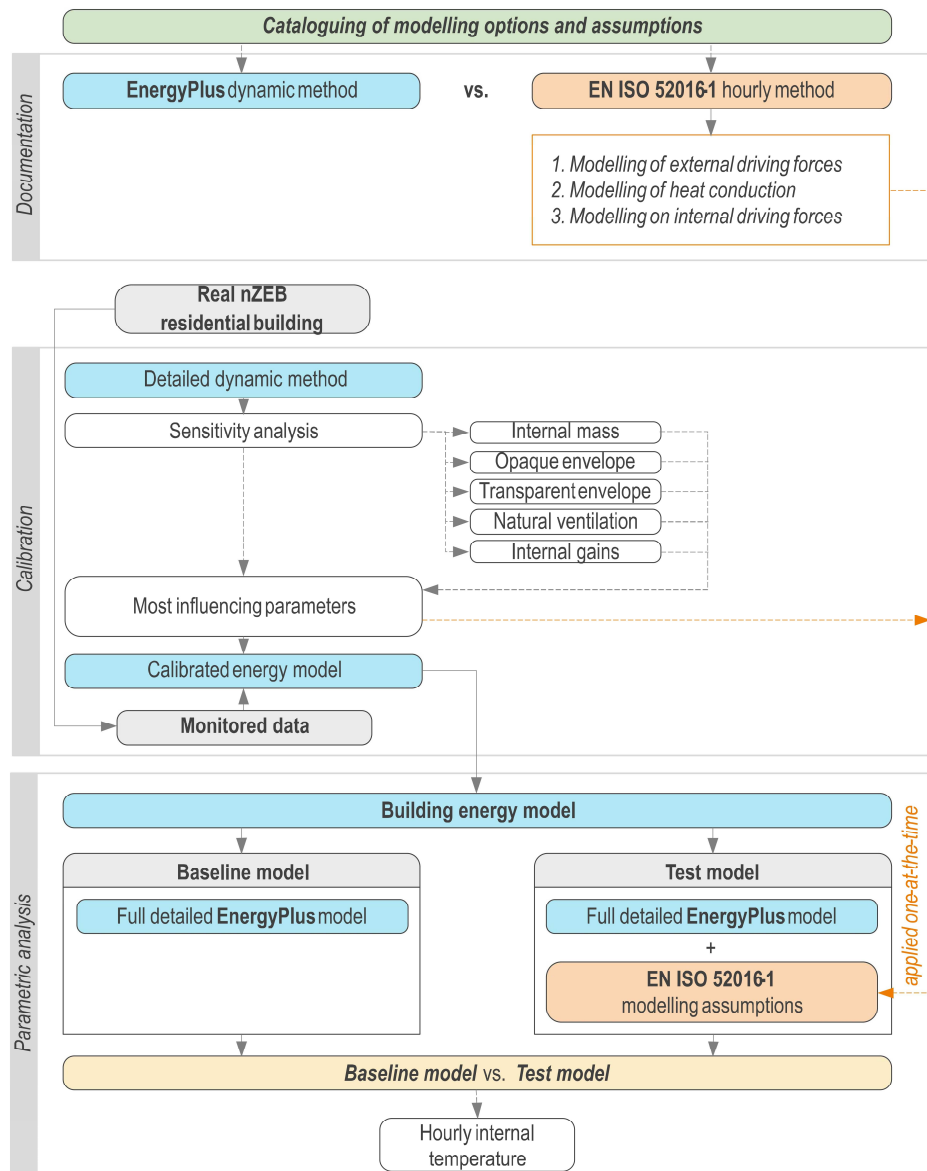


Figure 21: Methodology workflow for the evaluation of the EN ISO 52016-1 modelling assumptions to a real building, including the calibration step

A manual calibration procedure was adopted in the present work. Firstly, the building energy model is created in EnergyPlus, and a sensitivity analysis to the main parameters related to the building envelope (i.e., internal mass, opaque envelope, transparent envelope) and the users' behaviour (i.e., natural ventilation, internal gains) is carried out to identify the most influencing parameters on the thermal behaviour of the building, specifically on the indoor air temperatures. The most influencing parameters are then combined to calibrate the energy model. The overall agreement between simulation results and measurements on the whole

calibration period is evaluated through the Root Mean Squared Error (*RMSE*), calculated as presented in Equation (49),

$$RMSE = \left( \frac{1}{n} \cdot \sum_{k=1}^n (S_k - M_k)^2 \right)^{0,5} \quad (49)$$

where  $M_k$  and  $S_k$  represent the measured and simulated temperature (°C) at time step  $k$ , respectively, and  $n$  is the number of timestep considered. The model is considered calibrated when the *RMSE* is lower than the temperature measurement accuracy, equal to 0,5°C.

The evaluation of the EN ISO 52016-1 modelling assumptions is performed on the obtained calibrated energy model, which plays the role of the baseline model. Then, the modelling simplifications (documented in Section 5.2.1) are applied one-at-the-time in the test models. However, just the modelling assumptions linked to the most influencing parameters identified in the sensitivity analysis are tested to avoid not representative results. The effect of the tested simplifications is assessed as the variation in the accuracy of test model due to the implementation of each simplification, evaluated in terms of hourly indoor air temperatures and numerically assessed by means of the *RMSE* statistical index (Equation (49)).

## 5.5.2 Application

### 5.5.2.1 Case study

The case study considered is a five-storey residential building, fulfilling the nearly zero-energy building requirements, recently built in the province of Trento (Northern Italy). It was provided by the research group of the Università di Trento. The building is North- and South-oriented, and it is surrounded by equally high buildings (Figure 22); for the purpose of this work, an intermediate floor of the building, characterised by three conditioned apartments and an unconditioned stairwell, was chosen (Figure 23).

The building is characterised by a platform frame structure, and a reinforced concrete stairwell. The building envelope is highly thermally insulated; the non-load bearing external walls are characterised by a thermal transmittance of  $0,12 \text{ W} \cdot \text{m}^{-2} \cdot \text{K}^{-1}$ , while the transparent components are triple-layers Argon filled low-e glazings with  $U_{\text{win}} = 0,6 \text{ W} \cdot \text{m}^{-2} \cdot \text{K}^{-1}$  and  $g\text{-value} = 0,526$ . A radiant floor heating system supplies the building, while no active cooling is provided in summertime. A mechanical ventilation system with heat recovery provides external air to the apartments with a constant airflow rate of  $0,5 \text{ h}^{-1}$ ; it is supplied at  $18 \text{ }^{\circ}\text{C}$



during the heating period, while it is supplied at the outdoor air temperature during free-floating periods (i.e., intermediate and summer months).

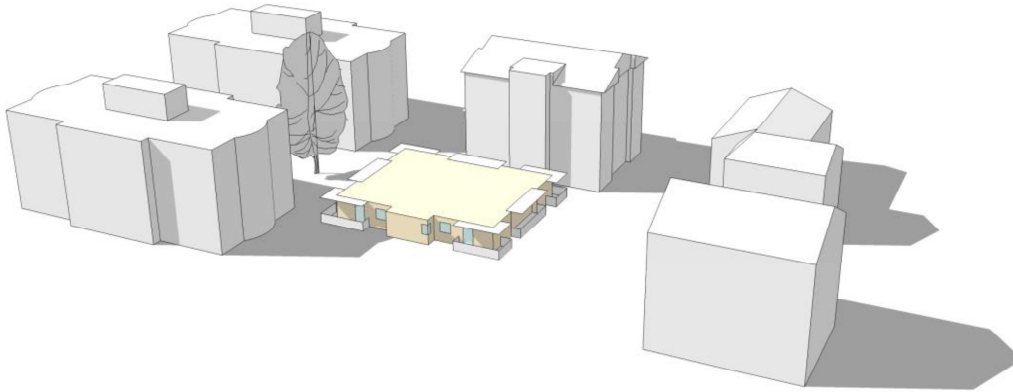


Figure 22: 3D model of the residential building and the surrounding buildings

The analysed floor was modelled as two thermal zones, corresponding to the set of the three apartments and to the stairwell. The upper and lower floors adjacent to the apartments were modelled considering a fixed air temperature (monitored air temperature profiles), while the slabs adjacent to the stairwell were modelled as adiabatic. A standardised user profile for residential buildings [266] was adopted. A constant mechanical ventilation flow rate equal to  $0,5 \text{ h}^{-1}$  was firstly assigned in the apartments; the stairwell, instead, was considered ventilated only by infiltration ( $0,3 \text{ h}^{-1}$ ). Window rolling shutters were supposed to be used only during night time (from 8 p.m. to 8 a.m.).

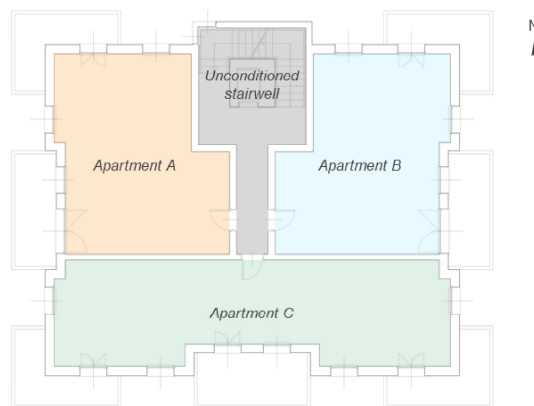


Figure 23: Plan of the analysed storey (2<sup>nd</sup> above-ground floor)

The temperatures of the three apartments, as well as those of the stairwell and the apartments on the two adjacent floors, were monitored for one year (from October 2017 to September 2018). The temperatures of the Apartment A, B, and C, were averaged to obtain a storey-average temperature profile (Figure 24); this

simplification was adopted in the present study to analyse the effects of basic and detailed monitored data sets on the calibration results within the collective calibration exercise (one University modelled the three apartments separately, while the others used an average storey temperature and a single thermal zone).

The analyses carried out in the present work were conducted for a free-floating period; the month of October 2017 was chosen for simulations, considering the first week as warm-up period, and the remaining three weeks as the calibration period.

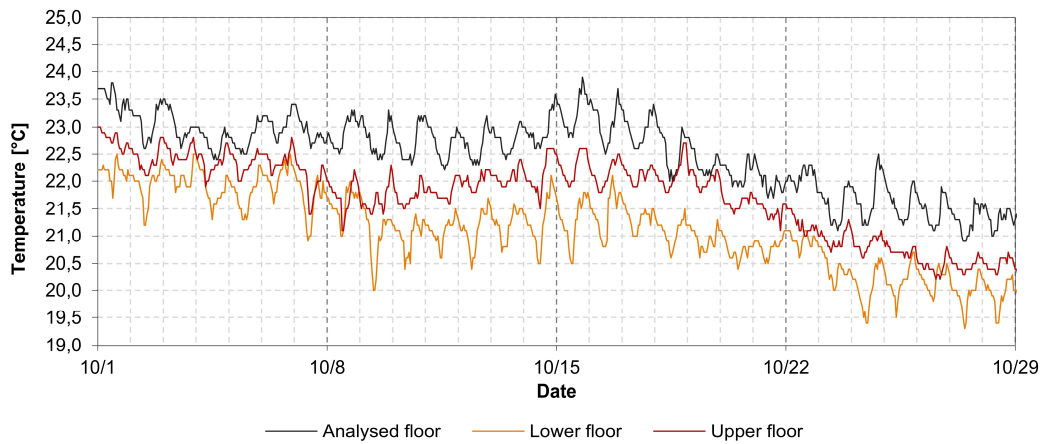


Figure 24: Monitored indoor air temperature for the analysed floor (intermediate) and the adjacent upper and lower floors

### 5.5.2.2 Parameters for sensitivity analysis

The building energy model calibration was preceded by a sensitivity analysis to the main building envelope parameters and user behaviour parameters. The envelope parameters considered included the following:

- thermal conductivity of the insulation layers ( $\lambda$  in  $\text{W}\cdot\text{m}^{-1}\cdot\text{K}^{-1}$ ),
- total solar energy transmittance of windows ( $g$ -value), and
- internal mass (internal walls and furniture), which was modelled following two different approaches: through a multiplier of the indoor air volume capacity ( $ACM$ ), and/or by explicitly modelling the internal partitions ( $S_{\text{part}}$  in  $\text{m}^2$ ).

Regarding the occupants, the following parameters were considered:

- internal gains value,
- daily operation of rolling-shutters, activated when a minimum solar irradiance is reached on the window ( $G_{\text{min}}$  in  $\text{W}\cdot\text{m}^{-2}$ ),
- introduction of natural ventilation, resulting from the opening of the windows (despite the presence of the mechanical ventilation system, the occupants are free to open the windows). This was modelled following two different approaches: opening according to a daily schedule, or opening

when the outside air temperature, or the indoor air temperature, reaches a threshold (deterministic rule). In both cases, the windows' opening determines a variation in the air change values ( $ACH_{NV}$ ).

In Table 21, the parameters tested in the sensitivity analysis, and their range of variation, are reported, as well as the base values used in the base model (prior to the building energy model calibration).

Table 21: Parameters varied in the sensitivity analysis

	Parameter	Base value	Variation
Envelope	Mineral wool/wood fibres thermal conductivity	$\lambda_{mw} = 0,038 \text{ W} \cdot \text{m}^{-1} \cdot \text{K}^{-1}$ $\lambda_{wf} = 0,050 \text{ W} \cdot \text{m}^{-1} \cdot \text{K}^{-1}$	+ 5% / + 10% / + 20%
	Glazings g-value	$g = 0,52$	$g = 0,34 / 0,40$
	Internal mass	Air capacity multiplier $ACM = 1$ Partitions surf. $S_{part} = 0$ No furniture	$ACM = 3 \div 10$ $S_{part} = 259 \text{ m}^2 \div 1034 \text{ m}^2$ (to include furniture)
Occupant behaviour	Internal gains schedule	Standard [266]	Reduced by factor 5% ÷ 50%
	Solar irradiance threshold for activation	No threshold for activation (scheduled activation)	$G_{min} = 200 \div 300 \text{ W} \cdot \text{m}^{-2}$
	Natural ventilation flow rate	$ACH_{NV} = 0$	$ACH_{NV} = 0,5 \div 2$ a) hourly schedule b) when $T_{ext} > T_{min}$ b) when $T_{ext} > T_{min}$ and $T_{int} > T_{max}$

## 5.5.3 Results

### 5.5.3.1 Base model and sensitivity analysis

In Figure 25 the temperature trend obtained from the base model simulation are reported and compared to the monitored data; specifically, both the hourly temperatures (straight lines) and the weekly average values (dotted lines) as reported for each week of the calibration period (i.e., second, firth, and fourth week of October). As it is shown, the simulated temperature trend is coherent with the monitored ones; however, compared with the measured profile, the base model tends to overestimate the indoor air temperature, both in terms of weekly average values (e.g., 1,6, 1,5, and 1,3 °C in the second, third, and fourth week respectively) and variation amplitude (e.g., the peak value for October 18 at 7 p.m. is overestimated of around 3,2 °C); moreover, it anticipates the peaks (e.g., the peak value for October 24 is anticipated of around 3 hours). These discrepancies lead the base model to overestimate the indoor air temperature with an overall error of 1,83 °C over the considered weeks (specifically, 1,92, 1,82, and 1,67 °C in the second, third, and fourth week respectively).

Considering the high discrepancies between the predicted indoor air temperatures in the base model and the monitored data, the sensitivity analysis essential to identify the most influencing parameters and to address the model calibration. The results are presented separately for the parameters concerning the

internal mass, the building envelope, the natural ventilation, and the internal gains. Specifically, they are reported in Figure 26 to Figure 29 for the 3<sup>rd</sup> week of October.

As regard the sensitivity to the internal mass parameters (Figure 26), the model appears to be more influenced by the modelling of the internal partitions as additional heat capacity applied to the internal air, rather than as exposed surface (i.e., explicit modelling). The latter approach leads to a slight variation of the temperature trend compared to the base model, moderately smoothing the temperature trend compared to the base model, moderately smoothing the temperature amplitude by damping the cold peaks. The former approach, instead, allows to damp both cold and warm temperature peak, and to fix the peaks anticipation that characterises the temperature trend in the base model. E.g., the peak value for October 18 occurs at 7 p.m. for the monitored and the simulation (4), while in the base model it occurs three hours in advance (at 4 p.m.). Nevertheless, the modelling of the internal partitions allows to decrease the *RMSE* values from 1,83 °C (base model) to 1,18 °C (simulation (3)).

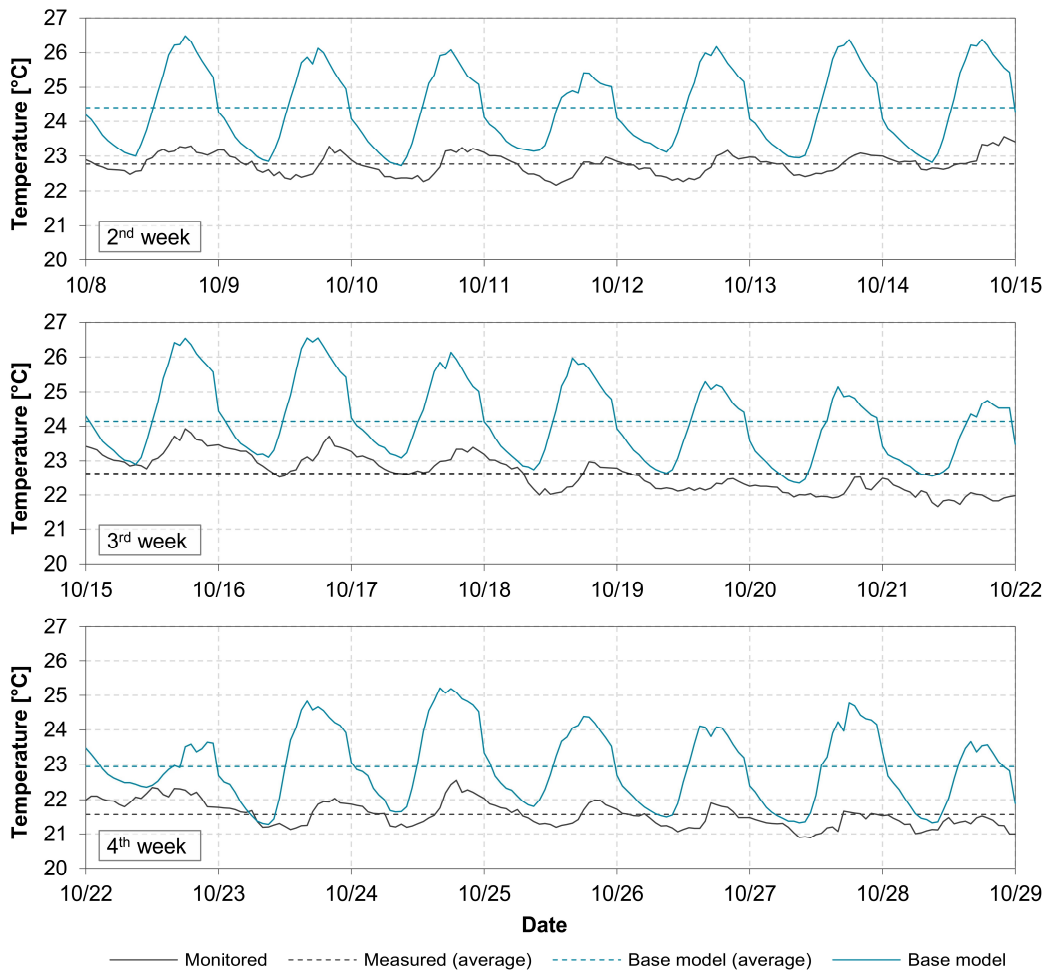
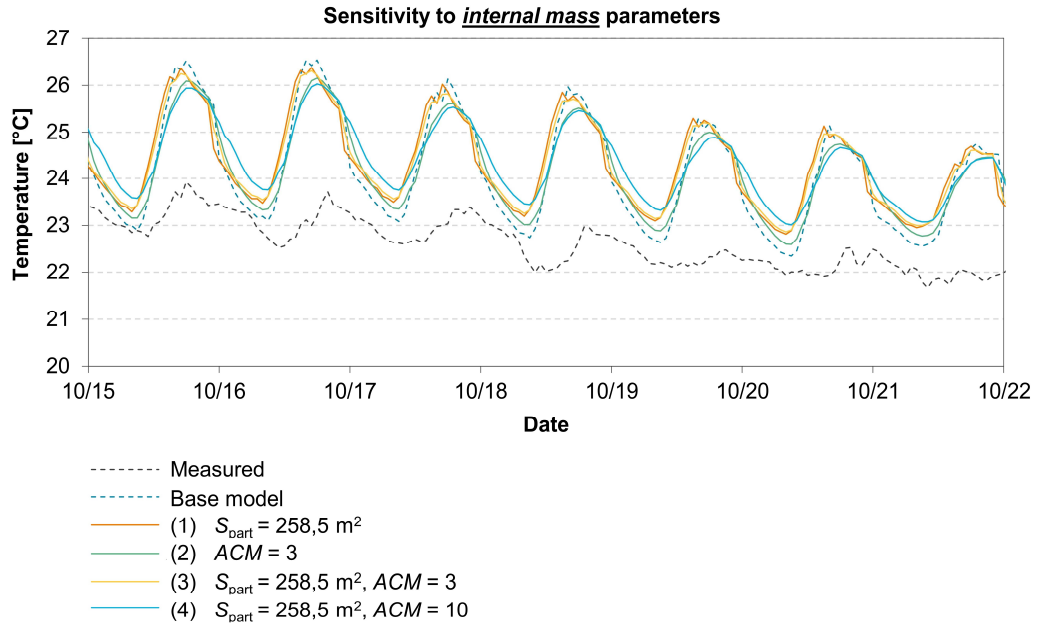
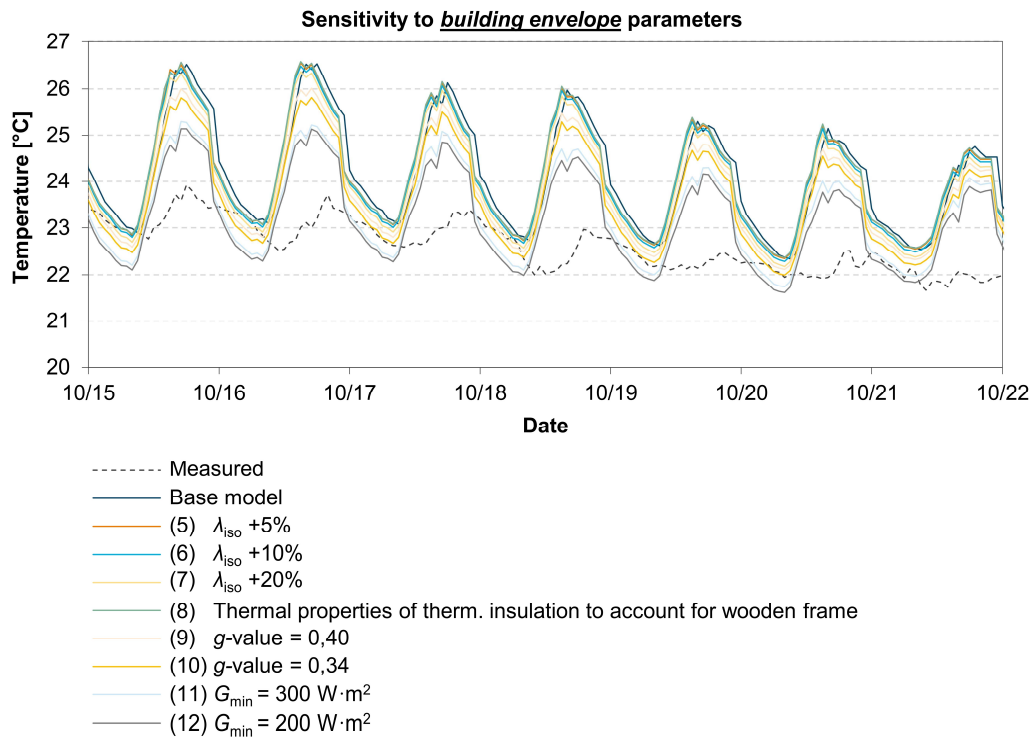


Figure 25: Base model simulations compared to measures

Figure 26: Sensitivity analysis to internal mass parameters (3<sup>rd</sup> week)Figure 27: Sensitivity analysis to building envelope parameters (3<sup>rd</sup> week)

Concerning the building envelope parameters (Figure 27), neither the increase of the insulation thermal conductivity (simulations (5)-(7)) nor its variation to consider the effect of the wooden structure (simulation (8)) influence the building

thermal behaviour. On the other hand, reducing the glazing  $g$ -value (simulation (9)-(10)) and the activation of the external solar shading (simulation (11)-(12)) greatly impact on the simulation outputs; in fact, both the variation of the parameters allows to reduce the committed errors, especially the solar shading activation, reaching a  $RMSE$  value of  $1,08\text{ }^{\circ}\text{C}$  (simulation (12)).

The introduction of natural ventilation (Figure 28) is the parameter that most allow to reduce the gap between the measured and the simulated indoor air. The scheduled windows' opening impacts more on the simulation outputs than the tested deterministic rule. Specifically, the windows' opening in the hottest hours of the day (e.g., from 12 a.m. to 9 p.m., or from 1 p.m. to 10 p.m.) with an  $ACH$  of  $1\text{ h}^{-1}$  allows to limit the warm peaks with respect to the base model, bringing the simulated temperature trend more in line with the monitored one, and reaching a  $RMSE$  of  $1,06$  and  $0,97\text{ }^{\circ}\text{C}$  for simulation (15) and (16) respectively. Instead, opening the windows in the morning, such as in simulation (13) and (14), lead to a pronounced cold peak due to the low external temperatures that does not comply with the monitored temperature trend.

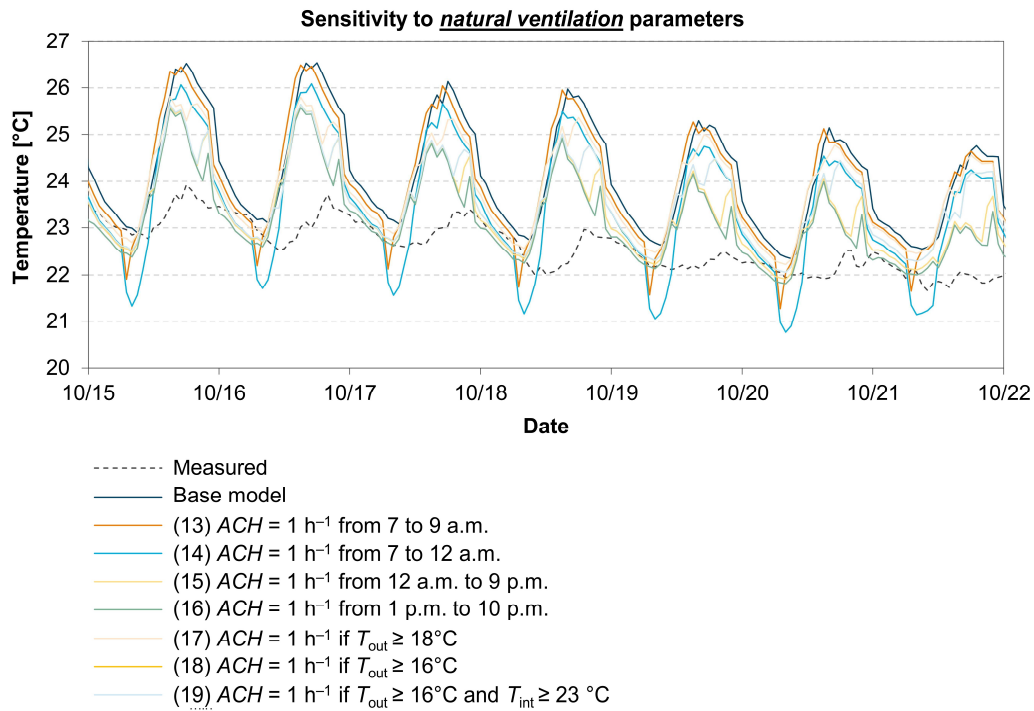


Figure 28: Sensitivity analysis to natural ventilation parameters (3<sup>rd</sup> week)

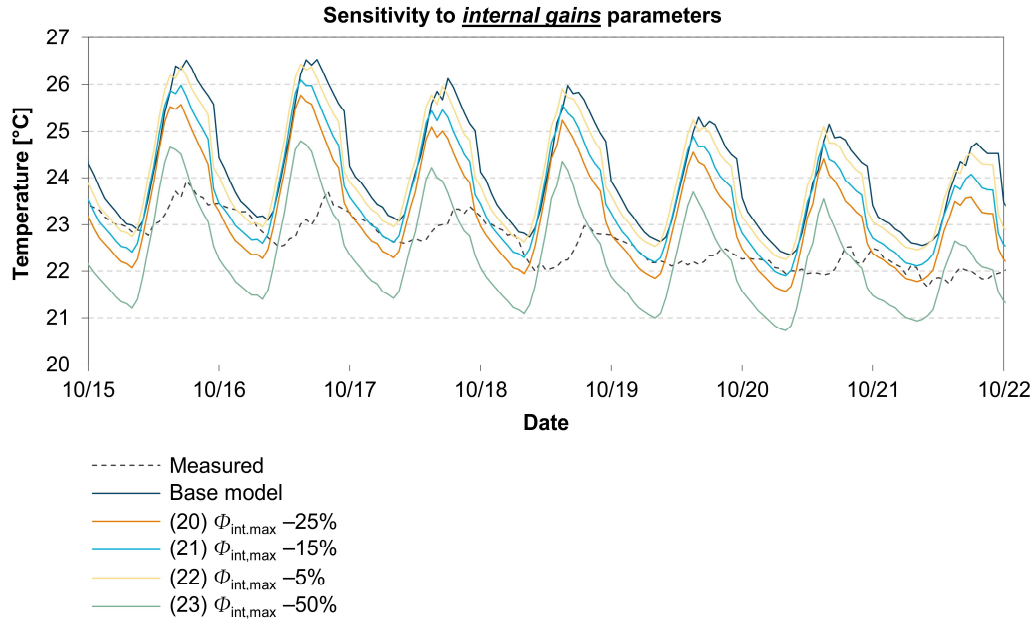


Figure 29: Sensitivity analysis to internal gains parameters (3<sup>rd</sup> week)

Finally, the reduction of the internal gains (Figure 29) lead to a general reduction of the indoor temperatures; however, these variations do not allow the damp the temperature peaks, thus not changing the base model temperature trend.

Therefore, the sensitivity analysis carried out showed a low influence of the parameters related to the opaque envelope, while the activation of the external shutters, the reduction of the internal gains, the addition of the internal partitions thermal mass, and the introduction of natural ventilation have a strong impact on the results of the simulations. Nevertheless, if varied individually, they do not guarantee the calibration of the energy model.

### 5.5.3.2 Building energy model calibration

The most influencing parameters selected from the sensitivity analysis were combined to calibrate the energy model, and four different calibrated solutions were obtained (Table 22). These are all characterised by the introduction of the internal partitions and furniture heat capacity, windows' opening during the hottest hours of the day, and the activation of the external shutters when a given incident solar irradiance threshold. Figure 31 shows the temperature trends for the combinations obtained.

Table 22: Calibrated models

Model	Internal mass	Natural ventilation	Internal gains	Solar shading activation threshold	RMSE
Comb. 1	$ACM = 5$ $S_{part} = 259 \text{ m}^2$	$ACH_{NV} = 0,5 \text{ h}^{-1}$ 1 p.m. – 10 p.m.	-	$300 \text{ W} \cdot \text{m}^{-2}$	$0,51 \text{ }^{\circ}\text{C}$
Comb. 2	$ACM = 5$ $S_{part} = 259 \text{ m}^2$	$ACH_{NV} = 0,5 \text{ h}^{-1}$ 1 p.m. – 10 p.m.	Profile PoliTO (daily reduction, night increase) <sup>a</sup>	$300 \text{ W} \cdot \text{m}^{-2}$	$0,43 \text{ }^{\circ}\text{C}$
Comb. 3	$ACM = 8$ $S_{part} = 0$	$ACH_{NV} = 0,5 \text{ h}^{-1}$ 1 p.m. – 10 p.m.	Profile PoliTO	$300 \text{ W} \cdot \text{m}^{-2}$	$0,44 \text{ }^{\circ}\text{C}$
Comb. 4	$ACM = 5$ $S_{part} = 259 \text{ m}^2$	$ACH_{NV} = 0,5 \text{ h}^{-1}$ 11 a.m. – 9 p.m.	Profile PoliTO	$300 \text{ W} \cdot \text{m}^{-2}$	$0,38 \text{ }^{\circ}\text{C}$

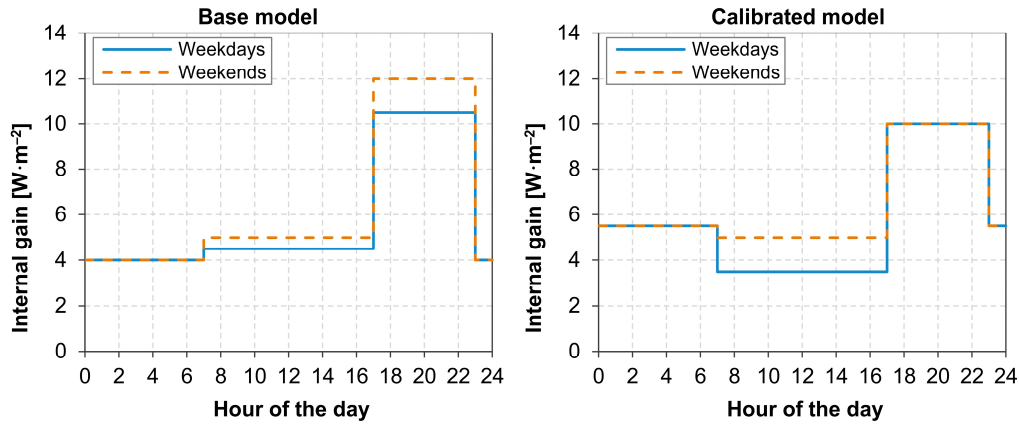
<sup>a</sup> As shown in Figure 30

Figure 30: Comparison between the base and the calibrated model internal gains profile

In the first combination (Comb. 1 in Table 22), resulting in a *RMSE* slightly above the limit value (*RMSE* equal to  $0,51 \text{ }^{\circ}\text{C}$ ), the internal partitions were explicitly modelled as exposed surface, while the heat capacity of the furniture (assumed equal to  $10 \text{ kJ} \cdot \text{m}^{-2} \cdot \text{K}^{-1}$  as suggested by the EN ISO 52016-1 technical standard [5]) was loaded on the air node (*ACM* equal to 5); the windows' opening was assumed from 1 to 10 p.m., and the shutters' activation threshold was supposed equal to  $300 \text{ W} \cdot \text{m}^{-2}$ . On the other hand, the internal gains were not modified. The modification of the internal gains profile (Comb. 2), i.e., reducing the internal gains during the day and increasing them during the evening/night while maintaining the daily mean value (Figure 30), lead to a reduction of the gap between the measured and the simulated indoor air temperatures, reaching a *RMSE* of  $0,43 \text{ }^{\circ}\text{C}$ . The last two combinations are characterised by the same parameters of Comb. 2, with a few modifications. In Comb. 3, all heat capacity of internal partitions and furniture was loaded on the air node (*ACM* equal to 8), reaching a *RMSE* of  $0,44 \text{ }^{\circ}\text{C}$ ; in Comb. 4, the anticipation of the windows' opening hours (from 11 a.m. to 9 p.m.) to exploit the favourable outdoor air temperatures leads to the best performing model among the obtained combinations (*RMSE* of  $0,38 \text{ }^{\circ}\text{C}$ ).



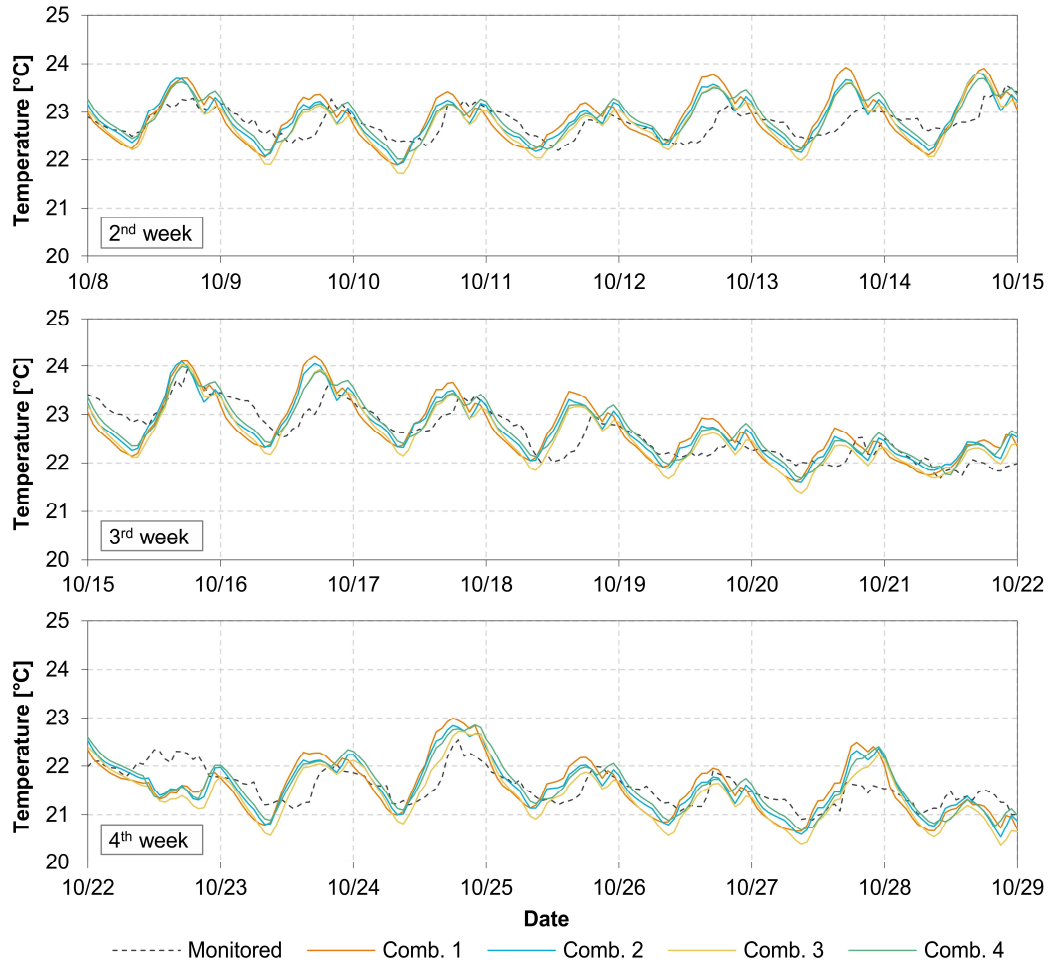


Figure 31: Calibrated models result

### 5.5.3.3 Modelling assumption testing

The evaluation of the EN ISO 52016-1 modelling assumptions was performed on the Comb. 4 calibrated model (i.e., the one with the lower *RMSE*). Beside addressing the model calibration, the sensitivity analysis performed in Section 5.5.3.1 allowed also to perform the present analysis only for the simplifications related to the most influencing modelling parameters on the building thermal behaviour. The exclusion of some modelling assumptions (related to not influencing parameters) is legitimated by the fact that they could lead to not representative results, since they may negligibly influence the building thermal behaviour.

The tested modelling assumptions concerns two parameters, namely the building heat capacity and the solar heat gains. Specifically, the following simplifications were considered.

1. *Simplified heat conduction model*: even though the parameters related to the opaque envelope showed a negligible influence on the thermal behaviour of the building, the EN ISO 52016-1 simplified heat conduction model (presented in Section 5.2.1.5) was considered in the present analysis due to its effect on the internal heat capacity. Only the standard heat conduction model was tested, since the Italian NA model proved to guarantee a high accuracy. External walls were assumed to belong to the mass distribution Class D (mass uniformly distributed), walls adjacent to the unconditioned stairwell to Class I (mass concentrated at internal side), and horizontal partitions to Class M (mass concentrated inside); the Crank-Nicolson finite difference algorithm was assumed as reference,
2. *Solar transmission*: the European modelling assumption of considering solar angle-independent window's optical properties (presented in Section 5.2.1.4) was tested, and an exposure correction factor ( $F_w$ ) equal to 0,9 was assumed. The procedure for correctly simulate this modelling assumption is presented in Section 5.4.2.2,
3. *Shadowing of diffuse solar radiation*: as described in Section 5.2.1.2, the simplified dynamic method does not consider the shadowing of the diffuse component of solar radiation. This modelling assumption was tested on the present case study since it is characterised by several external obstacles (i.e., neighbour building and balconies) that may be affected by this simplification. To this purpose, the EnergyPlus code was accordingly modified. Since the shutters activation control is based on the global (beam plus diffuse) incident solar irradiance on the windows, the same activation profile of the calibrated model was assumed in this test, to make the results comparable.

Table 23: Accuracy of tested modelling assumptions ( $RMSE$ , in  $^{\circ}C$ )

Period	Heat conduction model	Solar transmission	Shadowing of diffuse radiation
2 <sup>nd</sup> week	0,12	0,34	0,54
3 <sup>rd</sup> week	0,19	0,33	0,53
4 <sup>th</sup> week	0,40	0,26	0,44
<b>Overall</b>	<b>0,26</b>	<b>0,31</b>	<b>0,51</b>

The accuracy of the tested modelling assumptions in terms of  $RMSE$  (compared to the calibrated model) is reported in Table 23. The simplified heat conduction model is the assumption that less influences the thermal behaviour of the building among those tested; in fact, it allows to predict the indoor air temperatures with an overall accuracy of 0,26  $^{\circ}C$  with respect to the calibrated model, thus less than the assumed limit of 0,5  $^{\circ}C$ . It is worth highlighting that the accuracy of the model

worsens from the second to the third week of October. In fact, as it is shown in Figure 32, in the first two weeks the temperature trend is in line with the calibrated model, reaching weekly *RMSEs* of 0,12 and 0,19 °C respectively. In the last week, instead, the predicted temperature slightly increases and deviates from the baseline. This may be ascribed to a difference in warm-up due to the different modelling of thermal capacity in opaque structures.

Considering time- and solar angle-independent windows' solar properties leads to a slight increase of the indoor air temperatures as well. This may be due to an overestimation of the transmitted solar radiation in presence of high values of incidence solar angle (i.e., in the morning or evening), due to higher glazing solar transmittance values. Nevertheless, this modelling assumption negligibly affect the accuracy of the model in the prediction of the hourly temperatures, leading to an overall *RMSE* of 0,31°C.

The assumption related to the shadowing of diffuse solar radiation leads to a significant increase in the indoor temperatures. Its influence is critical on the analysed building due to the aforementioned external obstacles. For example, the incident diffuse irradiance on an obstructed surface (South-oriented facade) is almost doubled in a cloudy day (from 146 to 98 W·m<sup>-2</sup> for October 22<sup>nd</sup> at 3 p.m.) when the surface is considered not shaded to the diffuse component. Thus, not considering the shading of the diffuse solar radiation leads to not negligible discrepancies between the baseline and the test models, reaching a *RMSE* equal to 0,51 °C. Even though the error is just slightly above the assumed limit, it is worth underlining that this acceptable deviation may be driven by the high-performance transparent components (*g*-value of 0,526), which allows an effective control of solar heat gains. It is thus conceivable that higher deviations may occur for less performing glazing systems.

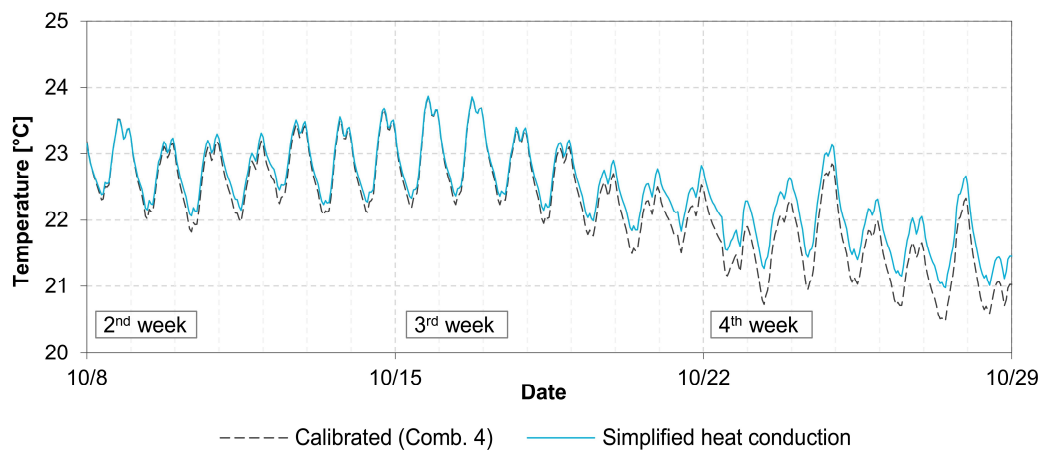


Figure 32: Comparison between the calibrated model and the test model implementing the simplified heat conduction model

#### **5.5.4 Lessons learned from a collective model calibration exercise**

Energy savings achievable through retrofit are correctly predicted if the simulation model adopted is carefully calibrated against measurements. However, calibration is a non-standard phase; as discussed in Section 2.4, a shared methodology for calibration is currently lacking, and it is often streamlined by the modeller's experience which may lead to non-unique solutions. Moreover, the calibration quality may be influenced by the kind of information on the building and system available, as well as of the extent of detailed metered data. The main open issues related to the calibration approach were addressed through a collective calibration exercise involving research groups from four Italian universities: Politecnico di Milano (PoliMI, in Milan), Politecnico di Torino (PoliTO, in Turin), Università di Trento (UniTN, in Trento), and Università degli Studi di Roma Tor Vergata (UniTOV, in Rome).

Three groups (PoliMI, PoliTO, and UniTOV) were provided of a set of basic information and measurements on the building, while detailed information and measured data were provided to the fourth one (UniTN). The different groups developed their own base models, and then calibrations were performed by minimising the discrepancy with the indoor air temperature measured profile. Two groups (PoliMI and PoliTO) adopted manual calibration, preceded by a sensitivity analysis to various parameters regarding the building envelope and users' behaviour, while the other two groups (UniTN and UniTOV) adopted automatic calibration by means of optimisation algorithms.

Section 5.5.4.1 deepens the possible impact of the use of different building energy simulation tools on the results of the calibration procedure. Section 5.5.4.2 discusses, instead, the advantages of automatic calibration over manual, and the importance of the checking the validity of the calibrated models in other periods (different from the calibration period) is investigated in Section 5.5.4.3.

##### **5.5.4.1 Comparison between tools**

The possible impact of the different building simulation tools was analysed by comparing the results obtained by the three research groups who had access to the same basic data set, namely PoliTO (using EnergyPlus), PoliMI (using TRNSYS) and UniTOV (using IDA ICE). The base models behave in a very similar way; they all capture the weekly trend, but they overestimate the indoor air temperature mean value and anticipate the peaks (Figure 33). From these outcomes, it can be derived that using different simulation tools do not lead to relevant discrepancies. In fact, given that the building is simulated in free floating, the potential differences among the tools are limited mainly to the processing of solar radiation data and to the

modelling of heat transfer across the components of the building envelope. However, none of the base model simulations match with measured data; *RMSE* values equal to 1,81, 1,76, and 1,58 °C were reached respectively by PoliTO, PoliMi, and UniTOV.

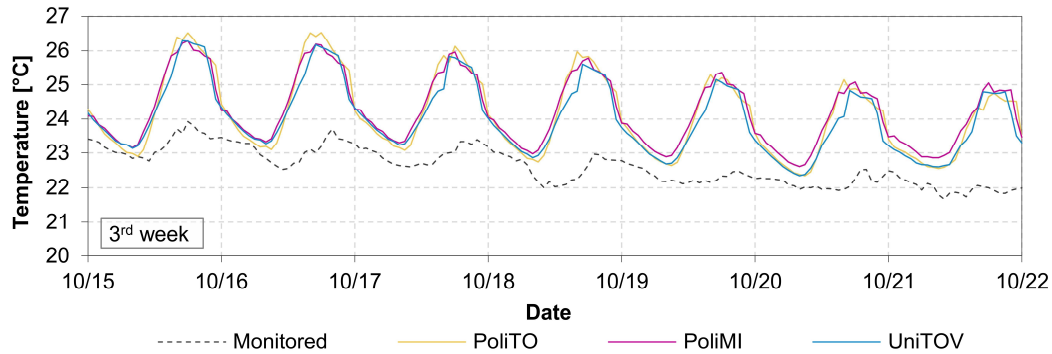


Figure 33: Base models simulations compared to measures for the 3<sup>rd</sup> week of October 2017

#### 5.5.4.2 Manual versus automatic calibration

The advantages of automatic calibration over manual are discussed by comparing the results obtained on the one side by UniTOV (automatic calibration) and on the other side by PoliTO and PoliMI (manual calibration).

The manual calibration lead PoliTO and PoliMI to define four and six calibrated models, respectively. These were obtained with a minimum of two and a maximum of four parameter variations together. All calibrated models required different modifications to the base one, identified in: (i) the modelling of additional internal mass, either through a lumped capacity approach applied to the air volume or through an explicit simulation of internal partitions; (ii) the introduction of either scheduled or rule-based window's opening; (iii) a reduction of internal gains, and (iv) the daily activation of the solar shutters. UniTOV, instead, defined a unique calibrated model. The automatically calibrated parameters include an air capacity multiplier, a modest thermal bridges correction, a small amount of natural ventilation in addition to the base mechanical ventilation rate, and a modified internal gains profile with respect to the base one. Moreover, different solar irradiance thresholds for shutters activation were found for different orientation of the windows; the small threshold irradiances resulting from calibration for the East and West orientation suggest that shutters are used primarily on these facades.

As the very low committed error ( $RMSE = 0,27$  °C) achieved by the UniTOV calibrated model demonstrates, automatic calibration can be more effective than manual one in reaching a more accurate matching with measured data, although managing more parameters (e.g., different thresholds for shutters activation rather than a unique). As far as the characteristics of the calibrated models are concerned,

it can be noticed that manually and automatically calibrated models coherently come to the presence of an important internal thermal mass, to modified internal gains profiles where gains are reduced in the central part of the day and in the evening hours, and to the activation of roll-up shutters during the day.

#### 5.5.4.3 Calibrated models' validation

In general, as it was expected, all the calibrated models perform worst in the validation periods (May and August) with a *RMSE* generally greater than defined the threshold representing the measurement uncertainty (Figure 34). While the mismatch with respect to measured data remains somehow limited in May, it becomes dramatic in most of the cases in August. It can be noticed that among the manually calibrated models, the ones named PoliMI 4 and PoliMI 5, where natural ventilation flow rates are provided through a deterministic rule, rather than in terms of constant or hourly variable values, are less prone to decrease their performance in both validation periods. The model obtained by UniTOV through automatic calibration process appear robust as long as the validation period is relatively similar to the calibration one, yet they not necessarily perform well in August. The more sophisticated model by UniTN, benefitting from the detailed measurement data set, performs well also in August; thus, it seems that having access to detailed monitoring data leads to a more robust calibrated model, namely performing well also outside the calibration month.

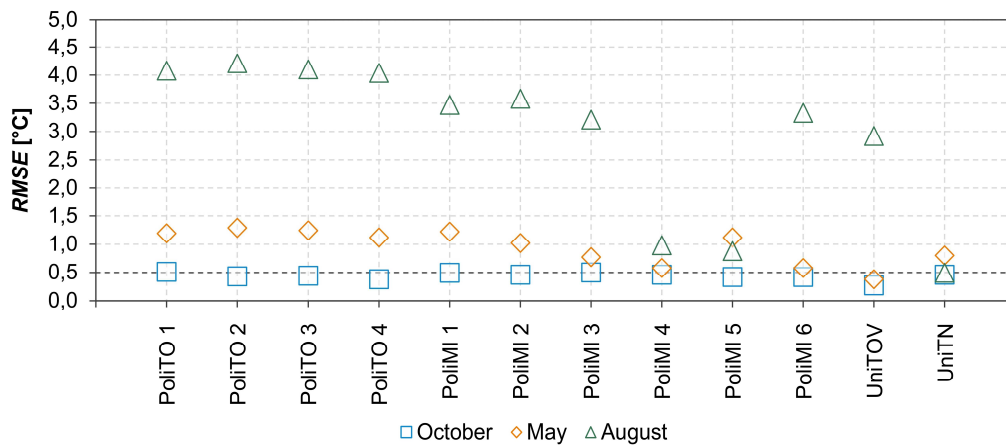


Figure 34: Performance of the calibrated models in the validation periods

The results of the validation process led the research groups who obtained unsatisfactory results to revise the models calibrated in October, with the idea that the occupants' behaviour was not properly captured by the previous approaches. PoliTO decided to implement a deterministic rule for natural ventilation during daytime, based on a minimum and a maximum outdoor air temperature. At the same

time, the solar irradiation threshold for activating the shutters during the day was set to  $200 \text{ W} \cdot \text{m}^{-2}$  (PoliTO 5) or  $300 \text{ W} \cdot \text{m}^{-2}$  (PoliTO 6). As it is shown in Table 24, the revised models by PoliTO perform in an acceptable way in both October and May, with PoliTO 5 better in May and PoliTO 6 better in October, suggesting that the threshold for shutters activation should be adjusted monthly or seasonally. Yet they both maintain an important discrepancy with measured data during August.

Table 24: Performance of the revised models (to be compared with Table 22)

Model	Internal mass	Natural ventilation	Internal gains	Solar shading activation threshold	RMSE [°C]		
					Oct.	May	Aug.
PoliTO 5	$ACM = 5$ $S_{\text{part}} = 259 \text{ m}^2$	11 a.m. – 11 p.m. $ACH_{\text{NV}} = 1,5 \text{ h}^{-1}$ if $18^\circ\text{C} < T_{\text{ext}} < 26^\circ\text{C}$	Profile PoliTO	$200 \text{ W} \cdot \text{m}^{-2}$	0,61	0,50	2,98
PoliTO 6	$ACM = 5$ $S_{\text{part}} = 259 \text{ m}^2$	11 a.m. – 11 p.m. $ACH_{\text{NV}} = 1,5 \text{ h}^{-1}$ if $18^\circ\text{C} < T_{\text{ext}} < 26^\circ\text{C}$	Profile PoliTO	$300 \text{ W} \cdot \text{m}^{-2}$	0,46	0,60	3,83

The validation phase proved to be crucial because: i) it helped discriminating among the different solutions, identifying the more robust calibrated models, and ii) it highlighted the necessity to refine them. It has to be noticed that the choice of the validation period is critical; in fact, if the latter is characterised by boundary conditions that are too similar to the calibration period (e.g., May versus October), the validation phase may fail to detect the weak points of a model.

## 5.6 Italian National Annex improved modelling options evaluation

The present study attempts to investigate the effects of the improved methods and assumptions of the Italian National Annex on the EN ISO 52016 1 calculation method. Although the body of literature on the evaluation of the EN ISO 52016-1 hourly method and its National Annexes has been growing in the recent years, there are not yet sufficient data to generalise the findings, as the existing works are generally based on specific case studies. For this purpose, the work presented in this section is intended to broaden this investigation field. Furthermore, the effect of the Italian National Annex modelling options on the computational effort of the calculation was also addressed.

### 5.6.1 Methodology

A case-study approach was used to facilitate the achievement of the research goals. Firstly, an energy model implementing the EN ISO 52016-1 standard method for the considered case study was created. Then, the improved modelling options introduced by the Italian NA were implemented one-at-the-time to the energy

model of the EN ISO 52016-1 standard method (which will be referred as test models). In particular, the following test models were considered (and named as follows):

1. *NA-Sky*: test model implementing the improved apparent sky temperature determination, described in Section 5.2.2.3,
2. *NA-Cond*: test model implementing the improved heat conduction model (discretisation of opaque components), described in Section 5.2.2.1,
3. *NA-Fw*: test model implementing the solar-angle dependency of windows properties, described in Section 5.2.2.2,
4. *NA*: test model implementing all the NA improved methods.

The standard and the test model simulations were performed by means of a publicly available Excel spreadsheet implementing the complete EN ISO 52016-1 algorithm. This was developed as part of the Mandate M/480 by the EPB Center to demonstrate the correctness of the calculation procedure, and it is available at the EPB Center website [243]. Although implementing the overall calculation algorithm, not every detail of the procedure is covered within the spreadsheet. For example, it is currently implemented to account only for a single thermal zone, and it does not account for adjacent thermally unconditioned zones. Therefore, for the sake of the present study, it was modified and implemented (within a cooperation agreement between the EPB Center and the Department of Energy of Politecnico di Torino) to overcome its current main limitations and to allow the modelling of the improved Italian NA options.

### 5.6.2 Application

The considered case study is an archetype of a two-storey single family, representative of the existing single-family house building stock in Northern Italy, built between 1977 and 1990 [263]. It is characterised by two conditioned stories, for a net floor area and volume of  $198 \text{ m}^2$  and  $537 \text{ m}^3$ , respectively, and an unconditioned basement (Figure 35).

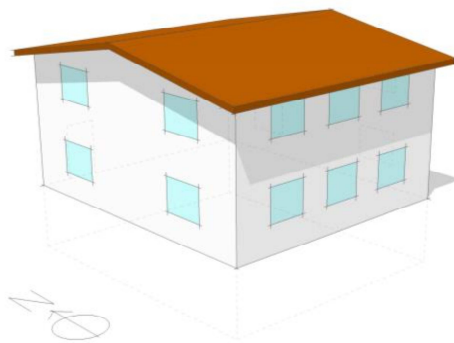


Figure 35: 3D visualisation of the case study



The East-, South- and West-oriented façades are characterised by windows for a total transparent surface of 7,6, 10,8 and 7,6 m<sup>2</sup>, respectively. The North-oriented façade presents an opaque door of 2,4 m<sup>2</sup>. The external vertical components are hollow-bricks walls with a partially insulated air-gap ( $U_{\text{wall}} = 0,76 \text{ W}\cdot\text{m}^{-2}\cdot\text{K}^{-1}$ ,  $\kappa_{\text{wall}} = 256 \text{ kJ}\cdot\text{m}^{-2}\cdot\text{K}^{-1}$ ), while the windows are characterised by a double glazing unit (DGU) with wooden frame ( $U_{\text{w}} = 2,8 \text{ W}\cdot\text{m}^{-2}\cdot\text{K}^{-1}$ ,  $g = 0,75$ ). The opaque door is made of a double wooden panel ( $U_{\text{door}} = 1,70 \text{ W}\cdot\text{m}^{-2}\cdot\text{K}^{-1}$ ,  $\kappa_{\text{door}} = 74 \text{ kJ}\cdot\text{m}^{-2}\cdot\text{K}^{-1}$ ). As far as the horizontal components are concerned, the roof is a scarcely insulated pitched slab ( $U_{\text{roof}} = 1,14 \text{ W}\cdot\text{m}^{-2}\cdot\text{K}^{-1}$ ,  $\kappa_{\text{roof}} = 270 \text{ kJ}\cdot\text{m}^{-2}\cdot\text{K}^{-1}$ ), while the floor adjacent to the unconditioned basement is characterised a barely insulated slab ( $U_{\text{floor}} = 0,98 \text{ W}\cdot\text{m}^{-2}\cdot\text{K}^{-1}$ ,  $\kappa_{\text{floor}} = 306 \text{ kJ}\cdot\text{m}^{-2}\cdot\text{K}^{-1}$ ). The internal vertical partitions ( $\kappa_{\text{wall,int}} = 120 \text{ kJ}\cdot\text{m}^{-2}\cdot\text{K}^{-1}$ ) and the intermediate slab ( $\kappa_{\text{floor,int}} = 306 \text{ kJ}\cdot\text{m}^{-2}\cdot\text{K}^{-1}$ ) were modelled for the sake of internal mass. In the EN ISO 52016 1 energy models (standard and test model), the envelope components were assumed to belong to the I, E, and IE mass distribution classes, for the roof, the floor adjacent to the unconditioned basement, and the external walls, respectively. Neither external obstacles nor solar shading devices were considered. The building was modelled as a single thermal zone.

A standardised user behaviour regarding occupancy, heat gains and natural ventilation was considered. In particular, the scheduled hourly values were derived from the EN 16798-1 standard [259]. A continuously operating heating and cooling system was considered to evaluate the thermal energy needs for heating and cooling of the case study. A dead-band thermostat set-point was assumed, equal to 20 °C and 26 °C for heating and cooling, respectively. The case study was supposed to be located in Milan (Northern Italy), and Palermo (Southern Italy). The evaluations were carried out using the International Weather for Energy Calculations (IWEC) data file [260] for the two cities.

### 5.6.3 Results

#### 5.6.3.1 Improved Italian NA options vs EN ISO 52016 1 standard method

In the present section, the effects of the improved options introduced by the Italian NA are evaluated. In particular, the percentage variation of the thermal energy needs for heating and cooling due to the implementation of the improved methods compared to the original approach are presented in Figure 36 for the considered case study in Milan and Palermo.

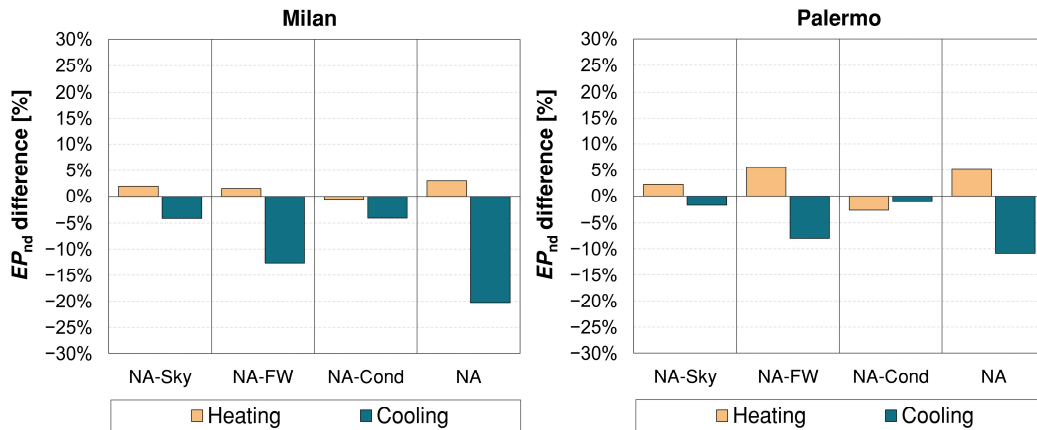


Figure 36: Percentage variation of the thermal energy needs due to the implementation of the NA options compared to the EN ISO 52016 1 standard method for Milan (a) and Palermo (b)

Generally, the same trend of variation can be highlighted in both climatic zones, even if at different extents. Moreover, analysing each improved option, the use of a solar angle and time dependent correction factor for the determination of the total solar energy transmittance of glazing leads to the highest variation in the simulation results, while little variations are reported for the other improved methods.

As far as the determination of the apparent sky temperature is concerned (*NA-Sky*), the implementation of a correlation based on the partial pressure of water vapour leads to an increase of the thermal energy need for heating, and a decrease of the thermal energy need for cooling, in both climatic zones. In particular, the annual thermal energy needs for heating increase by 1,9% and 2,3% in Milan and in Palermo, respectively; on the other hand, a higher variation is reported for the space cooling need in Milan (−4,2%). These variations in the annual thermal energy needs for space heating and cooling can be explained by analysing the profiles of the temperature differences between the apparent sky and the outdoor air, presented in Figure 37 and Figure 38, for Milan and Palermo, respectively. In particular, the grey and the black lines represent the hourly temperature difference, respectively for the NA and the standard model; instead, the green line represents the annual average temperature difference for the NA model. As shown in the figures, the NA average difference between the apparent sky and the air temperature is higher than the reference value of 11°C (i.e., equal to 13,2 °C for Milan, and 12,0 °C for Palermo), assumed in the EN ISO 52016-1 standard method. Thus, an increase in the temperature differences (so a decrease of the apparent sky temperatures) leads to an increase of the heat flux exchanged between the surfaces and the sky. Moreover, the higher difference between the apparent sky and the air temperature leads to higher variations in the results for the building in Milan than in Palermo.

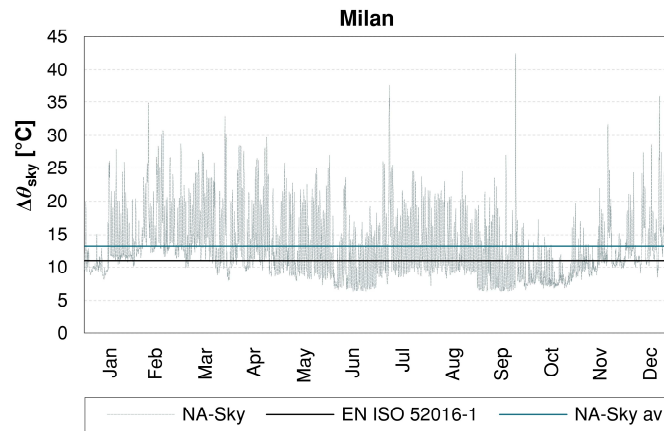


Figure 37: Outdoor air and apparent sky temperature difference in Milan

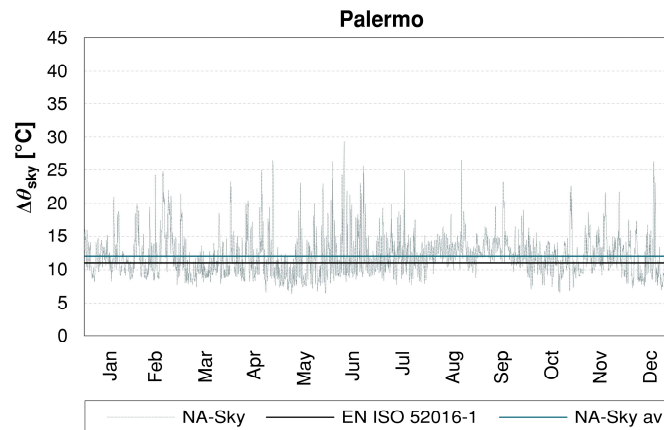


Figure 38: Outdoor air and apparent sky temperature difference in Palermo

Similar outcomes are reported for the correction factor of the total solar energy transmittance of glazing ( $NA-F_w$ ). In fact, also in this case, the thermal energy needs for heating are subject to an increase with respect to the standard method, and a decrease is instead shown for cooling. Nevertheless, the extent of the variation due to the implementation of this improved method is the highest among the tested improvements. In fact, a decrease of 12,6% is reported for the thermal energy need for cooling in Milan, and of 8,1% in Palermo; the thermal energy needs for heating, instead, increase by 1,5 and 5,5%, in Milan and in Palermo, respectively. As for the *NA-Sky* test, these results can be explained by analysing the differences in the monthly average  $F_w$  correction factors between the standard and the improved method. In particular, the monthly average  $F_w$  values are reported in Figure 39 and Figure 40 for different orientations, respectively for Milan and Palermo.

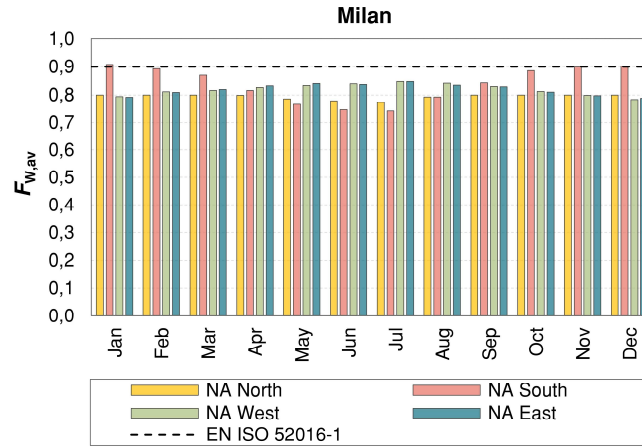


Figure 39: Monthly average correction factor of the total solar energy transmittance ( $F_W$ ) for different exposures in Milan

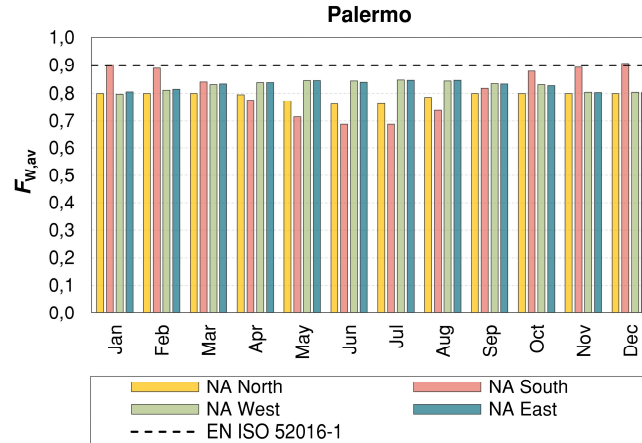


Figure 40: Monthly average correction factor of the total solar energy transmittance ( $F_W$ ) for different exposures in Palermo

The Italian NA formulation entails the use of a  $F_W$  correction factor equal to 0,8 in absence of incident beam solar radiation on the windows, while a 0,9 reference value is assumed over the calculation period in the standard method. Instead, the  $F_W$  values in presence of beam incident solar radiation on the windows varies according to the window orientation, and to the climate zone. In Milan, the monthly average  $F_W$  values are lower than the 0,9 reference value over the whole year for all orientations, except for the South-oriented windows. For this orientation, the monthly average values for the correction factors are close to the reference value in the winter months (e.g., the  $F_W$  average values are equal to 0,91 in January, 0,89 in February, and to 0,90 in November and December), while consistently lower values are reached in the summer months (e.g., 0,74 in July). For East- and West-oriented windows, the correction factors reach the maximum

monthly average values in the summer months, specifically in July (equal to 0,85 for both East- and West-orientations), while values of around 0,80 are reported in the winter and intermediate months. The same trend of the  $F_w$  correction factors monthly average can be highlighted in Palermo, even if lower values with respect to what is reported for Milan. Thus, these trends lead to the reported increases in the thermal energy needs for space heating and decreases in thermal energy needs for cooling. In fact, the NA formulation leads to an underrating of the solar heat gains with respect to the standard method (lower  $F_w$  values).

A general opposite trend is highlighted for the implementation of the improved conduction model (*NA-Cond*). This in fact leads to decreases in the thermal energy needs for both heating and cooling. Nevertheless, almost negligible variations are reported in the thermal energy needs for heating in Milan (−0,5%), and in the thermal energy needs for cooling in Palermo (−1,1%). The variation in the thermal energy needs for cooling and for heating in Milan and Palermo are instead comparable with the results of the NA-Sky simulations.

Finally, the implementation of all the improved options (NA) leads to considerable variation especially in the thermal energy needs for cooling (i.e., −20,3% and −10,8% in Milan and Palermo, respectively). Variations within 5% are instead reported for the thermal energy needs for heating in both climatic zones.

### **5.6.3.2 Computational time**

In Section 5.6.3.1, the variation in the thermal energy needs due to the implementation of the improved Italian National Annex modelling options was assessed, and negligible variations were highlighted for some of the tested options. Thus, to correctly address the evaluation of the implementation of the proposed procedures it is worth understating their influence on the complexity of the calculation and on the computational time. Therefore, an analysis of the variation in the computational time is presented in Table 25 for Milan, compared to the absolute variation in the thermal energy needs for space heating and cooling. The NA-Sky simulation leads to negligible variations in both thermal energy needs (2% and 4% for space heating and cooling, respectively) and computational time (from 8,1 to 8,9 min). A moderate increase in the computational time is instead reported for the NA- $F_w$  simulation (10,3 min, +27%); however, such an increase can be considered since it is linked to a consistent variation in the thermal energy needs, especially for space cooling (+13%). On the other hand, the NA-Cond simulation takes a consistently higher computational time (from 8,1 to 29,8 min, +268%) in the face of almost negligible variations in the thermal energy needs (lower than 4% for both space heating and cooling). Therefore, its implementation should be carefully evaluated in order to guarantee the simplicity of the assessment, as well

as to avoid increases in the computational time. Lastly, the simulation characterised by all the NA options (i.e., *NA*) leads to higher variations in both computational time (mainly related to the implementation of the improved conduction model) and thermal energy needs.

Table 25: Computational time vs. thermal energy needs variation for Milan

Simulation ID	Computational time (min) (%)		$ EP_{H,nd} \text{ variation} $ (%)	$ EP_{C,nd} \text{ variation} $ (%)
<i>Standard model</i>	8,1	-	-	-
<i>NA-Sky</i>	8,9	+10%	2%	4%
<i>NA-Fw</i>	10,3	+27%	2%	13%
<i>NA-Cond</i>	29,8	+268%	1%	4%
<i>NA</i>	33,0	+307%	3%	20%

## 5.7 Suitability of the modelling options

The validation of the modelling assumptions adopted by the EN ISO 52016-1 hourly calculation method was carried out by assessing the loss of accuracy of a detailed dynamic EnergyPlus energy model when the simplifications are implemented one-at-the-time. Seventeen different modelling simplifications, concerning the heat transfer phenomena on the outdoor and the indoor envelope surfaces (i.e., longwave radiation, shortwave radiation, and heat convection), and the heat conduction and storage inside the structures, were tested. Several case studies were considered, namely an enclosed office characterised by different building construction archetypes (Section 5.3), an office unit and a residential apartment characterised by different levels of thermal insulation (Section 5.4), and a residential storey in an existing nZEB (Section 5.5).

In some situations, certain tested assumptions resulted to differently affect the accuracy of the model for annual energy performance and hourly temperature evaluations. It is thus of crucial importance to understand for which purposes and conditions the simplifications are applicable or not. In Figure 41, the results of the analyses performed in the present dissertation are summarised in a comparative table in terms of modelling assumptions' suitability in predicting annual thermal energy needs (left-hand side) and indoor temperatures (right-hand side). For each considered case study, check marks and crosses are assigned to the tested assumptions if the variation limits (i.e., *MBE* for the energy needs evaluation, and *RMSD* for the hourly temperature evaluation) are, respectively, verified or not. The case studies are identified in Figure 41 through an identifier code:

- *Off – constr. arch.* is the enclosed office (sited in Milan) characterised by the Class I and IE building constructions representative of the existing Italian building stock (Section 5.3),

- *Off – scarcely ins.* is the office unit (sited in Milan and Palermo) characterised by a scarcely insulated building envelope (Section 5.4),
- *Off – well ins.* is the office unit (sited in Milan and Palermo) characterised by a highly insulated building envelope (Section 5.4),
- *Res – unins.* is the residential apartment unit (sited in Milan and Palermo) characterised by a scarcely insulated building envelope (Section 5.4),
- *Res – well ins.* is the residential apartment unit (sited in Milan and Palermo) characterised by a highly insulated building envelope (Section 5.4), and
- *Res – ext. nZEB* is the residential storey in the existing nZEB in Trento (Section 5.5).

	Thermal energy need						Indoor temperature					
	Off - constr. arch.	Off - scarcely ins.	Res - unins.	Off - well ins.	Res - well ins.	Res - exist. nZEB	Off - constr. arch.	Off - scarcely ins.	Res - unins.	Off - well ins.	Res - well ins.	Res - exist. nZEB
<b>External longwave radiation heat transfer</b>												
Direct sky temp. model		✓	✓	✓	✓			✓	✓	✓	✓	
Linearised LW, plus Clark-Allen sky temp. model		✓	✓	✓	✓			✓	✓	✓	✓	
Linearised LW, plus direct sky temp. model		✓	✓	✓	✓			✓	✓	✓	✓	
<b>External shortwave radiation heat transfer</b>												
No shading to diffuse irradiance												X
<b>External heat convection</b>												
TARP algorithm, annual av. wind speed		✓	✓	✓	✓			✓	✓	✓	✓	
EN ISO 6946 algorithm, hourly wind speed		-	✓	✓	✓			X	-	X	✓	
EN ISO 6946 algorithm, annual av. wind speed		-	-	✓	✓			X	X	X	✓	
EN ISO 6946 algorithm, reference wind speed		-	X	✓	✓			X	-	X	✓	
<b>Solar transmission</b>												
Constant windows' solar properties (CEN)		✓	✓	✓	-			✓	✓	✓	X	✓
Variable windows' solar properties (UNI)		✓	-	✓	X			-	✓	X	X	
<b>Heat conduction and storage</b>												
Simplified heat conduction model (CEN)	✓						✓					✓
Improved heat conduction model (UNI)	✓						✓					
<b>Internal longwave radiation heat transfer</b>												
Uniform distribution		✓	✓	✓	✓			✓	✓	✓	✓	
<b>Internal shortwave radiation heat transfer</b>												
No back reflection		✓	-	✓	✓			-	-	-	✓	
Uniform distribution		✓	✓	✓	✓			✓	✓	✓	-	
Uniform distribution, plus solar convective gains		✓	✓	✓	✓			✓	✓	-	-	
<b>Internal heat convection</b>												
EN ISO 6946 algorithm, reference values		✓	✓	✓	✓			✓	✓	✓	✓	

Verified MBE or RMSD limit: ✓

Not verified MBE or RMSD limit: X

Verified MBE or RMSD limit depending on climate: -

Not tested modelling assumption:

Figure 41: Modelling assumptions' suitability in predicting thermal energy needs and indoor temperatures (refer to the main text for case studies identifier code)

Based on the comparative table presented in Figure 41, it is possible to draw some considerations on the expected level of accuracy of the tested modelling assumptions for the different evaluation purposes and conditions. In particular:

1. the simplifications relative to the external longwave radiation heat transfer can guarantee a high level of accuracy in the outcomes. Both the linearisation of the phenomenon and the simplified determination of the apparent sky temperature (i.e., through a direct model assuming a constant temperature difference between the sky and the outdoor air) lead to negligible variation in the prediction of both annual energy needs and hourly temperatures in all the case studies considered. It is therefore possible to confirm that these assumptions are suitable for the application on both new and existing building, and for different purposes (e.g., check for energy performance requirement, energy audit, overheating risk assessment, etc.),
2. the use of an average wind speed value for the determination of the external convective heat transfer coefficients (through the detailed TARP formulation [247]) does not influence the expected accuracy of the model for the application purposes and conditions considered,
3. the use of either hourly or annual average wind speed values in the simplified EN ISO 6946 algorithm is generally applicable in well-insulated buildings for the evaluation of both energy needs for heating and cooling; on the other hand, significant errors are committed in the prediction of the indoor operative temperatures, especially in the warm season for office building uses. In uninsulated buildings, instead, the accuracy in predicting the energy needs mainly depends on the climate considered, while it is never guaranteed in predicting indoor temperatures. These results also highlight that the effectiveness of this modelling options is strictly related to the accuracy in the definition of the considered parameter. In fact, the use of a simplified model for the convective heat transfer coefficient calculation resulted to negatively affect the accuracy of the energy need assessment, even if applied on a timestep basis. This may indicate that the discrepancies are caused by a simplification of the equation used for the parameter definition rather than by a variation in its temporal discretisation,
4. the use of a reference wind speed value (thus of a reference convective heat transfer coefficient), instead, leads to acceptable deviations only for thermal energy needs prediction in well-insulated buildings. Thus, the EN ISO 52016-1 simplifications on the external convection heat transfer (referring to this and the previous point) may be applied in the design phases, or for compliance checks, for new buildings. However, for energy audits of existing buildings, or



for thermal comfort evaluations, it may be preferable to use more accurate calculation models,

5. the implementation of time- and solar angle-independent windows' solar properties differently affects the prediction of annual energy performance and hourly temperatures. In particular, this simplification can be safely adopted in buildings characterised by a small window-to-wall (WWR) ratios, while it may lead to inaccuracies in indoor temperature predictions in high WWR buildings, especially if well insulated,
6. the simplified heat conduction model can guarantee accurate predictions of internal surface and indoor temperatures, as well as of annual energy needs regardless of the construction typology, position of the mass inside the structure, and level of thermal insulation. It is therefore possible to confirm that these assumptions are suitable for the application on both new and existing building, and for different purposes (e.g., check for energy performance requirement, energy audit, overheating risk assessment, etc.),
7. a uniform distribution of radiative heat gains on the internal surfaces ensures an acceptable accuracy in all the considered case studies, and for all applications,
8. the simplifications on the solar radiation entering the zone (i.e., back reflection and convective solar gains) leads to inaccuracies in the temperature prediction, especially in summertime and in buildings characterised by high window-to-wall ratios. They generally guarantee, instead, an acceptable accuracy in terms of energy needs estimation,
9. finally, standard and constant internal convective heat transfer coefficients slightly affects the accuracy of the model. Thus, they may be applicable in all the considered case studies, and for all applications.

Therefore, for those modelling assumptions that ensures acceptable levels of accuracy, the use of more detailed approaches should be carefully evaluated to avoid the (unnecessary) increase of the model complexity. For example, the improved conduction model introduced by the Italian National Annex was proved to cause significant increases in the computational effort in the face of a slight variation of the outputs; thus, the use of a more simplified approach may be preferable to guarantee the “balanced accuracy” of the EN ISO 52016-1 model. For the other modelling options, instead, the implementation should be addressed accounting for the results here presented, as to increase the accuracy of the model.

## 5.8 Conclusion

In the present chapter, the effect of the specific simplifying modelling assumptions introduced by the EN ISO 52016-1 hourly method on the accuracy of a detailed dynamic simulation method was quantified, and the simplifications that may lead to non-negligible inaccuracies in the outcomes were identified by applying the *aware validation* approach proposed in the present dissertation.

The research underlined important aspects as regards the EN ISO 52016-1 hourly model validation. Firstly, the effectiveness of different modelling options proved to be strictly related to the accuracy in the definition of the considered parameters. For example, the use of a simplified model for the convective heat transfer coefficient calculation resulted to negatively affect the accuracy of the energy need assessment, even if applied on a timestep basis. This indicates that the discrepancies are caused by a simplification of the equation used for the parameter definition rather than by a variation in its temporal discretisation. Therefore, it would be preferable to select detailed approaches as to increase the accuracy of the calculation method. Other modelling options, instead, proved to guarantee an acceptable level of accuracy. For example, the linearisation of the external longwave radiation heat transfer phenomenon does not influence the accuracy of the model, not even a simplified definition of the apparent sky temperature. Therefore, the replacement of such simplifications with more detailed approaches should be carefully evaluated to avoid affecting the simplicity of the model. Moreover, the results proved the advantages of performing the validation separately for the different assumptions. The proposed approach led in fact to clearly detect specific inaccuracies in the modelling assumptions that a whole-model approach would not have allowed to identify. Therefore, the use of single component validation approaches should be enhanced to guarantee a complete and extensive energy performance assessment validation. Finally, it was shown how different assumptions are suitable for different applications. This furthermore highlighted the need to firstly define the purpose of the application of the calculation method to correctly address its validation, and to decide the level of modelling detail for eventual implementations of the method.

# Chapter 6

## Conclusions

A crucial role in fostering the employment of simplified dynamic methods in the legislative framework is played by their validation. However, ensuring a deep, rigorous, and correctly addressed validation is not straightforward. This is mainly due to the shortcomings of the existing validation procedures, identified in: (i) difficulties in identifying the source of possible errors among uncertainties in the input data or inaccuracies in the calculation method, and (ii) inabilities in evaluating the effect of specific modelling simplifications, parameters, standard values, etc., on the accuracy of the model.

Within this framework, the Ph.D. proposed a novel single-process comparative testing validation approach intended at identifying at which extent, for which conditions, and purposes, specific modelling simplifications (i.e., solution algorithms, modelling parameters, etc.) can affect the accuracy of the model undergoing validation. The proposed approach was then applied in the validation of the simplified dynamic method introduced by the EN ISO 52016-1 technical standard as to contribute to the enhancement of the standardisation activity.

The research demonstrated the advantages of performing the validation separately for the different modelling assumptions. On the one hand, it allowed to distinctly identify different sources of inaccuracies, namely the definition of specific calculation parameters and the simplification of specific heat transfer processes. Moreover, it enabled to demonstrate that the tested EN ISO 52016-1 assumptions are applicable only for defined conditions (e.g., level of thermal insulation of the building analysed) and applications (e.g., code compliance, energy

audits, etc.). Besides providing a clear overview of the suitability of the modelling simplifications, this result also allows to correctly address the choice of the level of modelling detail for eventual implementations of the method. This could furthermore be assisted by the extensive cataloguing of the existing modelling options and assumptions, the *comparison map*, performed within the research activity.

Based on the analyses carried out (and thus limited to the case studies considered), three main aspects relative to the EN ISO 52016-1 modelling of the building fabric should be implemented to control the source of errors and to increase the expected accuracy of the model, namely:

1. Inaccuracies related to the definition of the external convective heat transfer coefficients, caused by a simplification of the equation used for the parameter definition rather than by a variation in its temporal discretisation,
2. Inaccuracies due to the neglecting of the shadowing of the diffuse component of solar irradiance, and
3. Inaccuracies caused by the simplifications in the modelling of solar transmission (i.e., time- and solar-angle independent solar properties, and neglecting of the fraction of solar irradiance that is back reflected outside through the windows).

The main drawback related to the proposed validation approach regards the high level of expertise required for its correct application. In fact, it requires an advanced knowledge of building physics, of the simulation tool assumed as reference model, and of basic computer programming, to correctly implement the modelling assumptions to be tested. In fact, not straightforward workarounds and modification to the simulation tool's code were necessary to simulate some of the tested modelling options; for this reason, the application of this validation procedure may be suitable mainly for qualified academic or professional figures.

Starting from these findings, the following research perspectives are suggested to foster the application of the EN ISO 52016-1 hourly method in the legislative framework and to contribute to the enhancement of the standardisation activity:

1. The analyses presented were carried out on relatively simple case studies to avoid misleading results due to the complexity of the building being analysed. However, since the simplifications may influence the accuracy of the model depending on the building, it is essential to expand the sample of buildings analysed to enable the generalisation of the results, and thus to provide clear evidence of the calculation method's applicability in the Italian context. Different geometries, building uses (e.g., commercial buildings, schools, etc.), and climatic zones, should therefore be included,

2. The implementation of the calculation method should address the compliance with the models' requirements of simplicity and accuracy. Specifically, more detailed solution algorithms, equations, etc., should be defined as to increase the accuracy of the standard method, while guaranteeing its simplicity in terms of both input data (i.e., not additional input data should be requested, or at least easily accessible data) and calculation (i.e., increase in the complexity of the calculation and in the computational time should be avoided),
3. The proposed validation procedure is aimed at assessing the accuracy of the solution algorithms, while the accuracy of the input data used to describe the buildings is assumed. However, recent studies have demonstrated the poor quality data available to the practitioners and professionals to verify the compliance with the energy performance requirements (e.g., energy rating, energy performance certificate generation, etc.) [267,268]. The validation activity should be complemented with a rigorous investigation of the simulation errors that may arise from inaccurate input data. Additional research should therefore be focused on the improvement of the input data quality to limit the "garbage in garbage out" effect, and to complement the accurate building calculation model with accurate input data.

# References

- [1] European Commission, Eurostat, (2022). <https://ec.europa.eu/eurostat/data/database> (accessed June 14, 2022).
- [2] European Commission, Directive 2010/31/EU of 19 May 2010 on the energy performance of buildings (Recast), Off. J. Eur. Union. 18 (2010).
- [3] European Commission, Proposal for a Directive of the European Parliament and of the Council on the energy performance of buildings (Recast) - COM/2021/802 final, Off. J. Eur. Union. (2021).
- [4] H. van Dijk, M. Spiekman, P. de Wilde, A monthly method for calculating energy performance in the context of European building regulations, in: Proc. Ninth Int. Conf. Int. Build. Perform. Simul. Assoc., Montréal, Canada, 2005: pp. 255–262.
- [5] European Committee for Standardization (CEN), EN ISO 52016-1, Energy Performance of Buildings—Energy Needs for Heating and Cooling, Internal Temperatures and Sensible and Latent Heat Loads—Part 1: Calculation Procedures, (2016).
- [6] International Organization for Standardization (ISO), ISO/WD 52016-5, Energy performance of buildings — Energy needs for heating and cooling, internal temperatures and sensible and latent heat loads — Part 5: Specific criteria and validation procedures, (2022).
- [7] G. De Luca, F. Bianco Mauthe Degerfeld, I. Ballarini, V. Corrado, Accuracy of Simplified Modelling Assumptions on External and Internal Driving Forces in the Building Energy Performance Simulation, *Energies*. 14 (2021) 6841. <https://doi.org/10.3390/en14206841>.
- [8] A. Angelotti, L. Mazzearella, C. Cornaro, F. Frasca, A. Prada, P. Baggio, I. Ballarini, G. De Luca, V. Corrado, Calibrating the dynamic energy simulation model for an existing building: lessons learned from a collective exercise, *Submitt. to J. Build. Perform. Simul.* (2022).
- [9] V. Corrado, I. Ballarini, La nuova normativa tecnica nazionale ed europea quale risposta ai requisiti di accuratezza, semplicità, riproducibilità e trasparenza nelle procedure di certificazione energetica, in: *Proceeding Natl. AiCAAR Conf. “Certificazione Energ. Norm. e Model. Di Calc. per Sist. Edif. Posti a Confronto,”* 2008: pp. 21–37.
- [10] European Committee for Standardization (CEN), EN ISO 13790, Energy Performance of Buildings—Calculation of Energy Use for Space Heating and Cooling, (2007).
- [11] J.V. Beck, K.J. Arnold, *Parametric estimation in engineering and science*, John Wiley & Sons, New York, 1977.

- [12] American Society for Heating Refrigerating Air-conditioning Engineers (ASHRAE), Energy estimating and modelling methods, in: 2017 ASHRAE Handb. Fundam., SI Edition, ASHRAE, Tullie Circle, N.E., Atlanta, GA, 2017: pp. 19.1-19.53.
- [13] Y. Chen, M. Guo, Z. Chen, Z. Chen, Y. Ji, Physical energy and data-driven models in building energy prediction: A review, *Energy Reports*. 8 (2022) 2656–2671. <https://doi.org/10.1016/J.EGYR.2022.01.162>.
- [14] Z. Tian, X. Zhang, S. Wei, S. Du, X. Shi, A review of data-driven building performance analysis and design on big on-site building performance data, *J. Build. Eng.* 41 (2021) 102706. <https://doi.org/10.1016/J.JOBE.2021.102706>.
- [15] T. Ahmad, H. Chen, Y. Guo, J. Wang, A comprehensive overview on the data driven and large scale based approaches for forecasting of building energy demand: A review, *Energy Build.* 165 (2018) 301–320. <https://doi.org/10.1016/J.ENBUILD.2018.01.017>.
- [16] Y. Sun, F. Haghighat, B.C.M. Fung, A review of the-state-of-the-art in data-driven approaches for building energy prediction, *Energy Build.* 221 (2020) 110022. <https://doi.org/10.1016/J.ENBUILD.2020.110022>.
- [17] C. Deb, A. Schlueter, Review of data-driven energy modelling techniques for building retrofit, *Renew. Sustain. Energy Rev.* 144 (2021) 110990. <https://doi.org/10.1016/J.RSER.2021.110990>.
- [18] B. Grillone, S. Danov, A. Sumper, J. Cipriano, G. Mor, A review of deterministic and data-driven methods to quantify energy efficiency savings and to predict retrofitting scenarios in buildings, *Renew. Sustain. Energy Rev.* 131 (2020) 110027. <https://doi.org/10.1016/J.RSER.2020.110027>.
- [19] V. Corrado, E. Fabrizio, Steady-State and Dynamic Codes, Critical Review, Advantages and Disadvantages, Accuracy, and Reliability, *Handb. Energy Effic. Build. A Life Cycle Approach*. (2019) 263–294. <https://doi.org/10.1016/B978-0-12-812817-6.00011-5>.
- [20] European Committee for Standardization (CEN), EN ISO 52017, Energy Performance of Buildings—Sensible and Latent Heat Loads and Internal Temperatures—Part 1: Generic Calculation Procedures, (2017).
- [21] V. Corrado, H.E. Mechri, E. Fabrizio, Building energy performance assessment through simplified models: Application of the iso 13790 quasi-steady state method, in: *Proc. Tenth Int. Conf. Int. Build. Perform. Simul. Assoc.*, Beijing, China, 2007: pp. 79–86.
- [22] R. Bruno, P. Bevilacqua, N. Arcuri, Assessing cooling energy demands with the EN ISO 52016-1 quasi-steady approach in the Mediterranean area, *J. Build. Eng.* 24 (2019) 100740. <https://doi.org/10.1016/J.JOBE.2019.100740>.
- [23] Thermal Energy System Specialists, TRNSYS 17: a TRaNsient SYstem Simulation program, Mathematical Reference (Volume 4), (2010).
- [24] R. Bruno, N. Arcuri, C. Carpino, Study of innovative solutions of the building envelope for passive houses in Mediterranean areas, *Energy*

- [25] R. Bruno, N. Arcuri, C. Carpino, Cooling energy needs in non-residential buildings located in Mediterranean area: a revision of the quasi-steady procedure, in: Proc. Third Build. Simul. Appl. Conf. (BSA 2017), Bozen-Bolzano, Italy, 2017: pp. 293–300.
- [26] M. Filippi, E. Fabrizio, Introduzione alla simulazione termoeenergetica dinamica degli edifici, First edit, Editoriale Delfino, Milano, 2010.
- [27] D.B. Crawley, L.K. Lawrie, F.C. Winkelmann, W.F. Buhl, Y.J. Huang, C.O. Pedersen, R.K. Strand, R.J. Liesen, D.E. Fisher, M.J. Witte, J. Glazer, EnergyPlus: creating a new-generation building energy simulation program, *Energy Build.* 33 (2001) 319–331. [https://doi.org/10.1016/S0378-7788\(00\)00114-6](https://doi.org/10.1016/S0378-7788(00)00114-6).
- [28] U.S. Department of Energy, Building Energy Simulation Tools (BESTs) directory, (2022). <https://www.buildingenergysoftwaretools.com/> (accessed June 14, 2022).
- [29] D.B. Crawley, J.W. Hand, M. Kummert, B.T. Griffith, Contrasting the capabilities of building energy performance simulation programs, *Build. Environ.* 43 (2008) 661–673. <https://doi.org/10.1016/J.BUILDENV.2006.10.027>.
- [30] L. Giovannini, F. Favoino, A. Pellegrino, V.R.M. Lo Verso, V. Serra, M. Zinzi, Thermochromic glazing performance: From component experimental characterisation to whole building performance evaluation, *Appl. Energy.* 251 (2019) 113335. <https://doi.org/10.1016/J.APENERGY.2019.113335>.
- [31] E. Catto Lucchino, A. Gelesz, K. Skeie, G. Gennaro, A. Reith, V. Serra, F. Goia, Modelling double skin façades (DSFs) in whole-building energy simulation tools: Validation and inter-software comparison of a mechanically ventilated single-story DSF, *Build. Environ.* 199 (2021) 107906. <https://doi.org/10.1016/J.BUILDENV.2021.107906>.
- [32] F. Goia, G. Chaudhary, S. Fantucci, Modelling and experimental validation of an algorithm for simulation of hysteresis effects in phase change materials for building components, *Energy Build.* 174 (2018) 54–67. <https://doi.org/10.1016/J.ENBUILD.2018.06.001>.
- [33] D. Van Dijk, M. Spiekman, L. Hoes-Van Oeffelen, EPB standard EN ISO 52016: Calculation of the building's energy needs for heating and cooling, internal temperatures and heating and cooling load, *Fed. Eur. Heating, Vent. Air Cond. Assoc. J.* (2016) 18–22.
- [34] D. van Dijk, EN ISO 52016 1: The new International Standard to calculate building energy needs for heating and cooling, internal temperature and heating and cooling loads, in: Proc. Sixt. Int. Conf. Int. Build. Perform. Simul. Assoc., Rome, Italy, 2019.
- [35] I. Ballarini, E. Primo, V. Corrado, On the limits of the quasi-steady-state method to predict the energy performance of low-energy buildings, *Therm. Sci.* 2018 (2018) 1117–1127. <https://doi.org/10.2298/TSCI170724133B>.



- [36] G. De Luca, I. Ballarini, A. Paragamyran, A. Pellegrino, V. Corrado, On the improvement of indoor environmental quality, energy performance and costs for a commercial nearly zero-energy building, *Sci. Technol. Built Environ.* 27 (2021) 1056–1074. <https://doi.org/10.1080/23744731.2021.1940275>.
- [37] G. De Luca, I. Ballarini, A. Lorenzati, V. Corrado, Renovation of a social house into a NZEB: Use of renewable energy sources and economic implications, *Renew. Energy.* 159 (2020) 356–370. <https://doi.org/10.1016/j.renene.2020.05.170>.
- [38] V. Corrado, I. Ballarini, G. De Luca, E. Primo, Dynamic simulation to identify cost-optimal energy requirements for the Italian building stock, in: *Proc. Sixt. Int. Conf. Int. Build. Perform. Simul. Assoc.*, 2019: pp. 3948–3954.
- [39] I. Ballarini, A. Costantino, D. Dirutigliano, E. Fabrizio, S. Paduos, V. Corrado, On the cost-optimal design: Comparison of quasi-steady-state and dynamic simplified methods of calculation of H/C energy needs, in: *Proc. Third Build. Simul. Appl. Conf. (BSA 2017)*, 2017: pp. 129–136.
- [40] V. Corrado, I. Ballarini, S. Paduos, L. Tulipano, A new procedure of energy audit and cost analysis for the transformation of a school into a nearly zero-energy building, 140 (2017) 325–338. <https://doi.org/10.1016/j.egypro.2017.11.146>.
- [41] A. Lorenzati, I. Ballarini, G. De Luca, V. Corrado, Social housing in Italy: Energy audit and dynamic simulation towards a nZEB policy, in: *Proc. Sixt. Int. Conf. Int. Build. Perform. Simul. Assoc.*, 2019: pp. 4990–4997.
- [42] D. Dirutigliano, I. Ballarini, G. Murano, V. Corrado, Reference building approach combined with dynamic simulation in designing nZEBs, in: *Proc. Fifteenth Int. Conf. Int. Build. Perform. Simul. Assoc.*, San Francisco, U.S.A., 2017: pp. 648–657. <https://doi.org/10.26868/25222708.2017.627>.
- [43] European Commission, Directive (EU) 2018/844 of the European Parliament and of the Council of 30 May 2018 amending Directive 2010/31/EU on the energy performance of buildings and Directive 2012/27/EU on energy efficiency, *Off. J. Eur. Union.* 156 (2018).
- [44] V. Corrado, I. Ballarini, G. De Luca, M.P. Tootkaboni, Approfondimento teorico del modello di calcolo orario semplificato (UNI EN ISO 52016-1:2018) e applicazione al settore residenziale. Report RdS/PTR2019/035, 2019.
- [45] V. Corrado, I. Ballarini, F. Bianco Mauthe Degerfeld, G. De Luca, Approfondimento teorico del modello di calcolo orario semplificato (UNI EN ISO 52016-1:2018) e applicazione al settore terziario. Report RdS/PTR2019. In print, 2020.
- [46] V. Corrado, I. Ballarini, F. Bianco Mauthe Degerfeld, M. Piro, Aggiornamento della metodologia di calcolo dei livelli ottimali di prestazione energetica in funzione dei costi. Report RdS/PTR2019. In print, 2021.
- [47] E.M. Ryan, T.F. Sanquist, Validation of building energy modeling tools

- under idealized and realistic conditions, *Energy Build.* 47 (2012) 375–382. <https://doi.org/10.1016/j.enbuild.2011.12.020>.
- [48] R. Judkoff, D. Wortman, B. O’Doherty, J. Burch, A methodology for validating building energy analysis simulations, 2008.
  - [49] R. Judkoff, J. Neymark, Model Validation and Testing: The Methodological Foundation of ASHRAE Standard 140, *ASHRAE Trans.* 112 (2006).
  - [50] R. Judkoff, J. Neymark, The BESTEST method for evaluating and diagnosing building energy software, in: American Council for an Energy-Efficient Economy, Washington, DC (US), United States, 1998. <https://www.osti.gov/biblio/20001826>.
  - [51] D.P. Bloomfield, An overview of validation methods for energy and environmental software, *ASHRAE Trans.* 6 (1999) 685–693.
  - [52] I. Beausoleil-Morrison, B. Griffith, T. Vesanen, A. Weber, A demonstration of the effectiveness of inter-program comparative testing for diagnosing and repairing solution and coding errors in building simulation programs, *J. Build. Perform. Simul.* 2 (2009) 63–73. <https://doi.org/10.1080/19401490802559409>.
  - [53] A. Buonomano, Code-to-code validation and application of a dynamic simulation tool for the building energy performance analysis, *Energies.* 9 (2016). <https://doi.org/10.3390/en9040301>.
  - [54] S.A. Brideau, I. Beausoleil-Morrison, M. Kummert, A. Wills, Inter-model comparison of embedded-tube radiant floor models in BPS tools, *J. Build. Perform. Simul.* 9 (2016) 190–209. <https://doi.org/10.1080/19401493.2015.1027065>.
  - [55] R. Raslan, M. Davies, Results variability in accredited building energy performance compliance demonstration software in the UK: An inter-model comparative study, *J. Build. Perform. Simul.* 3 (2010) 63–85. <https://doi.org/10.1080/19401490903477386>.
  - [56] D. Bloomfield, Appraisal techniques for methods of calculating the thermal performance of buildings, *Build. Serv. Eng. Res. Technol.* 6 (1985) 13–20. <https://doi.org/10.1177/014362448500600103>.
  - [57] I. Ballarini, A. Costantino, E. Fabrizio, V. Corrado, A methodology to investigate the deviations between simple and detailed dynamic methods for the building energy performance assessment, *Energies.* 13 (2020). <https://doi.org/10.3390/en13236217>.
  - [58] J. Neymark, M. Kummert, R. Judkoff, Developing Equivalent Surface Heat Transfer Input Parameters for Updated Standard 140/BESTEST Thermal Fabric Test Cases, in: *Proc. Sixt. Int. Conf. Int. Build. Perform. Simul. Assoc.*, Rome, Italy, 2020. <https://doi.org/10.26868/25222708.2019.210588>.
  - [59] S.Ø. Jensen, Validation of building energy simulation programs: a methodology, *Energy Build.* 22 (1995) 133–144. [https://doi.org/10.1016/0378-7788\(94\)00910-C](https://doi.org/10.1016/0378-7788(94)00910-C).
  - [60] American Society for Heating Refrigerating Air-conditioning Engineers (ASHRAE), ANSI/ASHRAE 140-2020: Method Of Test For Evaluating

Building Performance Simulation Software, (2020).

- [61] J. Neymark, R. Judkoff, M. Kummert, R. Muehleisen, J. Allison, J. An, J. Glazer, R. Henninger, M. Hiller, Y. Jiang, A. Johannsen, N. Kruis, T. McDowell, E. Ono, P. Strachan, M. Witte, D. Yan, H. Yoshida, X. Zhou, Update of ASHRAE Standard 140/BESTEST Thermal Fabric Test Cases, in: Proc. Seventeenth Int. Conf. Int. Build. Perform. Simul. Assoc., Brugge, Belgium, 2021.
- [62] European Committee for Standardization (CEN), EN ISO 13791, Thermal Performance of Buildings—Calculation of Internal Temperatures of a Room in Summer without Mechanical Cooling—General Criteria and Validation Procedures, (2012).
- [63] A. Nicolai, S. Hirth, M. Madjidi, SimQuality: A novel test suite for dynamic building energy simulation tools, in: Proc. Seventeenth Int. Conf. Int. Build. Perform. Simul. Assoc., Brugge, Belgium, 2021.
- [64] R.D. Judkoff, Validation of building energy analysis simulation programs at the solar energy research institute, *Energy Build.* 10 (1988) 221–239. [https://doi.org/10.1016/0378-7788\(88\)90008-4](https://doi.org/10.1016/0378-7788(88)90008-4).
- [65] G. Augenbroe, Trends in building simulation, *Build. Environ.* 37 (2002) 891–902. [https://doi.org/10.1016/S0360-1323\(02\)00041-0](https://doi.org/10.1016/S0360-1323(02)00041-0).
- [66] A. Reddy, Literature review on calibration of building energy simulation programs: Uses, problems, procedure, uncertainty, and tools, *ASHRAE Trans.* 112 (2006) 226–240.
- [67] D. Coakley, P. Raftery, M. Keane, A review of methods to match building energy simulation models to measured data, *Renew. Sustain. Energy Rev.* 37 (2014) 123–141. <https://doi.org/10.1016/J.RSER.2014.05.007>.
- [68] E. Fabrizio, V. Monetti, Methodologies and Advancements in the Calibration of Building Energy Models, *Energies.* 8 (2015). <https://doi.org/10.3390/en8042548>.
- [69] H.E. Huerto-Cardenas, F. Leonforte, N. Aste, C. Del Pero, G. Evola, V. Costanzo, E. Lucchi, Validation of dynamic hygrothermal simulation models for historical buildings: State of the art, research challenges and recommendations, *Build. Environ.* 180 (2020) 107081. <https://doi.org/https://doi.org/10.1016/j.buildenv.2020.107081>.
- [70] C. Cornaro, F. Bosco, M. Lauria, V.A. Puggioni, L. De Santoli, Effectiveness of Automatic and Manual Calibration of an Office Building Energy Model, *Appl. Sci.* 9 (2019). <https://doi.org/10.3390/app9101985>.
- [71] American Society for Heating Refrigerating Air-conditioning Engineers (ASHRAE), Guideline 14—Measurement of Energy, Demand, and Water Savings, (2014).
- [72] T.A. Reddy, I. Maor, C. Panjapornpon, Calibrating Detailed Building Energy Simulation Programs with Measured Data—Part I: General Methodology (RP-1051), *HVAC&R Res.* 13 (2007) 221–241. <https://doi.org/10.1080/10789669.2007.10390952>.
- [73] A. Prada, A. Gasparella, P. Baggio, A Robust approach for the calibration of

- the material properties in an existing wall, in: Proc. Sixt. Int. Conf. Int. Build. Perform. Simul. Assoc., Rome, Italy, 2019: pp. 4554–4561.
- [74] I. Beausoleil-Morrison, Learning the fundamentals of building performance simulation through an experiential teaching approach, *J. Build. Perform. Simul.* 12 (2019) 308–325. <https://doi.org/10.1080/19401493.2018.1479773>.
  - [75] J. Hensen, E. Djunaedy, M. Radošević, A. Yahiaoui, Building Performance Simulation for better design: some issues and solutions, *Plea 2004*. (2004) 1185–1190.
  - [76] R. Judkoff, D. Wortman, B. O'Doherty, J. Burch, A methodology for validating building energy analysis simulations, *NREL Tech. Rep.* 550-42059. (2008) 1–192.
  - [77] H.E. Mechri, V. Corrado, Practical Applications of Uncertainty and Sensitivity Techniques in Building Energy Simulation, *Procedia - Soc. Behav. Sci.* 2 (2010) 7708–7709. <https://doi.org/10.1016/J.SBSPRO.2010.05.190>.
  - [78] W. Tian, Y. Heo, P. de Wilde, Z. Li, D. Yan, C.S. Park, X. Feng, G. Augenbroe, A review of uncertainty analysis in building energy assessment, *Renew. Sustain. Energy Rev.* 93 (2018) 285–301. <https://doi.org/10.1016/J.RSER.2018.05.029>.
  - [79] T. Hong, S.K. Chou, T.Y. Bong, Building simulation: an overview of developments and information sources, *Build. Environ.* 35 (2000) 347–361. [https://doi.org/10.1016/S0360-1323\(99\)00023-2](https://doi.org/10.1016/S0360-1323(99)00023-2).
  - [80] D. Bloomfield, The influence of the user on the results obtained from thermal simulation programs, in: Proc. Fifth Int. Symp. Use Comput. Environ. Eng. Relat. to Build., Guildhall, Bath, 1986.
  - [81] International Energy Agency, Calculation of Energy and Environmental Performance of Buildings - IEA ECBCS Annex 21 / IEA SHC Task 12B (Technical Synthesis Report), (1998). [https://www.iea-ebc.org/Data/publications/EBC\\_Annex\\_21\\_tsr.pdf](https://www.iea-ebc.org/Data/publications/EBC_Annex_21_tsr.pdf).
  - [82] G. Guyon, Role of the model user in results obtained from simulation software program, in: Proc. Fifth Int. Conf. Int. Build. Perform. Simul. Assoc., Prague, Czech Republic, 1997: pp. 377–384.
  - [83] P. Berkeley, P. Haves, E. Kolderup, Impact of modeler decisions on simulation results, 2014 ASHRAE/IBPSA-USA Build. Simul. Conf. (2014) 203–210.
  - [84] I. Beausoleil-Morrison, C.J. Hopfe, Teaching building performance simulation through a continuous learning cycle, in: Proc. Fourteenth Int. Conf. Int. Build. Perform. Simul. Assoc., 2015: pp. 2757–2764.
  - [85] S. Imam, D.A. Coley, I. Walker, The building performance gap: Are modellers literate?, *Build. Serv. Eng. Res. Technol.* 38 (2017) 351–375. <https://doi.org/10.1177/0143624416684641>.
  - [86] A. Gasparella, V. Corrado, Building simulation, *Sci. Technol. Built Environ.* 24 (2018) 459–460. <https://doi.org/10.1080/23744731.2018.1455358>.

- [87] N. Gentile, J. Kanters, H. Davidsson, A Method to Introduce Building Performance Simulation to Beginners, *Energies* . 13 (2020). <https://doi.org/10.3390/en13081941>.
- [88] J. Hand, D. Crawley, Forget the Tool when Training New Simulation Users, in: *Proc. Fifth Int. Conf. Int. Build. Perform. Simul. Assoc.*, Prague, Czech Republic, 1997: pp. 39–45.
- [89] S. Alsaadani, C. Bleil De Souza, Teaching BPS to architects: A closer look at the building performance simulation ‘consumer’ and ‘performer’ training paradigms, *IOP Conf. Ser. Earth Environ. Sci.* 397 (2019) 12004. <https://doi.org/10.1088/1755-1315/397/1/012004>.
- [90] S. Alsaadani, C. Bleil De Souza, Performer, consumer or expert? A critical review of building performance simulation training paradigms for building design decision-making, *J. Build. Perform. Simul.* 12 (2019) 289–307. <https://doi.org/10.1080/19401493.2018.1447602>.
- [91] G. De Luca, F. Bianco Mauthe Degerfeld, I. Ballarini, V. Corrado, The effect of the external driving forces modelling on the calculated building energy need through the use of dynamic simulation, in: *Proc. 2021 Build. Simul.*, Brugge, 2021.
- [92] U.S. Department of Energy, EnergyPlus, (2022). <https://energyplus.net/> (accessed June 14, 2022).
- [93] Energy Systems Research Unit, ESP-r, (2022). <https://www.strath.ac.uk/research/energysystemsresearchunit/> (accessed June 14, 2022).
- [94] D. Nong, pyEp: EnergyPlus cosimulation in Python, (n.d.). <https://pypi.org/project/pyEp/>.
- [95] R. Judkoff, D. Wortman, B. O’Doherty, J. Burch, *Methodology for Validating Building Energy Analysis Simulations*, United States, 2008. <https://doi.org/10.2172/928259>.
- [96] J.A. Clarke, 1 - Introduction, in: J.A.B.T.-E.S. in B.D. (Second E. Clarke (Ed.), Butterworth-Heinemann, Oxford, 2001: pp. 1–21. <https://doi.org/10.1016/B978-075065082-3/50001-2>.
- [97] C.O. Pedersen, D.E. Fisher, R.J. Liesen, Development of a heat balance procedure for calculating cooling loads, in: *American Society of Heating, Refrigerating and Air-Conditioning Engineers, Inc.*, Atlanta, GA (United States), United States, 1997. <https://www.osti.gov/biblio/349983>.
- [98] B. Griffith, Q.Y. Chen, Framework for Coupling Room Air Models to Heat Balance Model Load and Energy Calculations (RP-1222), *HVAC&R Res.* 10 (2004) 91–111. <https://doi.org/10.1080/10789669.2004.10391094>.
- [99] E. Mundt, *The performance of displacement ventilation systems: experimental and theoretical studies*, Royal Institute of Technology, 1996.
- [100] B.R. Morton, G.I. Taylor, J.S. Turner, Turbulent gravitational convection from maintained and instantaneous sources, *Proc. R. Soc. London. Ser. A. Math. Phys. Sci.* 234 (1956) 1–23. <https://doi.org/10.1098/rspa.1956.0011>.
- [101] P.F. Linden, G.F. Lane-Serff, D.A. Smeed, Emptying filling boxes: the fluid

- mechanics of natural ventilation, *J. Fluid Mech.* 212 (1990) 309–335. <https://doi.org/DOI: 10.1017/S0022112090001987>.
- [102] P. Stefanizzi, A. Wilson, A. Pinney, Internal long-wave radiation exchange in buildings: Comparison of calculation methods: I Review of algorithms, *Build. Serv. Eng. Res. Technol.* 11 (1990) 81–85. <https://doi.org/10.1177/014362449001100301>.
- [103] A. Trombe, L. Serres, M. Moisson, Solar radiation modelling in a complex enclosure, *Sol. Energy*. 67 (1999) 297–307. [https://doi.org/10.1016/S0038-092X\(00\)00077-3](https://doi.org/10.1016/S0038-092X(00)00077-3).
- [104] A.P. de A. Rocha, N. Mendes, R.C.L.F. Oliveira, Domus method for predicting sunlit areas on interior surfaces, *Ambient. Construído*. 18 (2018) 83–95. <https://doi.org/10.1590/s1678-86212018000300269>.
- [105] D.E. Fuller, A. McNeil, Radiance: A Validated Lighting Simulation Tool, (2017). <https://www.radiance-online.org/> (accessed June 14, 2022).
- [106] M. Feldmann, R. Kaspar, B. Abeln, A. Gessler, K. Langosch, J. Beyer, J. Schneider, S. Schula, G. Siebert, A. Haese, F. Wellershoff, P. Cruz, J. Belis, J. Colvin, T. Morgan, F. Ensslen, M. Eliasova, Z. Šulcová, G. Royer-Carfagni, L. Galuppi, C. Grenier, H. Hoegner, R. Kruijs, C. Louter, G. Manara, J. Neugebauer, V. Rajcic, R. Zarnic, Guidance for European Structural Design of Glass Components, Publications Office of the European Union, 2014.
- [107] U.S. Department of Energy, EnergyPlus™ Version 9.4.0 Documentation: Engineering Reference, (2020).
- [108] Big Ladder Software, Kiva™, 2018. (n.d.). <https://bigladdersoftware.com/projects/kiva/> (accessed June 14, 2022).
- [109] C. Huizenga, D.K. Arasteh, E. Finlayson, R. Mitchell, B. Griffith, D. Curcija, Teaching students about two-dimensional heat transfer effects in buildings, building components, equipment, and appliances using THERM 2.0, in: American Society of Heating, Refrigerating and Air-Conditioning Engineers, Inc., Atlanta, GA (US), United States, 1999. <https://www.osti.gov/biblio/20002366>.
- [110] J. Berger, S. Gasparin, W. Mazuroski, N. Mendes, An efficient two-dimensional heat transfer model for building envelopes, *Numer. Heat Transf. Part A Appl.* 79 (2021) 163–194. <https://doi.org/10.1080/10407782.2020.1836936>.
- [111] L. Evangelisti, C. Guattari, F. Asdrubali, On the sky temperature models and their influence on buildings energy performance: A critical review, *Energy Build.* 183 (2019) 607–625. <https://doi.org/10.1016/j.enbuild.2018.11.037>.
- [112] R.J. Cole, The longwave radiative environment around buildings, *Build. Environ.* 11 (1976) 3–13. [https://doi.org/10.1016/0360-1323\(76\)90014-7](https://doi.org/10.1016/0360-1323(76)90014-7).
- [113] D. Brunt, Notes on radiation in the atmosphere. I, *Q. J. R. Meteorol. Soc.* 58 (1932) 389–420. <https://doi.org/10.1002/qj.49705824704>.
- [114] C. Demain, M. Journée, C. Bertrand, Evaluation of different models to estimate the global solar radiation on inclined surfaces, *Renew. Energy*. 50

- (2013) 710–721. <https://doi.org/10.1016/j.renene.2012.07.031>.
- [115] C. Gueymard, An anisotropic solar irradiance model for tilted surfaces and its comparison with selected engineering algorithms, *Sol. Energy*. 38 (1987) 367–386. [https://doi.org/10.1016/0038-092X\(87\)90009-0](https://doi.org/10.1016/0038-092X(87)90009-0).
  - [116] A.J. Arnfield, A Note on the Diurnal, Latitudinal and Seasonal Variation of the Surface Reflection Coefficient, *J. Appl. Meteorol. Climatol.* 14 (1975) 1603–1608. [https://doi.org/10.1175/1520-0450\(1975\)014<1603:ANOTDL>2.0.CO;2](https://doi.org/10.1175/1520-0450(1975)014<1603:ANOTDL>2.0.CO;2).
  - [117] R.C. Temps, K.L. Coulson, Solar radiation incident upon slopes of different orientations, *Sol. Energy*. 19 (1977) 179–184. [https://doi.org/10.1016/0038-092X\(77\)90056-1](https://doi.org/10.1016/0038-092X(77)90056-1).
  - [118] T.M. McClellan, C.O. Pedersen, Investigation of outside heat balance models for use in a heat balance cooling load calculation procedure, in: American Society of Heating, Refrigerating and Air-Conditioning Engineers, Inc., Atlanta, GA (United States), United States, 1997. <https://www.osti.gov/biblio/349984>.
  - [119] A. Karn, V. Chintala, S. Kumar, An investigation into sky temperature estimation, its variation, and significance in heat transfer calculations of solar cookers, *Heat Transf. - Asian Res.* 48 (2019) 1830–1856. <https://doi.org/10.1002/htj.21459>.
  - [120] K. Zhang, T.P. McDowell, M. Kummert, Sky Temperature Estimation and Measurement for Longwave Radiation Calculation, *Proc. Fifteenth Int. Conf. Int. Build. Perform. Simul. Assoc.* (2017) 2093–2102.
  - [121] N. Daouas, Impact of external longwave radiation on optimum insulation thickness in Tunisian building roofs based on a dynamic analytical model, *Appl. Energy*. 177 (2016) 136–148. <https://doi.org/10.1016/j.apenergy.2016.05.079>.
  - [122] R. Evins, V. Dorer, J. Carmeliet, Simulating external longwave radiation exchange for buildings, *Energy Build.* 75 (2014) 472–482. <https://doi.org/10.1016/j.enbuild.2014.02.030>.
  - [123] Lawrence Berkeley National Laboratory, DOE-2: Building Energy Use and Cost Analysis Tool, (n.d.). <https://simulationresearch.lbl.gov/projects/doe2> (accessed June 14, 2022).
  - [124] D.C. Hittle, The building loads analysis and system thermodynamics (BLAST) program. Version 2. 0. Users manual. Volume II. Final report, United States, 1979.
  - [125] S. Aigarni, D. Nutter, Survey of sky effective temperature models applicable to building envelope radiant heat transfer, *ASHRAE Conf.* 121 (2015) 351–363. <https://doi.org/10.13140/RG.2.1.4212.5526>.
  - [126] L. Adelard, F. Pignolet-Tardan, T. Mara, P. Lauret, F. Garde, H. Boyer, Sky temperature modelisation and applications in building simulation, *Renew. Energy*. 15 (1998) 418–430. [https://doi.org/10.1016/S0960-1481\(98\)00198-0](https://doi.org/10.1016/S0960-1481(98)00198-0).
  - [127] S.A. Algarni, Modeling Radiation Heat Transfer for Building' s Cooling and

- Heating Loads: Considering the Role of Clear, Cloudy, and Dusty Conditions in Hot and Dry Climates, Univ. Arkansas. (2015). <http://scholarworks.uark.edu/etd><http://scholarworks.uark.edu/etd/1231>.
- [128] M. Aubinet, Longwave sky radiation, *Sol. Energy*. 53 (1994) 147–154.
  - [129] Italian Thermo-technical Committee (CTI), Typical Metereological Year Accessed, (2015).
  - [130] B.I. Höglund, G.P. Mitalas, D.G. Stephenson, Surface temperatures and heat fluxes for flat roofs, *Build. Sci.* 2 (1967) 29–36. [https://doi.org/10.1016/0007-3628\(67\)90005-9](https://doi.org/10.1016/0007-3628(67)90005-9).
  - [131] A. Aittomäki, A model for calculating heat balance of room and building, VTT Technical Research Centre of Finland, Helsinki, 1971.
  - [132] European Committee for Standardization (CEN), EN ISO 6946, Building Components and Building Elements—Thermal Resistance and Thermal Transmittance—Calculation Methods, (n.d.).
  - [133] R.J. Liesen, C.O. Pedersen, An evaluation of inside surface heat balance models for cooling load calculations, *ASHRAE Trans. Tech. Symp. Pap.* 103 (1997).
  - [134] European Committee for Standardization (CEN), EN ISO 13789, Thermal Performance of Buildings—Transmission and Ventilation Heat Transfer Coefficients—Calculation Method, (2017).
  - [135] J.R. Howell, M.P. Mengüç, Radiative transfer configuration factor catalog: A listing of relations for common geometries, *J. Quant. Spectrosc. Radiat. Transf.* 112 (2011) 910–912. <https://doi.org/10.1016/j.jqsrt.2010.10.002>.
  - [136] C. Miao, S. Yu, Y. Hu, H. Zhang, X. He, W. Chen, Review of methods used to estimate the sky view factor in urban street canyons, *Build. Environ.* 168 (2020) 106497. <https://doi.org/10.1016/j.buildenv.2019.106497>.
  - [137] Italian Thermo-technical Committee (CTI), Draft of Italian National Annex to EN ISO 52016-1 (restricted document), (2021). <https://www.cti2000.it/index.php?controller=documenti&action=schedaAllMsg&id=62539&tipodoc=4>.
  - [138] J.A. Clarke, 7 - Energy-related subsystems, in: J.A.B.T.-E.S. in B.D. (Second E. Clarke (Ed.), Butterworth-Heinemann, Oxford, 2001: pp. 202–280. <https://doi.org/https://doi.org/10.1016/B978-075065082-3/50007-3>.
  - [139] P.W. O’Callaghan, S.D. Probert, Sol-air temperature, *Appl. Energy*. 3 (1977) 307–311. [https://doi.org/10.1016/0306-2619\(77\)90017-4](https://doi.org/10.1016/0306-2619(77)90017-4).
  - [140] M. de Simón-Martín, C. Alonso-Tristán, M. Díez-Mediavilla, Diffuse solar irradiance estimation on building’s façades: Review, classification and benchmarking of 30 models under all sky conditions, *Renew. Sustain. Energy Rev.* 77 (2017) 783–802. <https://doi.org/10.1016/j.rser.2017.04.034>.
  - [141] F. Vignola, D.K. McDaniels, Beam-global correlations in the Pacific Northwest, *Sol. Energy*. 36 (1986) 409–418. [https://doi.org/10.1016/0038-092X\(86\)90088-5](https://doi.org/10.1016/0038-092X(86)90088-5).
  - [142] A. Louche, G. Notton, P. Poggi, G. Simonnot, Correlations for direct normal and global horizontal irradiation on a French Mediterranean site, *Sol.*



- Energy. 46 (1991) 261–266. [https://doi.org/10.1016/0038-092X\(91\)90072-5](https://doi.org/10.1016/0038-092X(91)90072-5).
- [143] E.L. Maxwell, A quasi-physical model for converting hourly global horizontal to direct normal insolation, United States, 1987. <https://www.osti.gov/biblio/5987868>.
  - [144] R. Perez, P. Ineichen, E.L. Maxwell, R.D. Seals, A. Zelenka, Dynamic global-to-direct irradiance conversion models, ASHRAE Trans. 98 (1992) 354–369.
  - [145] B.Y.H. Liu, R.C. Jordan, The interrelationship and characteristic distribution of direct, diffuse and total solar radiation, Sol. Energy. 4 (1960) 1–19. [https://doi.org/10.1016/0038-092X\(60\)90062-1](https://doi.org/10.1016/0038-092X(60)90062-1).
  - [146] J.C. Lam, D.H.W. Li, Correlation between global solar radiation and its direct and diffuse components, Build. Environ. 31 (1996) 527–535. [https://doi.org/10.1016/0360-1323\(96\)00026-1](https://doi.org/10.1016/0360-1323(96)00026-1).
  - [147] C.A. Gueymard, Parameterized transmittance model for direct beam and circumsolar spectral irradiance, Sol. Energy. 71 (2001) 325–346. [https://doi.org/10.1016/S0038-092X\(01\)00054-8](https://doi.org/10.1016/S0038-092X(01)00054-8).
  - [148] R.E. Bird, A simple, solar spectral model for direct-normal and diffuse horizontal irradiance, Sol. Energy. 32 (1984) 461–471. [https://doi.org/https://doi.org/10.1016/0038-092X\(84\)90260-3](https://doi.org/https://doi.org/10.1016/0038-092X(84)90260-3).
  - [149] T. Olofsson, K.E.A. Ohlsson, R. Östin, Measurement of the environmental temperature using the sol-air thermometer, Energy Procedia. 132 (2017) 357–362. <https://doi.org/10.1016/J.EGYPRO.2017.09.632>.
  - [150] X. Luo, Y. Tang, T. Hong, Efficient Computation Of Surface Sunlit Fractions In Urban-scale Building Modeling Using Ray-tracing Techniques, in: Proc. 2020 Build. Perform. Anal. Conf. SimBuild Co-Organized by ASHRAE IBPSA-USA, 2022. <https://escholarship.org/uc/item/9q02q8sd>.
  - [151] A. Yezioro, E. Shaviv, Shading: A design tool for analyzing mutual shading between buildings, Sol. Energy. 52 (1994) 27–37. [https://doi.org/10.1016/0038-092X\(94\)90078-G](https://doi.org/10.1016/0038-092X(94)90078-G).
  - [152] M.D.E. Hiller, W.A. Beckman, J.W. Mitchell, TRNSHD — a program for shading and insolation calculations, Build. Environ. 35 (2000) 633–644. [https://doi.org/10.1016/S0360-1323\(99\)00051-7](https://doi.org/10.1016/S0360-1323(99)00051-7).
  - [153] R. McCluney, Awning shading and algorithm for window energy studies, ASHRAE Trans. 92 (1986).
  - [154] V. Corrado, V. Serra, A. Vosilla, Performance Analysis of External Shading Devices, in: Proc. 21th Conf. Passiv. Low Energy Archit., 2004: pp. 19–22.
  - [155] Y. Cascone, V. Corrado, V. Serra, Calculation procedure of the shading factor under complex boundary conditions, Sol. Energy. 85 (2011) 2524–2539. <https://doi.org/10.1016/J.SOLENER.2011.07.011>.
  - [156] D.C. McKay, Estimating Solar Irradiance On Inclined Surfaces: A Review And Assessment Of Methodologies, Int. J. Sol. Energy. 3 (1985) 203–240. <https://doi.org/10.1080/01425918508914395>.
  - [157] R. Perez, R. Stewart, C. Arbogast, R. Seals, J. Scott, An anisotropic hourly

- diffuse radiation model for sloping surfaces: Description, performance validation, site dependency evaluation, *Sol. Energy*. 36 (1986) 481–497. [https://doi.org/10.1016/0038-092X\(86\)90013-7](https://doi.org/10.1016/0038-092X(86)90013-7).
- [158] D. Yang, Solar radiation on inclined surfaces: Corrections and benchmarks, *Sol. Energy*. 136 (2016) 288–302. <https://doi.org/10.1016/j.solener.2016.06.062>.
  - [159] J.W. Bugler, The determination of hourly insolation on an inclined plane using a diffuse irradiance model based on hourly measured global horizontal insolation, *Sol. Energy*. 19 (1977) 477–491. [https://doi.org/10.1016/0038-092X\(77\)90103-7](https://doi.org/10.1016/0038-092X(77)90103-7).
  - [160] D.T. Reindl, W.A. Beckman, J.A. Duffie, Evaluation of hourly tilted surface radiation models, *Sol. Energy*. 45 (1990) 9–17. [https://doi.org/10.1016/0038-092X\(90\)90061-G](https://doi.org/10.1016/0038-092X(90)90061-G).
  - [161] J.E. Hay, Calculation of solar irradiances for inclined surface: verification of models which use hourly and daily data, *Atmosphere-Ocean*,. 24 (1986) 16–41. <https://doi.org/10.1080/07055900.1986.9649238>.
  - [162] P.G. Loutzenhiser, H. Manz, C. Felsmann, P.A. Strachan, T. Frank, G.M. Maxwell, Empirical validation of models to compute solar irradiance on inclined surfaces for building energy simulation, *Sol. Energy*. 81 (2007) 254–267. <https://doi.org/10.1016/j.solener.2006.03.009>.
  - [163] M. David, P. Lauret, J. Boland, Evaluating tilted plane models for solar radiation using comprehensive testing procedures, at a southern hemisphere location, *Renew. Energy*. 51 (2013) 124–131. <https://doi.org/10.1016/j.renene.2012.08.074>.
  - [164] Bognár, R.C.G.M. Loonen, J.L.M. Hensen, Calculating solar irradiance without shading geometry: a point cloud-based method, *J. Build. Perform. Simul.* 14 (2021) 480–502. <https://doi.org/10.1080/19401493.2021.1971765>.
  - [165] A.P. Brunger, F.C. Hooper, Anisotropic sky radiance model based on narrow field of view measurements of shortwave radiance, *Sol. Energy*. 51 (1993) 53–64. [https://doi.org/10.1016/0038-092X\(93\)90042-M](https://doi.org/10.1016/0038-092X(93)90042-M).
  - [166] K. Källblad, A method to estimate the shading of solar radiation theory and implementation in a computer program, in: *Proc. Sixth Int. Conf. Int. Build. Perform. Simul. Assoc.*, Kyoto, Japan, 1999: pp. 595–601.
  - [167] C.A. Gueymard, Direct and indirect uncertainties in the prediction of tilted irradiance for solar engineering applications, *Sol. Energy*. 83 (2009) 432–444. <https://doi.org/10.1016/J.SOLENER.2008.11.004>.
  - [168] Y.Q. Tian, R.J. Davies-Colley, P. Gong, B.W. Thorrold, Estimating solar radiation on slopes of arbitrary aspect, *Agric. For. Meteorol.* 109 (2001) 67–74. [https://doi.org/10.1016/S0168-1923\(01\)00245-3](https://doi.org/10.1016/S0168-1923(01)00245-3).
  - [169] F.J. Olmo, J. Vida, I. Foyo, Y. Castro-Diez, L. Alados-Arboledas, Prediction of global irradiance on inclined surfaces from horizontal global irradiance, *Energy*. 24 (1999) 689–704. [https://doi.org/10.1016/S0360-5442\(99\)00025-0](https://doi.org/10.1016/S0360-5442(99)00025-0).

- [170] E.G. Evseev, A.I. Kudish, An assessment of a revised Olmo et al. model to predict solar global radiation on a tilted surface at Beer Sheva, Israel, *Renew. Energy*. 34 (2009) 112–119. <https://doi.org/https://doi.org/10.1016/j.renene.2008.04.012>.
- [171] D. Thevenard, K. Haddad, Ground reflectivity in the context of building energy simulation, *Energy Build.* 38 (2006) 972–980. <https://doi.org/10.1016/J.ENBUILD.2005.11.007>.
- [172] L. Evangelisti, C. Guattari, P. Gori, F. Bianchi, Heat transfer study of external convective and radiative coefficients for building applications, *Energy Build.* 151 (2017) 429–438. <https://doi.org/10.1016/j.enbuild.2017.07.004>.
- [173] H. Montazeri, B. Blocken, New generalized expressions for forced convective heat transfer coefficients at building facades and roofs, *Build. Environ.* 119 (2017) 153–168. <https://doi.org/10.1016/j.buildenv.2017.04.012>.
- [174] A. Awol, G.T. Bitsuamlak, F. Tariku, Numerical estimation of the external convective heat transfer coefficient for buildings in an urban-like setting, *Build. Environ.* 169 (2020) 106557. <https://doi.org/10.1016/j.buildenv.2019.106557>.
- [175] M. Mirsadeghi, D. Cóstola, B. Blocken, J.L.M. Hensen, Review of external convective heat transfer coefficient models in building energy simulation programs: Implementation and uncertainty, *Appl. Therm. Eng.* 56 (2013) 134–151. <https://doi.org/10.1016/j.applthermaleng.2013.03.003>.
- [176] T. Defraeye, B. Blocken, J. Carmeliet, Convective heat transfer coefficients for exterior building surfaces: Existing correlations and CFD modelling, *Energy Convers. Manag.* 52 (2011) 512–522. <https://doi.org/10.1016/j.enconman.2010.07.026>.
- [177] E.M. Sparrow, J.W. Ramsey, E.A. Mass, Effect of Finite Width on Heat Transfer and Fluid Flow about an Inclined Rectangular Plate, *J. Heat Transfer*. 101 (1979) 199–204. <https://doi.org/10.1115/1.3450946>.
- [178] J.A. Palyvos, A survey of wind convection coefficient correlations for building envelope energy systems' modeling, *Appl. Therm. Eng.* 28 (2008) 801–808. <https://doi.org/10.1016/j.applthermaleng.2007.12.005>.
- [179] A.D. Awol, G.T. Bitsuamlak, F.A. Tariku, Numerical Investigation of External Convective Heat Transfer Coefficient for Buildings in Different Land-Use Class, (2020) 214–221. [www.ibpsa.us](http://www.ibpsa.us).
- [180] European Committee for Standardization (CEN), EN 410, Glass in building. Determination of luminous and solar characteristics of glazing, (2011).
- [181] International Organization for Standardization (ISO), ISO 9050, Glass in building — Determination of light transmittance, solar direct transmittance, total solar energy transmittance, ultraviolet transmittance and related glazing factors, (2020).
- [182] J.L. Wright, Summary and comparison of methods to calculate solar heat gain, *ASHRAE Trans.* 101 (1995) 1517.

- [183] J. Karlsson, M. Rubin, A. Roos, Evaluation of predictive models for the angle-dependent total solar energy transmittance of glazing materials, *Sol. Energy*. 71 (2001) 23–31. [https://doi.org/10.1016/S0038-092X\(01\)00024-X](https://doi.org/10.1016/S0038-092X(01)00024-X).
- [184] M. Rubin, R. Powles, K. Von Rottkay, Models for the angle-dependent optical properties of coated glazing materials, *Sol. Energy*. 66 (1999) 267–276. [https://doi.org/10.1016/S0038-092X\(99\)00029-8](https://doi.org/10.1016/S0038-092X(99)00029-8).
- [185] I.E. Solutions, Virtual Environment (IES-Ve), (n.d.). <https://www.iesve.com/software/virtual-environment>.
- [186] Z. El Khoury, P. Riederer, N. Couillaud, J. Simon, M. Raguin, A multizone building model for matlab/simulink environment, *IBPSA 2005 - Int. Build. Perform. Simul. Assoc.* 2005. (2005) 525–532.
- [187] American Society for Heating Refrigerating Air-conditioning Engineers (ASHRAE), Fenestration, in: 2017 ASHRAE Handb. Fundam., SI Edition, ASHRAE, Tullie Circle, N.E., Atlanta, GA, 2017.
- [188] American Society for Heating Refrigerating Air-conditioning Engineers (ASHRAE), Nonresidential Cooling and Heating Load Calculations, in: 2017 ASHRAE Handb. Fundam., SI Edition, ASHRAE, Tullie Circle, N.E., Atlanta, GA, 2017.
- [189] A. Roos, P. Polato, P.A. Van Nijnatten, M.G. Hutchins, F. Olive, C. Anderson, Angular-dependent optical properties of low-e and solar control windows—: Simulations versus measurements, *Sol. Energy*. 69 (2001) 15–26. [https://doi.org/10.1016/S0038-092X\(01\)00019-6](https://doi.org/10.1016/S0038-092X(01)00019-6).
- [190] M. Montecchi, P. Polato, Simple equations to predict the daylighting behaviour of glazing by normal incidence spectrophotometry, *Riv. Della Stn. Sper. Del Vetro*. 5 (1995).
- [191] J. Karlsson, A. Roos, Modelling the angular behaviour of the total solar energy transmittance of windows, *Sol. Energy*. 69 (2000) 321–329. [https://doi.org/10.1016/S0038-092X\(00\)00083-9](https://doi.org/10.1016/S0038-092X(00)00083-9).
- [192] M.C. Singh, S.N. Garg, An empirical model for angle-dependent g-values of glazings, *Energy Build.* 42 (2010) 375–379. <https://doi.org/10.1016/J.ENBUILD.2009.10.004>.
- [193] F.C. McQuiston, J.D. Parker, J.D. Spitler, *Heating, Ventilating, and Air Conditioning: Analysis and Design*, 6th ed., Wiley, 2004.
- [194] I. Iu, D. Fisher, Application of Conduction Transfer Functions and Periodic Response Factors in Cooling Load Calculation Procedures, *ASHRAE Trans.* 110 (2004).
- [195] F. Haghighat, H. Liang, Determination of transient heat conduction through building envelopes - A review, *ASHRAE Trans.* 1 (1992) 284–290.
- [196] M.G. Davies, Current methods to handle wall conduction and room internal heat transfer, in: American Society of Heating, Refrigerating and Air-Conditioning Engineers, Inc., Atlanta, GA (US), United States, 1999. <https://www.osti.gov/biblio/20085611>.
- [197] A.P. Ramallo-González, M.E. Eames, D.A. Coley, Lumped parameter models for building thermal modelling: An analytic approach to simplifying

- complex multi-layered constructions, *Energy Build.* 60 (2013) 174–184. <https://doi.org/https://doi.org/10.1016/j.enbuild.2013.01.014>.
- [198] L. Mazzarella, R. Scoccia, P. Colombo, M. Motta, Improvement to EN ISO 52016-1:2017 hourly heat transfer through a wall assessment: the Italian National Annex, *Energy Build.* 210 (2020) 109758. <https://doi.org/10.1016/J.ENBUILD.2020.109758>.
- [199] E.Á. Rodríguez Jara, F.J. Sánchez de la Flor, S. Álvarez Domínguez, J.L. Molina Félix, J.M. Salmerón Lissén, A new analytical approach for simplified thermal modelling of buildings: Self-Adjusting RC-network model, *Energy Build.* 130 (2016) 85–97. <https://doi.org/https://doi.org/10.1016/j.enbuild.2016.08.039>.
- [200] C. Luo, B. Moghtaderi, H. Sugo, A. Page, A new stable finite volume method for predicting thermal performance of a whole building, *Build. Environ.* 43 (2008) 37–43. <https://doi.org/https://doi.org/10.1016/j.buildenv.2006.11.037>.
- [201] G. Fraisse, C. Viardot, O. Lafabrie, G. Achard, Development of a simplified and accurate building model based on electrical analogy, *Energy Build.* 34 (2002) 1017–1031. [https://doi.org/https://doi.org/10.1016/S0378-7788\(02\)00019-1](https://doi.org/https://doi.org/10.1016/S0378-7788(02)00019-1).
- [202] L. Laret, Use of general models with a small number of parameters, Part 1: Theoretical analysis, in: *Proc. Conf. Clima, 2000*: pp. 263–276.
- [203] M.M. Gouda, S. Danaher, C.P. Underwood, Building thermal model reduction using nonlinear constrained optimization, *Build. Environ.* 37 (2002) 1255–1265. [https://doi.org/https://doi.org/10.1016/S0360-1323\(01\)00121-4](https://doi.org/https://doi.org/10.1016/S0360-1323(01)00121-4).
- [204] B. Welt, A. Teixeira, K. Chau, M. Balaban, D.E. HINTENLANG, Explicit Finite Difference Methods for Heat Transfer Simulation and Thermal Process Design, *J. Food Sci.* 62 (2006) 230–236. <https://doi.org/10.1111/j.1365-2621.1997.tb03974.x>.
- [205] J.R. Waters, A.J. Wright, Criteria for the distribution of nodes in multilayer walls in finite-difference thermal modelling, *Build. Environ.* 20 (1985) 151–162. [https://doi.org/https://doi.org/10.1016/0360-1323\(85\)90010-1](https://doi.org/https://doi.org/10.1016/0360-1323(85)90010-1).
- [206] C.P. Underwood, An improved lumped parameter method for building thermal modelling, *Energy Build.* 79 (2014) 191–201. <https://doi.org/https://doi.org/10.1016/j.enbuild.2014.05.001>.
- [207] X. Xu, S. Wang, Optimal simplified thermal models of building envelope based on frequency domain regression using genetic algorithm, *Energy Build.* 39 (2007) 525–536. <https://doi.org/https://doi.org/10.1016/j.enbuild.2006.06.010>.
- [208] C. Luo, B. Moghtaderi, A. Page, Modelling of wall heat transfer using modified conduction transfer function, finite volume and complex Fourier analysis methods, *Energy Build.* 42 (2010) 605–617. <https://doi.org/https://doi.org/10.1016/j.enbuild.2009.10.031>.
- [209] J.D. Spitler, D.E. Fisher, Development of periodic response factors for use

- with the radiant time series method, in: American Society of Heating, Refrigerating and Air-Conditioning Engineers, Inc., Atlanta, GA (US), United States, 1999. <https://www.osti.gov/biblio/20085639>.
- [210] E. Kossecka, D. Ph., J. Nys, Conduction Z-transfer Function Coefficients for Common Composite Wall Assemblies, in: Proc. Therm. Perform. Exter. Envel. Build. VIII, 1995.
  - [211] American Society for Heating Refrigerating Air-conditioning Engineers (ASHRAE), Heat transfer, in: 2017 ASHRAE Handb. Fundam., SI Edition, ASHRAE, Tullie Circle, N.E., Atlanta, GA, 2017.
  - [212] G.N. Walton, A new algorithm for radiant interchange in room loads calculations, ASHRAE Trans. 86 (1980) 190–208.
  - [213] J.A. Carroll, An “MRT Method” of Computing Radiant Energy Exchange in Rooms, in: Proc. Build. Simul. 2011 12th Conf. Int. Build. Perform. Simul. Assoc., Sydney, 1980.
  - [214] E.R.G. Eckert, Radiative transfer, H. C. Hottel and A. F. Sarofim, McGraw-Hill Book Company, New York, 1967. 52 pages, AIChE J. 15 (1969) 794–796. <https://doi.org/https://doi.org/10.1002/aic.690150504>.
  - [215] T. Walker, S.-C. Xue, G.W. Barton, Numerical Determination of Radiative View Factors Using Ray Tracing, J. Heat Transfer. 132 (2010). <https://doi.org/10.1115/1.4000974>.
  - [216] H. Johra, P. Heiselberg, Influence of internal thermal mass on the indoor thermal dynamics and integration of phase change materials in furniture for building energy storage: A review, Renew. Sustain. Energy Rev. 69 (2017) 19–32. <https://doi.org/10.1016/j.rser.2016.11.145>.
  - [217] P. Raftery, E. Lee, T. Webster, T. Hoyt, F. Bauman, Effects of furniture and contents on peak cooling load, Energy Build. 85 (2014) 445–457. <https://doi.org/10.1016/j.enbuild.2014.09.081>.
  - [218] M. Cucumo, D. Kaliakatsos, V. Marinelli, Estimating effective solar absorptance in rooms, Energy Build. 23 (1995) 117–120. [https://doi.org/10.1016/0378-7788\(95\)00935-3](https://doi.org/10.1016/0378-7788(95)00935-3).
  - [219] M. Wall, Distribution of solar radiation in glazed spaces and adjacent buildings. A comparison of simulation programs, Energy Build. 26 (1997) 129–135. [https://doi.org/10.1016/S0378-7788\(96\)01026-2](https://doi.org/10.1016/S0378-7788(96)01026-2).
  - [220] T. Messadi, Mathematical Simulation for Correct Coupling of Direct Solar Gain to Thermal Mass Inside a Prototypical Space, in: Proc. Therm. Perform. Exter. Envel. Build. VII, n.d.
  - [221] J. Wen, T.F. Smith, Absorption of solar energy in a room, Sol. Energy. 72 (2002) 283–297. [https://doi.org/10.1016/S0038-092X\(01\)00107-4](https://doi.org/10.1016/S0038-092X(01)00107-4).
  - [222] K. Chatziangelidis, D. Bouris, Calculation of the distribution of incoming solar radiation in enclosures, Appl. Therm. Eng. 29 (2009) 1096–1105. <https://doi.org/10.1016/J.APPLTHERMALENG.2008.05.026>.
  - [223] Y. Boukhris, L. Gharbi, N. Ghrab-Morcos, Coupling the building simulation tool ZAER with a sunspot model. Case study in Tunis, Energy Build. 70 (2014) 1–14. <https://doi.org/10.1016/J.ENBUILD.2013.11.002>.

- [224] K.J. Kontoleon, Glazing solar heat gain analysis and optimization at varying orientations and placements in aspect of distributed radiation at the interior surfaces, *Appl. Energy*. 144 (2015) 152–164. <https://doi.org/10.1016/J.APENERGY.2015.01.087>.
- [225] K. Johnsen, K. Grau, TSBI3 Computer program for thermal simulation of buildings: User's Guide (version B.05), 1994.
- [226] J. Spitler, C.O. Pedersen, D. Fisher, Interior convective heat transfer in buildings with large ventilative flow rates, *ASHRAE Trans.* (1991) 505–515.
- [227] D.E. Fisher, C.O. Pedersen, Convective Energy and Heat Transfer Thermal Load in Building Calculations, in: *ASHRAE Trans. Tech. Symp. Pap.*, United States, 1997.
- [228] L. Peeters, I. Beausoleil-Morrison, A. Novoselac, Internal convective heat transfer modeling: Critical review and discussion of experimentally derived correlations, *Energy Build.* 43 (2011) 2227–2239. <https://doi.org/https://doi.org/10.1016/j.enbuild.2011.05.002>.
- [229] M. Camci, Y. Karakoyun, O. Acikgoz, A.S. Dalkilic, A comparative study on convective heat transfer in indoor applications, *Energy Build.* 242 (2021) 110985. <https://doi.org/https://doi.org/10.1016/j.enbuild.2021.110985>.
- [230] S.W. Churchill, R. Usagi, A general expression for the correlation of rates of transfer and other phenomena, *AIChE J.* 18 (1972) 1121–1128. <https://doi.org/https://doi.org/10.1002/aic.690180606>.
- [231] L. Peeters, I. Beausoleil-Morrison, B. Griffith, A. Novoselac, Internal convection coefficients for building simulation, *Proc. Twelfth Int. Conf. Int. Build. Perform. Simul. Assoc.* (2011) 2370–2377.
- [232] A.-J.N. Khalifa, Natural convective heat transfer coefficient – a review: I. Isolated vertical and horizontal surfaces, *Energy Convers. Manag.* 42 (2001) 491–504. [https://doi.org/https://doi.org/10.1016/S0196-8904\(00\)00042-X](https://doi.org/https://doi.org/10.1016/S0196-8904(00)00042-X).
- [233] A.-J.N. Khalifa, Natural convective heat transfer coefficient – a review: II. Surfaces in two- and three-dimensional enclosures, *Energy Convers. Manag.* 42 (2001) 505–517. [https://doi.org/https://doi.org/10.1016/S0196-8904\(00\)00043-1](https://doi.org/https://doi.org/10.1016/S0196-8904(00)00043-1).
- [234] European Committee for Standardization (CEN), EN ISO 15265, Ergonomics of the thermal environment - Risk assessment strategy for the prevention of stress or discomfort in thermal working conditions, (2004).
- [235] T. Berthou, P. Stabat, R. Salvazet, D. Marchio, Development and validation of a gray box model to predict thermal behavior of occupied office buildings, *Energy Build.* 74 (2014) 91–100. <https://doi.org/10.1016/J.ENBUILD.2014.01.038>.
- [236] G. De Luca, F. Bianco Mauthe Degerfeld, I. Ballarini, V. Corrado, Improvements of simplified hourly models for the energy assessment of buildings: The application of EN ISO 52016 in Italy, *Energy Reports*. 8 (2022) 7349–7359. <https://doi.org/10.1016/J.EGYR.2022.05.120>.
- [237] G. de Luca, I. Ballarini, F.G.M.B.M. Degerfeld, V. Corrado, Validation of the simplified heat conduction model of EN ISO 52016-1, 2069 (2021).

<https://doi.org/10.1088/1742-6596/2069/1/012136>.

- [238] A. Angelotti, M. Ballabio, L. Mazzarella, C. Cornaro, G. Parente, F. Frasca, A. Prada, P. Baggio, I. Ballarini, G. De Luca, V. Corrado, Dynamic simulation of existing buildings: Considerations on the model calibration, in: Proc. Sixt. Int. Conf. Int. Build. Perform. Simul. Assoc., 2019: pp. 4165–4172.
- [239] European Commission, Mandate M480, Mandate to CEN, CENELEC and ETSI for the elaboration and adoption of standards for a methodology calculating the integrated energy performance of buildings and promoting the energy efficiency of buildings, in accordance with the terms set in, (n.d.).
- [240] European Committee for Standardization (CEN), CEN ISO/TR 52016-2, Energy performance of buildings - Energy needs for heating and cooling, internal temperatures and sensible and latent heat loads - Part 2: Explanation and justification of ISO 52016-1 and ISO 52017-1 (ISO/TR 52016-2:2017), (2017).
- [241] I. Ballarini, A. Costantino, E. Fabrizio, V. Corrado, The Dynamic Model of EN ISO 52016-1 for the Energy Assessment of Buildings Compared to Simplified and Detailed Simulation Methods, 2019. <https://doi.org/10.26868/25222708.2019.210431>.
- [242] European Committee for Standardization (CEN), Energy performance of buildings – Basic Principles for the set of EPB standards (CEN/TS 16628), (2014).
- [243] E. Center, EPB Center, Consultancy and services on Energy Performance of Buildings, (2022). <https://epb.center/> (accessed June 14, 2022).
- [244] E. Parliament, Council of the European Union. Directive (EU) 2018/844 of the European Parliament and of the Council of 30 May 2018 amending Directive 2010/31/EU on the energy performance of buildings and Directive 2012/27/EU on energy efficiency, (2018).
- [245] D. van Dijk, J. Hogeling, The new EN ISO 52000 family of standards to assess the energy performance of buildings put in practice, E3S Web Conf. 111 (2019). <https://doi.org/10.1051/e3sconf/201911104047>.
- [246] G. Clark, C. Allen, The Estimation of Atmospheric Radiation for Clear and Cloudy Skies, in: Proc. 2nd Natl. Passiv. Sol. Conf., Philadelphia, Pennsylvania (U.S.), 1978.
- [247] G.N. Walton, Thermal Analysis Research Program Reference Manual, (1983).
- [248] M. Aubinet, Longwave sky radiation parametrizations, Sol. Energy. 53 (1994) 147–154. [https://doi.org/10.1016/0038-092X\(94\)90475-8](https://doi.org/10.1016/0038-092X(94)90475-8).
- [249] T. Zakula, M. Bagaric, N. Ferdelji, B. Milovanovic, S. Mudrinic, K. Ritosa, Comparison of dynamic simulations and the ISO 52016 standard for the assessment of building energy performance, Appl. Energy. 254 (2019) 113553. <https://doi.org/10.1016/j.apenergy.2019.113553>.
- [250] T. Zakula, N. Badun, N. Ferdelji, I. Ugrina, Framework for the ISO 52016



- standard accuracy prediction based on the in-depth sensitivity analysis, *Appl. Energy*. 298 (2021) 117089. <https://doi.org/10.1016/j.apenergy.2021.117089>.
- [251] M. Magni, F. Ochs, W. Streicher, Comprehensive analysis of the influence of different building modelling approaches on the results and computational time using a cross-compared model as a reference, *Energy Build.* 259 (2022) 111859. <https://doi.org/10.1016/J.ENBUILD.2022.111859>.
- [252] S. Summa, G. Remia, C. Di Perna, Comparative and Sensitivity Analysis of Numerical Methods for the Discretization of Opaque Structures and Parameters of Glass Components for EN ISO 52016-1, *Energies*. 15 (2022). <https://doi.org/10.3390/en15031030>.
- [253] F. Bianco Mauthe Degerfeld, I. Ballarini, G. De Luca, M.P. Tootkaboni, V. Corrado, Sensitivity Analysis of the Thermal Energy Need of a Residential Building Assessed by means of the EN ISO 52016 Simplified Dynamic Method, *E3S Web Conf.* 197 (2020). <https://doi.org/10.1051/e3sconf/202019702012>.
- [254] F. Bianco Mauthe Degerfeld, I. Ballarini, G. De Luca, V. Corrado, The application of the EN ISO 52016 standard and its Italian National Annex to assess the heating and cooling needs of a reference office building, *E3S Web Conf.* 312 (2021). <https://doi.org/10.1051/e3sconf/202131206003>.
- [255] D. Palladino, D. Iatauro, P. Signoretti, Application of hourly dynamic method for nZEB buildings in Italian context: analysis and comparisons in national calculation procedure framework, *E3S Web Conf.* 312 (2021). <https://doi.org/10.1051/e3sconf/202131202006>.
- [256] A. Angelotti, M. Martire, L. Mazzarella, M. Pasini, I. Ballarini, V. Corrado, G. De Luca, P. Baggio, A. Prada, F. Bosco, C. Cornaro, Building Energy Simulation for Nearly Zero Energy Retrofit Design: The Model Calibration, in: 2018 IEEE Int. Conf. Environ. Electr. Eng. 2018 IEEE Ind. Commer. Power Syst. Eur. (EEEIC / I&CPS Eur., 2018: pp. 1–6. <https://doi.org/10.1109/EEEIC.2018.8493777>.
- [257] European Committee for Standardization (CEN), EN ISO 13786, Thermal performance of building components. Dynamic thermal characteristics. Calculation methods, (2017).
- [258] Italian Organisation for Standardisation (UNI), UNI/TR 11552, Opaque Envelope Components of Buildings—Thermo-Physical Parameters, (2014).
- [259] European Committee for Standardization (CEN), EN 16798-1, Energy performance of buildings. Ventilation for buildings. Indoor environmental input parameters for design and assessment of energy performance of buildings addressing indoor air quality, thermal environment, lighting and acoustics. Module M, (2019).
- [260] U.S. Department of Energy, EnergyPlus Weather Data Sources, (2022). <https://energyplus.net/weather> (accessed June 14, 2022).
- [261] Italian Republic, Inter-Ministerial Decree of 26 June 2015, Applicazione delle Metodologie di Calcolo delle Prestazioni Energetiche e Definizione

- delle Prescrizioni e dei Requisiti Minimi Degli Edifici, Off. J. Ital. Repub. 162 (2015).
- [262] T. Loga, N. Diefenbach, B. Stein, Typology Approach for Building Stock Energy Assessment. Main Results of the TABULA Project, (n.d.).
  - [263] Italian Ministry of the Economic Development and Ministry of the Environment, Updating of the Italian Application of the Cost-Optimal Calculation Methodology for the Minimum Energy Performance Requirements (Directive 2010/31/EU Art. 5), (2018).
  - [264] Italian Organisation for Standardisation (UNI), UNI 10349-3, Heating and cooling of buildings - Climatic data - Part 3: Accumulated temperature differences (degree-days) and other indices, (2016).
  - [265] G. Clark, C. Allen, The Estimation of Atmospheric Radiation for Clear and Cloudy Skies, in: Proc. 2nd Natl. Passiv. Sol. Conf., Philadelphia, PA, USA, 1978.
  - [266] Italian Organisation for Standardisation (UNI), UNI/TS 11300-1, Energy performance of buildings - Part 1: Evaluation of energy need for space heating and cooling, (2014).
  - [267] A. Hardy, D. Glew, An analysis of errors in the Energy Performance certificate database, Energy Policy. 129 (2019) 1168–1178. <https://doi.org/10.1016/J.ENPOL.2019.03.022>.
  - [268] M. Mangold, M. Österbring, H. Wallbaum, Handling data uncertainties when using Swedish energy performance certificate data to describe energy usage in the building stock, Energy Build. 102 (2015) 328–336. <https://doi.org/10.1016/J.ENBUILD.2015.05.045>.

# Annex A – Modifications to EnergyPlus’s source code

## A.1 General specifications

The EnergyPlus’s source code was modified following the rules presented in the EnergyPlus’s Module Developer document, and using the tools indicated at the following link: <https://github.com/NREL/EnergyPlus/wiki/Building-EnergyPlus>.

Firstly, it has to be stated that the modifications applied to the EnergyPlus’s code were made only for research purposes, and specifically to test specific modelling simplifications, assumptions, or calculation modules, namely those for which appropriate modelling strategies could not be applied. Therefore, the modified code is currently at an early, basic, but working, stage. It was modified within the Microsoft Visual Studio software, and debug executables were built to run the code (release executables were not built).

Different routines of the source code were modified to test three modelling simplifications, as presented in the main text of the present dissertation; these regard the following phenomena:

1. Solar transmission, presented in Section 5.2.1.4 and 5.2.2.2,
2. Shadowing of diffuse solar radiation, presented in Section 5.2.1.2, and
3. Heat conduction, presented in Section 5.2.1.5 and 5.2.2.1.

As for the first two phenomena, only few changes have been implemented in the source code in the *SolarShading* routine; specifically, some variables were overridden. The latter, instead, required extensive modifications and additions to correctly implement it in the source code. Therefore, the main changes and additions related to the latter modelling assumptions are presented in the following paragraphs.

## A.2 Modifications to the source code

For simulating the simplified heat conduction model presented in the EN ISO 52016-1 technical standard, the *HeatBalFiniteDiffManager* routine of the source code was modified. This module contains the heat balance simulation routines, and

manages the finite difference heat balance simulation on the building; the *HeatBalFiniteDiffManager*'s main subroutines are presented in Table A1.

Table A1: *HeatBalFiniteDiffManager*'s main subroutines

<b><i>HeatBalFiniteDiffManager</i></b>	
<i>ManageHeatBalFiniteDiff</i>	Manages the moisture balance method
<i>CalcHeatBalFiniteDiff</i>	Controls the calculation of the fluxes and temperatures using finite difference procedures for all building surface constructs
<i>ExteriorBCEqns</i>	Calculates the heat transfer at the node on the surfaces outside face (facing outdoor environment)
<i>InteriorNodeEqns</i>	Calculates finite difference heat transfer for nodes inside material layers
<i>IntInterfaceNodeEqns</i>	Calculates finite difference heat transfer for nodes that interface two different material layers inside construction
<i>InteriorBCEqn</i>	Calculates the heat transfer at the node on the surfaces inside face (facing zone)
<i>CalcNodeHeatFlux</i>	Calculate heat flux at each node
<u><i>ExtSurfNode52016</i></u>	Calculates the heat transfer at the node on the surfaces outside face according to the EN ISO 52016-1 algorithm
<u><i>IntSurfNode52016</i></u>	Calculates the heat transfer at the node on the surfaces inside face according to the EN ISO 52016-1 algorithm
<u><i>IntNode52016</i></u>	Calculates finite difference heat transfer for inside nodes according to the EN ISO 52016-1 algorithm

Black underlined = modified subroutines

Red underlined = added subroutines

As reported in Table A1, three different routines were added to the code to solve the heat balances at the external surface, internal surface, and inside nodes (i.e., ***ExtSurfNode52016***, ***IntSurfNode52016***, and ***IntNode52016*** respectively), according to the simplified dynamic method; then, the main subroutine which controls the calculation of the heat fluxes and temperatures (i.e., ***CalcHeatBalFiniteDiff***) was modified to use the added subroutines.

In the modified main subroutine, the number of resistive-capacitive nodes for each construction (e.g., an external wall with a given stratigraphy, or a slab with another stratigraphy, etc.) is defined, as well as the internodal conductances and the node heat capacities (as required by the simplified heat conduction algorithm). For the sake of the present dissertation, the EnergyPlus's source code was not implemented with a function for an automatic definition of these parameters; thus, these are calculated externally (following the specifications of the technical standard) and manually implemented within the code as arrays (for each construction type).

The added subroutines, and the modifications to the main one, are reported below.

#### ***ExtSurfNode52016* – External surface node heat balance**

```

void ExtSurfNode52016(int const NodeNum,           // NODE NUMBER
    float const Cap_Delt,                          // Heat capacity at node / 3600 seconds
    float const CondH_p,                          // Conductance between node and node + 1
    int const Surf,                                // Surface number
    Array1D<Real64> const &TD,                    // The old dry Temperature at each node for the CondFD algorithm..
    Array1D<Real64> &TDT                          // The current or new Temperature at each node location for the CondFD solution..
)
{
    using DataHeatBalSurfFace::QdotRadOutRep;
    using DataHeatBalSurfFace::QdotRadOutRepPerArea;
    using DataHeatBalSurfFace::QradOutReport;
    using DataSurfFaces::HeatTransferModel1_CondFD;
    using DataSurfFaces::OSCM;
    using DataSurfFaces::OtherSideCondModeledExt;

```

```

auto const &surface(Surface(Surf));
int const surface_ExtBoundCond(surface.ExtBoundCond);
auto const TD_i(TD(NodeNum)); // temperature at node (n) at timestep - 1
auto TDT_i(TDT(NodeNum)); // temperature at node (n) at timestep
auto const TDT_p(TDT(NodeNum + 1)); // temperature of inner node (node + 1) at timestep

Real64 Tsky;
Real64 QRadSWOutFD; // Short wave radiation absorbed on outside of opaque surface
Real64 QRadSWOutMvInsulFD(0.0); // SW radiation at outside of Movable Insulation
Real64 const hconvo(HConvExtFD(Surf));
Real64 const hrad(HAirFD(Surf));
Real64 const hsky(HSkyFD(Surf));
Real64 const hgnd(HGrndFD(Surf));
Real64 const Toa(TempOutsideAirFD(Surf));
Real64 const Tgnd(TempOutsideAirFD(Surf));

if (surface_ExtBoundCond == OtherSideCondModeledExt) {
    // CR8046 switch modeled rad temp for sky temp.
    Tsky = OSCM(surface.OSCMPtr).TRad;
    QRadSWOutFD = 0.0; // eliminate incident shortwave on underlying surface
} else { // Set the external conditions to local variables
    QRadSWOutFD = QRadSWOutAbs(Surf);
    QRadSWOutMvInsulFD = QRadSWOutMvIns(Surf);
    Tsky = SkyTemp;
}

if (surface_ExtBoundCond == Surf) { // adiabatic surface, solved as an exterior node but considering
    // hce = hre = 0, asol = 0 (no absorbed solar radiation), and Qsky = 0 (no radiation to sky)
    TDT_i = (Cap_Delt * TD_i + CondH_p * TDT_p) / (Cap_Delt + CondH_p);
} else if (surface_ExtBoundCond <= 0) { // regular outside conditions
    TDT_i = (Cap_Delt * TD_i + hgnd * Tgnd + (hconvo + hrad) * Toa + hsky * Tsky + QRadSWOutFD + CondH_p * TDT_p) /
        (Cap_Delt + hconvo + hgnd + hrad + hsky + CondH_p);
}

// Limit clipping
if (TDT_i < MinSurfaceTempLimit) {
    TDT_i = MinSurfaceTempLimit;
} else if (TDT_i > MaxSurfaceTempLimit) {
    TDT_i = MaxSurfaceTempLimit;
}

TDT(NodeNum) = TDT_i;

Real64 const Toa_TDT_i(Toa - TDT_i);
Real64 const QNetSurfFromOutside(QRadSWOutFD + (hgnd * (-TDT_i + Tgnd) + (hconvo + hrad) * Toa_TDT_i + hsky * (-TDT_i + Tsky)));

// Same sign convention as CTFs
OpaqSurfOutsideFaceConductionFlux(Surf) = -QNetSurfFromOutside;
OpaqSurfOutsideFaceConduction(Surf) = surface.Area * OpaqSurfOutsideFaceConductionFlux(Surf);

// Report all outside BC heat fluxes
QdotRadOutRepPerArea(Surf) = -(hgnd * (TDT_i - Tgnd) + hrad * (-Toa_TDT_i) + hsky * (TDT_i - Tsky));
QdotRadOutRep(Surf) = surface.Area * QdotRadOutRepPerArea(Surf);
QRadOutReport(Surf) = QdotRadOutRep(Surf) * TimeStepZoneSec;
}

```

### IntSurfNode52016 – Internal surface node heat balance

```

void IntSurfNode52016(int const NodeNum,
    float const Cap_Delt,
    float const CondH_m,
    int const Surf, // Surface number
    Array1D<Real64> const &TD, // INSIDE SURFACE TEMPERATURE OF EACH HEAT TRANSFER SURF.
    Array1D<Real64> &TDT, // INSIDE SURFACE TEMPERATURE OF EACH HEAT TRANSFER SURF.
    Array1D<Real64> &TDTreport // Temperature value from previous HeatSurfaceHeatManager iteration's value
)
{
    using DataHeatBalFanSys::MAT;
    using DataHeatBalFanSys::QCoolingPanelSurf;
    using DataHeatBalFanSys::QElecBaseboardSurf;
    using DataHeatBalFanSys::QHTRadSysSurf;
    using DataHeatBalFanSys::QHWBaseboardSurf;
    using DataHeatBalFanSys::QSteamBaseboardSurf;
    using DataHeatBalFanSys::ZoneAirHumRat;
    using DataSurfaces::HeatTransferModel_ConvFD;

    auto const &surface(Surface(Surf));
    int const ConstrNum(surface.Construction);

    // Set the internal conditions to local variables
    Real64 const NetLWRadToSurfFD(NetLWRadToSurf(Surf)); // Net interior long wavelength radiation to surface from other surfaces
    Real64 const QRadSWInFD(QRadSWInAbs(Surf)); // Short wave radiation absorbed on inside of opaque surface
    Real64 const QHTRadSysSurfFD(
        QHTRadSysSurf(Surf)); // Current radiant heat flux at a surface due to the presence of high temperature radiant heaters
    Real64 const QHWBaseboardSurfFD(
        QHWBaseboardSurf(Surf)); // Current radiant heat flux at a surface due to the presence of hot water baseboard heaters
    Real64 const QSteamBaseboardSurfFD(
        QSteamBaseboardSurf(Surf)); // Current radiant heat flux at a surface due to the presence of steam baseboard heaters
    Real64 const QElecBaseboardSurfFD(
        QElecBaseboardSurf(Surf)); // Current radiant heat flux at a surface due to the presence of electric baseboard heaters
    Real64 const QCoolingPanelSurfFD(
        QCoolingPanelSurf(Surf)); // Current radiant heat flux at a surface due to the presence of simple cooling panels
    Real64 const QRadThermInFD(QRadThermInAbs(Surf)); // Thermal radiation absorbed on inside surfaces

    // Boundary Conditions from Simulation for Interior
    Real64 hconvi(HConvInFD(Surf));
    Real64 const Tia(MAT(surface.Zone));
    auto TDT_i(TDT(NodeNum));
    auto const TDT_m(TDT(NodeNum - 1));
    auto const TD_i(TD(NodeNum));
    Real64 const QFac(NetLWRadToSurfFD + QHTRadSysSurfFD + QHWBaseboardSurfFD + QSteamBaseboardSurfFD + QElecBaseboardSurfFD + QRadSWInFD +

```

```

        QRadThermInFD + QCoolingPanelSurfFD);
// Real64 const QFac(QHtRadSysSurfFD + QHwBaseboardSurfFD + QSteamBaseboardSurfFD + QElecBaseboardSurfFD + QRadSWInFD + QRadThermInFD +
// QCoolingPanelSurfFD);

TDT_i = (QFac + hconvi * Tia + Cap_Delt * TD_i + CondH_m * TDT_m) / (Cap_Delt + hconvi + CondH_m);

if (TDT_i < MinSurfaceTemplimit) {
    TDT_i = MinSurfaceTemplimit;
} else if (TDT_i > MaxSurfaceTemplimit) {
    TDT_i = MaxSurfaceTemplimit;
}

TDT(NodeNum) = TDT_i;

Real64 const QNetSurfInside(-(QFac + hconvi * (-TDT_i + Tia)));
// Pass inside conduction Flux [W/m2] to DataHeatBalanceSurface array
OpaqSurfInsFaceConductionFlux(Surf) = QNetSurfInside;
// QFluxZoneToInsurf(Surf) = QNetSurfInside
OpaqSurfInsFaceConduction(Surf) = QNetSurfInside * surface.Area; // for reporting as in CTF, PT
}

```

### ***IntNode52016 – Inside nodes heat balance***

```

void IntNode52016(int const NodeNum,
                 float const Cap_Delt,
                 float const CondH_p,
                 float const CondH_m,
                 int const Surf,           // Surface number
                 Array1D<Real64> const &TD, // INSIDE SURFACE TEMPERATURE OF EACH HEAT TRANSFER SURF.
                 Array1D<Real64> &TDT      // INSIDE SURFACE TEMPERATURE OF EACH HEAT TRANSFER SURF.
)
{
    int const ConstrNum(Surface(Surf).Construction);
    auto const TD_i(TD(NodeNum));

    auto const TDT_m(TDT(NodeNum - 1)); // temperature of outer node
    auto TD_i(TD(NodeNum));              // temperature of node to calculate
    auto const TDT_p(TDT(NodeNum + 1)); // temperature of inner node

    TDT_i = (Cap_Delt * TD_i + CondH_m * TDT_m + CondH_p * TDT_p) / (Cap_Delt + CondH_m + CondH_p);

    // Limit clipping
    if (TDT_i < MinSurfaceTemplimit) {
        TDT_i = MinSurfaceTemplimit;
    } else if (TDT_i > MaxSurfaceTemplimit) {
        TDT_i = MaxSurfaceTemplimit;
    }

    TDT(NodeNum) = TDT_i;
}

```

### ***CalcHeatBalFiniteDiff***

```

void CalcHeatBalFiniteDiff(int const Surf,           // Surface number
                           Real64 &TempSurfInTmp, // INSIDE SURFACE TEMPERATURE OF EACH HEAT TRANSFER SURF.
                           Real64 &TempSurfOutTmp  // Outside Surface Temperature of each Heat Transfer Surface
)
{
    { ... }
}

```

```

using DataHeatBalance::CondFDRelaxFactor;

static Real64 MaxDelTemp(0.0);

int const ConstrNum(Surface(Surf).Construction);
int const TotNodes(ConstructFD(ConstrNum).TotNodes);
int const TotLayers(dataConstruction.Construct(ConstrNum).TotLayers);

TempSurfInTmp = 0.0;
TempSurfOutTmp = 0.0;

int const Delt(ConstructFD(ConstrNum).DeltaTime); // (seconds)

// Aliases
auto &surfaceFD(SurfaceFD(Surf));
auto const &T(surfaceFD.T);
auto &TT(surfaceFD.TT);
auto const &Rhov(surfaceFD.Rhov);
auto &RhoT(surfaceFD.RhoT);
auto const &TD(surfaceFD.TD);
auto &TDT(surfaceFD.TDT);
auto &TDTLast(surfaceFD.TDTLast);
auto &TDreport(surfaceFD.TDreport);
auto &RH(surfaceFD.RH);
auto &EnthOld(surfaceFD.EnthOld);
auto &EnthNew(surfaceFD.EnthNew);
auto &EnthLast(surfaceFD.EnthLast);
auto &GSLoopCounter(surfaceFD.GSLoopCounter);
auto &MaxNodeDelTemp(surfaceFD.MaxNodeDelTemp);

Real64 HMovInsul; // Equiv H for TIM layer, Comes with call to
int RoughIndexMovInsul; // roughness Movable insulation
Real64 AbsExt; // exterior absorptivity movable insulation
EvalOutsideMovableInsulation(Surf, HMovInsul, RoughIndexMovInsul, AbsExt);
// Start stepping through the slab with time.

for (int J = 1, J_end = nint(TimeStepZoneSec / Delt); J <= J_end; ++J) { // PT testing higher time steps
    int GSiter; // iteration counter for implicit repeat calculation
    for (GSiter = 1; GSiter <= MaxGSiter; ++GSiter) { // Iterate implicit equations

```

```

TDTLast = TDT; // Save last iteration's TDT (New temperature) values
EnthLast = EnthNew; // Last iterations new enthalpy value

// For each construction number ... to be repeated for each
if (ConstrNum == ConstrNum_) {
    int TotNodeNum = n;
    float Caps[n + 1] = {0, // always zero
        Caps_1 / TimeStepZoneSec, // node 1
        Caps_2 / TimeStepZoneSec, // node 2
        Caps_3 / TimeStepZoneSec,
        ...
        Caps_n / TimeStepZoneSec}; // last node (n)
    float CondHs[n + 1] = {0, // always zero
        CondHs_1, // between node 1 and 2
        CondHs_2, // between node 2 and 3
        ...
        CondHs_n, // between node n-1 and n
        0.0}; // always zero
    for (int i = 1; i <= TotNodeNum; ++i) {
        if (i == 1) { // External surface node
            float const Cap_Delt = Caps[i];
            float const CondH_p = CondHs[i];
            ExtSurfNode52016(i, Cap_Delt, CondH_p, Surf, T, TT, Rhov, RhoT, RH, TD, TDT, EnthOld, EnthNew, TotNodes, HMovInsul);
        } else if (i == TotNodeNum) { // Internal surface node
            float const Cap_Delt = Caps[i];
            float const CondH_m = CondHs[i - 1];
            IntSurfNode52016(i, Cap_Delt, CondH_m, Surf, T, TT, Rhov, RhoT, RH, TD, TDT, EnthOld, EnthNew, TDreport);
        } else { // Interior nodes
            float const Cap_Delt = Caps[i];
            float const CondH_p = CondHs[i];
            float const CondH_m = CondHs[i - 1];
            IntNode52016(i, Cap_Delt, CondH_p, CondH_m, Surf, T, TT, Rhov, RhoT, RH, TD, TDT, EnthOld, EnthNew);
        }
    }
    /// Repeat for each construction
    /// From here it starts the original code loop
} else {
    // Original loop version
    int i(1); // Node counter
    for (int Lay = 1; Lay <= TotLayers; ++Lay) { // Begin layer loop ...
        { ... }
    }
}

```